ONTOGENY OF MONO- AND DIKARYOTIC HAUSTORIA OF *Puccinia coronata avenae*: ULTRASTRUCTURE, CYTOCHEMISTRY AND ELECTRON-PROBE X-RAY ANALYSIS

by

James Y.N. Chong

A thesis

submitted in partial fulfillment

of the requirements for the degree of

Doctor of Philosophy in the Department of Botany

The University of Manitoba

August, 1981

ONTOGENY OF MONO- AND DIKARYOTIC HAUSTORIA OF *Puccinia coronata avenae*: ULTRASTRUCTURE, CYTOCHEMISTRY AND ELECTRON-PROBE X-RAY ANALYSIS

BY

JAMES Y.N. CHONG

A thesis submitted to the Faculty of Graduate Studies of the University of Manitoba in partial fulfillment of the requirements of the degree of

DOCTOR OF PHILOSOPHY

TABLE OF CONTENTS

Page

LIST OF FIGURES

LIST OF TABLES

LIST OF ABBREVIATIONS

C	- collar
CH	- chloroplast
Cl	- chlorine
Con A	- Concanavalin A
Con A-gold	- gold-bound Con A
Cu	- copper
CW	- host wall
EDX	- energy dispersive X-ray analysis
EM	- extrahaustorial matrix
ER	- endoplasmic reticulum
Fe	- iron
G	- glycogen
GB	- Golgi body
Glt	- glutaraldehyde
H	- haustorium
HB	- haustorial body
HN	- haustorial neck
HNW	- haustorial neck wall
HMC	- haustorial mother cell
H_2O_2	- hydrogen peroxide
HS	- hyphal septum
IL	- inner layer
IPL	- invaginated host plasmalemma
K	- potassium
$K_3Fe(CN)_6$	- potassium ferricyanide
M	- mitochondria
Mg	- magnesium
MH	- M-haustorium
ML	- middle layer
MS	- haustorial mother cell septum
N	- nucleus
OL	- outer layer
OsO_4	- osmium tetroxide
P	- phosphorous
PA	- periodic acid
PACP	- periodic acid-chromic acid-phosphotungstic acid
PA-TCH-SP	- periodic acid-thiocarbohydrazide-silver proteinate
Pb	- lead citrate
PL	- plasmalemma
S	- sulphur
SG	- starch granule
SE	- sieve element
Si	- silicon
SP	- silver proteinate
TC	- terminal cell

TCH-SP	- thiocarbohydrazide-silver proteinate
Ua	- uranyl acetate
V	- vacuole
WGL	- wheat germ lectin
WGL-gold	- gold-bound WGL
X	- mature xylem vessel

ACKNOWLEDGEMENTS

I wish to express my sincere appreciation to Dr. D.E. Harder, my supervisor, for his guidance, constant encouragement, and constructive criticism during this study, and in the preparation of this manuscript. I would also like to thank the other members of the advisory committee, Dr. P.K. Isaac, Dr. I. Morrison, Dr. D. Punter, and Dr. J. Reid, for their valuable assistance.

I am very grateful to Dr. W.G. McDonald, Dr. R. Rohringer, and Dr. G. Dorrell (Research Station, Agriculture Canada, Winnipeg, Canada), for their kind support and for making available the facilities at the Research Station. I am also grateful to Dr. R. Rohringer for providing the gold-bound lectin preparations during the course of this study.

I am indebted to Dr. F.N. Ghadially and Mr. N.K. Yong, Department of Pathology, University Hospital, University of Saskatchewan, Saskatchewan, Canada, for making the energy dispersive X-ray analytical facilities available to me, and I would also like to thank Mr. N.K. Yong for his assistance and training.

A special note of gratitude is due to all my friends, Mr. W. Mauthe, and Ms. D. Derksen, for their valuable assistance, and notably Mr. K. Shewchuk, for his very capable technical assistance and preparation of the early draft.

Finally, I would like to express my sincere appreciation to my wife, Cecilia, and to my three young children, Patrick, Ivy and Peter. Without their understanding, patience and faith this work would not have been possible.

ABSTRACT

Puccinia coronata Cda. f. sp. avenae Eriks. was chosen for a study of haustorial development during the dikaryotic (D) and monokaryotic (M) life cycles. Less extensive studies were carried out on the D-haustoria of P. graminis Pers. f. sp. tritici Eriks. and Henn. Haustorial development was studied using cytochemical procedures: periodic acid-thiocarbohydrazide-silver proteinate (PA-TCH-SP), and periodic acid-chromic acid-phosphotungstic acid (PACP) staining; cellulase, protease, acetone, chloroform/methanol, and ether/ethanol extraction; Concanavalin A- and wheat germ lectin-gold binding; and energy dispersive X-ray (EDX) analysis. Further differentiation of structures was obtained by varying the fixation of tissues with glutaraldehyde alone, glutaraldehyde/osmium tetroxide, or glutaraldehyde/osmium tetroxide-potassium ferricyanide.

In the dikaryotic phase of both fungi specialized haustorial mother cells became differentiated at the hyphal tips prior to haustorium formation. Characteristically, the mitochondria of the mother cells were located around the inner periphery of their protoplasts. Another distinctive feature was the septum which delimited these cells from the rest of the mycelium. During early haustorium formation elaborations of the fungal plasmalemma occurred to form long protrusions on the hyphal side of the septum. Reduction in size of the protrusions subsequently occurred as the haustoria developed inside the host cells.

In P. coronata the septal protrusions contained a matrix which was similar in composition to the walls of young haustoria. They contained

protein, an unsaturated lipid, and PA-TCH-SP positive materials, but no chitin. These materials were likely present in complex forms. The haustorial mother cell walls on the other hand were little affected by protease, and contained PA-TCH-SP positive materials and a saturated lipid. Wheat germ lectin receptors were also common. The extrahaustorial matrix (EM) was composed of PA-TCH-SP positive materials, Concanavalin A receptors, a saturated lipid, protein and cellulose, but no chitin.

The neck ring in mature haustoria of P. coronata was composed of two cylindrical bands (designated as the α and β bands). The EDX analysis indicated that silicon was the major element in the α band, and iron and phosphorous the major elements in the β band. The EDX analysis also showed many haustorial mother cells near the centre of the infection colonies to be silicified, and these were usually associated with aberrant D-haustoria.

In D-infections of P. coronata there was a close association between haustoria and the host nuclei. This host response was marked by a proliferation of tubule complexes in the host cytoplasm between the haustoria and the host nuclei, and direct continuity between the tubules and the EM was observed. Cellulase treatment suggested that cellulose was present in the tubules. Another common host response was the formation of collars around the necks of some older haustoria. Cytochemical tests indicated that the materials making up the collars were mainly polysaccharides.

In contrast to the dikaryotic haustorial apparatus of P. coronata, the M-haustoria appeared as relatively undifferentiated hyphae. There were no septal membrane protrusions as in the dikaryotic phase. The position of the last septum outside the host cell varied during growth of

the M-haustoria. Older M-haustoria were septate. The walls of M-haustoria were continuous with those of the fungal cells outside the host cells and remained uniform in thickness and structure through the penetration site. The M-haustoria possessed an extrahaustorial matrix analogous to that of the D-haustorial apparatus. The EM of M-haustoria, however, was electron-opaque after uranyl acetate-lead citrate staining. Around the distal end in particular, the EM contained material that was intensely stained with the PACP method, whereas the haustorial wall remained largely unstained.

INTRODUCTION

The cereal rust diseases are economically important. Although efforts to control these diseases by the use of resistant varieties have been largely successful, continuing variation in the pathogen population makes the finding and incorporation of new resistant genes increasingly difficult. Many hundreds of virulence types exist in the pathogen population of many of the rusts, and whether a compatible or incompatible relationship with the host occurs probably depends on recognition factors, namely the putative products of the genes for resistance and avirulence in the host and parasite respectively (Rohringer et al, 1980). A major advance in breeding for resistance would be to understand and manipulate these recognition factors.

Rust fungi form intracellular haustoria, thereby establishing an intimate interfacial relationship with their hosts. The structural aspects of haustoria and their relationship with their hosts have been quite well characterized (Bracker and Littlefield, 1973; Littlefield and Heath, 1979). However, to understand fully the dynamics of this relationship, more detailed information is needed on the process of host cell invasion and on the chemical composition of the component parts of the host-pathogen interface. Detailed information on the latter aspect is almost totally lacking.

To study these aspects, the heteroecious oat crown rust system (Puccinia coronata Cda. f. sp. avenae Eriks./Avena sativa L.) was chosen.

This fungus is common to Manitoba both in the dikaryotic phase on Avena sp. and in its monokaryotic phase on Rhamnus cathartica L. Preliminary studies have shown that haustoria produced by this fungus during the monokaryotic and dikaryotic stages of the life cycle are morphologically distinct (Harder, 1978). Supplementary studies were also carried out on the wheat stem rust (Puccinia graminis Pers. f. sp. tritici Eriks. and Henn./Triticum aestivum) system for comparison. Specifically the following were to be studied:

1) The ultrastructural features of the haustorial mother cells and changes which occur just prior to or during the formation of young haustoria.

2) The structural aspects of the development of haustoria.

3) The ultrastructural changes of the host cells, particularly at the host-pathogen interface, in response to the fungal invasion.

During these studies various histochemical methods and electron-probe X-ray analysis (EDX) were applied to provide information on the chemical nature of the component parts of the haustorial apparatus and the host-pathogen interface. The significance of these results is discussed in connection with the probable mode of formation of these haustoria and the possible location of recognition factors between host and pathogen.

LITERATURE REVIEW

According to Rice (1927), de Bary (1863) was the first to describe in detail the occurrence and structure of haustoria and apparently first used the term haustorium for the knob-like organs of Cystopus. He correctly regarded the haustorium as a specialized organ that maintained the interrelations between parasite and host (Rice, 1927).

The word haustorium comes from a Latin term meaning "to drink" (Snell and Dick, 1971). Karling (1932) regarded haustoria as feeding organs. Although the role of haustoria as organs of nutrient absorption has never been unequivocally proven, it is universally accepted that this is the case (Littlefield and Heath, 1979). Bushnell (1972) defined haustorium as " ... a specialized organ which is formed inside a living host cell as a branch of an extracellular (or intercellular) hypha or thallus, which terminates in that host cell, and which probably has a role in the interchange of substances between host and fungus". Haustoria are, therefore, distinct from intracellular hyphae which may continue to grow for some time after penetration and they may grow from cell to cell (Bracker and Littlefield, 1973).

With rust fungi, in infections originating from aeciospores or urediospores, haustoria usually show determinate growth and clearly fall within Bushnell's (1972) definition of haustoria. However, in basidiospore-derived infections, the intracellular structures produced differ in many ways from the haustoria found in dikaryotic infections. Indeed,

there is some controversy whether the intracellular structures found in monokaryotic rust infections should be designated as haustoria or as intracellular hyphae. What is known of the structural features of dikaryotic and monokaryotic haustoria in rust fungi and problems of terminology have been dealt with in detail by Littlefield and Heath (1979). The dikaryotic and monokaryotic haustoria were designated (Littlefield and Heath, 1979) respectively as D- and M-haustoria, and this terminology will be retained in this thesis.

I. Dikaryotic (D-) Haustoria

The foundations of many subsequent cytological studies of the rust fungi are found in several classical papers: Allen (1923a), Ruttle and Fraser (1927), Rice (1927). These were among the first investigators to look at the intercellular hyphae and the haustoria, and the relations of these fungal organs to the host cells. Allen (1923a) described the stages leading to haustorium formation by P. graminis tritici in susceptible wheat. As a hypha was about to form a haustorium, it stopped growing in length and its tip became swollen into a "club" with its end closely applied to the wall of the host cell. The pair of nuclei near the hyphal tip underwent nuclear division. Two of the daughter nuclei then moved into the swollen terminal portion, while the other two remained a short distance behind. At this stage these four nuclei were about equal in size. A septum was then formed, thus giving rise to a short terminal cell, the haustorial mother cell. The two nuclei in the haustorial mother cell then underwent a marked decrease in size to become about one-half of their previous size.

In a similar study Ruttle and Fraser (1927) showed that the haustorial mother cells of P. coronata avenae were initiated essentially in

the same way as that described for P. graminis tritici (Allen, 1923a). The two nuclei in the haustorial mother cells of P. coronata avenae also became smaller in size. A similar decrease in nuclear size also occurred during haustorial mother cell formation in Uromyces fabae (Savile, 1939). The nuclei of the haustorial mother cells were smaller than those of the intercellular hyphae of U. phaseoli vignae in an electron microscope study (Heath and Heath, 1978), but the mechanism by which this reduction occurred was not known.

The initially formed haustoria within the host cells were described by early light microscopists as a peg-like projection (Allen, 1923a; Ruttle and Fraser, 1927), slender rod (Rice, 1927) or slender filament (Savile, 1939). It was believed that growth of a haustorium into the host cell was accompanied by a corresponding invagination of the host protoplast (Allen, 1923a; Rice, 1927). The young haustoria then differentiated into two parts: a small dense staining globular body and a slender neck. The haustorial body expanded rapidly and much of the contents of the mother cell passed into the haustorium. In P. graminis tritici (Allen, 1923a) and U. fabae (Saville, 1939), two nuclei were found in the mature haustorium. With P. coronata avenae, however, only a single nucleus was consistently seen in many of the mature haustoria (Ruttle and Fraser, 1927). No trace of a second nucleus was ever found. Ruttle and Fraser (1927) suggested that both nuclei entered and then either fused or one of them degenerated, but evidence of either process is lacking.

The use of the electron microscope in recent years has enabled electron microscopists to examine rust infections in finer detail and has resulted in a large volume of descriptive information on the ultrastructure of D-haustoria and their associations with higher plants. Much of this

information has been extensively reviewed (Bracker and Littlefield, 1973; Bushnell, 1972; Ehrlich and Ehrlich, 1971; Littlefield and Heath, 1979), thus only literature of immediate relevance to the work presented here is included.

Ehrlich and Ehrlich (1963) pioneered the work in using electron microscopy to study host-parasite relationships in stem rust of wheat. Their observations confirmed the early findings of Allen (1923a, b) on the morphology of haustoria. In addition they showed that at the site of host wall penetration a bulge-like thickening occurred on the inside of the haustorial mother cell wall. This thickened region was closely appressed to the host cell wall, and it was through this area that host penetration was accomplished by the fungus. This thickening of the haustorial mother cell wall at the site of host penetration was in time found to be a constant feature of many rust fungi.

In Melampsora lini (Littlefield and Bracker, 1972) and U. phaseoli vignae (Heath and Heath, 1971) the thickening has been attributed to the presence of an electron-dense, lens-shaped layer deposited between the two fibrillar layers which comprise the rest of the haustorial mother cell wall. With P. coronata avenae, Harder (1978) reported the presence of only two layers in the thickened region. The inner layer of the fungal wall was visible as a very narrow, denser staining region through either side of the penetration site. Other variations in terms of number of layers of the haustorial mother cell wall at the thickened region have been reported in other rust species. As commented on by Littlefield and Heath (1979), the reality of these differences is hard to interpret, especially in some cases where different interpretations have been made from micrographs produced by different workers of the same rust species.

It appears that appearance and position of wall layers in the penetration region of the haustorial mother cell is affected by minor differences in preparative procedures.

An early event in haustorium formation is the development, from the thickened region of the haustorial mother cell wall, of a penetration peg which breaches the host wall (Littlefield, 1972). The diameter of the site of penetration through the host wall is usually less than 0.5 μm (Littlefield and Bracker, 1972). This represents the area of host wall actually removed by the action of the penetrating fungus. There is very little ultrastructural information on the penetration process in rust fungi. Ultrastructural evidence from post-penetration stages, however, suggests that penetration involves mainly enzymatic action rather than physical force, since the host wall, and often wall fibrils, end abruptly at the penetration peg and do not appear distorted or displaced inward (Littlefield and Heath, 1979).

The fungal wall in the penetration region is usually much thinner than the walls of the haustorial mother cell or haustorium. In U. appendiculatus (or U. phaseoli typica) the fungal wall was so thin at the penetration site as to appear absent in some micrographs (Hardwick et al, 1971). In other cases, the host and fungal walls may merge such that their distinction is obscure (Coffey et al, 1972; Littlefield and Bracker, 1972; Hardwick et al, 1971). These diffuse regions of integrated host and fungal walls may signify sites at which the walls of the two organisms have grown together (Bracker and Littlefield, 1973).

Two cases have been documented showing the early stages of penetration peg formation. These were reported in M. lini (Littlefield and Bracker, 1972) and U. phaseoli vignae (Heath and Heath, 1975). In both

the peg developed as a localized evagination of the haustorial mother cell plasmalemma and the inner layer of the haustorial mother cell wall. The outer wall layer did not seem to play a part in peg development. The penetration pegs reported by Bossányi and Oláh (1974) in P. graminis tritici were clearly oblique sections of well-developed haustorial necks, as the haustorial mother cells shown in their micrographs were largely vacuolated, a good indication that much of their cytoplasm had emigrated into the haustoria.

The cytoplasm of all the penetration pegs reported in U. phaseoli vignae was characterized by the presence of electron-opaque granules about 30 nm in diameter (Heath and Heath, 1975). With M. lini multivesicular structures were found instead of electron-opaque granules (Littlefield and Bracker, 1972). It is possible that these granules or the multivesicular structures play a role in effecting the localized degradation of host wall in advance of the penetrating pathogen.

After host wall penetration Ehrlich and Ehrlich (1963) claimed that the incipient haustorium consisted only of a membrane, and the initial contact between the nascent haustorium and the host cell protoplast was between naked protoplasts. This led to their proposal that penetration is accomplished by a "blow-out" of the fungal protoplast (Ehrlich and Ehrlich, 1971). This "blow-out" hypothesis, however, has not been supported by further ultrastructural evidence. Rather the penetration peg appears to elongate and expand somewhat to form a structure, the nascent haustorial neck (Littlefield, 1972; Heath and Heath, 1975). Ultrastructurally, only a single example has been reported of a nascent haustorial neck, 4 μm in length, which shows no sign of development of the haustorial body (U. phaseoli vignae; Heath and Heath, 1975). This neck

was completely surrounded by a discrete fungal wall (see later). The neck cytoplasm was densely packed with ribosomes and contained longitudinally arranged microtubules. A few cytoplasmic membrane-bound vesicles were found close to the tip but mitochondria and nuclei were absent.

In U. phaseoli vignae early haustorium formation was characterized by changes associated with the septum delimiting the haustorial mother cell (Heath and Heath, 1975). Elaborations of the plasmalemma occurred on both sides of the septum. These appeared as irregular whorls and tangles of membrane on the haustorial mother cell side and tubular membrane protrusions on the hyphal side. Mitochondria accumulated on the haustorial mother cell side and became associated with the masses of membranes. These membranes disappeared and the mitochondria dispersed when the penetration peg began to enter the host cell. The maximum development of the tubular protrusions on the hyphal side was accomplished by a marked association with numerous mitochondria and coincided with penetration of the host wall. Significant changes also occurred in the septal pore at this stage. By the time the haustorial neck had reached its full length, the plasmalemma protrusions had greatly shrunk in length and the accumulated mitochondria had dispersed.

After the tubular neck has reached a length of about 4 μm, the distal end of the neck begins to expand into the haustorial body in M. lini (Littlefield, 1972). The initial swelling of the body apparently coincides with the migration of mitochondria from the haustorial mother cell, as a large number of mitochondria were seen packed in a partly expanded body (Harder et al, 1978). Migration of the two nuclei from the haustorial mother cell into the haustorium eventually followed (Heath and Heath, 1975; Mendgen, 1975). Preformed cytoplasmic micro-

tubules in the neck may play a role in organelle migration (Heath and Heath, 1971, 1975).

Thatcher (1943) using plasmolysis, was able to separate haustoria of P. graminis tritici from the invaginated host protoplasts and thus demonstrated that the entire haustorium is surrounded by the invaginated host plasma membrane (or extrahaustorial membrane). There is now ample ultrastructural evidence to show that young and mature haustoria are separated from the host cytoplasm by the invaginated host plasma membrane and clear continuity has been established between this membrane and the host plasma membrane at the base of the haustorial neck (Coffey et al, 1972; Hardwick et al, 1971; Littlefield and Bracker, 1972).

The neck ring, sometimes referred to as a neck band (Ehrlich and Ehrlich, 1971; Heath and Heath, 1971; Coffey et al, 1972), is a specialized structure occurring in D-haustorial necks of all rust fungi so far examined ultrastructurally, but it is usually absent in very young haustoria (Heath and Heath, 1975; Harder et al, 1978). This structure was first described by Rice (1927) as a broad or narrow ring-like zone seen along the neck. Hardwick et al (1971) have shown that it is a specialized region of the neck wall. The neck ring is marked by an extremely tight association of host and fungal plasma membrane, which is reminiscent of the Casparian strip of endodermal cells of vascular plants (Littlefield and Bracker, 1972; Heath, 1976). Bossányi and Oláh (1974) claimed that the neck ring in P. graminis tritici is associated with acid phosphatase activity. Their interpretation is questionable as there is no mention of a control treatment (ie. excluding lead nitrate in the incubation medium) being done to demonstrate that the observed electron-opacity of the neck ring is actually due to localized acid phosphatase

activity.

The neck ring stains intensely after conventional (glutaraldehyde-OsO_4/uranyl acetate-lead citrate) preparation procedures for electron microscopy (Coffey et al, 1972; Harder, 1978; Hardwick et al, 1971; Heath, 1972; Heath and Heath, 1971; Rijo and Sargent, 1974; Van Dyke and Hooker, 1969). It is generally accepted that the neck ring is intensely osmiophilic (Bracker and Littlefield, 1973; Littlefield and Heath, 1979), although the neck ring in unstained sections of glutaraldehyde fixed, unosmicated material has never been examined to verify that this is the case. Littlefield and Bracker (1972) have shown that the neck ring of M. lini is extractable with periodic acid but it is not known if the neck rings of other rust species will respond to periodic acid in the same way.

One view (Heath, 1976) of the function of the neck ring is that it prevents apoplastic flow of substances along the haustorial neck wall and out of the infected cell, a parallel function to that of the Casparian strip of endodermal cells in roots of higher plants. The restriction of apoplastic flow may then favor the uptake of substances into the haustorial body (Heath, 1976). That the neck ring is capable of preventing apoplastic flow has been demonstrated for P. sorghi (Heath, 1976). Despite the importance of this view, nothing is known about the chemical composition of the neck ring.

There is ultrastructural evidence that there are two types of organization of structures found between the protoplasts of the fungus and the host in the neck region (Littlefield and Heath, 1979). In M. lini the region proximal to the neck ring stains uniformly and has been described as consisting entirely of fungal wall (Coffey, 1976; Coffey et al, 1972; Littlefield and Bracker, 1972). On the distal side

of the neck band two layers were found which were continuous around the haustorial body (Coffey, 1976; Coffey et al, 1972). Coffey has interpreted the outer more electron-lucent region as being the extrahaustorial matrix and the inner more electron-opaque layer as being a new type of fungal wall. That the composition of the neck wall of M. lini does seem to change at the neck ring is indicated by Littlefield and Bracker (1972) who showed that the neck wall proximal to the neck ring is more strongly stained with the periodic acid-chromic acid-phosphotungstic acid (PACP) technique than the part distal to it.

The other type of organization in the neck region is characterized by the presence of two distinct layers along the whole length of the neck as shown in U. phaseoli typica (Hardwick et al, 1971; Muller et al, 1974), U. phaseoli vignae (Heath and Heath, 1971), P. helianthi (Coffey et al, 1972), and P. sorghi (cited in Littlefield and Heath, 1979). In all the above cases where the penetration region is illustrated, the inner layer proximal to the neck ring is shown to be continuous with the wall of the penetration peg, and therefore is assumed to have fungal origin. The outer layer of this region, which shows a different structure than the inner layer, has been interpreted as extrahaustorial matrix material (see later) in U. phaseoli vignae (Heath and Heath, 1971) or as a layer of collar material of host origin (Hardwick et al, 1971; Muller et al, 1974). On the other side of the neck ring, the inner layer is shown to be similar in staining and thickness to the inner layer proximal to the neck ring and the outer layer gradually becomes more electron-lucent. These two layers continue around the haustorial body and have been interpreted as fungal wall and extrahaustorial matrix respectively (Heath and Heath, 1971). The presence of two such layers along the whole neck is

evident in young haustoria of U. phaseoli vignae before the neck ring develops (Heath and Heath, 1975).

Around the haustorial body, the protoplasts of fungus and host are separated by two or more ultrastructurally distinct layers. Where two layers are present, the more discrete electron-opaque layer next to the fungal plasmalemma has been interpreted as fungal wall while the remaining more electron-lucent layer is considered as part of the extrahaustorial matrix (Calonge, 1969; Harder, 1978; Heath and Heath, 1971; Heath, 1972; Van Dyke and Hooker, 1969). However, where more than one discrete electron-opaque layer is present, opinions varied among workers in deciding whether all layers should be considered as part of the fungal walls or only the innermost layer (see Littlefield and Heath, 1979). This contrast in opinions is perhaps due to the fact that the above interpretations are based on morphological appearances resulting from "standard" preparations and as yet there are no other criteria to distinguish between fungal walls and the extrahaustorial matrix. Clearly, histochemical data are needed to clarify the above distinctions.

The extrahaustorial matrix (termed by Bushnell, 1972) is equivalent to the encapsulation shown by Heath (1972), Heath and Heath (1971), Ehrlich and Ehrlich (1963, 1971), Calonge (1969), and Shaw and Manocha (1965), and the haustorial sheath (Bracker and Littlefield, 1973). It is the medium which surrounds the haustorium and little is known of its composition. The extrahaustorial matrix is usually more pronounced around the body of the haustorium and it gradually tapers off in the transition region from the haustorial body to the neck (Coffey et al, 1972; Harder, 1978; Heath and Heath, 1971; Mares, 1979). The extrahaustorial matrix may be uniformly granular in appearance, suggesting that

the major constituents are distributed uniformly throughout the matrix or it may contain irregular or more discrete layers of amorphous or fibrillar electron-opaque material (Bracker and Littlefield, 1973; Littlefield and Heath, 1979).

The extrahaustorial matrix may stain only faintly or not at all with conventional stains (Adu-Zinada et al, 1975; Coffey et al, 1972; Harder, 1978; Heath, 1972; Heath and Heath, 1971; Littlefield and Bracker, 1972; Manocha and Lee, 1971; Van Dyke and Hooker, 1969). Such images pose the question whether there is actually any material in the matrix or whether it is an artifact of preparation. Recently, Allen et al (1979), from their plasmolytic studies on rusted flax indicated that the electron-lucent matrices of young dikaryotic, rust haustoria may arise through loss of turgor during fixation, allowing the invaginated host plasma membrane to pull away from the haustorial wall in regions where the two structures were not firmly attached. They did, however, point out that matrices of older haustoria, that contain dense granular or fibrillar materials (eg. Coffey, 1976) are presumed to be real structures. The concept of the electron-lucent matrix as an artifact of preparation is supported by light microscope observations of living haustoria of the powdery mildew, Erysiphe graminis, where the extrahaustorial matrix was seen to expand when fixatives (osmium tetroxide and potassium permanganate) were added (Bushnell, 1971). Bushnell (1972) suggested that the invaginated host plasma membrane is in close contact with the living, undisturbed, young powdery mildew haustorium.

On the other hand, the best argument for the reality of the extrahaustorial matrix is the fact that it can be found around all rust haustoria (including those fixed with glutaraldehyde and freeze-etched;

(Littlefield and Bracker, 1972) as well as around intracellular structures in a wide variety of symbiotic relationships (Bracker and Littlefield, 1973) fixed and prepared by a variety of procedures (see references in Littlefield and Heath, 1979). There are other observations which can be used to support the above argument. Armentrout and Wilson (1969) detected reaction products indicating acid phosphatase activity in the matrix region around haustoria of Piptocephalis virginiana. Mendgen and Fuchs (1973) showed occasional peroxidase activity in the inner portion of the matrix of U. phaseoli typica. Moreover, the extrahaustorial matrix often seems to change with age. The electron-opaque component, as well as the overall thickness of the matrix have been claimed to increase with haustorium age for several rust infections (Ehrlich and Ehrlich, 1971; Harder, 1978; Manocha and Shaw, 1967; Orcival, 1969; Shaw and Manocha, 1965). Accepting the interpretations above, the changing status of the extrahaustorial matrix is at least an indication that the matrix is not entirely a result of preparation artifact. Hardwick et al (1971) regarded the extrahaustorial matrix as part of the fungal wall. In Zimmer's (1970) study of Safflower rust, the extrahaustorial matrix became stratified into three layers as the haustoria aged in a compatible host, and glandular appendages with fibrillar contents were sometimes found at the periphery. The fibrillar portions of the matrix resembled loosely organized cell wall material, but it was not clear whether this possible attempted wall formation was a property of the host, fungus, or both. Coffey (Fig. 68; Littlefield and Heath, 1979) showed that the electron-dense material in the extrahaustorial matrix around a mature haustorium of M. lini was also associated with host cytoplasmic tubules located in the vicinity of the haustorium. A

distinct connection was seen between these tubules and the extrahaustorial matrix, suggesting that this region may contain substances of host origin.

The above interpretations of the origin of the matrix are at best based on visual observations of electron micrographs and again, biochemical data is needed to support any of these views. The best available evidence related to the origin of the matrix so far is obtained from the high resolution autoradiographic studies of a mycoparasite, Piptocephalis virginiana (Manocha and Lee, 1972; Manocha and Letourneau, 1978). Labels from feeding experiments with (^{3}H) N-acetyl-glucosamine, a precursor of chitin, are located in the extrahaustorial matrix and host wall, but not in the wall of the parasite. These results, therefore suggest that the extrahaustorial matrix around the mature haustoria of Piptocephalis virginiana contains some host cell wall material, ie. chitin. Contribution by the parasite to the matrix, however, is not ruled out.

There have been other attempts at using high resolution autoradiography to help elucidate the nature of the extrahaustorial matrix and to determine the route of nutrient transfer. Ehrlich and Ehrlich (1970) inoculated wheat leaves with prelabelled ($^{14}CO_2$) stem rust urediospores and demonstrated the passage of radioactivity from the parasite to the host. No label was detected in the extrahaustorial matrix. Using a similar host-parasite system and feeding the infected host plant with (^{3}H) leucine, Manocha (1975) also did not find label accumulated in the extrahaustorial matrix. In contrast to the results of Ehrlich and Ehrlich (1970), however, Manocha showed that the migration of label when (^{3}H) leucine was used, was from the host to the parasite.

Absence of label in the extrahaustorial matrix around haustoria of U. phaseoli typica was similarly demonstrated when bean leaves were inoculated with urediospores previously labelled with (^{3}H) orotic acid (Mendgen and Heitefuss, 1975). It is evident from the above studies that the extrahaustorial matrix does not act as a sink for the radioactive substances involved. However, it is possible that the absence of label in this region may have been due to extraction during preparation.

More recently, Spencer-Phillips and Gay (1980) found significant labelling occurred in the haustorial complexes of Erysiphe pisi isolated from infected leaves of Pisum sativum that had been exposed to $^{14}CO_2$. Their results indicated that (^{14}C) photosynthate was incorporated into the haustorial complexes. Further, the invaginated host plasmalemma was heavily labelled, but more importantly, this was the first occasion on which significant matrical labelling was shown, and the level attained suggested that the matrix was derived directly from the host.

II. Monokaryotic (M-) Haustoria

Early light microscope studies have shown that the intracellular structures found in the basidiospore-derived infections (Allen, 1930, 1932a, b, 1934; Colley, 1918) are filamentous and more irregular in shape than those haustoria found in the uredial stage of the life cycle (Allen, 1923a, b; Ruttle and Fraser, 1927; Rice, 1927). Electron microscopy has supplemented these studies and has clearly shown that the intracellular structures of many rust species have little of the structural specialization characteristic of the D-haustorial apparatus (Cronartium ribicola, Robb et al, 1975; M. lini, Gold and Littlefield,

cited in Gold et al, 1979; Peridermium pini, Walles, 1974; P. coronata avenae, Harder, 1978; P. malvacearum, cited in Gold et al, 1978; P. poarum, Al-Khesraji et al, 1980; Al-Khesraji and Lösel, 1980; P. podophylli, Borland and Mims, 1980; P. recondita, Gold et al, 1979; P. sorghi, Rijkenberg and Truter, 1973; U. phaseoli vignae, Heath, cited in Littlefield and Heath, 1979). Harder (1978) was the first to directly compare the haustoria in uredial and pycnial infections of one rust fungus by electron microscopy. The differences reported between the haustoria of uredial and pycnial infections in the heteroecious rusts such as P. coronata avenae may possibly be due to varying influences by the different host species. However, studies of the autoecious rusts P. podophylli (Borland and Mims, 1980) and M. lini (Gold et al, 1979) indicate that the host does not influence the type of intracellular structures formed. Gold et al (1979), from their studies and review of others, suggested that the type of intracellular structure in many rusts may be linked to the genetic and nuclear condition of the thallus and depends on whether the thallus is derived from a monokaryotic spore or a dikaryotic spore, and not on the host species infected.

The intracellular structures of the pycnial-aecial thallus have been variously designated; haustorium (Allen, 1930, 1932a, b, 1934; Borland and Mims, 1980; Colley, 1918; Kozar and Netolitzky, 1975; Walles, 1974); P-haustorium (Harder, 1978); intracellular hypha (Allen, 1935; Coffey, 1977; Gold et al, 1979; Kohno et al, 1976, 1977; Rijkenberg and Truter, 1973; Al-Khesraji et al, 1980; Al-Khesraji and Lösel, 1980) and intracellular mycelium (Hunt, 1968; Pady, 1935). The ultrastructural observations in the literature indicate that the intra-

cellular structures of heteroecious or autoecious rusts share many features in common. Recently, much of this information has been reviewed (Littlefield and Heath, 1979). Following Littlefield and Heath's (1979) terminology M-haustorium will be used in this review to designate all intracellular structures in basidiospore-derived infections, and the term "haustorium" is retained to indicate that both the monokaryotic and dikaryotic intracellular structures represent analogous portions of the fungus in terms of the close association with the host protoplast (Littlefield and Heath, 1979).

In general terms, the M-haustoria may be characterized as follows. No localized thickenings occur in the walls of the "haustorial mother cells" at the penetration site. Lack of penetration attachments of the mother cells to host cells is also common as shown in P. coronata avenae (Harder, 1978), P. recondita (Gold et al, 1979), M. lini and P. malvacearum (cited in Gold et al, 1979), although in some instances, material that is thought to have an adhesive role in dikaryotic infections is seen at the penetration site of M-haustoria of P. sorghi (Rijkenberg and Truter, 1973) and in U. phaseoli vignae (Tighe and Heath, cited in Littlefield and Heath, 1979). At the penetration region the degradation of the host wall suggests that penetration is primarily enzymatic (Harder, 1978; Rijkenberg and Truter, 1973; Walles, 1974). Penetration appears to be accomplished by a protuberance of the mother cell entering the host cell (Harder, 1978) and does not involve the formation of a specialized penetration peg as that found in dikaryotic infections (Heath and Heath, 1975; Littlefield and Bracker, 1972). The fungus shows relatively little constriction as it passes through the host wall. The fungal wall through the penetration region is equal in

thickness to and continuous with the haustorial mother cell and haustorial body wall. The walls of both the mother cells and the M-haustoria of U. phaseoli vignae responded similarly to periodic acid-chromic acid-phosphotungstic acid (PACP) staining (Heath, cited in Littlefield and Heath, 1979).

In all rust-fungal species examined, M-haustoria are hypha-like in appearance and lack a distinct neck region (Littlefield and Heath, 1979). There is no dense staining neck ring, with the exception of M-haustoria of tissue-culture grown Cronartium ribicola, in which electron-opaque neckband-like structures have been reported (Robb et al, 1975). Nevertheless, the presence of neckband-like structures is not consistent and as commented on by Littlefield and Heath (1979), the so-called "neckbands" reported in Cronartium ribicola do not seem to be the same structure seen in the dikaryotic haustorial apparatus.

Many M-haustoria are septate but the position of the septum appears to vary depending on the species. In haustoria of Cronartium ribicola (Robb et al, 1975), Kuehneola japonica (Kohno et al, 1977), M. pinitorqua (Coffey, cited in Littlefield and Heath, 1979), Peridermium pini (Walles, 1974), and P. podophylli (Borland and Mims, 1980), a septum was normally found in the penetration region separating the mother cell from the M-haustorium. In other species, a septum may be positioned in the haustorium at some distance away from the penetration site (P. coronata avenae, Harder, 1978; P. sorghi, Rijkenberg and Truter, 1973).

The M-haustoria invaginate the host plasmalemma (Harder, 1978; Kohno et al, 1977; Rijkenberg and Truter, 1973; Walles, 1974). In P. coronata avenae (Harder, 1978), and Cronartium ribicola (Robb et al, 1975), an ingrowth of host wall-like material which invaginates the host

plasmalemma has been reported to form in advance of the penetrating fungus. The remnants of this ingrowth are believed to later form a collar around the proximal end of the M-haustorium (Harder, 1978). The presence of a collar in the penetration region appears to be a common feature associated with M-haustoria (Cronartium ribicola, Robb et al, 1975; Peridermium pini, Walles, 1974; P. coronata avenae, Harder, 1978; P. podophylli, Borland and Mims, 1980).

The appearance of the extrahaustorial matrix found in different monokaryotic infections is variable (Littlefield and Heath, 1979). It may be relatively electron-opaque (Gold et al, 1979; Robb et al, 1975; Walles, 1974) or it may appear more heterogeneous with both translucent and opaque components (Kohno et al, 1977; Harder, 1978). In U. phaseoli vignae, it stains strongly after PACP treatment while the haustorial wall remains largely unstained (Heath, cited in Littlefield and Heath, 1979). Rijkenberg and Truter (1973) did not distinguish between the extrahaustorial matrix and the invaginated collar at the penetration region in P. sorghi, but it is more likely that matrix material blended imperceptibly with the collar material as suggested by Littlefield and Heath (1979).

From the foregoing review, the morphology of M-haustoria among different rust species appears to be very similar. However, they may differ in other respects. From a few available studies, it is evident that M-haustoria are characteristically restricted to one host cell (eg. P. coronata, Allen, 1932b; Harder, 1978; Cronartium ribicola in parenchyma cells, Colley, 1918; Peridermium pini, Walles, 1974; P. poarum, Al-Khesraji and Lösel, 1980). However, other studies have shown that M-haustoria of some species may exit the invaded host cell and may

pass from one host cell to the next (Cronartium ribicola in phloem cells, Colley, 1918; M. lini, Gold and Littlefield, 1979; P. malvacearum, Allen, 1935; Gold et al, 1979). It appears then that some of the M-haustoria conform to Bushnell's (1972) definition of a haustorium while others do not. Because of this reason, and because of their ultrastructural differences from D-haustoria, a number of authors cited earlier, have regarded these intracellular structures as "intracellular hyphae", rather as haustoria. This difference in terminology is not likely to be resolved until better criteria can be found and more specific information relating to their function is available.

III. Host Responses

A. Cytoplasmic Changes

Most of the ultrastructural studies of host responses to rust infection have focused on the interface between the M- or D-haustoria and the host. The invaginated host plasma membrane has received considerable attention because presumably it is through this membrane that materials are exchanged between the host and fungus.

There is ultrastructural evidence that the invaginated host plasma membrane differs in some way from the non-invaginated portion. In some infections the invaginated host plasma membrane appears to be thicker than the non-invaginated portion (P. graminis tritici, Ehrlich and Ehrlich, 1963; Harder, personal communication), while in others, it may appear thinner (some M-haustoria of P. coronata avenae, Harder, 1978) or it may not change in thickness at all (P. sorghi, Van Dyke and Hooker, 1969; M. lini, Littlefield and Bracker, 1970, 1972). In

M. lini, freeze-etching or treatment with periodic acid-chromic acid-phosphotungstic acid (PACP) respectively, revealed that the membrane around the D-haustoria contained fewer granules and stained less intensely (Littlefield and Bracker, 1972). The position of the neck ring appeared to mark the transition in stainability with the PACP method. A similar lack of PACP staining of the invaginated host plasma membrane occurs around the M-haustoria of U. phaseoli vignae (Heath, cited in Littlefield and Heath, 1979). In contrast, in uredial infections of P. graminis tritici (Harder et al, 1978) and U. phaseoli vignae (Heath, cited in Littlefield and Heath, 1979), this membrane is often shown to have a greater PACP staining than the rest of the host plasma membrane. The above observations indicate that there is a change in the nature of the invaginated host plasma membrane as compared to the non-invaginated membrane. Littlefield and Bracker (1972) concluded from their study of M. lini that the change in nature, be it in structure and/or composition, of this membrane represented a response to the pathogen.

Host cells invaded by compatible strains initially show little disorganization of the host protoplasts, and most of the differences in ultrastructure between infected and uninfected cells appears to involve the frequency of distribution of certain components (Littlefield and Heath, 1979). Cisternae of endoplasmic reticulum are commonly found lying parallel to the invaginated host plasma membrane in almost every study of M- and D-haustoria (Littlefield and Heath, 1979). The association between endoplasmic reticulum and D-haustoria seems to develop soon after penetration, prior to haustorial body formation (Heath and Heath, 1975), and in some infections the early expansion phase of the D-haustorium is marked by extensive proliferation of endoplasmic reticulum,

particularly around the upper portion of the neck, where some of the cisternae appear to radiate from the haustorium (P. graminis tritici, Harder et al, 1978; U. phaseoli vignae, Heath, cited in Littlefield and Heath, 1979). Continuity between endoplasmic reticulum and the invaginated host plasma membrane in the neck region has never been observed. Profiles of endoplasmic reticulum in the neck region of P. graminis tritici became less prominent as the haustoria matured (Harder et al, 1978). Endoplasmic reticulum-derived membranous complexes, consisting of a lattice arrangement of large and small, apparently interconnected, ribosome-free tubules then occurred around the bodies of more mature haustoria (Harder et al, 1978). These complexes formed part of the interface between host and pathogen through connections with the invaginated host plasma membrane. Somewhat similar structures have been reported in haustoria of Peronospora pisi (Hickey and Coffey, 1977), young D-haustoria of P. graminis tritici (Ehrlich and Ehrlich, 1971), older D-haustoria of M. lini and P. helianthi (Coffey et al, 1972), and D-haustoria of P. recondita (Yudkin and Reiter, 1979).

Associations between host mitochondria, the nucleus, chloroplasts, Golgi bodies, and cytoplasmic vesicles and haustoria have been reported, but only the host nucleus-haustorial association is more convincingly shown to be a characteristic response (Littlefield and Heath, 1979). Early light microscopists (Allen, 1923a, 1932b; Colley, 1918; Rice, 1927; Ruttle and Fraser, 1927) have shown that there is a definite attraction between host nuclei and haustoria in many rust infections. With corn rust, the association was so close that the host nucleus was described as amoeboid-like, to enwrap the haustorium, or it was indented by a haustorial lobe (Rice, 1927). Recent studies with

the electron microscope have shown the close association of the host nucleus and the D-haustorium (Al-Khesraji and Lösel, 1980; Coffey, 1975; Coffey et al, 1972; Heath and Heath, 1971; Manocha and Shaw, 1966; Van Dyke and Hooker, 1969) or M-haustorium (P. recondita, Gold et al, 1979; M. pinitorqua and U. phaseoli vignae, Coffey and Heath respectively, cited in Littlefield and Heath, 1979). Bracker and Littlefield (1973) suggested that the apparent lack of association with host nuclei in other ultrastructural studies may be due to unfavorable plane of sectioning, or it is possible that the association may only exist during the early stages of haustorium formation as suggested for D-haustoria of U. phaseoli vignae (Heath and Heath, 1971).

Late in the infection process and often after the onset of sporulation, the most frequently observed response of the host tissue is a general disorganization of the cytoplasm and a disruption of the cell membrane (for details see the review by Littlefield and Heath, 1979).

B. Collars

A common response of the host cell to the presence of both M- and D-haustoria is the deposition of a "collar" of material at the point where the fungus enters the host cell. Some collars are primarily electron-lucent, and contain some membranous vesicles (eg. Coffey et al, 1972; Ehrlich et al, 1968; Littlefield and Bracker, 1972) or more extensive electron-opaque patches (eg. Ehrlich et al, 1968; Rijkenberg and Truter, 1973). Some collars are fibrillar (eg. Harder, 1978; Hardwick et al, 1971; Walles, 1974). There are collars that contain both fibrillar and electron-lucent components, and primarily translucent, or primarily fibrillar, collars may occur in single rust infections (Coffey et al, 1972; Hardwick et al, 1971).

Littlefield and Heath (1979), after reviewing different collars found in different rust infections, have designated two types of collars based on their probable mode of formation. One type of collar (usually the more electron-translucent ones) appears to form by a "growing up" process from the host wall during (Littlefield and Bracker, 1972), or possibly after, fungal penetration in such a manner that the collar is surrounded inside and out by the host plasma membrane. This type of collar, designated as Type I is found, for example, in D-infections of M. lini (Coffey et al, 1972; Littlefield and Bracker, 1972), or P. coronata avenae (Harder, 1978). The other type of collars comprise the more fibrillar ones, and these collars are often not separated from the haustorium by any discernable membranes (Type II collar) as shown in M-infections of P. coronata avenae (Harder, 1978) or Peridermium pini (Walles, 1974). This type of collar appears to be formed either as the fungus grows through material deposited on the host cell wall before penetration, or it is deposited directly over the surface of the young haustorium as it enters the host cell (Harder, 1978; Walles, 1974). Type II collars are frequently found around M-haustoria but rarely around D-haustoria, whereas Type I collars have been observed around both M- and D-haustoria.

IV. Cytochemical Methods

The ultrastructural information shows rust fungal haustoria to be complex specialized structures. However, little is known of the chemical composition of component parts of the haustorial apparatus, or how haustoria relate to their host protoplasts on a chemical basis. This type of information is lacking mainly because it is not yet possible to isolate rust fungal haustoria from their host cells, thus traditional

methods of chemical analysis are not suitable to analyze these haustoria.

The advent of ultrastructural cytochemistry has allowed precise intracellular location of a number of substances. Through various means, groups of polysaccharides, proteins, and lipids may be identified and located. Use of these methods hold considerable promise to increase our understanding of the nature of rust fungus-host interactions. A number of cytochemical methods were employed in this study, and the following review is restricted to those methods used.

A. Periodic Acid-Thiocarbohydrazide-Silver Proteinate Method (Thiery, 1967)

In this method the staining procedure involves initial oxidation of vicinal hydroxyl groups present in polysaccharides to yield aldehyde groups, coupling of the latter with thiocarbohydrazide (TCH) and subsequent reaction of the thiol group of TCH with silver proteinate. According to Thiéry (1969) the degree to which polysaccharides are complexed to other substances like proteins is directly related to the time necessary in TCH to achieve maximal staining. Pure polysaccharides such as starch or glycogen stain maximally after 1 hour or less in TCH, while mucopolysaccharides require 24 hours, and glycoproteins may need a longer incubation period in TCH.

Controls for the selectivity of the oxidation are performed by substituting hydrogen peroxide as the oxidizing agent (Hall, 1978). This treatment removes osmium but does not specifically oxidize glycols. Polysaccharides containing glycols therefore will not react but other reactive compounds (eg. argentophilic structures) are stained. Additional controls include using aldehyde blocking reagents (eg. sodium

borohydride, dimedone) to block aldehydes produced by periodic acid oxidation of polysaccharides in thin sections (Craig, 1974), and omitting periodic acid or thiocarbohydrazide or both from the Thiéry staining procedures (Courtoy and Simar, 1974) to demonstrate the presence of any endogenous reducing groups.

The Thiéry staining procedure has been used to demonstrate the presence of polysaccharides in a variety of organisms, eg. glycogen in rhizobial bacteroids (Craig, 1974) and fungal tissue (Harder, 1978), polysaccharides in fungal walls (Harder, 1978; Scannerini and Bonfante-Fasolo, 1979; van der Valk et al, 1977), and starch and polysaccharides in cell walls of both higher and lower plants (Courtoy and Simar, 1974; Hanchey, 1980; Hickey and Coffey, 1978). However, not all polysaccharides containing vicinal hydroxyl groups are stained with the Thiéry procedure. When vicinal hydroxyl groups are not available due to numerous lateral branches or substitution, the reaction is weak or does not occur at all (Hall, 1978). On the other hand, polysaccharides such as callose, a β-1,3-glucan (Kessler, 1958; Eschrich, 1961) and chitin, a polymer of N-acetylglucosamine, are unstained (Heath and Heath, 1971; van der Valk et al, 1977) because they do not contain vicinal hydroxyl groups. Certain groups of fatty acids and polypeptides may also react to periodic acid oxidation, thus may also react positively with the Thiéry staining procedures (Hall, 1978).

B. Phosphotungstic Acid Staining at Low pH

The mechanism and specificity of phosphotungstic acid (PTA) staining at low pH have been reviewed recently (Hayat, 1975; Hall, 1978). It is an anionic stain, and the effectiveness of staining is strictly

pH-dependent and decreases rapidly above pH 3. However, controversy exists on the type of interaction and affinity of PTA for organic substrates. In some studies, it has been indicated that PTA has a specific affinity for highly polymerized polysaccharides when used in strongly acidic solutions of pH 1.4 to 2.0 (Pease, 1968). At this pH the stain may complex with glycogen, glycoproteins, mucus and mucoid layers, and chondroitin sulphate. By lowering the pH further to 0.3 by acidifying with chromic acid, an increase in contrast and specificity of the cell surface containing sialic acid has been demonstrated (Rambourg, 1967; Rambourg et al, 1969). Tsuchiya and Ogawa (1973) have used PTA in chromic acid for selective staining of glycoproteins.

On the other hand, there are studies which do not hold the view that PTA has a special affinity for polysaccharides (see Hayat, 1975). For example, Silverman and Glick (1969) indicated that PTA selectivity stains tissue protein while no apparent reactivity with acid polysaccharides was observed. This is supported by the fact that under test tube conditions, peptide bonds and amide groups in proteins do react with PTA (Scott and Glick, 1971).

For plant cells, PTA used at low pH (acidified with chromic acid) has been found to be a specific stain for the plasma membrane (Roland, 1973); the ribosomes and plant cell wall are also stained to some extent, but other cytomembranes are not contrasted at all. The chemistry of the reactions is not understood (Hall, 1978). Van der Woude (1973) suggested that phosphotungstic acid-chromic acid reacts with glycolipids involved in the synthesis of cell wall polysaccharides, while Bowers and Korn (1974) have implicated the synthesis of cell wall phosphonoglycans as responsible for staining the plasmalemma of

Acanthamoeba. As indicated by Hall (1979), the staining is usually reproducible and constant enough to be used to study problems such as the modification and differentiation of plasma membrane within the cell. Littlefield and Bracker (1972) were the first workers to use this staining method to study the host-parasite interface in the flax rust system.

C. De Bruijn Potassium Ferricyanide Method

De Bruijn (1973) showed that the application of osmium tetroxide in combination with potassium ferricyanide to the aldehyde-fixed tissue specimens results in selective staining of glycogen particles in ultrathin sections. Sections do not need post-staining to show this staining. The membranes and lipids are also stained, but ribosomes remain unstained. The exact reaction mechanism responsible for this selective staining is not known (Hayat, 1975).

D. Extraction and Subtractive Localization

To improve the specificity of staining reactions, selective chemical or enzymatic extractions of subcellular components can be performed. Sites where the extracted compounds were present will then appear "negative" in comparison with the unextracted controls. Such subtractive localizations will increase the chance of identification in situ. Structures with known chemical composition may act as internal controls to determine the specificity of the extraction. Selective extraction(s) can be used in combination with cytochemical test(s). For example, some information on the composition of the component parts of the host-parasite interface in Pisum sativum infected by Peronospora pisi has been provided by a cytochemical study involving enzymic digestions, chemical extractions; and specific staining methods (Hickey and Coffey,

1978).

E. Lectin-Colloidal Gold Markers

Chitin microfibrils are poorly visible by electron microscopy when prepared by glutaraldehyde/osmium fixation and uranyl acetate/lead citrate staining (Pearlmutter and Lembi, 1978). When converted to chitosan by hydrolysis in potassium hydroxide and then bound to osmium tetroxide during fixation, the deacetylated polymer becomes electron-dense (Pearlmutter and Lembi, 1978). In this way chitin can be identified in thin sections. However, the conditions required to hydrolyze chitin to chitosan are drastic (slow hydrolysis of 2 - 6 days at 65° C in 60% KOH or autoclaved at 15 psi for 1.5 - 3 hours in a saturated aqueous solution). Consequently, extensive extraction and distortions can occur throughout the whole specimen, resulting in a great loss in ultrastructural details. Other methods are, therefore, needed for localization of chitin *in situ* in haustorial structures.

Faulk and Taylor (1971) have described an immunocolloid method for electron microscopy to study surface antigen on *Salmonella* using an antiserum labelled with colloidal gold. Horisberger and Rosset (1976) modified the colloidal gold technique. Utilizing the fact that wheat germ lectin binds specifically to chitin or its oligomers (Goldstein et al, 1975), they attempted to use wheat germ lectin labelled with colloidal gold to study budding yeast cells with scanning electron microscopy. They located wheat germ lectin receptor sites on the surface of the yeast cells after the cells had been treated with α-mannanase. This wheat germ lectin marking was totally inhibited by pentaacetyl chitopentaose. The receptor sites were attributed to the pre-

sence of chitin. In subsequent studies, Horisberger and colleagues extended the colloidal gold technique to the marking of thin sections of yeasts (Horisberger and Rosset, 1977; Horisberger and Vonlanthan, 1977). In yeast cells chitin or its oligomers were located in the bud scars and cell wall and in the cytoplasm near the plasmalemma (Horisberger and Vonlanthan, 1977). This distribution of chitin has been confirmed in a recent, more elegant study of the same organism using three complementary methods: electron microscopy of colloidal gold particles but labelled either with wheat germ lectin or a chitinase, fluorescence microscopy with fluorescein isothiocyanate derivatives of the same markers, and enzymatic treatments of (^{14}C) glucosamine labelled cells (Molano et al, 1980). This demonstrates that the lectin-colloidal gold method of Horisberger and Rosset (1977) for the detection of chitin, or its oligomers, is quite reliable. The method is simple as binding can be performed directly on sections of any glutaraldehyde fixed, non-osmicated specimens.

The lectin Concanavalin A (Con A) has been employed in various methods for studying carbohydrate composition of cell surfaces and these methods have been reviewed (see Hayat, 1975). Like wheat germ lectin, Con A can be labelled with colloidal gold and used as a marker. In thin sections of budding yeast cells, mannan (a polysaccharide) was located with gold-labelled Con A in the cell walls, on the plasmalemma and within the cytoplasm sometimes associated with vesicles and vacuoles (Horisberger and Vonlanthan, 1977). The significance of these observations is that mannan is synthesized within the cytoplasm and then transported to the cell wall.

Unlike wheat germ lectin, Con A can form a precipitate with

numerous polysaccharides that contain multiple terminal non-reducing α-D-glucopyranosyl, α-D-mannopyranosyl, β-D-fructofuranosyl, or α-D-arabinofuranosyl residues (Sharon and Lis, 1972). These include glucans such as glycogen, amylopectin and dextrans; yeast mannans and phosphomannans; D-fructans and arabinogalactan. Glycoproteins containing some of the above residues can also combine with Con A. As Con A has affinities for different substrates, the gold-labelled Con A method of Horisberger and Vonlanthan (1977) will have considerable potential for cytochemical studies of other organisms.

MATERIALS AND METHODS

I. Urediospore-Derived Infections

A.. Plant Material and Inoculation with P. coronata avenae

Seedlings of Avena sativa L. cv Pendek (compatible with known races of rust) were grown in growth cabinets at 19° C, a photoperiod of 18 hours/day, and light intensity averaging 20,000 lx at the pot surface. Four days after emergence, seedlings were placed in a spore settling tower and inoculated with urediospores of P. coronata avenae race 326 on the adaxial leaf surface, placed in a dew chamber, and incubated overnight for 12 hours in the dark. After incubation, plants were covered with Sisal glaze vinyl hoods and placed in a growth cabinet and grown under the conditions above. The hoods were removed after 12 hours in the growth cabinet.

B. Plant Material and Inoculation with P. graminis tritici

Seedlings of Triticum aestivum L. cv Chinese Spring were grown in growth cabinets at 19° C under cool-white fluorescent light, averaging 20,000 lx at the pot surface for 16 hours/day. Three to 4 days after emergence seedlings were placed in a spore settling tower and inoculated with urediospores of P. graminis tritici race C17 (56) on the adaxial surface, placed in a dew chamber, and incubated overnight for 12 hours in the dark. After incubation plants were covered with Sisal glaze vinyl hoods and placed in a growth cabinet under the conditions above. The hoods were removed at the end of the first light period.

C. Conventional Fixing and Staining for Electron Microscopy

Developing pustules of crown rust or stem rust were sampled at various times beginning 5 days after inoculation. Infected tissue was fixed in 3% glutaraldehyde for 3 hours at room temperature under partial vacuum in 0.025 M phosphate buffer, pH 6.8, then either post-fixed for 2 hours at 4° C in 2% osmium tetroxide (OsO_4) in the same phosphate buffer or processed further without OsO_4 fixation. After fixation, both osmicated and unosmicated glutaraldehyde fixed tissue was dehydrated in a graded ethanol series. Some of the tissue was then embedded in Spurr resin mixture (Spurr, 1969). Other tissue was followed by successive changes through a graded propylene oxide series and finally embedded in a plastic resin mixture of Epon 812, Araldite 6005, and dodecenylsuccinic anhydride (DDSA) using DMP 30 as an accelerator. Ultrathin sections were cut with a diamond knife on a Reichert OM-U2 ultramicrotome. Sections were usually taken near the edge and the centre of the developing rust colonies, and some colonies were sectioned right through. Sections were mounted on formvar and carbon coated 100 mesh or single-hole (for serial sections) copper grids and stained with 5% uranyl acetate in 50% ethanol aqueous solution and lead citrate. These "conventional" stains will be referred to as Ua/Pb in the text. Magnification was calibrated with a grating replica grid bearing 58,000 lines per square inch. Unless otherwise stated, all electron microscope examinations were carried out with an Hitachi HU-12 transmission electron microscope at an accelerating voltage of 50 kV. Electron images were taken on Kodak electron image 3¼ x 4 inch sheet film.

During this study the haustorial neck walls of *P. coronata avenae* were usually intensely stained after post-staining with uranyl acetate

and lead citrate. Thus details of the neck ring structure tended to be obscured. To make the neck ring more visible, some of the ultrathin sections were treated with 20% hydrogen peroxide for 20 minutes before post-staining with uranyl acetate and lead citrate.

D. Histochemical Methods

1. Periodic Acid - Chromic Acid - Phosphotungstic Acid (PACP) (Roland et al, 1972)

Ultrathin sections of glutaraldehyde/OsO_4 fixed tissue were floated on aqueous 1% periodic acid for 30 minutes in a high humidity chamber (Nagahashi et al, 1978), rinsed in five changes of distilled water for 5 minutes each, and treated with an aqueous solution containing 1% phosphotungstic acid and 10% chromic acid. The sections were then washed in five changes of distilled water for 5 minutes each and mounted on grids. For control treatments, the chromic acid, phosphotungstic acid, and subsequent washes were omitted from the procedure. It was found necessary to conduct the periodic acid treatment in a saturated aqueous atmosphere to obtain consistent oxidation by periodic acid.

2. Periodic Acid - Thiocarbohydrazide - Silver Proteinate (PA-TCH-SP) (Thiéry, 1967)

This test is generally specific for polysaccharides which contain vicinal hydroxyl groups. Unless otherwise stated, structures reacting positively to this test will be referred to as containing polysaccharide. Ultrathin sections of glutaraldehyde/OsO_4 fixed tissue or glutaraldehyde fixed, unosmicated tissue were floated on 1% periodic acid for 30 minutes in a high humidity chamber (Nagahashi et al, 1978), washed in five changes of distilled water for 5 minutes each, and were floated on 0.2% thiocarbohydrazide (TCH) in 20% acetic acid for 0.2, 1, 24, or 72 hours. After

washing successively in 10, 5, and 1% acetic acid for a 30 minute period and in three changes of distilled water for 10 minutes each, the sections were floated in aqueous 1% silver-proteinate for 30 minutes in the dark. For controls, either periodic acid, TCH, or silver proteinate was omitted (Courtoy and Simar, 1974). Two additional controls were also used. In one control, ultrathin sections were treated with sodium borohydride to block free aldehyde groups created by periodic acid oxidation (Craig, 1974). Oxidized sections were placed in 0.1% sodium borohydride for 45 minutes prior to TCH-silver proteinate treatment. With the other control, ultrathin sections were oxidized in 10% hydrogen peroxide for 30 minutes (Hall, 1978) instead of 1% periodic acid prior to TCH-silver proteinate treatment.

3. The $K_3Fe(CN)_6$ Fixation Method (de Bruijn, 1973)

Infected tissue was fixed for 16 hours at 4° C in 3% glutaraldehyde in 0.1 M cacodylate buffer, pH 6.9 containing 0.05 M anhydrous $CaCl_2$. The tissue pieces were then thoroughly washed in several changes of buffer, and post-fixed for 16 hours at 4° C in a combination of 1% OsO_4 and 0.05 M $K_3Fe(CN)_6$ in the same cacodylate buffer. The tissue was dehydrated and embedded as before, and examined directly or stained as before with uranyl acetate and lead citrate.

4. Lectin-Gold Markers (Horisberger and Rosset, 1977)

Gold granules with an average diameter of 5 nm were prepared and coated with Concanavalin A (Con A) or wheat germ lectin according to Horisberger and Rosset (1977) by Dr. R. Rohringer (Research Station, Agriculture Canada, Winnipeg). Infected tissue was fixed with 3% glutaraldehyde as above and embedded either in Spurr embedding medium or Epon-

Araldite. Ultrathin sections were floated for 2 hours on solutions containing gold-bound lectin, washed overnight with the appropriate buffer (Horisberger and Rosset), deposited on copper grids, and post-stained 20 minutes with 1% uranyl acetate aqueous solution. Control treatments were performed by floating the ultrathin sections on solutions containing gold-bound Con A or gold-bound wheat germ lectin in the presence of methyl α-D-methyl-mannopyranoside or chitin hydrolysate respectively.

5. Solvent Extractions

After fixation in 3% glutaraldehyde at room temperature as before, infected tissue was subjected at room temperature to one or the other of the following organic solvent extractions according to Hickey and Coffey (1978).

a. Ether/ethanol (2:1) for 3 hours.

b. A graded series of acetone concentrations over a period of 20 minutes followed by 20 minutes in 100% acetone.

c. Chloroform/methanol (3:1) for 2 hours followed by 1 hour in chloroform.

After solvent extraction tissue was post-fixed in 0.025 M phosphate buffered 2% OsO_4 for 2 hours at 4° C, and finally embedded in Epon-Araldite. Ultrathin sections of specimens treated with organic solvents were post-stained with uranyl acetate and lead citrate as above.

6. Enzyme Treatments

Following fixation for 3 hours at room temperature in 3% glutaraldehyde as before, infected tissue was incubated at room temperature in one or the other of the following enzyme preparations according to Hickey and Coffey (1978).

a. Protease (Sigma, type V, purified), 1 to 5 mg/ml in 0.05 M Tris-Hcl buffer, pH 7.5.

b. Cellulase (Sigma, type 1, practical grade), 5 mg/ml in 0.05 M phosphate buffer, pH 5.5.

After enzyme treatment tissue was post-fixed in 0.025 M phosphate buffered 2% OsO_4 for 2 hours at 4° C, and finally embedded in Epon-Araldite. Ultrathin sections of specimens treated with enzymes were post-stained with uranyl acetate and lead citrate as above.

E. Energy Dispersive X-Ray Analysis

Glutaraldehyde fixed, unosmicated infected leaf tissue, processed as described earlier, was used for X-ray analysis. Sections with a thickness giving a blue interference colour were mounted on formvar and carbon coated grids. Energy dispersive X-ray analyses on unstained sections were carried out using a Philips EM-400 transmission electron microscope to which was connected a computerized energy dispersive X-ray analysis system (Edax-Edit). In general, the method of X-ray analysis was as follows. When an area of interest (target) such as a neck ring or any electron-dense area was located, the electron beam was reduced to a spot size of about 0.2 μm and aligned to focus on the target. Counts of X-ray pulses were then collected for a period of 100 seconds live time. The spectrum thus obtained was displayed on a cathode-ray screen and photographed. To obtain control data, spectra were similarly obtained from the background, ie. from an area in the host cytoplasm adjacent to the neck ring, the fungal cytoplasm inside the haustorial neck and from the adjacent portion of the haustorial neck wall. All X-ray analyses were carried out at an accelerating voltage at 60 kV. The energy values of the spectral peaks were also

obtained by computer print-out and the atomic ratios of the elements present was computed in each final spectrum.

II. Basidiospore-Derived Infections

Buckthorn (Rhamnus cathartica L.) leaves naturally infected in late spring with basidiospores from overwintering telia of P. coronata avenae were collected and processed for electron microscopy as described previously (Harder, 1978). Infected leaf pieces were fixed with glutaraldehyde and post-fixed with OsO_4, and finally embedded in Spurr resin mixture (Spurr, 1969).

Ultrathin sections of infected tissue were generally stained with uranyl acetate and lead citrate. Other sections were treated with the PACP or PA-TCH-SP staining methods as described above.

RESULTS AND DISCUSSION

I. Urediospore-Derived Infections of P. coronata avenae and P. graminis tritici

A. Haustorial Mother Cells

Prior to haustorium formation a terminal cell of an intercellular hypha becomes differentiated to form the haustorial mother cell. The first stage in haustorial mother cell differentiation is the formation of a septum near the tip of an infection hypha (Littlefield and Heath, 1979). Heath and Heath (1975) pointed out that it was impossible from ultrastructural studies to predict that any particular hyphal tip was an incipient haustorial mother cell. The haustorial mother cell in rusts (Littlefield and Heath, 1979) at the early stage after its formation is full of cytoplasm and is non-vacuolated. The present study showed that young haustorial mother cells contained small vacuoles (Figs. 1 - 4) and frequently, electron-dense deposits were found in these vacuoles (see section F later for details). Although the cytoplasmic contents were similar to those of the other intercellular hyphal cells in terms of nuclei, mitochondria, endoplasmic reticulum, glycogen particles and lipid droplets, the present study also showed that the haustorial mother cells could be readily differentiated from the other hyphal cells after their formation.

A characteristic pattern of distribution of mitochondria was evident in the haustorial mother cell protoplasts in both P. coronata avenae and P. graminis tritici. All mitochondria in the haustorial mother cells

were located around the periphery of the cell adjacent to the plasmalemma (Figs. 1 - 4). They were never found at or near the center of the cell lumen. Figures 1 - 4 are of four closely adjacent sections taken from a series of serial sections of the same young haustorial mother cell. In this case breaching of the host wall had occurred but the haustorium had not yet formed (Fig. 1). In cross-sections of another young haustorial mother cell, a similar pattern of distribution was observed and the mitochondria appeared as a ring around the inner periphery of the cell (Fig. 5). In hyphal cells the mitochondria were scattered, frequently in small groups, at random locations in the protoplast (Fig. 6). During early haustorium formation the characteristic distribution of mitochondria in the haustorial mother cell protoplast was altered and they accumulated at the penetration site (Fig. 7) as they began their migration into the young haustorium.

In both P. coronata avenae and P. graminis tritici, haustorial mother cells could be distinguished from other hyphal cells by differences in wall structure as revealed by different staining methods. Also the haustorial mother cell septum differed from the septa found elsewhere in the mycelium. With uranyl acetate and lead citrate (Ua/Pb) staining, four layers were visible in the haustorial mother cell septum (Figs. 8 and 9). Of these four layers two were electron-opaque. These were separated by a third more lightly stained layer. The fourth layer had a similar staining intensity as the third layer and was found adjacent to the fungal plasmalemma on the haustorial mother cell side of the septum. The third layer ended at the periclinal wall of the fungus while the two electron-opaque layers were continuous with it (Fig. 9). The fourth layer that was located adjacent to the haustorial mother cell plasmalemma was continuous around the rest of the haustorial mother cell (Figs. 8 and 9). In all septa

elsewhere in the fungal hyphae only three layers were observed: two electron-opaque layers separated by a narrow electron-translucent central lamella that ended at the periclinal wall (Fig. 10). The two electron-opaque layers were continuous with the periclinal wall. In both P. coronata avenae and P. graminis tritici the walls of the haustorial mother cells and hyphal cells differed structurally. In P. coronata avenae the haustorial mother cell wall was thicker and it contained more layers than the hyphal wall (Figs. 8 and 11). In P. graminis tritici the haustorial mother cell wall contained only two main layers, whereas only a single layer was seen in the hyphal walls (Fig. 12).

Using the Thiéry PA-TCH-SP staining method to locate areas rich in polysaccharides, the septa and walls of haustorial mother cells of P. coronata avenae and P. graminis tritici were similar in appearance. Two electron-opaque layers separated by a middle electron-translucent layer were seen in hyphal septa (Figs. 13 and 14), whereas in the haustorial mother cell septa more layers could be resolved (Figs. 15 and 16). The haustorial mother cell walls of both fungi were composed of three layers: two electron-opaque layers separated by a middle moderately stained layer (Figs. 17 and 18). The innermost electron-opaque layer of the haustorial mother cell wall was continuous around the septum (Figs. 15 and 16). In contrast the hyphal walls were made up of a single layer (Figs. 13 and 14).

In both P. coronata avenae and P. graminis tritici the earliest stage at which an apparent haustorial mother cell could be recognized was after the formation of the haustorial mother cell septum. After septum formation and during early stages of haustorium formation, elaborations of membranes (referred to as membrane protrusions) characteristically developed on the hyphal side of the haustorial mother cell septum (see Figs. 1 - 4).

Observation of these protrusions was an accurate indicator of a haustorial mother cell. No such structures were ever found in association with other hyphal septa (Figs. 9 and 10). These membrane protrusions will be described in greater detail in section C.

B. General Haustorium Development

The precise age of individual haustoria is not easily determined, and the criteria used to estimate the relative stage of haustorial development in this study were similar to those outlined for P. graminis tritici (Harder et al, 1978). Where possible the haustorial mother cells were located and the protoplasmic contents of the haustorial mother cells and haustoria were determined. The size and shape of haustoria in serial sections were used as further indicators. The present study showed that characteristic changes occurred at the haustorial mother cell septum during haustorium development and the structural appearance of the haustorial mother cell septum at any one time was characteristic of the level of haustorium development (see section C) and this could be used as an additional indicator. Haustoria were considered mature when the nuclei along with most of the cytoplasm from the haustorial mother cells had migrated into the haustoria.

The first event in haustorium formation was the development, from the young haustorial mother cell, of a penetration peg which breached the host cell wall. Penetration of the host wall appeared to be mainly enzymatic since distortion of the host wall was never observed at the site of penetration (Figs. 19 and 21). Only one example of the earliest stage of penetration peg formation in P. coronata avenae was found (Figs. 19 and 20). Figures 19 and 20 are micrographs of two closely adjacent sections from a

series of serial sections, thus they represent true sections of the median point of penetration peg formation. These sections had been stained with the Thiéry PA-TCH-SP method. The haustorial mother cell wall was thickened around the site of host penetration and two layers were evident in the thickened portion of the haustorial mother cell wall: a thin densely stained, outer layer and a thick lightly stained, inner layer (Fig. 19). The penetration peg developed as a localized evagination of the haustorial mother cell plasmalemma, which was very lightly stained (Fig. 20). This occurred in the center of the thickened region of the haustorial mother cell wall. A thin, lighter stained layer was seen in the penetration region adpressing the evaginated portion of the haustorial mother cell plasmalemma and this layer appeared to be continuous with the thick inner layer of the haustorial mother cell wall (Fig. 19). It was not clear however, if the thin lighter stained layer adpressing the evaginated fungal plasmalemma was actually fungal wall material or whether it was a lighter staining region of the host wall resulting from enzymatic digestion during the breaching process.

Using conventional stains (Ua/Pb) on sections of P. coronata avenae, Harder (1978) showed that there was swelling of the haustorial mother cell wall around the penetration site. In the present study it was further shown that the swelling in this region apparently resulted from the addition of an electron-dense layer (Fig. 11), but there was no continuity between the newly deposited wall material and the other existing wall layers of the haustorial mother cell. However, variations in staining density and the number of layers in this region were observed. For example, the thickened region of the haustorial mother cell wall shown in Figure 21 was mainly electron-opaque, and that in Figure 22 was mainly electron-

translucent. After haustorium formation there was no clear continuity between any of the wall layers of the haustorial mother cell and the haustorial neck (Fig. 21), although in some cases, it appeared that there was a thin fungal wall layer through the penetration region (Fig. 22).

In P. graminis tritici the haustorial mother cell wall usually contained three layers at the thickened region around the penetration site as seen with Ua/Pb staining (Fig. 23). The thickening of the haustorial mother cell wall in this region apparently resulted from the addition of a thick electron-opaque, convex lens-shaped middle layer between the two existing wall layers of the haustorial mother cell wall (Fig. 23). While fungal wall material was reported to be absent in the penetration region in earlier work on the same fungus (Ehrlich and Ehrlich, 1971), the present study showed that fungal wall material occurred through the penetration region, and there appeared to be continuity between the middle wall layer of the haustorial mother cell wall and the haustorial neck wall (Fig. 23). Similar continuity between the convex lens-shaped middle layer and the haustorial neck wall could be demonstrated in sections treated with the PACP procedure (Fig. 24). However, the fungal wall material was more lightly stained and more diffuse through the penetration region.

In P. coronata avenae the cytoplasm of the haustorial mother cell at the penetration region was characterized by the presence of small electron-dense granules, microtubules and membranous materials (Figs. 25 and 26). Some of these electron-dense granules were membrane-bound (Fig. 27). After host wall penetration the fungus formed a tubular finger-like projection extending into the host cell (Figs. 28 and 29). This projection later became the neck of the haustorium. Electron-dense granules or amorphous materials were found in the cytoplasm of the young haustorial neck, but

mitochondria and nuclei were absent at this stage. In P. graminis tritici a single example of a similar young haustorial neck with no sign of a haustorial body at the distal end of the neck was found (Fig. 30). Characteristic of this stage was the presence of electron-dense granules in the cytoplasm of the young haustorial neck and in the haustorial mother cell near the penetration region (Fig. 30).

The cytoplasm in young haustorial necks was continuous with that in the haustorial mother cells. Mitochondrial migration from the haustorial mother cell apparently coincided with the initial expansion of the haustorial body at the distal end of the neck. The protoplasts of young haustorial bodies (about 2 μm in diameter) of P. coronata avenae (Fig. 31) were typically packed with mitochondria. At this stage the haustorial neck of P. coronata avenae did not possess a neck ring. Using conventional Ua/Pb staining the entire neck wall could be resolved into three distinct layers: two moderately-stained layers separated by a middle electron-opaque layer (Fig. 32). At the junction of the haustorial neck and body, these three layers appeared to merge to give rise to a single electron-opaque wall layer which continued around the newly formed haustorial body (Fig. 33). The invaginated host plasmalemma adhered tightly to the entire length of the neck wall (Fig. 32) and became separated from the fungal wall near the base of the haustorial body (Fig. 33). The invaginated host plasmalemma continued around the haustorial body; a less well defined region, the extrahaustorial matrix, occurred between the membrane and the haustorial body wall (Fig. 34). The profile of the invaginated host plasmalemma was irregular in sections due to its undulating nature. Diffuse electron-opaque material was present in the extrahaustorial matrix of young haustoria and this matrix material was quite distinct from the more discrete

body wall (Fig. 34). In contrast to the three neck wall layers in P. coronata avenae, the haustorial neck walls of P. graminis tritici were composed of one main layer (Harder et al, 1978) and this layer continued around the young haustorial body. The haustorial body wall contained no pores or channels and no direct connections were seen between the protoplasts of the host and fungus as was reported in earlier work on the same fungus (Ehrlich and Ehrlich, 1971).

In P. coronata avenae the neck ring was first observed as an electron-dense region after Ua/Pb staining in the neck wall when the haustorial body was about 5 μm in diameter and when the nuclei were still within the haustorial mother cells. The neck ring was located about one-third of the way down the neck from the haustorial body (Fig. 35). In haustoria in an intermediate stage of development, the neck ring measured about 0.15 μm in width (Fig. 35) and in mature haustoria it reached a width of about 0.38 μm in P. coronata avenae (Fig. 36). In P. graminis tritici the haustorial neck also did not possess a neck ring structure up to the stage when the haustorial body was about 2.8 μm in diameter (Harder et al, 1978). After the neck ring was formed it was seen as an electron-dense region after Ua/Pb staining in the neck wall and was located about mid-way down the neck from the haustorial body (Fig. 37).

As the haustoria matured two layers became evident in the haustorial body wall of P. coronata avenae. The outer body wall layer was strongly stained whereas the inner layer was lightly stained (Fig. 38). In glutaraldehyde/OsO_4 fixed tissue and after staining with Ua/Pb, diffuse electron-opaque and lightly stained fibrillar materials were often observed in the extrahaustorial matrix of the mature haustoria of P. coronata avenae (Fig. 39). The development of the extrahaustorial matrix was accompanied by

massive proliferation of large tubular complexes (Fig. 39) located in certain areas of the host cytoplasm (see section G for details). The thickness of the extrahaustorial matrix and the amount of stained material appeared to increase with haustorium age, especially at the distal end of the haustorial body (Fig. 40). The latter interpretation was based on serial sections through haustoria. In glutaraldehyde fixed, unosmicated tissue, the extrahaustorial matrix was consistently electron-lucent after Ua/Pb staining (Fig. 41). However, using the PA-TCH-SP method intense staining was observed in the extrahaustorial matrix (Figs. 42 - 44). Evidently the extrahaustorial matrix in the glutaraldehyde fixed, unosmicated tissue had a low affinity for the Ua/Pb stains. A similar interpretation was made earlier by Bracker and Littlefield (1973). Failure of a structure to stain does not necessarily mean organic material is absent, but that it may have a low affinity for the stains that were used.

Mature haustoria of P. coronata avenae or P. graminis tritici were generally elongated (Fig. 40) but occasionally they appeared to be branched (Fig. 45). Mature haustoria contained nuclei, mitochondria, endoplasmic reticulum, lipid droplets and many free ribosomes. The attached haustorial mother cell was largely vacuolate with very little cytoplasm left. No septum separating the haustorial mother cell from its haustorium was ever found. A distinctive pattern of distribution of mitochondria was evident in the haustorial protoplasts. Mitochondria were consistently found around the periphery of the cell adjacent to the plasmalemma (Fig. 40). This was confirmed by examining serial sections of mature haustoria. This particular pattern of distribution in the haustorial protoplasts was also evident in cross-sections (Fig. 46). Occasionally mitochondria appeared to be dispersed randomly in some haustoria, but this was probably due to a portion

of the haustoria being sectioned obliquely (eg. see Fig. 45). The haustorial body walls could also be used as a marker for the plane of sectioning because the walls appear thicker and more diffuse in oblique sections. This pattern of mitochondrion distribution was similar to that observed in the haustorial mother cell protoplast prior to haustorium formation (see Fig. 1). The above pattern of mitochondrion distribution has not been previously reported in haustoria of other rust fungi and the significance of this observation is not known. However, mitochondria are a rich source of energy which can be used to facilitate transport of substances across membranes. If it is accepted that haustoria have a role as absorbing organs and that it is through the extrahaustorial matrix and fungal plasmalemma that materials are taken, the location of mitochondria in the haustorium in close proximity to the fungal plasmalemma and extra-haustorial matrix may be advantageous to the fungus in effecting a more rapid transport.

Aberrant, necrotic-appearing haustoria were occasionally found at or near the colony centers of P. coronata avenae. Necrosis occurred in these haustoria regardless of the stage of their development. Figure 47 shows one of these aberrant haustoria that became necrotic during its early stage of development, but the haustorium mother cell still appeared healthy. Examples of mature haustoria that became necrotic are shown in Figures 48 and 49. These haustoria were usually irregular in shape. Some of these haustoria were found in previously infected host cells which were largely devoid of the normal host cytoplasmic components (Fig. 50). Other aberrant haustoria occurred in host cells with normal appearing cytoplasm (Fig. 49). In other instances, both aberrant and more normal looking haustoria were found within the same host cell (Fig. 50). Collars or encasements were not usually associated with these aberrant haustoria (Figs. 47 and 48). All

of these aberrant haustoria were found at or near the center of the infection colonies as determined by serially sectioning through three 6-day old colonies. The fact that many haustoria regardless of age became necrotic, suggests that the physiology of the host cells at the center of the colony has changed resulting in a physiologically incompatible relationship between these haustoria and the host cells.

C. The Haustorial Mother Cell Septum

Characteristic changes at the haustorial mother cell septum were observed in P. coronata avenae and P. graminis tritici during the early stages of haustorium formation. Elaborate membrane protrusions together with a marked aggregation of mitochondria occurred on the hyphal side of the haustorial mother cell septum (Figs. 51 and 52). This large accumulation of mitochondria near the septum was evident in Figure 53, a micrograph of a closely adjacent section to that shown in Figure 54. In glutaraldehyde/OsO_4 fixed tissue and after staining with Ua/Pb, the membrane protrusions contained an electron-dense matrix (referred to as the protrusion matrix). However, in similarly stained sections of glutaraldehyde fixed, unosmicated tissue, the protrusion matrix was mainly electron-lucent (Fig. 55). Serial sections showed that these membrane protrusions originated from the plasma membrane along the septum. The membrane protrusions were long, flattened cisternae closed at the end furthest from the septum. In some views the membranes of these protrusions were convoluted at the edges, and serial sections showed possible interconnections between these membranes (Figs. 56 - 58).

At the earliest stage of membrane protrusion formation that could be found, they were very small, measuring about 0.2 μm long (Fig. 59). At this stage other membrane formations in the form of small whorls appeared

in close proximity to the fungal plasma membrane on the haustorial mother cell side of the septum (Figs. 59 and 60). Similar to the membranes of the membrane protrusions (Fig. 56), membranes of these whorls showed a trilamellar structure (Fig. 59) typical of fungal plasma membrane. These also stained in a manner characteristic of fungal plasma membrane after treatment with the PACP procedure (Fig. 60). The duration of these small whorls apparently was very short, as apart from the four examples observed in the present study, they were not found in other situations when haustorial mother cells were involved in breaching of the host wall. Similar whorls of membranes have also been reported in U. phaseoli vignae (Heath and Heath, 1975). They too disappeared prior to the formation of the penetration peg.

In P. coronata avenae the membrane protrusions extended to a length of 4.2 μm during the period of host wall penetration. After host wall penetration many stages of subsequent haustorium development were easily recognizable and correlation was observed between haustorium development and the temporal changes associated with this septum. The septal membrane protrusions decreased in length during the subsequent formation of the haustorial neck. By the time the haustorial neck was about 4 μm in length, the mitochondria associated with the membrane protrusions had dispersed and the protrusions had shrunk to less than 0.4 μm in length (Fig. 61). The "angular" appearance of the membrane protrusions at this stage suggested that their reduction in size was caused by a rapid loss of their contents. This decrease in size continued as the haustorial body formed at the distal end of the haustorial neck and the membrane protrusions now appeared as small angular projections along the haustorial mother cell septum (Fig. 62). When sectioned favourably in a plane to reveal the cross-section of the

hyphal region adjacent to the haustorial mother cell septum, these protrusions were seen to be interconnected to form ridges (Figs. 63 and 64). The membrane protrusions persisted and remained as tiny flattened papillae on the haustorial mother cell septum (Fig. 65) as the haustoria matured.

In haustorial mother cell septa with long membrane protrusions, the central pore was always completely blocked by a pulley-wheel shaped plug of electron-dense material (Figs. 66 and 67). In only one example did the pore appear open (Fig. 68). This septum apparently was still in the formative stage but membrane protrusions were already present. The septal pore remained plugged throughout the subsequent stages of haustorium development until the membrane protrusions had shrunk to the size of small papillae (Fig. 69). The hyphal septum penultimate to the haustorial mother cell septum was similarly plugged with an electron-dense material during this time (Fig. 70). The haustorial mother cell septal pore structure then underwent further changes as the haustorium developed. By the time nuclear migration had occurred the pore had become electron-translucent and it was delimited on either side by an irregularly shaped electron-opaque diaphragm (Fig. 72). The diameter of the pore of the haustorial mother cell septum was very small, about 9.5 nm (Figs. 71 - 73). In contrast, septal pores in the rest of the mycelium were usually much larger in diameter, about 23 nm to 66 nm. Some of these pores were found to contain an electron-lucent area bound by an electron-opaque diaphragm on either side of the pore (Fig. 10). Although this perforate type of septum is typical for the rust fungi (Littlefield and Heath, 1979), pores of other hyphal septa were occasionally found to be occluded with an electron-opaque material having the same pulley-wheel shape as that outlined by the diaphragms in the more typical septum (Figs. 74 and 156), as reported earlier by Harder (1976).

D. Cytochemistry of the D-Haustorial Apparatus

Using the Thiéry PA-TCH-SP technique to locate polysaccharides with vicinal glycols, sites with low affinity for the stain contained a fine deposit of discrete electron-opaque silver particles, while highly reactive sites appeared densely granular or amorphous in consistency. In P. coronata avenae infected tissue, the host walls were seen to be composed of two layers: a matrix of coarsely granular particles in the thinner inner layer and finer granular particles in the thicker outer layer (Fig. 75). Maximum staining of the host walls occurred after 24 hours in TCH. Starch granules in the chloroplasts were highly reactive and were densely granular in structure. Thylakoid membranes showed a lower affinity for the Thiéry stain and the plastoglobuli structures known to contain lipids were unstained (Fig. 75). Maximum staining of starch granules was attained after 30 minutes in TCH.

When sections were treated with sodium borohydride prior to TCH and silver proteinate (Craig, 1974), there was complete suppression of staining of the host walls and starch granules (Fig. 76). In a control treatment in which periodate oxidation had been omitted (the thiocarbohydrazide-silver proteinate control, TCH-SP) the host walls and starch granules were largely unstained, but the plastoglobuli, thylakoid membranes (Fig. 77) as well as all other cellular membranes of host and fungus were intensely stained. No silver deposits were observed in the host walls, starch granules, plastoglobuli, and thylakoid membranes when sections were treated with silver proteinate alone (Fig. 78). The staining of plastoglobuli and thylakoid membranes in Figure 78 was due to osmium binding by their lipid components. When periodate oxidation was replaced by hydrogen peroxide treatment prior to TCH and silver proteinate, no staining was observed in both starch

granules (Fig. 79) and the host walls. The resulting reactions of starch and the host walls in the above control treatments therefore conform to what would be expected for structures containing polysaccharides with vicinal glycols (see section IV.A Literature Review for specificity of Thiéry staining and control treatments).

The Thiéry procedure is commonly used to stain glycogen in thin sections (see Hayat, 1975). Using this method glycogen granules were located in the fungal cytoplasm of hyphal and haustorial mother cells, but not in the cytoplasm of the haustoria of P. coronata avenae. These granules reacted strongly to the PA-TCH-SP procedure after 30 minutes in TCH (Fig. 80). Staining was largely absent in glycogen granules when sodium borohydride was used prior to TCH and silver proteinate (Fig. 81) or in the control treatment in which the periodate oxidation had been omitted (TCH-SP) (Fig. 82). The presence of glycogen in P. coronata avenae was confirmed by the de Bruijn (1973) potassium ferricyanide method. With this method glycogen was seen as electron-opaque granules in the fungal cytoplasm of the hyphal (Fig. 83) and haustorial mother cells (Fig. 84) but not in the cytoplasm of haustoria, regardless of age. These results are similar to those reported earlier by Harder (1978) on the same fungus. Both fungal walls and protrusion matrix of P. coronata avenae were largely electron-lucent after the de Bruijn method (Figs. 83 and 85).

In unstained sections of glutaraldehyde/OsO_4 fixed specimens of P. coronata avenae both the protrusion matrix and the haustorial neck walls were osmiophilic (Figs. 86 and 87). After PA-TCH-SP treatment the protrusion matrix and all fungal walls were intensely stained (Figs. 88 - 90). No further intensity in staining was obtained by more than 24 hours TCH treatment. Unlike the three haustorial neck wall layers seen in Ua/Pb

stained material (Fig. 32), the PA-TCH-SP procedure revealed only two layers: a thin, densely stained inner layer and a thick, lighter stained outer layer (Fig. 89). In mature haustoria these two layers continued around the haustorial body (Fig. 90). In all controls for the PA-TCH-SP treatment, mycelial walls remained unstained (Figs. 91 - 93). The positive staining of the mycelial walls with the PA-TCH-SP procedure suggests that they contained polysaccharides. However, intense silver staining was observed in the protrusion matrix (Figs. 94 and 95) and haustorial walls (Figs. 96 and 97) in a control treatment in which periodate oxidation had been omitted (the thiocarbohydrazide-silver proteinate control, TCH-SP) from the Thiéry procedure. The protrusion matrix and haustorial walls were not argentophilic as no silver deposits were observed in these structures when sections were treated with silver proteinate alone (Fig. 98). These properties were shared with lipid droplets, plastoglobuli, thylakoid membranes, and other membrane structures that are osmiophilic and are known to contain lipids (see Fig. 99). The positive silver staining of the protrusion matrix and haustorial walls in the control treatment with TCH-SP was perhaps due to unsaturated lipids, as they are known to be osmiophilic and the reduced osmium present after fixation reacts with thiocarbohydrazide (Hayes et al, 1963; Marinozzi, 1961; Seligman et al, 1966), with subsequent binding of silver proteinate (Sannes et al, 1979).

In glutaraldehyde fixed, unosmicated specimens all fungal walls and the protrusion matrix were stained by the PA-TCH-SP procedure (Figs. 100 and 101). However, when ultrathin sections of the unosmicated specimens were subjected to the TCH-SP procedure, no silver staining was evident in the protrusion matrix (Fig. 102) and haustorial walls (Fig. 103), or in the plastoglobuli (Fig. 104). This is because the lack of osmication results

in the extraction of all lipid components from samples (see Fig. 105) during subsequent preparation steps (Hayat, 1970). This substantiates the above hypothesis that the previous staining of the protrusion matrix and haustorial walls in osmicated specimens with this procedure (TCH-SP) was due to the presence of unsaturated lipid.

To determine the possible presence of unsaturated lipids in the protrusion matrix and haustorial walls, specimens were fixed with glutaraldehyde first, treated with lipid solvents (ether/ethanol, acetone or chloroform/methanol) and then post-fixed with osmium tetroxide. If unsaturated lipid was normally present in haustorial walls and the protrusion matrix, this would be extracted by the lipid solvents prior to post-fixation with OsO_4. After the above treatments the haustorial walls (Fig. 106), protrusion matrix (Fig. 107), plastoglobuli and membrane structures (Fig. 108) were no longer osmiophilic and remained largely unstained after the TCH-SP treatment. The plastoglobuli in particular, normally seen as electron-opaque globules in Ua/Pb stained sections of unextracted tissue had become electron-lucent after the solvent treatment (Fig. 109), indicating that lipid had been extracted from these structures. While host walls appeared to be unaltered after solvent treatment, there was a reduction in staining intensity by Ua/Pb of the hyphal walls, haustorial walls (Fig. 110) and protrusion matrix (Fig. 111), indicating that there was lipid present in the latter structures but not in the host walls. However, the hyphal walls were non-osmiophilic, and as only unsaturated lipid is osmiophilic (Hayes et al, 1963; Marinozzi, 1961; Seligman et al, 1966), the lipid present in the hyphal walls was likely in the saturated form.

The fact that the hyphal walls, haustorial walls and the protrusion matrix was not completely extracted after the solvent treatments suggested

that there were other components remaining in these structures. Treatment with PA-TCH-SP showed that the material remaining in the hyphal walls, haustorial walls and protrusion matrix contained some polysaccharide. However, as compared to unextracted specimens stained by the same method (Figs. 88 and 89), the staining intensity of the protrusion matrix (Fig. 112) and haustorial walls (Fig. 113) was much reduced after solvent treatment, whereas the hyphal walls remained unchanged. The large reduction in staining in haustorial walls and protrusion matrix after solvent treatment therefore indicates that much of the PA-TCH-SP stainable material was extractable by lipid solvents. The significance of this point will be discussed later.

To determine the presence of protein in haustorial structures, P. coronata avenae infected tissue was treated with protease. Protease treatment in general caused marked erosion of both fungal and host cytoplasm while host walls appeared to be little affected by the treatment (Fig. 114). Structural integrity of the chloroplasts was markedly affected and the stroma was extensively extracted, but the plastoglobuli remained unchanged and showed no loss in staining intensity (Fig. 114). Protease digestion showed protein to be a major component making up the protrusion matrix. At 1 mg/ml concentration of protease in buffer, the protrusion matrix was completely extracted (Fig. 115). At a higher concentration (5 mg/ml), extensive disruption occurred but the membrane structures delimiting the protrusions were still visible (Fig. 116). The hyphal and haustorial mother cell walls on the other hand were more resistant to protease digestion (Fig. 117). With Ua/Pb stains these walls appeared more fibrillar and less discrete in outline than the untreated ones and their usual layered appearance was now lacking (compare Fig. 117 to Fig. 11). Staining of the mycelial walls with PA-TCH-SP after protease treatment, however, was not affected (Fig. 118).

Extensive extraction of the haustorial walls occurred after protease treatment, leaving a thin wall layer immediately adjacent to the fungal plasmalemma (Fig. 119). Although the entire haustorial neck wall was affected, it appeared that extraction was more extensive in the neck wall proximal to the neck ring than distal to it. In contrast, both bands of the neck ring remained unchanged and remained in place in their usual position along the neck, with the invaginated host plasmalemma still tightly adhered to it (Fig. 119). Along the extracted portions of the neck wall the invaginated host plasmalemma now appeared convoluted, similar to that normally seen around the haustorial body. Normally, the invaginated host plasmalemma adheres tightly to the entire neck wall (Fig. 32) (Harder, 1978; Harder et al, 1978).

With protease treatment extraction also occurred in the haustorial body wall. The extent of extraction, however, depended upon the age of the haustorium. In young haustoria almost the entire haustorial body wall was extracted (Fig. 120). In the body wall of mature haustoria extraction was less extensive (Fig. 121). It appeared that the composition of the haustorial body wall changed as the haustorium developed. This was supported by the detection of N-acetylglucosamine binding sites (suggesting the presence of chitin) in the body wall of mature haustoria but not in young haustoria (see later this section).

In protease treated tissue the remaining wall material of the haustorium reacted positively to the PA-TCH-SP treatment (Figs. 122 and 152) but remained unstained in the control treatment where periodate oxidation had been omitted (TCH-SP procedure) (Fig. 123). However, in comparing the remaining wall of a younger haustorium (Fig. 122) with a haustorial wall that had not been treated with protease (Fig. 90), it was apparent that

much of the PA-TCH-SP stainable material had been removed by the protease treatment. Furthermore, Figure 123 shows that the TCH-SP type of staining normally found in haustorial walls that had not been treated with protease (Fig. 96), was absent in the same structure after protease digestion. It was demonstrated above that the component in the haustorial wall stained by the TCH-SP procedure was an unsaturated lipid. The fact that this lipid was completely removed by the protease treatment (Fig. 123) suggests that the lipid was protein-bound.

After protease treatment all haustorial mother cells of P. coronata avenae were dislodged from the host cells and their haustoria (Figs. 119 and 123). Figure 123 shows the detachment of the haustorium from its mother cell at the site of penetration. Protein is thus likely a major component of the substance by which the haustorial mother cells adhere to the host cell walls. Removal of this adhesive material appeared to weaken the attachment site and resulted in the detachment of the haustorial mother cell from its haustorium during the subsequent preparation steps for electron microscopy.

The above extraction studies with lipid solvents and protease therefore showed that protein, lipid and PA-TCH-SP positive material were major components in the haustorial walls. However, much of the PA-TCH-SP positive material in the haustorial walls was readily extracted by either lipid solvents or protease, whereas that in the mycelial walls was not. The question now arises as to whether the extractable PA-TCH-SP positive material in the haustorial walls was a polysaccharide or some other component(s). This is because certain groups of fatty acids and polypeptides react to periodic acid oxidation and are stained with the PA-TCH-SP procedure (Hayat, 1975; Hall, 1978), although the PA-TCH-SP procedure generally stains 1,2-

glycols of polysaccharides. It is possible that the solvent extractable PA-TCH-SP positive material in the haustorial wall was a polysaccharide or it could be a lipid or protein stainable with the PA-TCH-SP procedure. Assuming that it was a protein component in the haustorial wall that was stainable with the PA-TCH-SP procedure and as almost all of the PA-TCH-SP positive material was removed by protease treatment (compare Fig. 122 to Fig. 90), this would mean that the haustorial wall contained almost pure protein. This is unlikely, because lipid was shown to be present in the haustorial walls of P. coronata avenae. Also, glucans are known to be common polysaccharide components in fungal walls (Bartnicki-Garcia, 1968; Hunsley and Burnett, 1970; Trocha and Daly, 1974; van der Valk et al, 1977; Wessels, 1969) and glucans with β-1,3 linkages have been shown to be in the haustorial walls of Peronospora pisi (Hickey and Coffey, 1978). It is most likely that polysaccharides, proteins and lipids are present in complex forms. Another method was then used to localize polysaccharides in the haustorial walls of P. coronata avenae.

The Concanavalin A-colloidal gold method of Horisberger and Vonlanthan (1977) was used as a preliminary study because Concanavalin A (Con A) will bind to various polysaccharides containing α-D-glucopyranosyl, α-D-mannopyranosyl and β-D-fructofuranosyl residues (Goldstein et al, 1969). These include starch, glycogen, mannan and other glucans or glycoproteins containing the above residues (see section IV.E Literature Review). Using this method, heavy binding with Con A was observed to glycogen granules in P. coronata avenae (Fig. 125) and to starch grains in the host (Fig. 124). There was no binding to the host walls, but binding occurred in the fungal walls and protrusion matrix (Figs. 126 - 128). This binding was largely inhibited by the presence of methyl α-D-mannopyranoside in the Con

A-gold preparations (Fig. 129). It is not known however, whether this Con A binding in the fungal structures was due to glucan and/or mannan, as Con A has an affinity for both (Goldstein et al, 1969). As mannan is known to be a major wall component of yeasts and not of other fungi (Bartnicki-Garcia, 1968; Boer, 1979), the above Con A binding was probably due to glucans. Glycoproteins containing the appropriate carbohydrate moieties could also serve as receptor sites for Con A. In any case, the binding of Con A to haustorial wall was extensive (Fig. 128) suggesting that receptor sites containing carbohydrate moieties were abundant throughout the haustorial walls. The fact that the haustorial neck wall was almost completely extracted after protease treatment (Figs. 119 and 122) is indicative that many of these carbohydrates receptor sites had been removed by the treatment. However, further investigations are needed to determine the nature of these carbohydrate receptor sites in the above fungal structures.

Cellulose, a β-1,4-glucan, is known to be a component in some fungal walls (Boer, 1979). It contains vicinal glycols and is stained by the PA-TCH-SP procedure (Hall, 1978). Treatment of glutaraldehyde fixed specimens with cellulase resulted in the removal of material from the host walls (Figs. 130 and 131). Cellulase treatment did not affect fungal walls (Figs. 132-135) or the protrusion matrix (Figs. 132 and 134) of P. coronata avenae indicating that cellulose was absent from these structures.

Chitin is also a common wall polysaccharide of many fungi (Bartnicki-Garcia, 1968) and has been shown to be present in haustorial walls of Erysiphe graminis hordei (Shiraishi et al, 1976). Chitin is not visible in Ua/Pb stained sections of glutaraldehyde/OsO_4 fixed tissue (Pearlmutter and Lembi, 1978) or in sections stained with the PA-TCH-SP method (van der Valk et al, 1977). To determine the presence of chitin in

P. coronata avenae the colloidal gold - wheat germ lectin method of Horisberger and Rosset (1977) was used. Wheat germ lectin will bind specifically to polymers containing N-acetylglucosamine residues and has been used as a chitin marker in budding yeasts. Wheat germ lectin will also bind to glycoprotein with available N-acetylglucosamine moieties.

In the present study N-acetylglucosamine-containing receptors were demonstrated in septa and walls of hyphal cells and haustorial mother cells but not in the protrusion matrix (Fig. 136), or young haustorial neck and body walls (Figs. 137 and 138). As haustoria matured, binding of wheat germ lectin occurred in the body walls of P. coronata avenae (Fig. 139), but never on neck walls regardless of age of the haustoria (Fig. 140). The binding of wheat germ lectin to the above hyphal walls and matured haustorial body walls was inhibited by the presence of chitin oligomers in the wheat germ lectin preparation (eg. see Fig. 141). The binding was therefore specific to N-acetylglucosamine-containing receptors and this would most likely indicate the presence of chitin in these fungal structures.

As described earlier in section C, diffuse electron-opaque materials were present in the extrahaustorial matrix during the early expansion phase of a young haustorium of P. coronata avenae (Fig. 34). After PA-TCH-SP treatment the extrahaustorial matrix of another haustorium at a similar stage of development was stained and was not clearly differentiated from the haustorial body wall (Fig. 142). In contrast, PA-TCH-SP stained material was located mainly in isolated patches in the extrahaustorial matrix of a young haustorium of P. graminis tritici at about the same stage of development, and the extrahaustorial matrix was clearly differentiated from the more discrete haustorial wall (Fig. 143). As the haustoria of P. coronata avenae matured, the extrahaustorial matrix became distinct

from the haustorial wall and the stained material of the matrix looked frayed (Fig. 144). The matrix material remained unstained in the control treatments where sodium borohydride was used prior to TCH and silver proteinate (Fig. 145), or where periodate oxidation had been omitted (Fig. 146). Similar patterns of staining occurred in the extrahaustorial matrix in glutaraldehyde fixed, unosmicated material, except that the extrahaustorial matrix stained more densely (Figs. 42 - 44). Cellulase treatment removed much of the Ua/Pb stainable (Fig. 147) and PA-TCH-SP (Fig. 148) stainable material from the extrahaustorial matrix, indicating that cellulose may have been present in the extrahaustorial matrix.

Solvent extraction with chloroform/methanol removed much matrix material stainable with Ua/Pb (Fig. 149) but it did not affect the amount of PA-TCH-SP stainable material in the extrahaustorial matrix (Fig. 150). Protease treatment, however, removed almost all of the extrahaustorial matrix materials that were stainable with Ua/Pb stains (Figs. 121 and 151) and the PA-TCH-SP procedure (Fig. 152). There were no wheat germ lectin receptor sites in the extrahaustorial matrix (Fig. 139), indicating that the extrahaustorial matrix was free of chitin. Con A receptor sites were common in the extrahaustorial matrix, suggesting the presence of polysaccharides or glycoproteins (Fig. 153).

Although lipid appeared to be present in the extrahaustorial matrix as indicated by the solvent extraction experiments, this material was not osmiophilic and did not react with the TCH-SP treatment (Fig. 146), indicating any lipid present was in the saturated form. Also, the fact that the extrahaustorial matrix was almost completely electron-lucent after protease treatment suggests that protein was a major component. Further, because almost all of the PA-TCH-SP stainable material was removed by pro-

tease treatment it is possible that at least some of the PA-TCH-SP stainable material is a protein because certain groups of polypeptides are stained with the PA-TCH-SP procedure. Alternatively, the polysaccharides in the extrahaustorial matrix may be present in the form of glycoprotein and were removed along with the protein component by the protease treatment.

As shown in section C, the pores of the haustorial mother cell septa during early haustorium formation (Figs. 66 and 69) and some of the hyphal septa (Fig. 74) were plugged with an electron-opaque material. This plugging material was electron-lucent after the de Bruijn fixation method (Fig. 154) and reacted negatively to the Thiéry staining method for polysaccharides (Fig. 155). It was resistant to lipid solvents (Fig. 156), suggesting that lipid was not a major component. With the perforate type of septum, PA-TCH-SP type of polysaccharide was not detected in the electron-lucent area which was bound by a lightly stained diaphragm (Fig. 157). The diaphragm was normally electron-opaque after Ua/Pb staining (Fig. 10). After chloroform/methanol treatment, while membrane structures were largely extracted, the diaphragm found on either side of the septal pore structure remained unchanged (Fig. 158). After protease treatment however, the fungal plasmalemma generally remained intact (Fig. 117) but the diaphragm was completely extracted (Fig. 159). The above observations suggest that the diaphragm associated with the septal pore was mainly proteinaceous in nature.

E. Composition of the Neck Ring of P. coronata avenae

On close examination of mature haustoria, two closely adjacent cylindrical bands could be distinguished within the neck ring structure (Fig. 36). This was a regular feature of all neck rings examined in mature

haustoria (over 50 examined). These two bands were usually located very close together or they were separated by a narrow strip of neck wall material between them (Fig. 160). For convenience, these two bands of the neck ring are designated as: (i) the alpha (α) band, which is the band nearer to the haustorial mother cell, (ii) the beta (β) band, which is the one nearer to the haustorial body. The term neck ring refers to both α and β bands combined.

When the PACP staining method was used the α band remained electron-opaque, while the β band was electron-lucent (Figs. 161 and 162), indicating that these bands differ in chemical composition. It was found that the β band was preferentially extracted with periodic acid in such a way that holes were often left on the sections at the location of the β band (Fig. 161). In unstained sections treated with periodic acid, the β band was also electron-lucent, whereas the α band was electron-dense. The β band was completely extracted after 30 minutes in 1% periodic acid, whereas the α band remained unchanged after prolonged (overnight) oxidation in 1% periodic acid or after 1 hour in 3% periodic acid (Fig. 163). These results indicate that the Thiéry (1967) PA-TCH-SP method could also be used to differentiate the α and β bands. The Thiéry method, when applied to the neck ring of a mature haustorium, differentiated the α and β bands (Fig. 164) in the same way as with the PACP method (Fig. 161). However, when the same treatment was applied to the neck ring of a young haustorium, only one densely-staining band was observed (Fig. 165). There was no sign of an adjacent electron-lucent (β) band as seen in older haustoria. Also, the entire densely-staining band seen in younger haustoria by the Thiéry method always corresponded in size to the α band seen in younger haustoria stained with Ua/Pb. It was thus concluded that the α band was formed first and was

followed by formation of the β band during haustorial development.

In using the Thiéry test, the β band was extracted by periodic acid oxidation before TCH-SP was applied, thus it was not possible to demonstrate the presence of polysaccharide with this method. On the other hand, the α band consistently remained electron-opaque in the controls where periodic acid had been omitted (TCH-SP) (Fig. 166) or where sodium borohydride was applied prior to TCH-SP treatment (Fig. 167). Therefore, proof for the presence of polysaccharide also could not be obtained (Courtoy and Simar, 1974; Craig, 1974). However, in the studies using colloidal gold-lectins (Concanavalin A or wheat germ lectin) as cytochemical markers to elucidate the chemical composition of haustorial walls, neither glucan, mannan nor chitin could be demonstrated in the neck ring (Figs. 127 and 140).

The resistance of the α band to prolonged periodic acid oxidation prompted further investigation into the nature of the neck ring. Unstained sections from glutaraldehyde fixed, unosmicated older haustoria also showed two electron-opaque bands in the neck ring structure (Fig. 168). This indicated that both bands may contain mineral substances that may be suitable for energy dispersive X-ray analysis (EDX). This method has been used to detect the presence of all elements with an atomic number of 11 or higher on the periodic table at a detection sensitivity of 10^{-17} to 10^{-18} grm (Russ, 1972) and has been used to demonstrate the various elements in different tissues (Mills and Chong, 1977; Lott and Buttrose, 1978; Lalonde et al, 1977; Heath, 1979).

Three haustoria containing well defined α and β bands in the neck ring were located and subjected to EDX analysis. These neck rings consistently showed a similar elemental composition. One such analysis, carried

out on the haustorial neck in Figure 168 is presented (Figs. 169 to 174). Analysis was made on both bands from each side of the neck ring.

In the α band silicon was detected as the major element present (Figs. 169 and 170). The peak representing copper was assumed to have originated from the copper support grid. To test whether the silicon peak was significant, the host cytoplasm adjacent to each side of the neck ring was also analyzed. This revealed a small peak of silicon (Figs. 173 and 174) as did the other background controls, ie. the haustorial neck wall (Figs. 175 and 176) and the fungal cytoplasm inside the neck (Fig. 177). Analysis of the formvar-coated support film also showed trace amounts of silicon (Fig. 178) which could account for the silicon in the other controls. The small chlorine peak present in the α band was also present at about the same levels in all the other background controls (Figs. 173 - 176) and probably originated from the Epon embedding plastic (Lalonde et al, 1977).

In the β band iron, phosphorus and chlorine peaks were observed (Figs. 171 and 172) and a silicon peak significantly higher than the background (Fig. 173) was detected, but only on one side of the neck (Fig. 171). This discrepancy was attributed to a technical difficulty encountered during this particular analysis. In Figure 168 the β band measured 0.13 μm as compared to 0.27 μm for the α band and the smallest electron beam spot size possible for the EDX analysis was 0.2 μm. Furthermore, due to the close proximity of the α band to the β band, it was difficult to align the beam on the β band without touching the α band. In contrast the β band seen on the top side of the neck ring in Figure 168 (where an analysis was also made as illustrated in Fig. 172) was located slightly further away from the α band, thus allowing a more accurate analysis of the β band.

This would explain why there was less silicon present in the β band in Figure 172 than in the same band in Figure 171. On the other hand, iron, phosphorous and chlorine peaks were detected consistently in all the β bands analyzed (Figs. 171 and 172). While it was apparent that some of the chlorine present was due to the background as mentioned earlier, significant amounts of chlorine were always observed even after background consideration. Regarding the presence of iron and phosphorous in the β band, it is of interest to note that the Fe:P atomic ratio obtained from computer analysis, varied from 1:1.20 to 1:1.68 (an average ratio of 1:1.41). The theoretical expected ratio of Fe:P in ferric pyrophosphate $\left[Fe_4(P_2O_7)_3\right]$ is 1:1.50 and the results are within the limits of experimental error. Thus one possible compound present in the β band is ferric pyrophosphate.

While the above EDX analyses indicated that silicon, iron and phosphorous were the major elements present in the neck ring, they did not exclude the possibility that some other components such as lipid and protein could also be present, perhaps in smaller amounts. After treatment with lipid solvents (ether/ethanol, acetone or chloroform/methanol), both bands of the neck ring remained unchanged (Fig. 110). In protease treated samples, both bands of the neck ring apparently remained unchanged and remained in place in their usual position along the neck (Fig. 119). The above results therefore, indicate the presence of little, if any, protein or lipid materials in the neck ring. However, samples used for this study have been subjected to fixation and embedding procedures and the possibility exists that soluble materials may have been washed away during preparation.

The occurrence of two distinct bands in the neck ring structure of P. coronata avenae is unique relative to the rust fungi so far described. There is little known about the chemical composition of the neck ring other

than in P. coronata avenae. However, the β band in P. coronata avenae was shown to have the same response to periodic acid oxidation as the entire neck ring structure found in M. lini (Littlefield and Bracker, 1972) and in P. graminis tritici (Fig. 24). Thus the β band in P. coronata avenae and the neck rings in M. lini and P. graminis tritici are possibly similar in composition. It would be of interest therefore, to more closely examine the neck rings in M. lini and other rust fungi to verify their chemical composition. Nevertheless, even if it can be demonstrated that the β band in P. coronata avenae and the neck rings of other rust fungi are the same in composition, there is still a further difference between P. coronata avenae and M. lini. In P. coronata avenae the α band was formed first and appeared to be the major band in the neck ring structure. This is in contrast to the smaller, later-formed β band which appears to correspond to the M. lini-type neck ring.

The silicon in the α band may possibly function as a permeability barrier. This is based on the fact that the α band was highly resistant to most of the chemical treatments performed in the present study. Heath (1976) provided strong evidence that the neck ring of P. sorghi was capable of preventing apoplastic flow of substances along the haustorial neck and drew a parallel between the neck ring and the Casparian strip of higher plants. In the present study the invaginated host plasmalemma remained tightly adhered to both the α and β bands of the neck ring after digestion of the remainder of the neck wall by protease. The binding of the plasmalemma to the neck ring also has a parallel in the tight binding between the plasmalemma and radial walls in the region of the Casparian strip (Bonnett, 1965; Robards et al, 1973) and strengthens the argument that the neck ring may function to prevent apoplastic flow.

F. Electron-Opaque Deposits in the D-Haustorial Apparatus

In sections of glutaraldehyde/OsO_4 fixed materials of both P. coronata avenae and P. graminis tritici and after staining with Ua/Pb, electron-opaque deposits were observed in the protrusion matrix and in the walls and septa of many haustorial mother cells located at or near the center of the infection colonies. Examples are shown in Figures 179 - 181. In the thickened wall region of some haustorial mother cells at the penetration site, these deposits appeared as large, electron-opaque granules (Fig. 180). In walls of other haustorial mother cells more deposits were found and they formed a denser layer around the whole haustorial mother cell (Fig. 181). As mentioned earlier (see section B), aberrant haustoria were found at or near the colony centers of P. coronata avenae. Many of these haustoria were shown to be associated with those haustorial mother cells which had heavy wall deposits (Fig. 48). Similar electron-opaque deposits were not observed in the septa or in the walls of the haustorial mother cells located at the edge of the same infection colonies. The appearance of the deposits in the above structures found at or near infection colony centers was more common in older colonies than in those sampled at 5 days after inoculation.

In Ua/Pb stained sections of glutaraldehyde fixed, unosmicated materials, the deposits were seen as small electron-opaque aggregates, and in the earliest stage of deposition that could be detected, these deposits were found in the membrane protrusions (Fig. 182) but not in the haustorial mother cell wall or in the septum. They were quite distinct from the rest of the protrusion matrix which was more electron-lucent (Fig. 182). For comparison, Figure 55 shows some membrane protrusions that were free of these deposits. These electron-opaque deposits were prominent in unstained

sections and could be detected very readily in fungal materials (Fig. 183).

New haustoria were observed to form in cells near the colony centers of 6-day old infections. After haustorium formation but prior to nuclear migration, granular electron-opaque deposits appeared in the thickened portion of the haustorial mother cell wall at the site of host penetration (Fig. 184). At around this time or shortly after, granular deposits began to appear in the haustorial mother cell septum and in the rest of the wall around the haustorial mother cell (Fig. 185). At this time, more deposits accumulated in the membrane protrusions, haustorial mother cell walls and septa. Eventually the walls of the haustorial mother cells were completely obscured with these deposits. The deposits were continuous with those in the septum (Fig. 186). However, a small portion of the haustorial mother cell septum around the septal pore was always free of these deposits (Fig. 179), as determined in serial sections of this region. The haustorial mother cells with heavy wall deposits finally collapsed (Fig. 189).

The electron-opaque deposits found in the above structures were resistant to both lipid solvent extraction (Fig. 187) and protease digestion (Fig. 188). Similar to the α band of the neck ring of P. coronata avenae, they were resistant to periodic acid treatment (Fig. 189). Since these deposits were electron-opaque in unstained sections of glutaraldehyde-fixed, unosmicated materials, they may also consist of element(s) suitable for electron-probe X-ray analysis (EDX).

A 7-day old colony of P. coronata avenae was chosen for EDX analysis of these deposits. Sections were taken from various areas of the colony to obtain haustorial mother cells undergoing different stages of development. Stages showing the initial deposition of electron-opaque material in the membrane protrusions and in the thickened portion of the haustorial mother cell wall at the site of host penetration, as well as the subsequent heavy

accumulation of the deposits in the rest of the haustorial mother cell wall and septum were located readily within or near the centers of colonies. Analysis was made on these structures, but only one example of each will be presented. For comparison, membrane protrusions, haustorial mother cell walls and septa found at the edge of the colony, and other mycelial walls that were free of any electron-opaque deposits were also analyzed.

Where electron-opaque deposits appeared inside the membrane protrusions (Fig. 190), silicon was detected as the major element present (Fig. 200). The peak representing copper was assumed to have originated from the copper support grid. To show that the silicon peak was significant, the hyphal wall adjacent to the above membrane protrusion was also analyzed. This revealed only a small peak of silicon (Fig. 201). Analysis of the formvar-carbon support film also showed trace amounts of silicon (see Fig. 178), which could account for the small amounts of silicon detected in the hyphal wall. The above therefore demonstrated that silicon was the major element present in the electron-opaque deposits.

At the site of host penetration (Fig. 191), EDX analysis of the electron-dense deposits in the thickened portion of the haustorial mother cell wall indicated that silicon was the major element in these dense deposits (Fig. 202). With older haustorial mother cells (Fig. 186), EDX analysis similarly revealed a major silicon peak in the electron-opaque wall (Fig. 203) and septum (Fig. 204). Evidently silicon was also the major element in this modified haustorial mother cell wall and septum. In contrast no silicon was detected in significant amounts in the walls (Fig. 205) and septal (Fig. 206) structures of the haustorial mother cells regardless of age, that were located at the edge of infection colonies.

Changes in wall appearance of the haustorial mother cells located

in the central regions of older infection colonies have been reported in P. coronata avenae and also in P. graminis tritici by light microscopy. In the central regions of the colonies the walls of many haustorial mother cells usually became swollen and were described as having a "glassy" appearance (Allen, 1923b; Ruttle and Fraser, 1927). The present study supplemented these findings. The silicon that was frequently found in the walls and septa of many haustorial mother cells located mainly in the center of the colonies of P. coronata avenae may be responsible for the "glassy" appearance observed by light microscopy. While the electron-dense deposits found in similar locations in P. graminis tritici (Figs. 180 and 181) were not analyzed, it is believed that silicon is also present in these dense deposits.

The finding of silicon in the haustorial mother cells of P. coronata avenae appears unique relative to the rust fungi so far described. There is little information on the occurrence and distribution of silicon in fungal tissue. Silicon has been reported in sporangia of Metatrichia vesparium (Nelson et al, 1977) and in conidia of Erysiphe graminis after germination on a compatible host (Kunoh et al, 1978; Kunoh and Ishizaki, 1980). Kunoh et al (1978) suggested that silicon in germinated conidia was translocated from the host cells through primary germ tubes and/or conidial cell walls, because the level of silicon in germinated conidia was higher than that in ungerminated conidia. To determine the possible source of silicon in the haustorial mother cells of P. coronata avenae, air-dried ungerminated urediospores were examined by EDX analysis. No significant amounts of silicon could be detected in the walls of the urediospores (Fig. 207). Also, no electron-dense deposits were observed in unstained sections of urediospores of P. coronata avenae fixed in

glutaraldehyde alone (Fig. 193). Thus it appears that the dense silicon deposits in many of the haustorial mother cells found in older colonies were derived from the host plant.

During the course of EDX analysis large electron-opaque deposits were detected in the protoplasts of older haustoria (Fig. 194) and haustorial mother cells (Figs. 190 and 192) of P. coronata avenae in unstained sections of glutaraldehyde fixed, unosmicated tissue. Spectra of these deposits found in older haustoria and in haustorial mother cells are shown in Figures 208 and 209 respectively. They were similar in composition and EDX analysis showed that they contained high concentrations of phosphorous with some amounts of iron and sulphur. In Ua/Pb stained sections of glutaraldehyde/OsO_4 fixed tissue, large electron-opaque deposits of varying shape were observed in vacuoles of hyphal cells (Figs. 195 and 198) and young haustorial mother cells (Figs. 196 and 197) of P. coronata avenae. Similar deposits were also found in P. graminis tritici (Fig. 199). However, EDX analysis was not employed and it is not known if the above electron-opaque deposits found in stained sections were analogous to those in older haustorial mother cells and haustoria (Figs. 192 and 194) that had been subjected to EDX analysis. Using transmission electron microscopy and EDX analysis, White and Brown (1979) and Bullock et al (1980) showed that phosphorous-rich (most likely polyphosphate) inclusions were common in some fungi and characteristically, all of these inclusions were detected within vacuoles. However, it appeared that general morphological appearance and location were not adequate criteria for the identification of phosphorous-rich inclusions as White and Brown (1979) noted that some electron-opaque deposits found in vacuoles in the mycorrhizal fungus that had been fixed with glutarldehyde/OsO_4 and stained with Ua/Pb were not preserved in

glutaraldehyde fixed, unosmicated tissue, and thus could not be identified by X-ray analysis. Phosphorous-rich inclusions were normally preserved in glutaraldehyde fixed, unosmicated tissue. Further investigation is needed to determine if the electron-opaque deposits seen in young haustorial mother cells of P. coronata avenae or P. graminis tritici fixed with glutaraldehyde OsO_4 and stained with Ua/Pb were phosphorous-rich deposits.

Polyphosphates (or inorganic phosphates) have been reported in bacteria, algae, several ecto- and endo-mycorrhizae, and in several fungi including Rozella allomycis, Glomus mosseae, Aspergillus niger and P. graminis tritici in saprophytic cultures (see White and Brown, 1979). In Glomus mosseae, Callow et al (1978) reported that more than 40% of the total fungal phosphorous occurred as polyphosphate. It is probable that the phosphorous-rich iron-containing deposits found in the older haustorial mother cells and haustoria of P. coronata avenae, as determined by the present EDX analysis were analogous to the inorganic phosphates described in the organisms above.

G. Host Responses

1. Cytoplasmic Changes

In newly invaded host cells one of the earliest host responses that could be detected was the association of endoplasmic reticulum with the developing haustoria. General disorganization of the host cell protoplast was not apparent at this stage. In P. coronata avenae infections, endoplasmic reticulum cisternae were seen lying parallel to the invaginated host plasmalemma along the young haustorial neck, before expansion of the haustorial body (Figs. 28 and 29). After the haustorial body was formed, profiles of endoplasmic reticulum cisternae were found associated with the

invaginated host plasmalemma that continued around the haustorial body (Fig. 35).

In P. graminis tritici infections the association of the endoplasmic reticulum with developing haustoria was more striking. As reported elsewhere (Harder et al, 1978), the early expansion phase of the haustorial body was accompanied by extensive proliferation of endoplasmic reticulum, particularly around the upper portion of the neck, where some of the cisternae appeared to radiate from the haustorium out into the host cytoplasm. As the haustorium matured, the proliferation of endoplasmic reticulum around the haustorial neck became less marked and this was preceded by the development of endoplasmic reticulum-derived membranous complexes. These complexes consisted of a lattice arrangement of large and small, apparently interconnected, ribosome-free tubules around the haustorial body. It was shown that the large tubules were continuous with the endoplasmic reticulum, and both large and small tubules were apparently connected to the invaginated host plasmalemma around the haustorial body (Harder et al, 1978).

While organized endoplasmic reticulum-derived membranous complexes were not observed in P. coronata avenae infections, the development of the extrahaustorial matrix was accompanied by a marked proliferation of large tubular complexes (Fig. 210). These complexes consisted of large randomly arranged tubules, some of which in turn were connected to membrane structures with circular profiles (Fig. 210). As will be detailed later, these tubular complexes were located mainly in the part of the host cytoplasm between the host nucleus and the adjacent developing haustorium.

The tubules making up the complexes contained an electron-dense matrix and a thread of denser staining material at their centers (Fig. 210). The tubules were distinct from the host endoplasmic reticulum (Fig. 211).

While the membranes of these tubules were often seen connected to the invaginated host plasmalemma around the haustorial body, results from PACP staining showed that the invaginated plasma membrane consistently stained more densely than the tubule membranes and other membrane structures both in the host and fungus (Figs. 212 and 213). Similar staining behaviour was observed with the invaginated host plasmalemma and tubules around the haustorial body of P. graminis tritici (Harder et al, 1978). In P. coronata avenae, the invaginated plasmalemma at the more distal portion of the haustorial body stained more intensely than the rest of the invaginated plasmalemma. The exact location where this transition occurred was not determined. The above observations with the PACP staining were different from those described for uredial infections of M. lini in that the invaginated host plasmalemma around the haustorial body was always more lightly stained than the non-invaginated portion (Littlefield and Bracker, 1972). While the specificity of this stain for plasmalemma is still unclear (see section IV.B Literature Review), the consistent more dense staining of the distal portions of the invaginated plasmalemma observed in the present study indicates variability in composition of various portions of the invaginated plasmalemma, and that the PACP method is sensitive to these differences. Littlefield and Bracker (1972) concluded from their M. lini study that either the change in nature of the invaginated host plasmalemma occurred after its formation, or that the new portion of the plasmalemma differed from the rest from the outset.

After the PA-TCH-SP treatment the contents of the tubules that made up the large tubular complexes found in the vicinity of the haustoria of P. coronata avenae were intensely stained (Figs. 144 and 214). The contents of the tubules were continuous with the PA-TCH-SP stainable

materials in the extrahaustorial matrix and direct connection between the tubule membranes and the invaginated host plasmalemma was evident (Fig. 144). After cellulase treatment both the Ua/Pb stainable (Fig. 147) and PA-TCH-SP stainable (Fig. 148) materials were removed, suggesting that cellulose was present in these structures. As described earlier, much of the PA-TCH-SP stainable material in the extrahaustorial matrix was also removed after cellulase treatment (Fig. 148), suggesting that cellulose was also present as a component of the matrix. This is consistent with the suggestion that the extrahaustorial matrix may contain substances of host origin (Littlefield and Heath, 1979). The contents of the large tubules that made up part of the endoplasmic reticulum-derived tubular complexes found in P. graminis tritici were also stained with PA-TCH-SP (Fig. 215). The cellulase treatment was not performed to determine if cellulose was also present in these structures.

As the haustoria developed the host nuclei were frequently seen appressed to one side of the haustorium and occasionally the nucleus was indented by a haustorial lobe (Fig. 216). Close association of haustoria with host nuclei has been reported in other rust infections and this appears to be a general phenomenon (Littlefield and Heath, 1979). However, the present results indicate a more extensive association between the haustoria of P. coronata avenae and host nuclei than has been previously indicated. As mentioned above there was extensive ramification of large tubules and circular membranous structures in the host cytoplasm in the vicinity of the haustoria. On close examination these tubules were found mainly in the cytoplasmic region between the host nuclei and the nearby haustoria (Fig. 217). The frequency of this observation in the present study suggests that the association may be a characteristic response of the host. The proli-

feration of these tubules and circular membranous structures was more pronounced especially in the indented region of the nucleus where a haustorial lobe was located (Figs. 217 - 220). In this region the portion of the nucleus adjacent to the cytoplasm containing these tubules was highly lobed (Figs. 217 - 220), more so than the rest of the nucleus. While direct continuity was observed between these tubules and the invaginated host plasmalemma around the extrahaustorial matrix (Figs. 144 and 212), continuity between the tubular membranes and the nuclear envelope was not found despite extensive efforts made to find these connections. The occasional association of these tubules with some chloroplasts seen in some cases (Fig. 221) was likely by chance and due to the nucleus being just out of the plane of sectioning. Figure 220 shows a general view of the association of a mature haustorium with the lobed portion of the host nucleus. Tubular and membranous complexes were located mainly in the cytoplasmic region between the host nucleus and haustorium, and not in other cytoplasmic areas which contained chloroplasts and mitochondria. There was no particular association of chloroplasts and mitochondria with the developing haustoria nor was any change in their ultrastructure observed in the time period up to the onset of sporulation. However, other host organelles such as Golgi bodies were often seen in the vicinity around the developing haustoria of P. coronata avenae. Figures 222 and 223 are micrographs of adjacent sections of a young haustorium stained with the PA-TCH-SP method. The age is indicated by the presence of only the α band in the neck ring (Fig. 222). An aggregation of Golgi bodies and vesicles was clearly evident around the haustorial neck region. The contents of the vesicles were stained intensely with PA-TCH-SP and appeared to have budded off from the Golgi bodies (Figs. 222 and 223). Golgi bodies were also abundant in the

host cytoplasm around the haustorial body and they appeared to be active in budding off vesicles (Fig. 224). An increase in the number of Golgi bodies in the host cytoplasm around haustoria has been reported in other rust infections (see Littlefield and Heath, 1979). In P. coronata avenae infections however, and without quantitative data, it was difficult to determine if the apparent increase in number of host Golgi bodies around the haustoria resulted from a redistribution of such organelles in the host protoplast or whether it was due to an increase in the total number of Golgi bodies in each infected cell. The Golgi bodies did not appear to be particularly involved in any of the described associations of the endoplasmic reticulum and the invaginated host plasmalemma, despite their accumulation around haustoria. They also did not appear to be involved in the large tubular complexes associated with the haustoria. The Golgi bodies normally have an intermediary role in the transformation of endoplasmic reticulum-type to plasmalemma-type membranes (Morré, 1975). It is not clear if the Golgi bodies have a similar role in the host membrane-haustorial association. One possibility is that the tubular complexes play a similar synthetic-transport-intermediary role, but in a specialized way to meet the needs of the parasitic fungus.

2. Collars

A common response of the host cell to the presence of rust fungal haustoria is the deposition of a "collar" of material at the point where the fungus enters the host cell (see section III.B Literature Review). In compatible infections of P. coronata avenae or P. graminis tritici deposition of material against the host cell occasionally occurred at the point where the haustorium entered the cell. Such wall deposits usually resulted in the formation of a collar around the haustorial neck but they rarely

extended beyond the haustorial neck. In both P. coronata avenae and P. graminis tritici infections, collars were generally associated with older haustoria.

After Ua/Pb staining, a small collar in the early development stage around the neck region of P. coronata avenae was mainly electron-translucent with some electron-opaque patches (Fig. 225). The area of the collar immediately adjacent to the neck was electron-translucent. Host plasmalemma was seen lining both sides of the collar which was separated from the haustorial neck by both the host plasmalemma and the invaginated host plasmalemma (Fig. 225). Some mature collars were electron-opaque (Fig. 226) while others contained membranous material and extensive electron-opaque patches (Fig. 227). After PA-TCH-SP treatment, the material making up most of the collar was intensely stained, although some compartments and especially the portion of the collar immediately adjacent to the haustorial neck remained unstained (Figs. 228 and 229). By using the same staining method two host wall layers were revealed: a thicker lighter stained outer layer and a thinner denser stained inner layer (Fig. 75). In all cases the collar material was continuous with the inner layer of the host wall (Figs. 228 - 230). This inner layer of the host wall increased in thickness initially in regions around the penetration site as the collar developed. In some infections where well-developed collars were present, deposition of collar material into the inner host wall in these regions was so intense that this inner layer of the host wall became much thicker than the outer layer (compare Fig. 230 to Fig. 231). Where there were large collars, these wall appositions could be observed at some distance away from the penetration site of the haustorium (Fig. 230). In compatible P. graminis tritici infections the appearance of the collar deposits stained with the PA-TCH-SP

procedure was quite distinct from those associated with P. coronata avenae infections. The materials in the wall appositions as well as the collar were more diffuse and granular in the P. graminis tritici infections (Fig. 232).

In P. coronata avenae infections the onset of wall apposition was initiated by deposition of material against the host cell wall at the penetration site of the haustorium (Fig. 231). Small membrane-bound vesicles, some containing electron-opaque material, appeared and became attached to the invaginated host plasmalemma along the haustorial neck (Fig. 233). More vesicles then appeared (Fig. 234) and these probably coalesced together to form the collar. A collar formed in this manner would contain trapped membranous materials which are remnants of the vesicles after having released their contents during fusion. It is not clear however, whether the invaginated host plasmalemma along the neck region was involved with the vesicle-membrane fusion. The absence of trapped membranes in some collars (Fig. 226) suggested that not all collars were formed in the manner as described above. Furthermore, collars found in P. coronata avenae infections were variable in shape. Many collars had long projections radiating out from the main collars into the host cytoplasm (Figs. 235 - 237). In some views, these projections resembled large vesicles (Fig. 236), but this appearance was due to the plane of sectioning. When these projections were present, profiles of host endoplasmic reticulum and Golgi bodies were always found associated with them (Figs. 236 and 237). Most interesting was the fact that these large projections apparently were linked by profiles of endoplasmic reticulum, although actual connections between these structures were not demonstrated. Figure 236 shows a network of endoplasmic reticulum-projection system occurring in the host cytoplasm around a collar.

Characteristic organization and distribution patterns of endoplasmic reticulum cisternae have been associated with cell wall formation in higher plants (Chrispeels, 1976), including callose deposition (Northcote and Wooding, 1966; Clowes and Juniper, 1969). The characteristic association of the endoplasmic reticulum cisternae with the collar projections seen in the present study is probably representative of a stage in the growth of the collar. It has been implicated that endoplasmic reticulum plays a role in the development of the more extensive, but otherwise similar, collars and encasements found in some incompatible rust-host interactions (Heath and Heath, 1971), and endoplasmic reticulum involvement in polysaccharide synthesis has been suggested for other systems (Chrispeels, 1976). However, collar deposits and the contents of the nearby endoplasmic cisternae always stained differently. As pointed out by Heath and Heath (1971), it was possible that precursors of collar material were synthesized in the endoplasmic reticulum, then either the contents changed in composition or degree of polymerization after discharge, or it is possible that the substances of the collar were secreted in some other way.

Collars containing fibrillar and electron-lucent components have been observed in a number of rust infections (Coffey et al, 1972; Hardwick et al, 1971; Littlefield and Bracker, 1972; Heath and Heath, 1971). Since callose is typically electron-lucent (Frey-Wyssling and Mühlethaler, 1965; Heslop-Harrison, 1966), one would expect callose was at least present in those collars containing electron-lucent components. In compatible interactions with U. phaseoli typica (Hardwick et al, 1971) and in incompatible interactions with U. phaseoli vignae (Heath, 1971), histological studies with light microscopy suggested that a callose-like compound was present in these collars. It is likely that callose was present in the electron-

lucent compartments of the collars found in P. coronata avenae infections. However, the collars were not wholly electron-lucent, and they probably contained other materials as well.

Using the PA-TCH-SP test for polysaccharides most regions within the collars in P. coronata avenae infections were intensely stained (Fig. 238), and this staining reaction was blocked by sodium borohydride (Fig. 239). The collar material remained unstained in the control treatment (TCH-SP) where periodate oxidation had been omitted (Fig. 240). The staining pattern of the collar with the PA-TCH-SP procedure apparently was not affected after cellulase treatment, suggesting that cellulose was not a major constituent of the collar material (Fig. 241). The de Bruijn fixation method did not reveal the presence of any glycogen (Fig. 242). After protease treatment extensive extraction occurred in the haustorial neck wall, but the collar material that was stainable with Ua/Pb (Fig. 243) and PA-TCH-SP treatment (Fig. 244) remained unchanged. Solvent extraction did not affect the appearance of the collar (Fig. 245) nor did it affect the amount of polysaccharide in it (Fig. 246).

The above cytochemical tests therefore suggested that carbohydrates were the main constituents of the collar deposits in susceptible plants infected with P. coronata avenae. These carbohydrates reacted positively to the PA-TCH-SP treatment, indicating that they were polysaccharides containing vicinal hydroxyl groups. Callose on the other hand, is known to be a β1-3 glucan (Kessler, 1958; Eschrich, 1961). Such glucans are resistant to periodate oxidation (Heath and Heath, 1971) and thus should be PA-TCH-SP negative. If it could be confirmed that callose was also present in the translucent compartments of the collars found in P. coronata avenae infections, this would suggest that there were at least two types of carbohydrates

making up the collar deposits. A number of studies have shown that callose deposition could be induced, increased or decreased by such factors as mechanical injury, temperature, application of various chemicals, or by changes brought about by senescence (see Jagels and Garner, 1979). The formation of primarily callose-containing collars may similarly represent a nonspecific response to invasion of the host cell. However, other carbohydrates were often found in apparently large concentrations in the collars of P. coronata avenae infections and the development of such collars appeared to be closely associated with host endoplasmic reticulum, thus representing a kind of host response that is perhaps more specific than that elicited by injury alone.

It is of interest that collars were not induced in every invaded cell. As pointed out by Heath and Heath (1971) and Heath (1974), this could indicate a suppression of this response in compatible associations as long as the haustorium remained alive and unimpaired. Such a hypothesis would further explain why collars were more frequent in older infections seen in the present study and in other rust infections (Coffey et al, 1972; Heath and Heath, 1971). Further, it has been indicated that the degree of compatibility between host and fungus, and the health of the latter, could decrease with time, particularly after the onset of sporulation (Littlefield and Heath, 1979).

II. Basidiospore-Derived Infections of P. coronata avenae

Monokaryotic (M-) haustoria are intracellular structures found in basidiospore-derived infections. They are formed from a terminal cell of a hyphal branch, are rather filamentous in shape and they more closely resemble the intercellular hyphae than the "true" D-haustoria (see Littlefield and

Heath, 1979). Using the Thiéry PA-TCH-SP staining method a moderately-stained layer of extracellular substance was often observed on the outside of this terminal cell, which commonly filled part of the angle of contact between host and fungus (Fig. 247). After Ua/Pb staining this layer was electron-lucent and the boundary between this layer and the fibrillar host wall was indistinct (Fig. 248). This layer was continuous with that covering the rest of the intercellular mycelium and probably served to adhere the fungus to the host wall.

In D-haustoria the haustorial mother cell septum is the last septum formed in the D-haustorial apparatus. In M-haustoria the position of the last septum relative to the host cell varied with age of the M-haustoria. During early haustorium development these septa were found at some distance external to the penetration region (Fig. 249) and no structural changes comparable to those in dikaryotic infections were observed. When the haustoria were more mature the last septum outside the host cell occurred close to or at the site of penetration (Fig. 250). In older infections some M-haustoria were septate (Fig. 251) (Harder, 1978). No structural differences could be observed between the last haustorial septum (Fig. 249) and septa in other portions of the fungus (Fig. 252). The variable location of the M-haustorial septa appears to be due to continuous formation of new septa during haustorial growth, similar to that occurring during normal hyphal growth.

After PA-TCH-SP treatment all fungal walls were intensely stained (Fig. 253). Invasion of host cells did not involve the formation of a specialized penetration peg. There was no localized thickening of the fungal wall at the penetration site (Figs. 247 and 253). Penetration was accomplished by a protuberance of the terminal cell entering the host wall

(Fig. 247). At the tip of the protuberance the fungal wall was slightly thinner than that around the rest of the cell, and dense granules and membranous material were seen in the cytoplasm of this region (Fig. 247). After host penetration the fungal wall was similar in thickness throughout the penetration region and relatively little constriction of the fungus was observed at the penetration site (Fig. 253). The host wall did not appear distorted or displaced inward at the penetration region (Figs. 253 and 254) suggesting that penetration of the host wall was accomplished largely by enzymatic action.

The ingrowth of host wall-like material formed in advance of the penetrating fungus (Harder, 1978) was not observed in the present study, though infrequently a collar was found around the proximal (adjacent to the host wall) portion of the M-haustoria. When present, the collar was fibrillar and appeared rather heterogenous in nature, and its presence was usually associated with older haustoria (Fig. 255).

The M-haustoria of P. coronata avenae had a much simpler structure than the D-haustoria. They did not possess a structure resembling the neck ring typical of D-haustoria and a clearly differentiated neck region was absent. They were usually filamentous and closely resembled intercellular hyphae (Fig. 254). The walls of M-haustoria were separated from the surrounding invaginated host plasmalemma by an intervening layer, designated as an extrahaustorial matrix analogous to that of the D-haustorial apparatus. The extrahaustorial matrix was usually thin around most of the haustorial body, but was more pronounced at the distal portion of the haustorium (Fig. 254).

After Ua/Pb staining the extrahaustorial matrix was moderately electron-opaque around the entire haustorial body, but was usually more

densely stained in the proximal region (Fig. 256) than in the other regions (Fig. 257). Using the PA-TCH-SP staining method the extrahaustorial matrix was electron-opaque but not as densely stained as the fungal wall (Figs. 258 and 259). In the control treatment in which periodate oxidation was omitted from the PA-TCH-SP procedure (TCH-SP), silver staining was observed in all fungal walls (Fig. 254) as well as the extrahaustorial matrix, but there was more staining in the matrix along the proximal region of the M-haustoria (Fig. 260) than that in the distal region (Fig. 261). After PACP treatment the extrahaustorial matrix in the distal region of the haustoria was strongly stained (Fig. 263). The extrahaustorial matrix in the proximal region as well as the fungal walls remained largely unstained (Fig. 262). The above observations from the PACP treatment suggest that the extrahaustorial matrix in the distal region of the haustorium has a higher concentration of PACP positive material than the matrix in the proximal region.

In studying the component parts of the D-haustorial apparatus in dikaryotic infections it was demonstrated that the TCH-SP type of silver staining in the D-haustorial wall was most likely due to the presence of unsaturated lipids (see section D above). The D-haustorial wall was markedly different from the mycelial walls because no TCH-SP type of silver staining was evident in the latter walls. In the monokaryotic infections however, all fungal walls stained intensely after the TCH-SP treatment. This suggests that walls of M-haustoria and intercellular hyphal cells were similar in composition. This is further supported by similar staining in the walls of the M-haustoria and those of other hyphal cells of the fungus after Ua/Pb, PA-TCH-SP and PACP treatments. Further investigation is needed to determine if the TCH-SP type of silver staining seen in the walls

of the fungus in the monokaryotic infections was due to unsaturated lipids.

The protoplasts of young M-haustoria contained the usual hyphal organelles such as mitochondria, endoplasmic reticulum and nuclei. Large vacuoles were not present in the young haustoria except for some small membrane-bound electron-translucent structures which resembled tiny vacuoles (Fig. 257). Storage material such as glycogen and lipid droplets were uncommon at this stage. The cytoplasm was densely packed with ribosomes but it stained normally with Ua/Pb (Fig. 257). Older haustoria became vacuolated (Fig. 255) and contained considerable numbers of lipid droplets. Initially, the host protoplasts did not appear to be affected by the presence of the fungus but there were usually cisternae of endoplasmic reticulum (Figs. 256 and 258) in the host cytoplasm near the M-haustoria.

Like uredial infections in the Avena host, aberrant M-haustoria were found, but these were usually limited to certain areas of the infection sites. Similar to the M-haustoria described earlier (Harder, 1978), these haustoria were very irregular in shape with sharply contoured outlines (Fig. 264). Usual organelles such as nuclei, mitochondria and endoplasmic reticulum were present and lipid droplets were abundant in the protoplasts, which were typically densely staining, suggesting that the haustoria were necrotic. As shown elsewhere (Harder, 1978) the density of the protoplast most often increased at the point of entry into the host cell. Both normal looking and aberrant haustoria were occasionally found in the same host cell (Fig. 251), but it was not clear whether they were part of one haustorium or two separate haustoria. In a typical area of the infection site where several of these aberrant haustoria were found, the intercellular hyphal cells all appeared normal but host cells showed some

signs of disorganization (Fig. 264). It is possible that the necrosis seen in these haustoria was a deleterious response to the disrupted host cells. Alternatively, it is also possible that certain M-haustoria, perhaps at particular stages of development, were more sensitive to the preparative procedures, resulting in the more dense staining and irregular outlines of these haustoria. Aberrant M-haustoria were also reported in Peridermium pini (Walles, 1974). Walles (1974) suggested that the necrosis of these haustoria was probably due to an incompatibility reaction with the host protoplasts.

In monokaryotic infections of P. coronata avenae in the Rhamnus host, invasion of the host cells was not limited to the leaf epidermal and mesophyll tissues. As reported elsewhere (Harder, 1978; Al-Khesraji et al, 1980), invasion of host vascular tissue often occurred. Figure 265 shows the presence of a M-haustorium in a sieve element. The haustoria found in these vascular cells usually contained very dense cytoplasms and were irregular in outline, similar to the aberrant haustoria found in the mesophyll cells. Fungal structures were also found in mature xylem vessels (Fig. 265). They resembled intercellular hyphae in structure, and lacked an extrahaustorial matrix around them. The M-haustoria of P. poarum found in vascular tissue of Tussilago host also contained electron-dense cytoplasm (Al-Khesraji et al, 1980). These workers attributed the dense cytoplasm of these haustoria to metabolic activity. In uredial infections of P. coronata avenae in the Avena host, invasion of the host vascular tissue has not been observed.

LEGEND

Figures 1-4. A young haustorial mother cell of P. coronata avenae.

Figures 1-4. Four closely adjacent sections taken from a series of serial sections of the same young HMC. Host wall penetration had begun (arrow), but the haustorium had not yet formed. Mitochondria (M) are densely stained and located around the periphery of the cell adjacent to the plasmalemma. The protoplast contains two nuclei (N), small vacuoles (V) and an abundance of ribosomes. Characteristic membrane protrusions with a dense matrix (open arrow) are found on the hyphal side of the HMC septum (MS). Glt/OsO_4. Ua/Pb. All Figures x8,700.

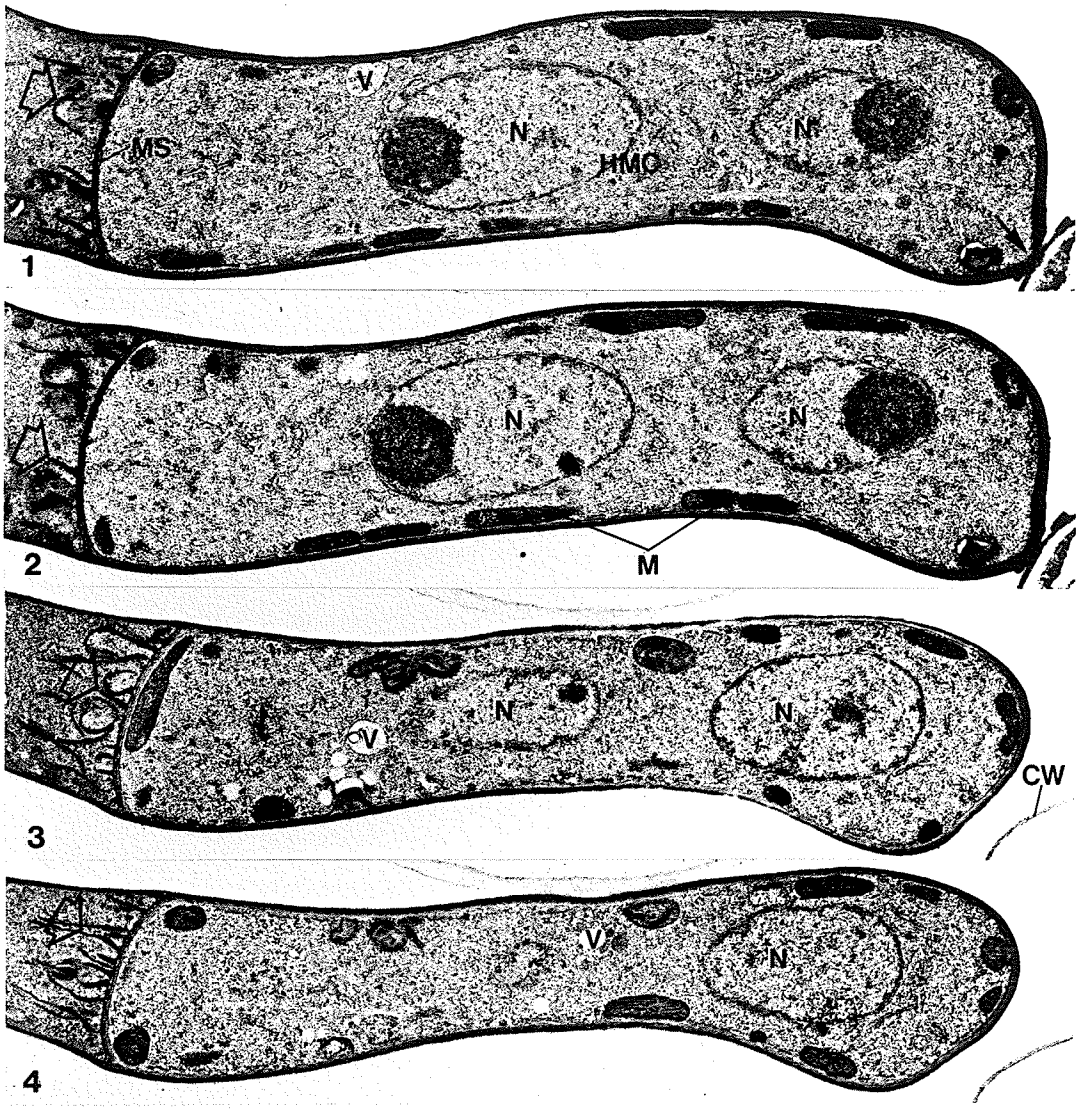
V
MS
N
HMC
N
1
N
N
M
2
N
N
V
CW
3
V
N
4

LEGEND

Figures 5-9. Hyphal and haustorial mother cells of P. coronata avenae (Figs. 5, 6 and 8) and P. graminis tritici (Figs. 7 and 9).

Figure 5. Cross-section of a young HMC with mitochondria (M) arranged as a ring around the inner periphery of the cell, adjacent to the plasmalemma. Glt/OsO_4. Ua/Pb. x22,500.

Figure 6. Part of a hyphal cell with mitochondria (M) scattered at random locations in the cell lumen. Glt/OsO_4. Ua/Pb. x15,000.

Figure 7. A section taken from a serial set showing a HMC during early haustorium formation. Mitochondria (M) have aggregated at the site of penetration (arrow). Glt/OsO_4. Ua/Pb. x15,700.

Figure 8. A section showing part of a HMC septum (MS) which is composed of four layers. The two electron-opaque layers (long arrows) are continuous with the periclinal wall (open arrow). A third more lightly stained layer (short arrow) separates the two electron-opaque layers and ends at the periclinal wall. The fourth lightly stained layer (arrowhead) is continuous around the rest of the HMC. The haustorial mother cell wall is multi-layered, and contains more layers than the hyphal wall. Glt/OsO_4. Ua/Pb. x47,100.

Figure 9. A section showing part of a HMC septum (MS) composed of four layers. The two electron-opaque layers (long arrows) are continuous with the periclinal wall (open arrow). A third more lightly stained layer (short arrow) separates the two electron-opaque layers and ends at the periclinal wall. The fourth lightly stained layer (arrowhead) is continuous around the rest of the HMC. Glt/OsO_4. Ua/Pb. x39,600.

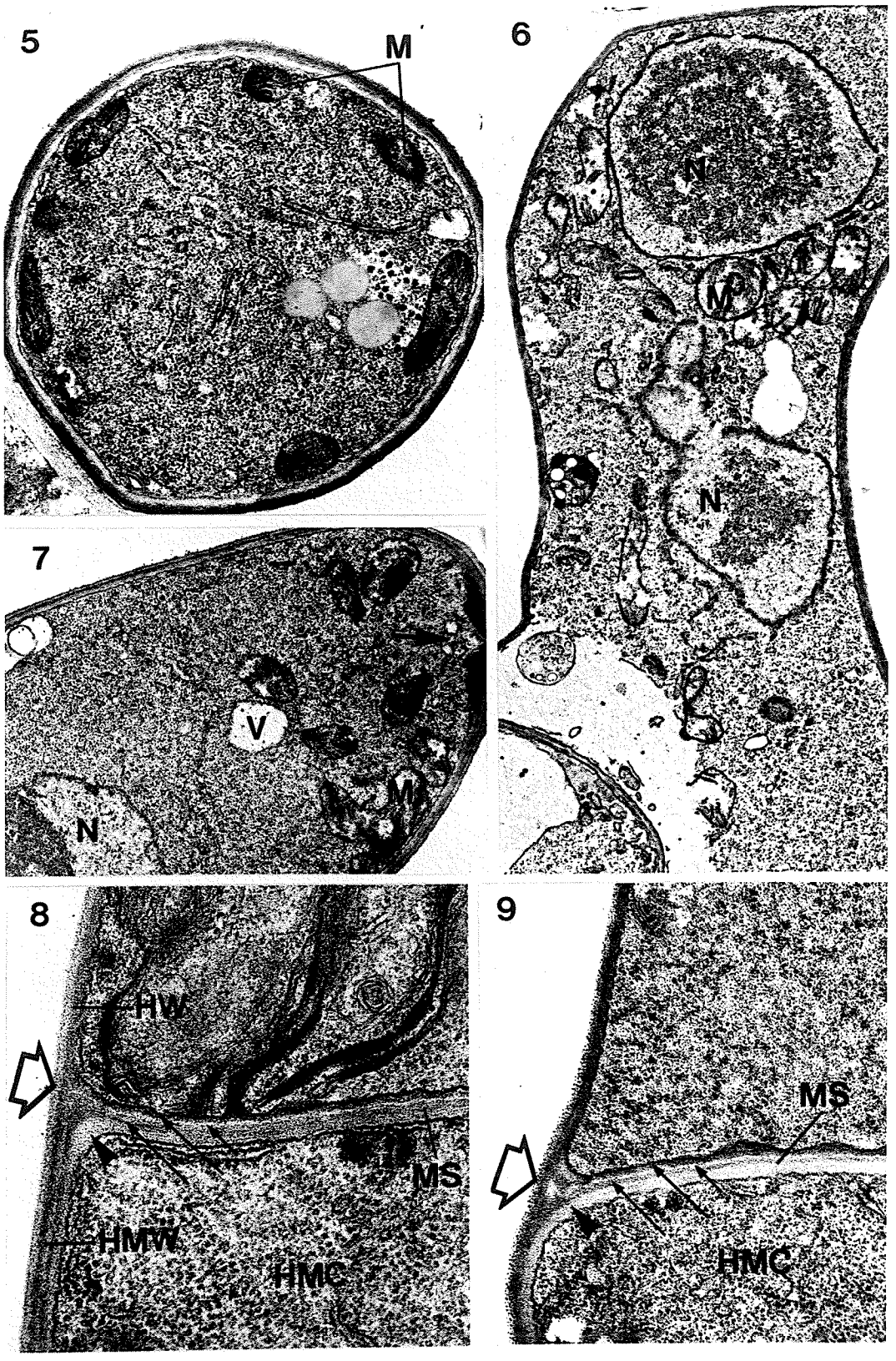
5
M
6
N
M
N
7
V
M
N
8
HW
MS
HMW
HMC
9
MS
HMC

LEGEND

Figures 10-16. Hyphal and haustorial mother cells of P. coronata avenae (Figs. 10, 11, 13 and 15) and P. graminis tritici (Figs. 12, 14 and 16).

Figure 10. Part of a hyphal septum showing two electron-opaque layers separated by a narrow electron-translucent central lamella which ends at the periclinal wall (arrowhead). The septal pore is the perforated type and is bounded by a pulley-wheel shaped diaphragm on either side of the pore (arrow). Glt/OsO_4. Ua/Pb. x30,400.

Figure 11. A HMC sectioned near the site of host-penetration. A densely staining layer (arrows) is seen at the thickened region of the HMC wall. There is no continuity between this dense staining layer and the other existing wall layers. Glt/OsO_4. Ua/Pb. x37,500.

Figure 12. The haustorial mother cell wall (arrow) is composed of two layers, a densely staining outer layer and a lightly staining inner layer. The hyphal wall (arrowhead) contains one layer and is continuous with the outer layer of the mother cell wall. Glt/OsO_4. Ua/Pb. x25,000.

Figures 13 and 14. The hyphal septa (long arrow) appear as two electron-opaque layers separated by a middle electron-translucent layer. The hyphal walls (arrowheads) are composed of one densely staining layer, excluding the lightly stained layer of extracellular substance. Both septa are plugged with material (short arrow) which is unstained by this staining method. Glt/OsO_4. PA-TCH-SP. Figure 13, x44,300. Figure 14, x37,600.

Figures 15 and 16. The HMC septa (MS) of older HMC showing their multilayered composition. Three layers are observed in the haustorial mother cell walls (arrows), two electron-opaque layers separated by a middle moderately stained layer. The innermost electron-opaque layer is continuous around the septum (arrowhead). Glt/OsO_4. PA-TCH-SP. Figure 15, x44,300. Figure 16, x37,500.

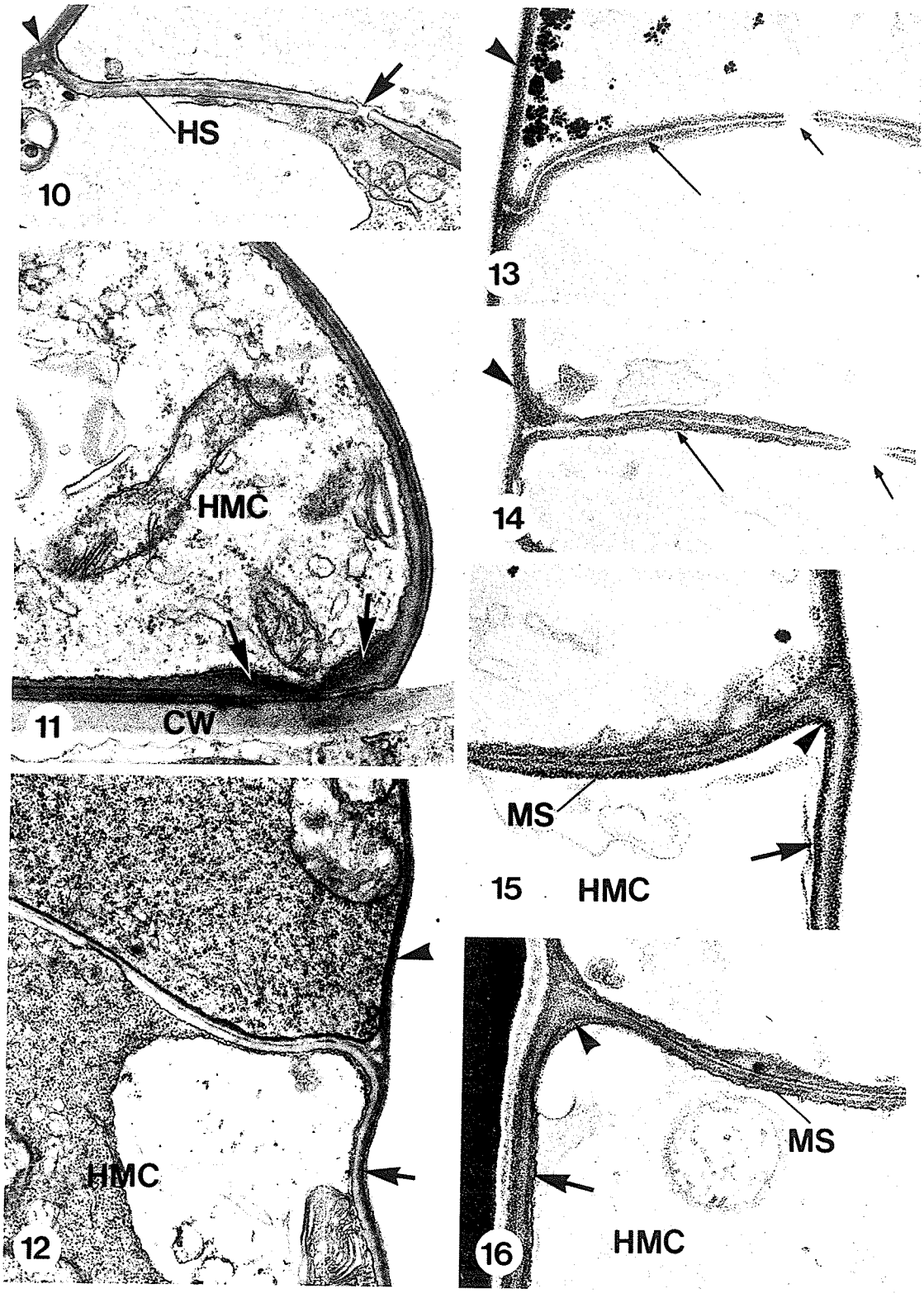
HS
10
HMC
11
CW
HMC
12
13
14
MS
15
HMC
MS
16
HMC

LEGEND

Figures 17-23. Haustorial mother cells of P. graminis tritici (Figs. 18 and 23) and P. coronata avenae (Figs. 17 and 19-22).

Figures 17 and 18. Three layers can be seen in the HMC wall (arrowhead); two electron-opaque layers separated by a moderately stained middle layer. Glt/OsO_4. PA-TCH-SP. Figure 17, x12,000. Figure 18, x18,600.

Figures 19 and 20. Two sections taken from a series of serial sections to show a young penetration peg (asterisk) which has developed as a localized evagination of the HMC plasmalemma (PL). The thickened region of the HMC wall is composed of two layers; a thin, densely stained outer layer (OL) and a thick, more lightly stained inner layer (IL). A thin, lighter stained region is seen between the invaginated portion of PL and IL (arrows) and appears to be continuous with the IL (Fig. 19). Glt/OsO_4. PA-TCH-SP. Figure 19, x51,000. Figure 20, x65,000.

Figure 21. A HMC sectioned at the site of host-penetration. The thickened region (arrows) of the HMC wall is electron-opaque. Continuity is not seen between the HMC wall and the haustorial neck wall (arrowhead). Glt/OsO_4. Ua/Pb. x44,900.

Figure 22. An oblique section through the penetration region. The thickened region of the HMC wall is largely electron-translucent (arrows). A thin fungal wall layer (arrowheads) is seen through the penetration region and is continuous with the dense staining haustorial neck wall (HNW). Glt/OsO_4. Ua/Pb. x55,400.

Figure 23. A thick electron-opaque convex lens-shaped middle layer (ML) is seen between the two existing wall layers (IL and OL) of the HMC wall. Note the presence of a more diffuse fungal wall layer (arrows) through the penetration region, and continuity can be seen between the ML and the haustorial neck wall (arrowhead). Glt/OsO_4. Ua/Pb. x32,800.

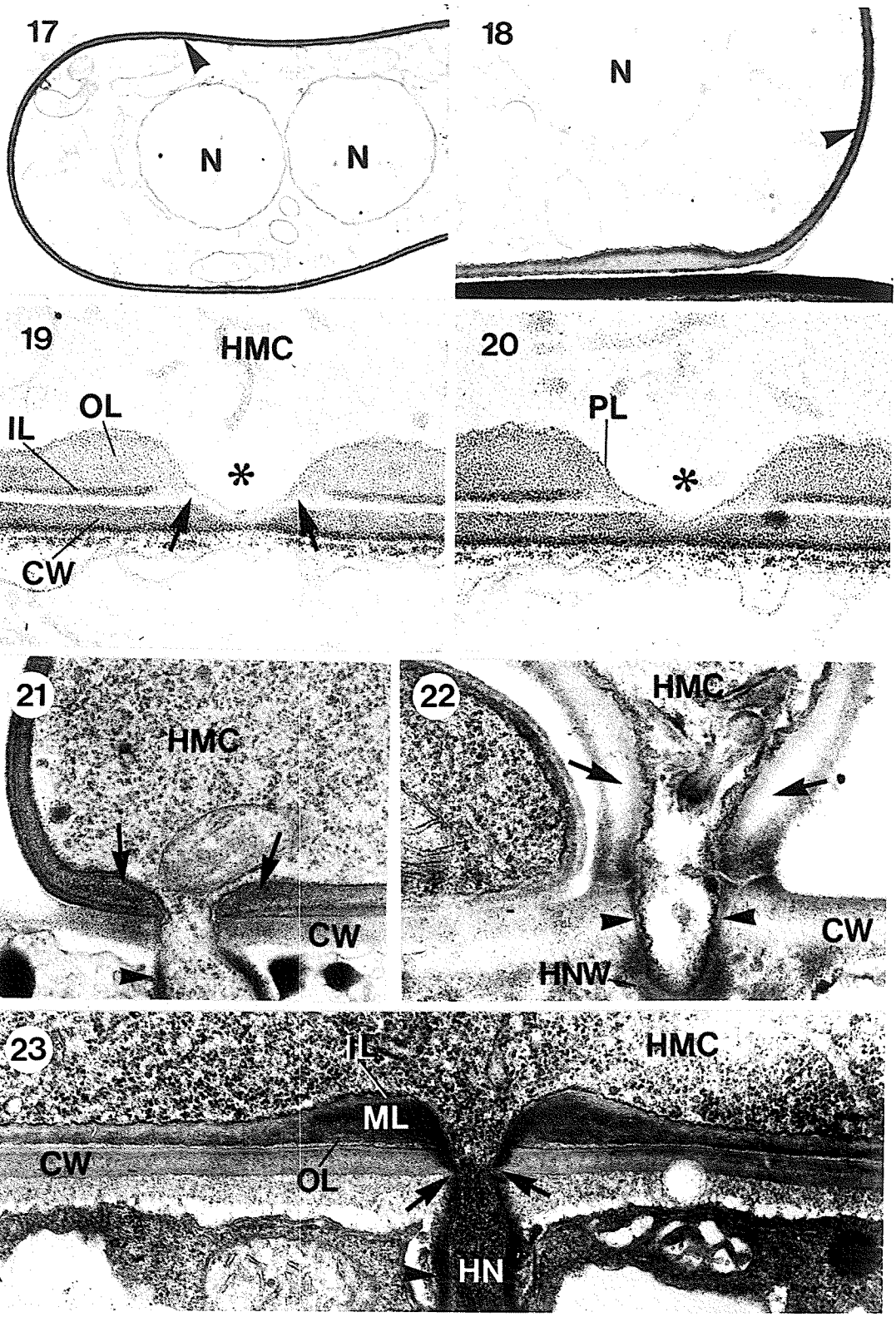
17
N
N
18
N
19
HMC
IL
OL
*
CW
20
PL
*
21
HMC
CW
22
HMC
CW
HNW
23
IL
HMC
ML
CW
OL
HN

LEGEND

Figures 24-27. Penetration regions through host cell walls of cells infected by P. graminis tritici (Fig. 24) and P. coronata avenae (Figs. 25-27).

Figure 24. Three layers (IL, ML and OL) can be seen at the thickened region of the HMC wall. Continuity can be established between the ML and the densely stained neck wall (HNW), but the fungal wall material (arrowheads) is more lightly staining and more diffuse through the penetration region. The neck ring (arrow) has been etched out by this staining method. Glt/Os04. PACP. x43,900.

Figures 25 and 26. Two closely adjacent sections of the same young HMC showing the presence of microtubules, membranous materials, and electron-dense granules in the HMC cytoplasm at the penetration region. Glt/$Os0_4$. Ua/Pb. Figure 25, x50,000. Figure 26, x51,800.

Figure 27. Membrane-bound electron-dense granules in the HMC cytoplasm at the penetration region. Glt/$Os0_4$. Ua/Pb. x60,700.

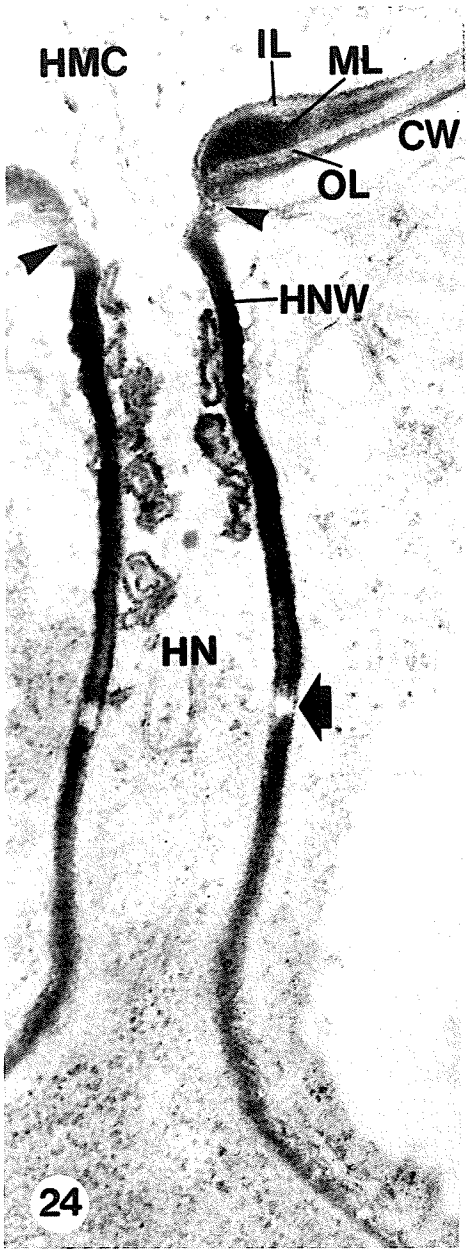
HMC
IL
ML
CW
OL
HNW
HN
24

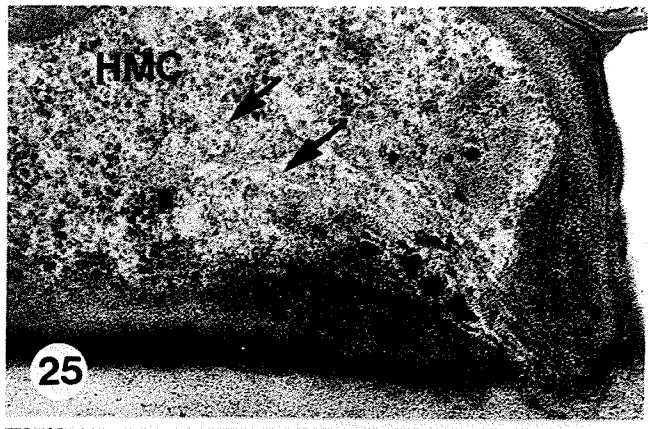
HMC
25


26

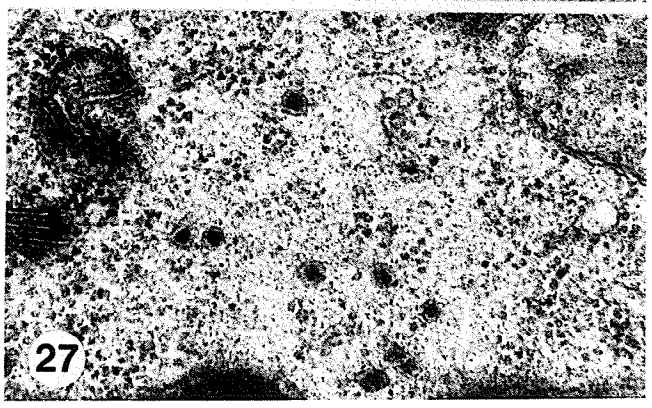
27

LEGEND

Figures 28-30. Early haustorium formation in P. graminis tritici (Fig. 30) and P. coronata avenae (Figs. 28 and 29).

Figure 28. A young haustorium (H) consisting of a tubular finger-like projection, about 2.6 μm long, extending into the host cell. Inset. Note the presence of electron-dense granules (arrow) and ribosomes in the fungal cytoplasm. The haustorial wall is seen as one densely staining layer. Host endoplasmic reticulum (ER) is seen lying parallel to and around the tip of the neck. Adjacent sections did not reveal the presence of a haustorial body. Glt/OsO_4. Ua/Pb. Figure 28, x13,300. Inset, x33,900.

Figure 29. A young haustorium (H) consisting of a tubular finger-like projection, about 4.1 μm long. Amorphous materials (arrows) are seen in the cytoplasm. The haustorial wall is seen as one densely staining layer. Note the presence of host ER lying parallel to the entire length of the neck. Glt/OsO_4. Ua/Pb. x28,300.

Figure 30. A young haustorium (H) consisting of a tubular finger-like projection. Mitochondria (arrowheads) in the HMC have not migrated through the site of penetration. Note the electron-dense granules (arrows) in the cytoplasm. Glt/OsO_4. PACP. x26,400.

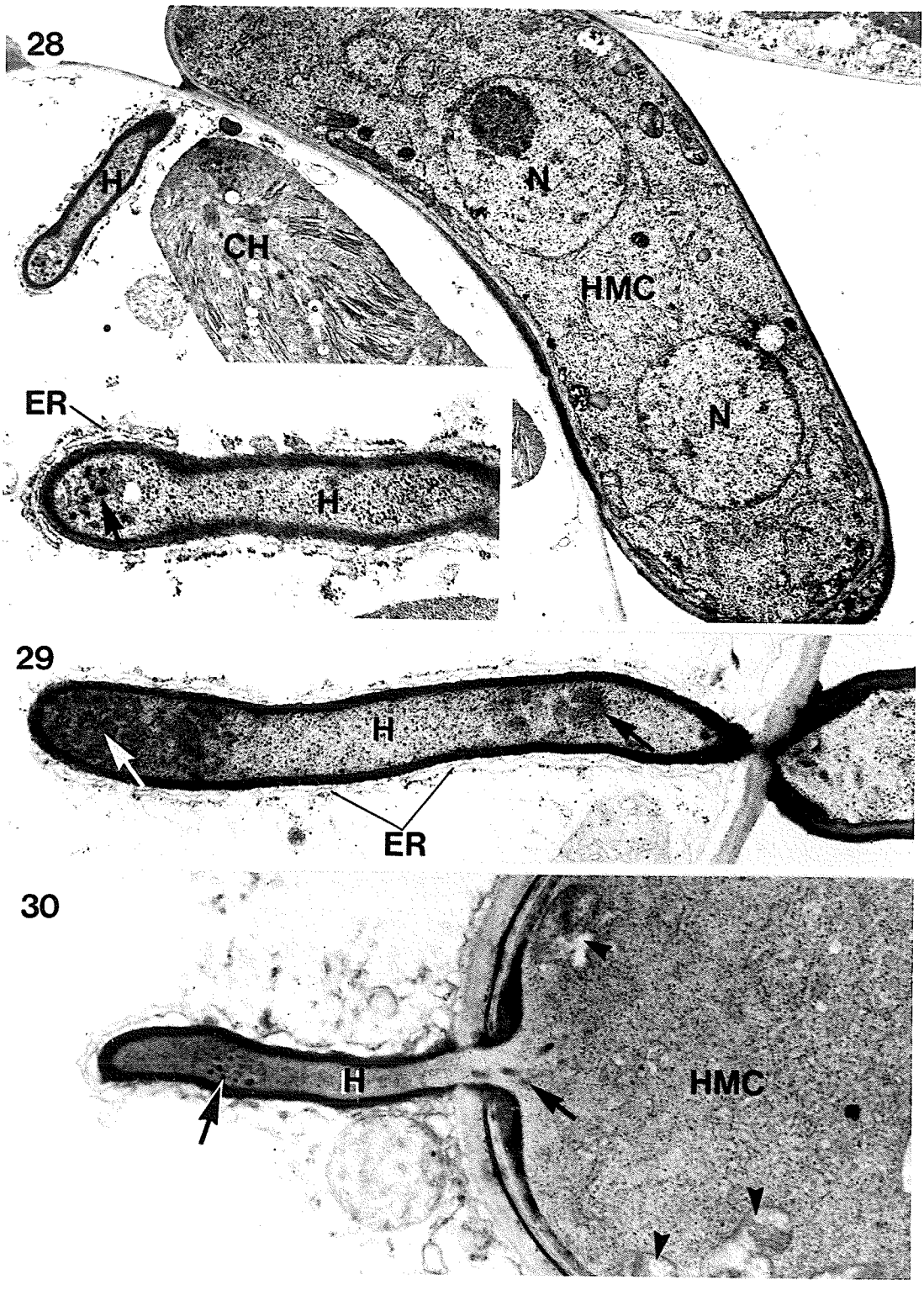
28
H
CH
N
HMC
N
ER
H
29
H
ER
30
H
HMC

LEGEND

Figures 31-34. Young haustorial bodies of P. coronata avenae. Figures 31, 32 and 34 are closely adjacent sections taken from a series of serial sections of the same young haustorium.

Figure 31. A young haustorial body, about 2 μm in diameter, formed at the distal end of the haustorial neck (not seen in this section) is packed with mitochondria. Glt/OsO_4. Ua/Pb. x34,300.

Figure 32. Two moderately-stained layers separated by a middle electron-opaque layer can be seen in the entire neck wall. The invaginated host plasmalemma (arrows) adheres tightly to the entire length of the neck. Glt/OsO_4. Ua/Pb. x66,400.

Figure 33. Same section as in Figure 31 at a higher magnification to show the presence of only one layer making up the haustorial body wall. The IPL separates somewhat near the base (arrow) of the haustorial body to form the extrahaustorial matrix (EM) between the IPL and the body wall. Glt/OsO_4. Ua/Pb. x64,300.

Figure 34. Diffuse electron-opaque material is seen in the EM. Glt/OsO_4. Ua/Pb. x53,600.

Figures 35 and 36. Sections of the neck ring of P. coronata avenae.

Figure 35. A densely stained neck ring (arrows) in the neck wall of a young haustorium. It is located about one-third of the way down the neck (HN) from the haustorial body (HB). Note the presence of host ER (arrowheads) along the HN and HB. Glt/OsO_4. Sections treated with H_2O_2 before Ua/Pb. x25,700.

Figure 36. A neck ring in a mature haustorium. The ring is about 0.38 μm wide. Note the distinction of two bands at the position of the arrows. Both bands are densely stained. Glt/OsO_4. Sections treated with H_2O_2 before staining with Ua/Pb. x37,500.

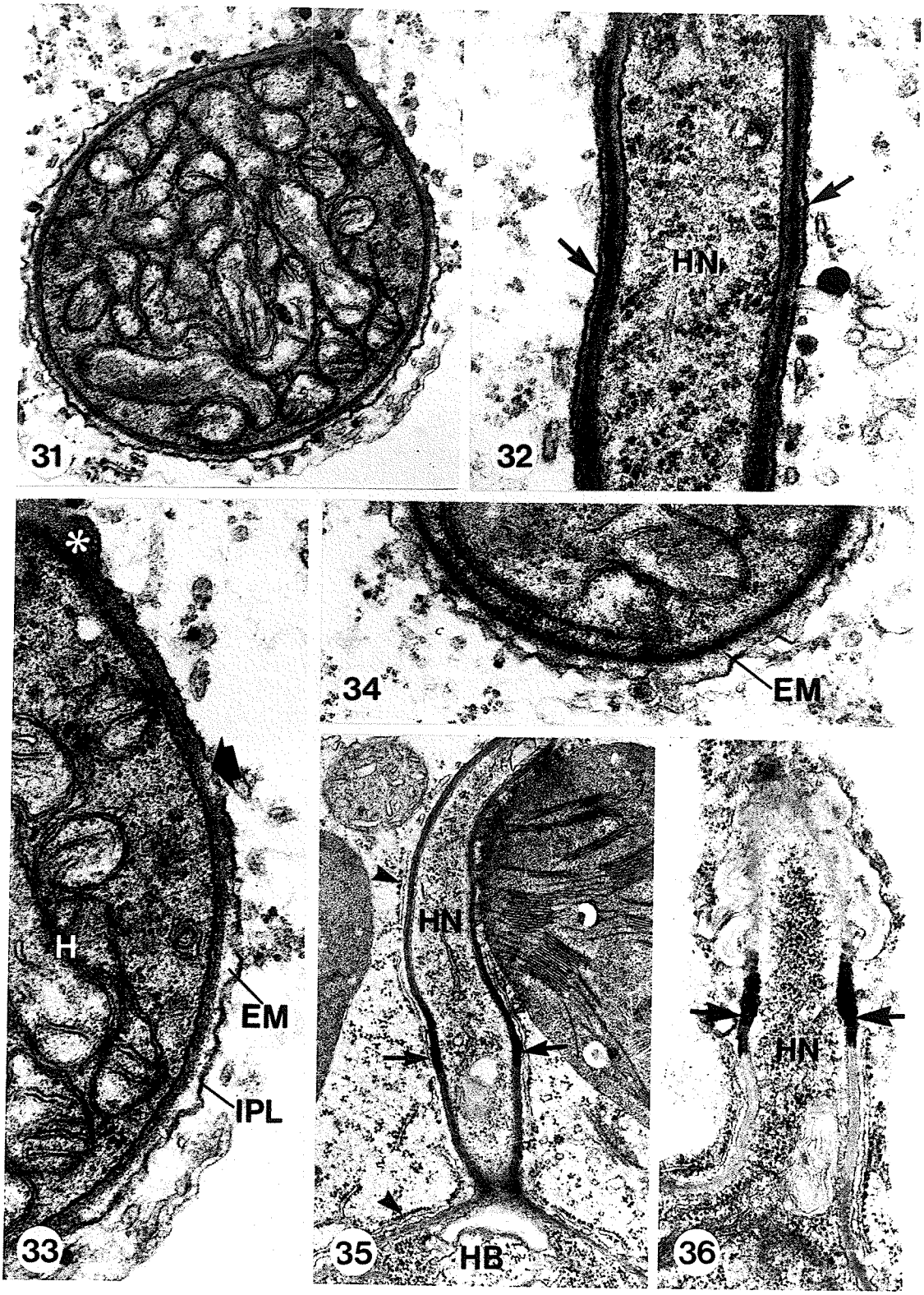
31
32
HN
34
EM
*
H
EM
IPL
33
HN
35
HB
HN
36

LEGEND

Figure 37. Neck ring of P. graminis tritici.

Figure 37. A densely stained neck ring (arrows) in the neck wall of a young haustorium. Glt/$0s0_4$. Ua/Pb. x22,300.

Figures 38-40. Haustorial bodies and extrahaustorial matrix of P. coronata avenae.

Figure 38. Two layers are evident in the body wall (arrow) of a nearly mature haustorium. The outer layer is electron-opaque and the inner layer is moderately stained. Glt/$0s0_4$. Ua/Pb. x27,900.

Figure 39. Diffuse electron-opaque and lightly stained fibrillar materials in the extrahaustorial matrix (EM) of a mature haustorium. Note the massive proliferation of large tubular complexes in the adjacent host cytoplasm. Many of these tubules contain a dense matrix or a dense core. Glt/$0s0_4$. Ua/Pb. x23,600.

Figure 40. Section taken from a serial set to show the increase in thickness of the EM from the proximal end (arrow) to the distal end (open arrow) of a mature haustorium. This haustorium is elongated but curves slightly at the distal end. Mitochondria (M) are located mainly around the periphery of the cell adjacent to the fungal plasmalemma. Glt/$0s0_4$. Ua/Pb. x9,400.

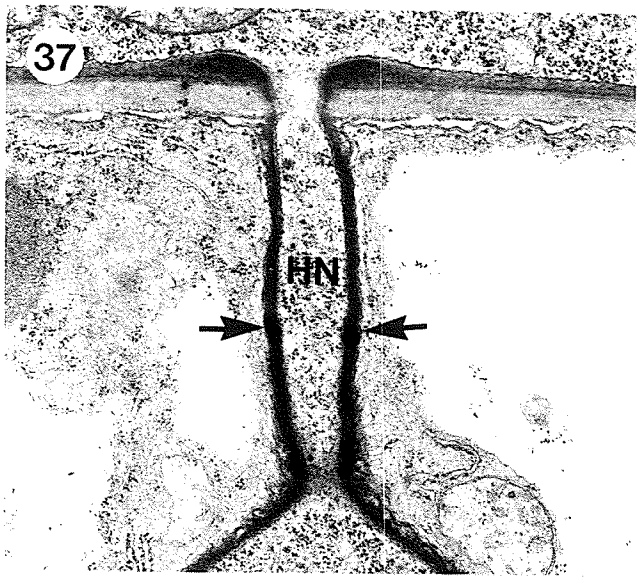
37
HN

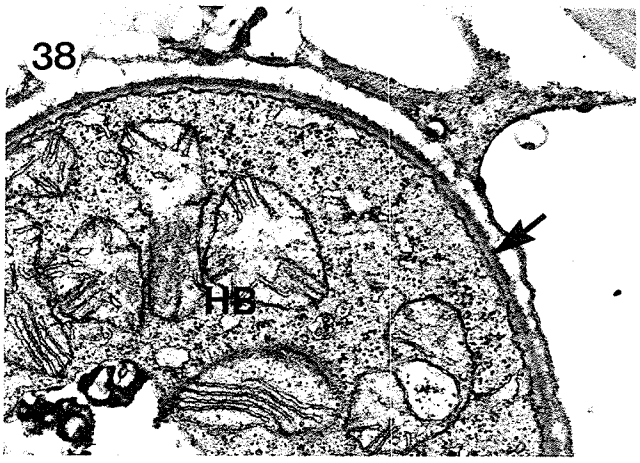
38
HB

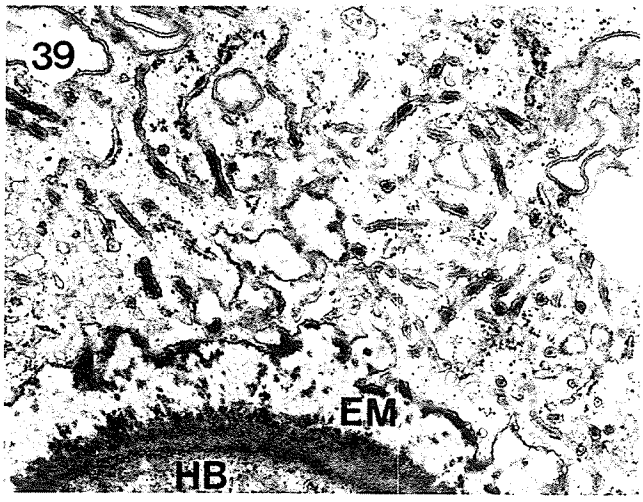
39
EM
HB

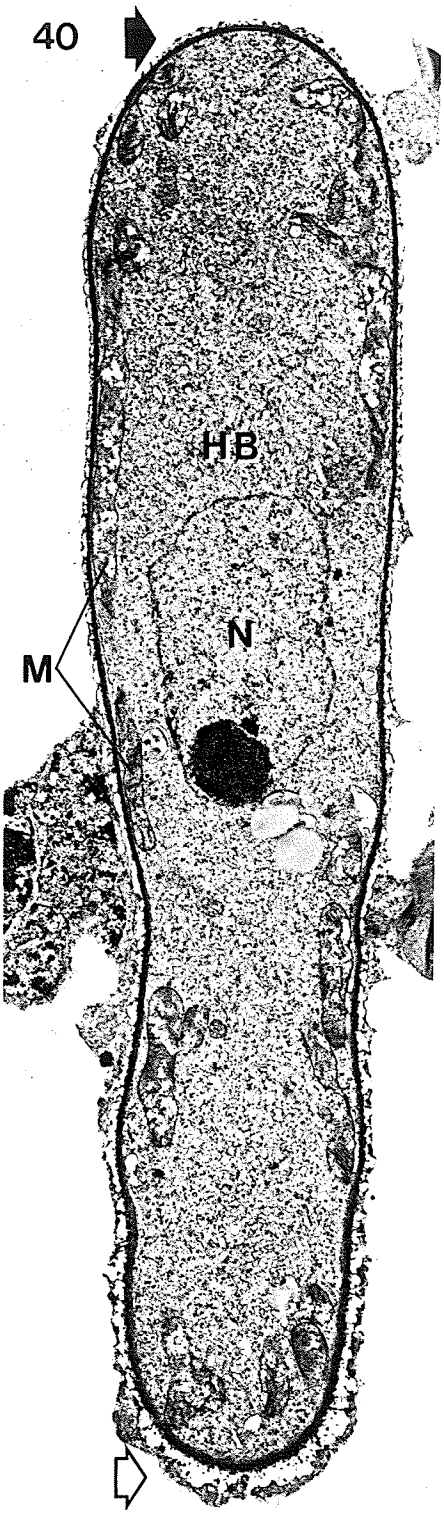
40
HB
N
M

LEGEND

Figures 41-44. The extrahaustorial matrix of P. coronata avenae.

Figure 41. The extrahaustorial matrix (EM) is electron-lucent, and the two-layered haustorial body wall (arrow) is lightly stained. Glt. Ua/Pb. x58,900.

Figure 42. The EM near the distal end of a haustorium is intensely stained. Glt. PA-TCH-SP. x47,100.

Figure 43. The EM at the distal end of a haustorium is intensely stained. Glt. PA-TCH-SP. x58,900.

Figure 44. A near tangential section through a haustorium at the distal region showing abundant stained material in the EM. Glt. PA-TCH-SP. x30,000.

Figure 45. A mature haustorium of P. coronata avenae.

Figure 45. The mature haustorium appears to be branched. In the unbranched portion of the haustorium, mitochondria (M) are located mainly around the periphery of the cell adjacent to the fungal plasmalemma. In the branched portion (lower right) mitochondria appear to be randomly dispersed, due to this portion of the haustorium being sectioned obliquely, as indicated by the more diffuse appearance of the walls (arrows). Glt/OsO_4. Ua/Pb. x10,000.

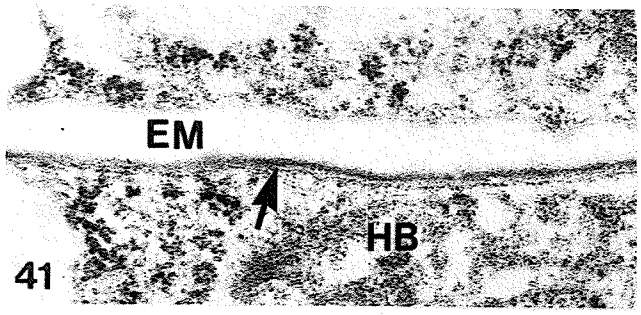

41

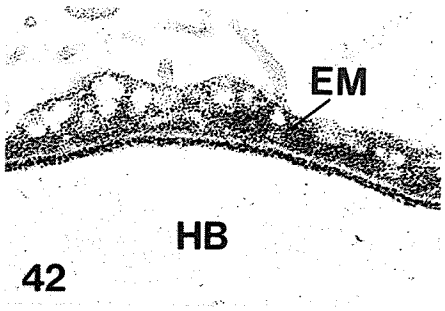

42

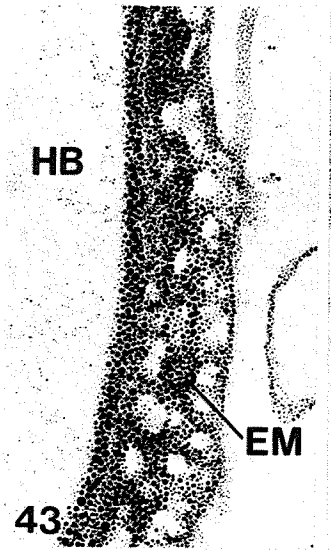

43

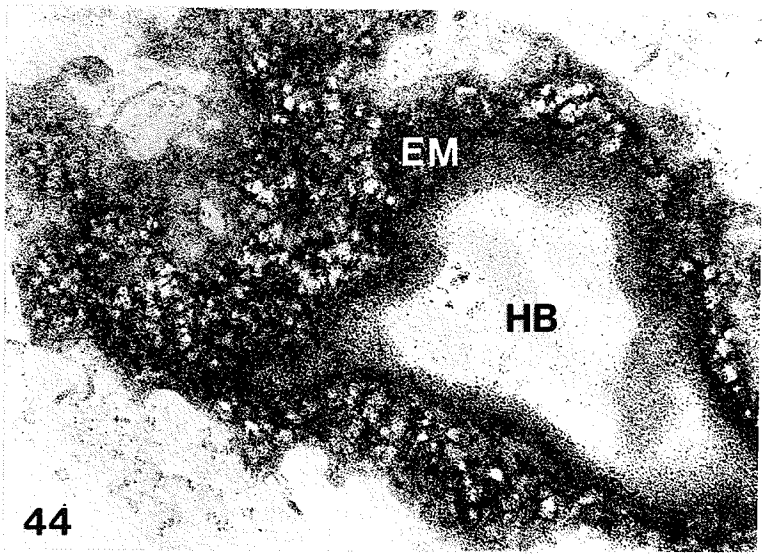

44

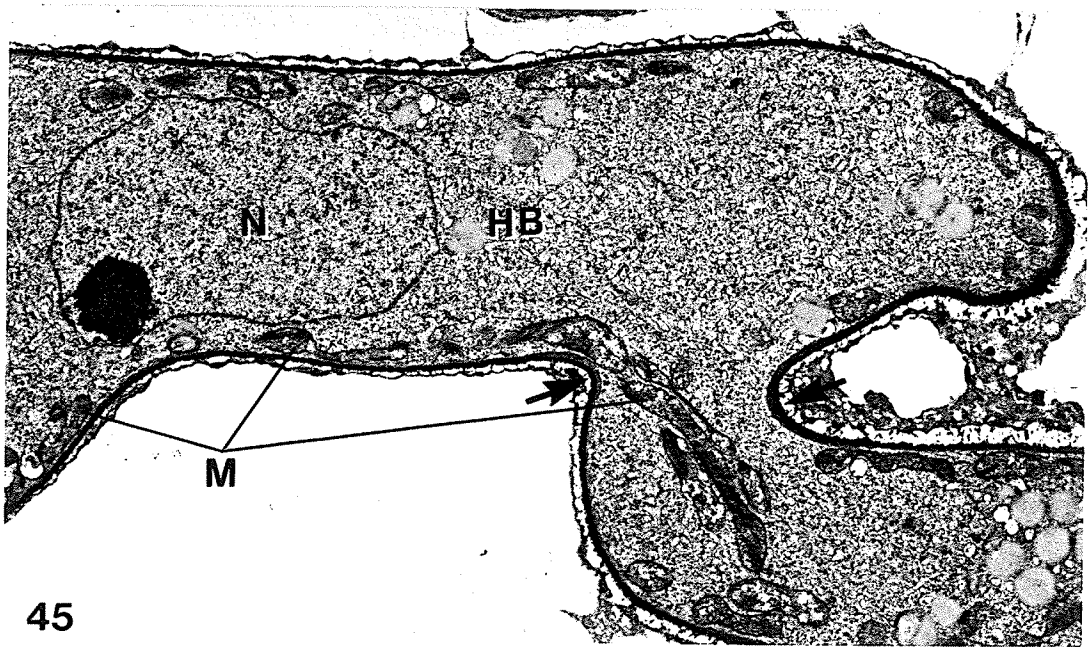

45

LEGEND

Figure 46. Mitochondria in a mature haustorium of P. coronata avenae.

Figure 46. Cross-section of a mature haustorium with mitochondria (M) arranged as a ring around the periphery of the cell. Glt/$0s0_4$. Ua/Pb. x14,100.

Figures 47-50. Aberrant haustoria in urediospore-derived infections of P. coronata avenae.

Figure 47. A small necrotic haustorium, but the HMC still appears healthy. Glt/$0s0_4$. Ua/Pb. x13,600.

Figure 48. A mature necrotic haustorium (H) with an empty and abnormally-shaped HMC (asterisk). The inset shows a higher magnification of the HMC wall. Electron-dense deposits (arrow) normally not found in healthy HMC walls, are found in the wall of this HMC. These electron-dense deposits can be differentiated from the coarsely granular HMC wall stained by the Thiéry method. Glt/$0s0_4$. PA-TCH-SP. x13,100. Inset, x75,000.

Figure 49. A mature necrotic haustorium (H) found in a host cell with normal appearing cytoplasm. Glt/$0s0_4$. Ua/Pb. x5,400.

Figure 50. Aberrant and more normal looking haustoria (H) found within the same host cell. It is not known if the two "haustoria" are lobes of the same haustorium. Note the lack of normal host cytoplasmic components in this cell. Glt/$0s0_4$. Ua/Pb. x12,900.

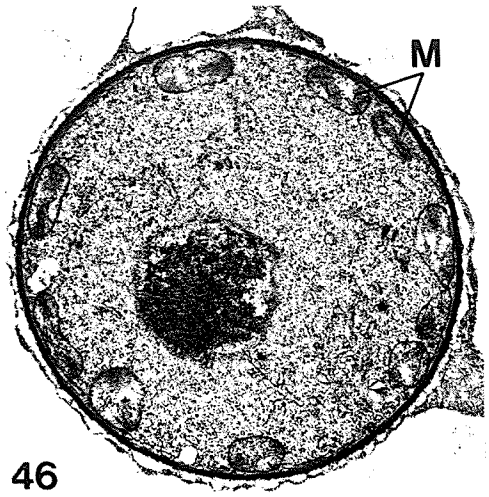

46

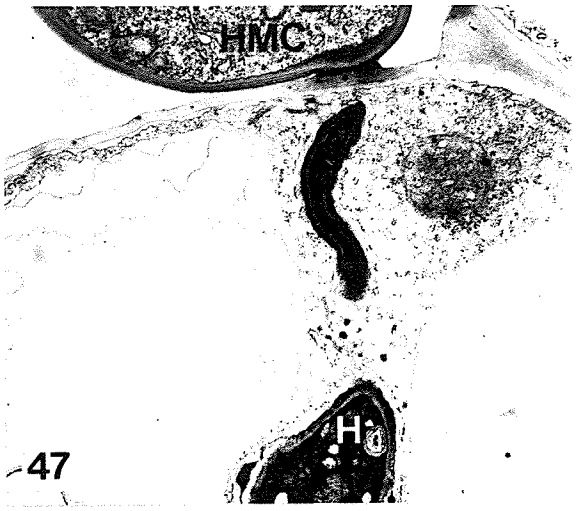

47

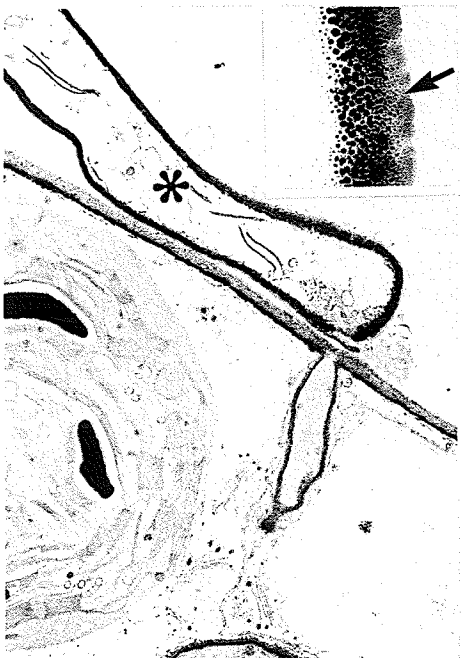

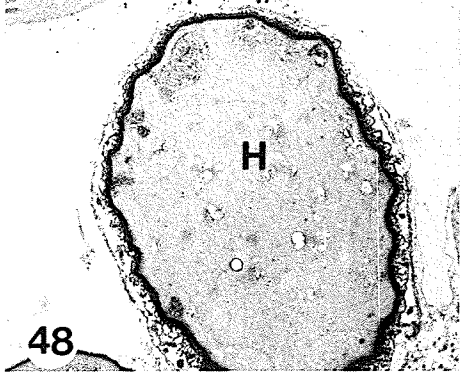

48

49

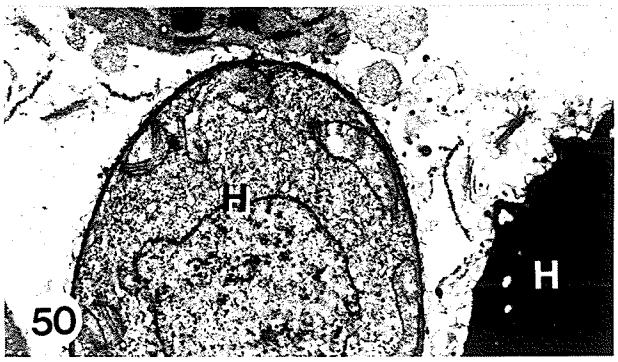

50

LEGEND

Figures 51-55. Membrane protrusions associated with HMC septum in P. coronata avenae.

Figure 51. Longitudinal view of fungal plasma membrane protrusions (arrow) and associated mitochondria (M) on the hyphal side of the HMC septum. Glt/OsO_4. Ua/Pb. x13,700.

Figure 52. Higher magnification of Figure 51 to show the dense matrix (arrows) of the septal protrusions. Glt/OsO_4. Ua/Pb. x39,600.

Figures 53 and 54. Two closely adjacent sections to show the cross-sectional views of membrane protrusions (Fig. 54) and associated mitochondria (Fig. 53) near the HMC septal region. Glt/OsO_4. Ua/Pb. Fig. 53, x27,100. Fig. 54, x23,100.

Figure 55. The protrusion matrix (arrowheads) is largely electron-translucent in glutaraldehyde fixed, unosmicated tissue. Glt. Ua/Pb. x79,500.

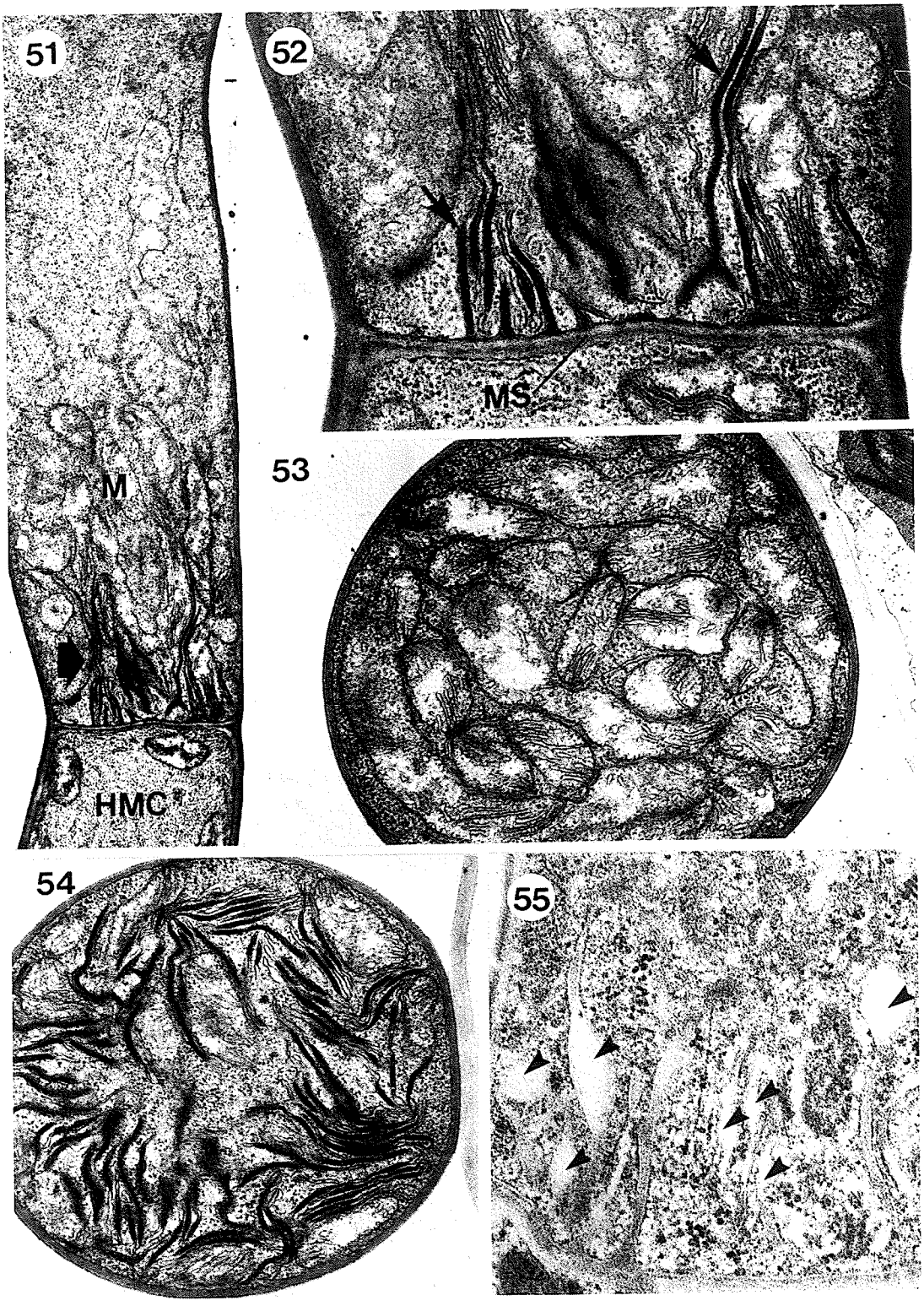
51
M
HMC
52
MS
53
54
55

LEGEND

Figures 56-62. Membrane protrusions and whorls of membranes associated with HMC septum in P. coronata avenae.

Figures 56, 57 and 58. Three serial sections to show the convolution of the membranes at the edges of the protrusions, suggesting that interconnections may occur. The arrow indicates the same membrane protrusion. Membranes of these protrusions have a trilemma structure. Glt/OsO_4. Ua/Pb. All Figures x45,000.

Figure 59. Small membrane protrusions (arrow), about 0.2 μm long, appear on the hyphal side of the HMC septum. Small whorls of membranes (arrowheads) with a trilemma structure, occur in close proximity to the fungal plasma membrane on the HMC side of the septum. Glt/OsO_4. Ua/Pb. x51,600.

Figure 60. Whorls of membranes (asterisks) found on the HMC side of the septum, and the fungal plasmalemma (arrow) are stained densely relative to the mitochondrial (M) membranes. Glt/OsO_4. PACP. x86,700.

Figure 61. Membrane protrusions on the hyphal side of the HMC septum, decreased in size and became angular in shape. This occurred after the finger-like stage of haustorium development, illustrated in Figure 28. Glt/OsO_4. Ua/Pb. x45,300.

Figure 62. Further reduction in size of the membrane protrusions. This occurred as the haustorial body formed at the distal end of the haustorial neck (not shown). Glt/OsO_4. Ua/Pb. x34,300.


56


57


58

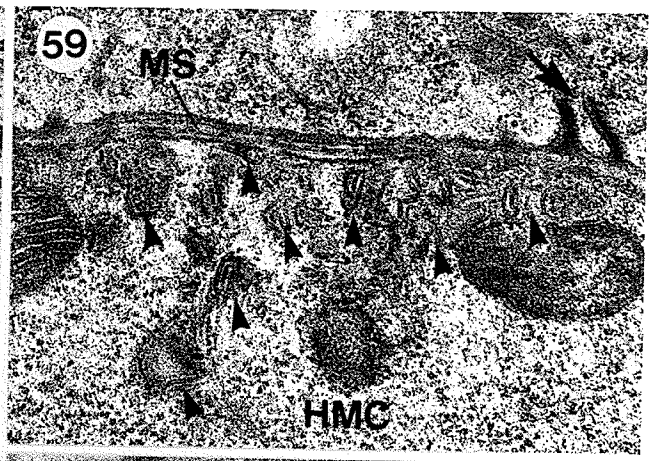
59
MS
HMC

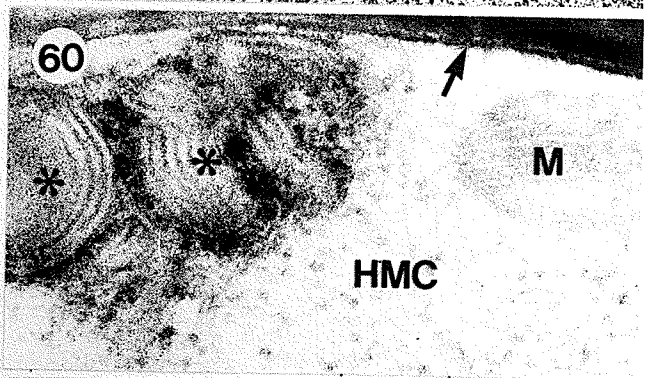
60
M
HMC

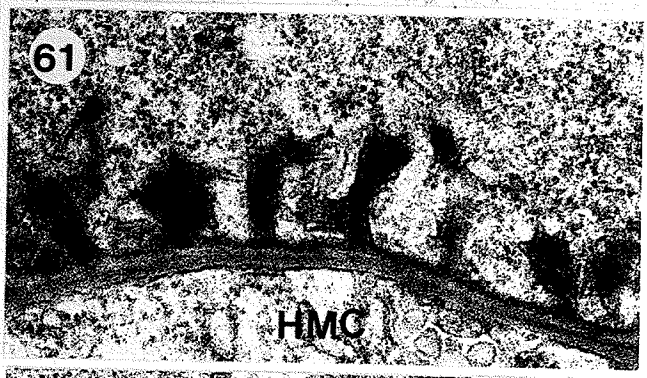
61
HMC

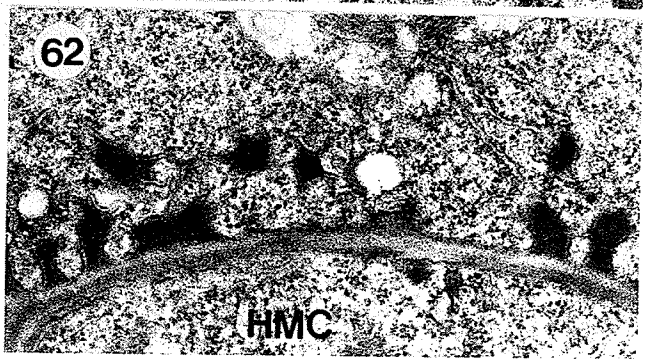
62
HMC

LEGEND

Figures 63-65. Membrane protrusions in P. coronata avenae after haustorium formation.

Figure 63. An oblique section at the hyphal septal region near the HMC septum showing the interconnections of membrane protrusions (arrows). Glt/OsO_4. Ua/Pb. x22,500.

Figure 64. A near cross-sectional view showing the interconnections of membrane protrusions (arrows). Glt/OsO_4. PA-TCH-SP. x35,200.

Figure 65. Membrane-protrusions (arrowheads) as reduced papillae. The HMC is largely vacuolated. Glt/OsO_4. Ua/Pb. x35,200.

Figures 66-68. Septal pore structure of the HMC septum. Figure 66, P. graminis tritici; Figures 67 and 68, P. coronata avenae.

Figure 66. The septal pore is blocked by a pulley-wheel shaped plug of electron-dense material (arrow). Long membrane protrusions (arrowheads) are present on the hyphal side of the HMC septum. Glt. Ua/Pb. x58,600.

Figure 67. An unstained section of the HMC septum after lipid-solvent extraction. The plugging material of the septal pore is electron-dense (arrow). Long membrane protrusions (arrowheads) are present. Glt-acetone-OsO_4. x58,300.

Figure 68. A large open pore (opposing arrows) of the HMC septum which apparently is still in the formative stage. Note the presence of long membrane protrusions (arrowheads). Glt/OsO_4. TCH-SP. x52,900.

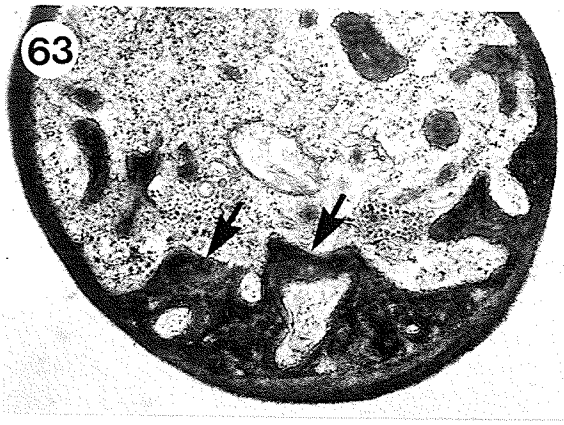
63

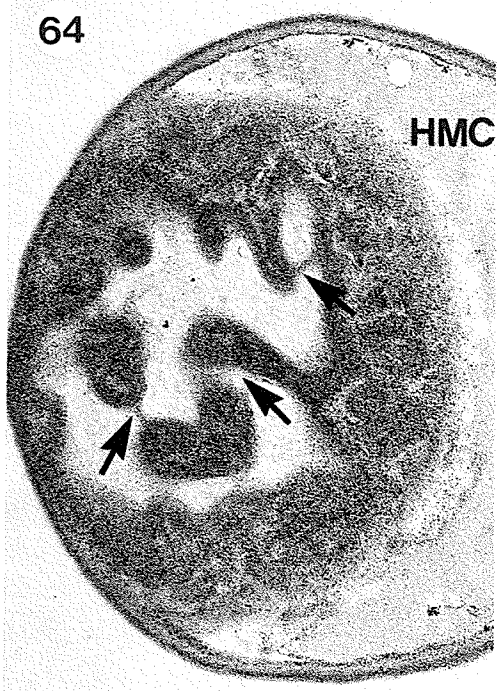
64
HMC

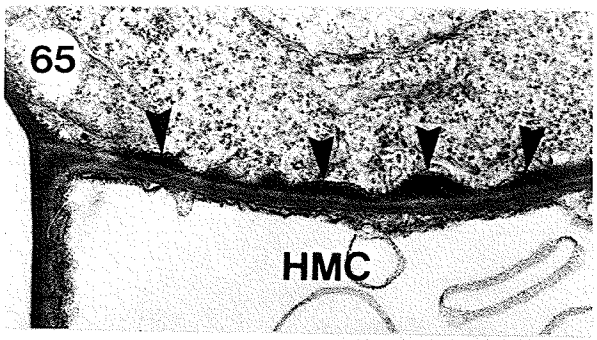
65
HMC

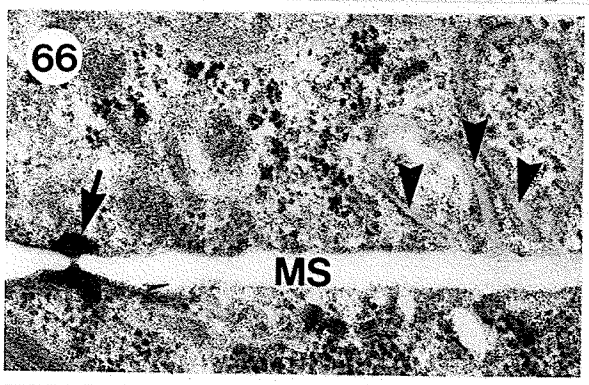
66
MS

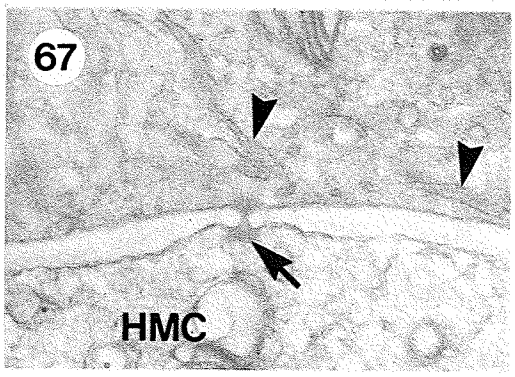
67
HMC

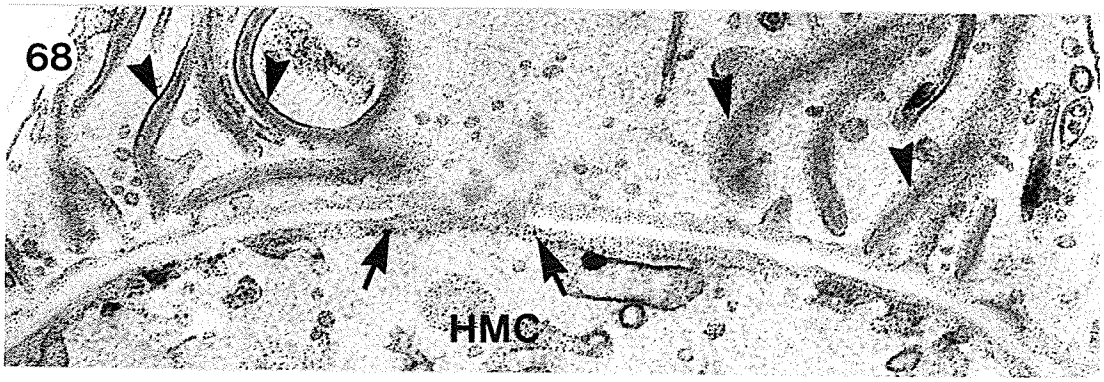
68
HMC

LEGEND

Figures 69, 71-73. Septal pore structure of the HMC septum of *P. coronata avenae*.

Figures 70 and 74. The septal pore structure of a hyphal septum of *P. graminis tritici*.

Figure 69. The septal pore is plugged with an electron-dense material (open arrow) after membrane protrusions had shrunk to the size of small papillae (arrowheads). Glt/OsO_4. Ua/Pb. x77,700.

Figure 70. An electron-dense plug (open arrow) in the pore of the hyphal septum penultimate to the HMC septum. Glt/OsO_4. Ua/Pb. x24,300.

Figures 71-73. Three serial sections showing the small open pore (about 9.5 nm) in Figure 72. The pore is delimited on either side by an irregularly shaped electron-opaque diaphragm (arrows). Glt/OsO_4-$K_3Fe(CN)_6$. Ua/Pb. All Figures x52,900.

Figure 74. Higher magnification of Figure 70 to show the electron-dense plug of the hyphal septal pore. Glt/OsO_4. Ua/Pb. x48,000.

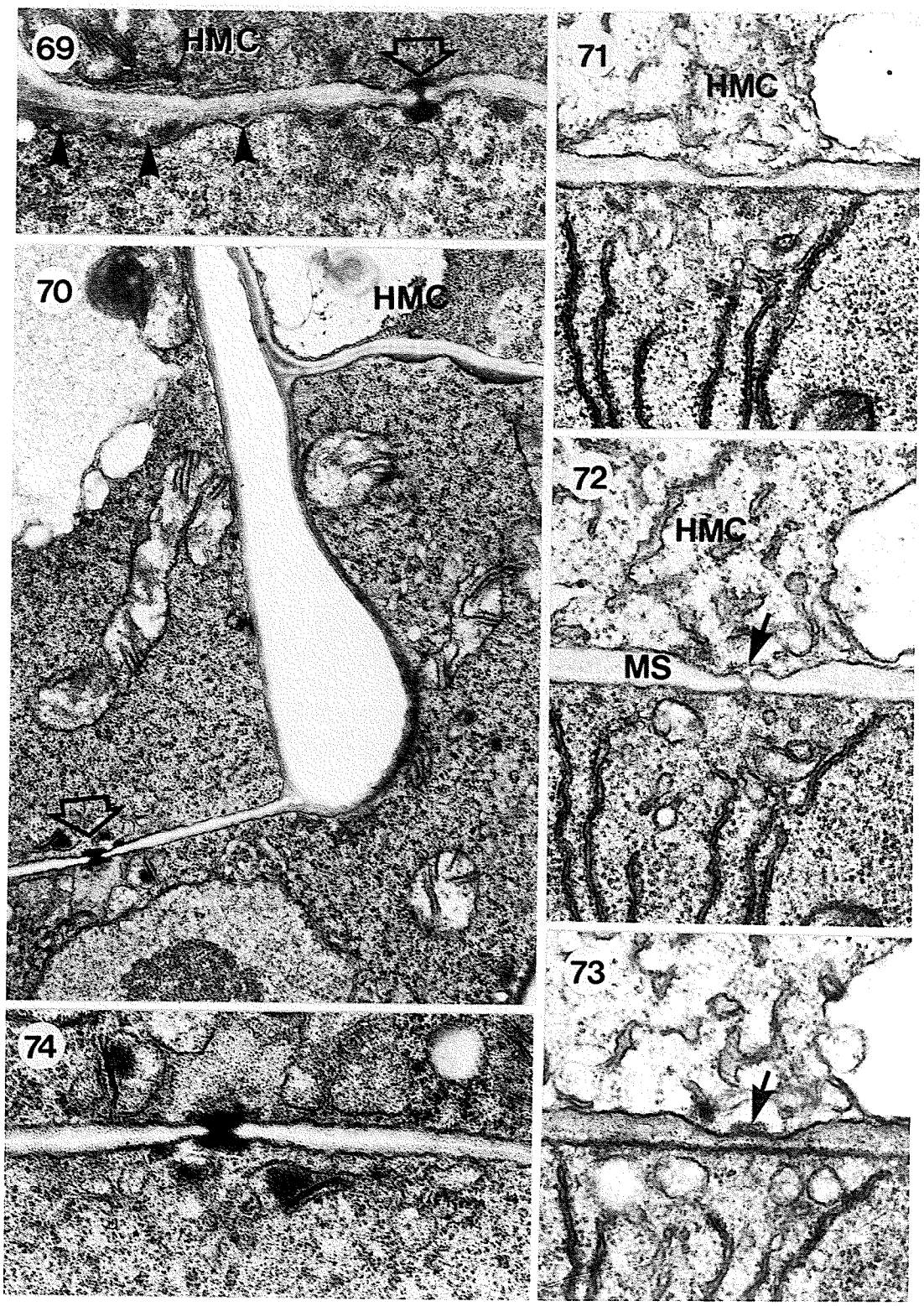
69
HMC
71
HMC
70
HMC
72
HMC
MS
73
74

LEGEND

Figures 75-79. Chloroplasts in the P. coronata infected Avena host.

Figure 75. Thiéry staining of starch granules (SG) in a chloroplast (CH), and the host wall, which is seen as two layers (IL and OL). The OL is finely granular and the IL is coarsely granular. The fungal wall (arrow) is intensely stained. Plastoglobuli (arrowheads) are unstained, and thylakoid membranes are lightly stained. Glt/OsO_4. PA-TCH-SP. x26,800.

Figure 76. Host wall (CW) and starch granules (SG) not stained in a control treatment where sodium borohydride was used. Glt/OsO_4. PA-sodium borohydride-TCH-SP. x20,000.

Figure 77. Plastoglobuli (arrowheads) and thylakoid membranes are intensely stained but the starch granules (SG), host wall (CW) and fungal wall (arrow) are largely unstained in a control treatment in which periodate oxidation had been omitted. Glt/OsO_4. TCH-SP. x37,500.

Figure 78. No silver deposits observed in starch granules (SG). The staining of thylakoid membranes and plastoglobuli is due to their osmiphilia. Glt/OsO_4. SP. x51,800.

Figure 79. Starch granules not stained when periodate oxidation was replaced by hydrogen peroxide treatment. Glt/OsO_4. H_2O_2-TCH-SP. x41,000.

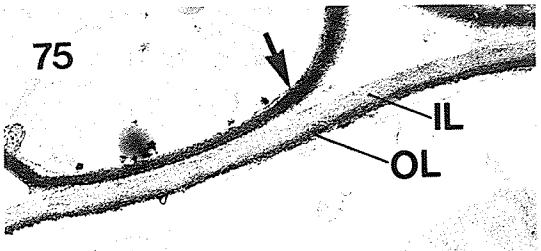
75
IL
OL

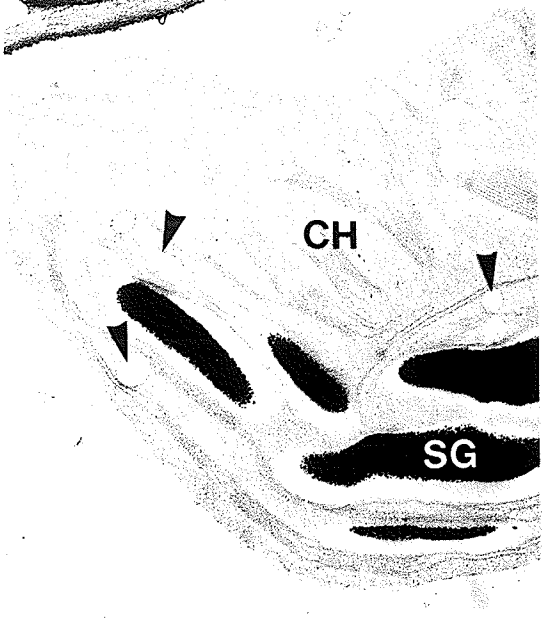
CH
SG

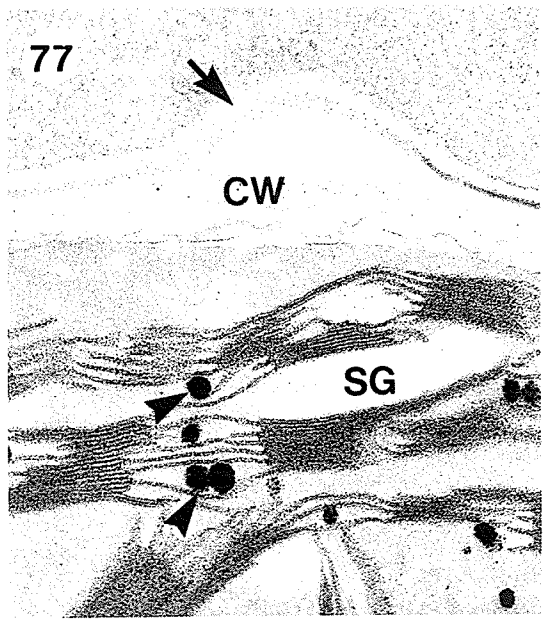
77
CW
SG


76
CW

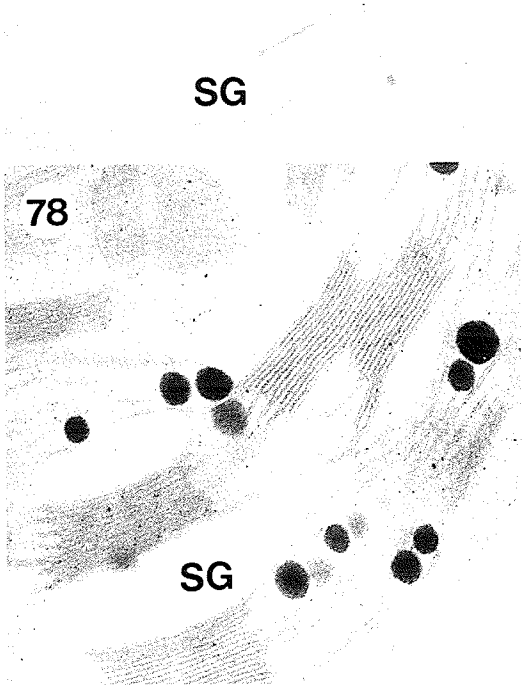
SG
78
SG


79
SG

LEGEND

Figures 80-82. Glycogen granules in P. coronata avenae.

Figure 80. Thiéry staining of glycogen granules (G). Glt/OsO_4. PA-TCH-SP. x32,100.

Figure 81. Glycogen granules (G) not stained in a control treatment. Glt/OsO_4. PA-sodium borohydride-TCH-SP. x24,000.

Figure 82. Glycogen granules (G) largely unstained in a control treatment. Glt/OsO_4. TCH-SP. x35,000.

Figures 83-85. Tissue of P. coronata avenae fixed by the de Bruijn method.

Figure 83. Glycogen granules (arrows) and membranes are electron-opaque. Protrusion matrix (arrowheads), HMC septum and HMC wall are moderately electron-lucent. Glt/OsO_4-$K_3Fe(CN)_6$. Unstained section. x26,400.

Figure 84. Glycogen granules (arrow) are electron-opaque, as well as lipid and membranes. Glt/OsO_4-$K_3Fe(CN)_6$. Unstained section. x37,700.

Figure 85. Haustorial neck wall (arrow) and body wall (arrowhead) are largely electron-lucent. Membranes are more electron-opaque. Glt/OsO_4-$K_3Fe(CN)_6$. Unstained section. x39,600.

Figures 86-87. Osmiophilia of fungal structures.

Figure 86. Protrusion matrix (arrowheads) is moderately electron-dense but not the hyphal wall (arrow). Glt/OsO_4. Unstained section. x41,300.

Figure 87. Oblique section of part of the haustorial neck (HN) and neck ring (asterisk). Neck walls (arrows) are electron-dense. Glt/OsO_4. Unstained section. x48,600.

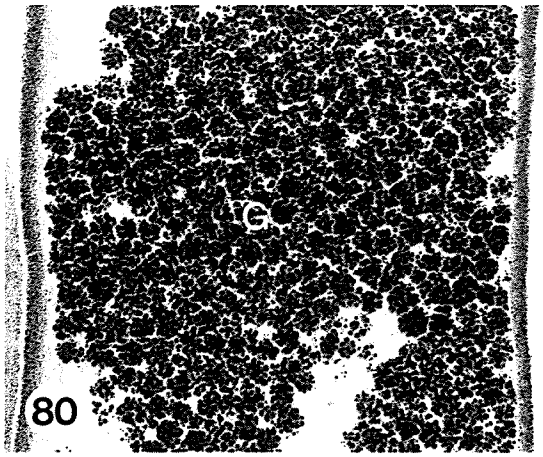
G
80

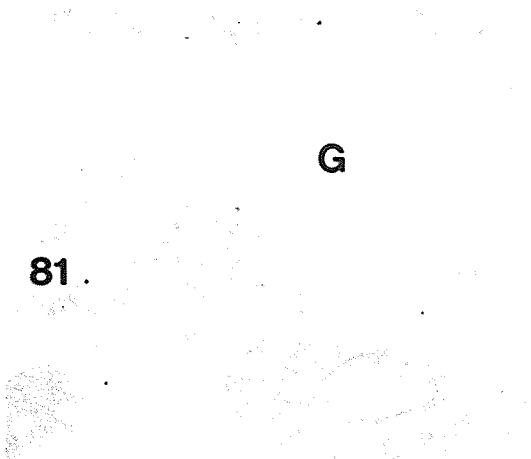
G
81

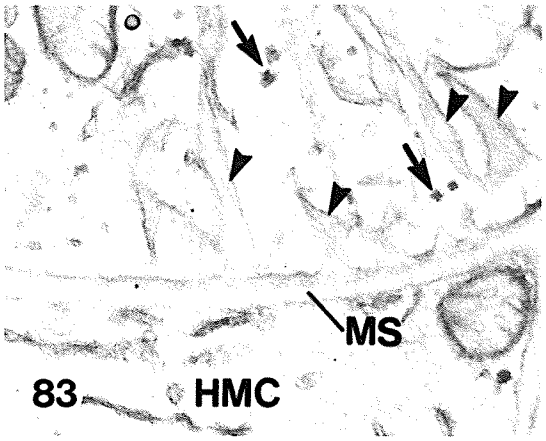
MS
83
HMC

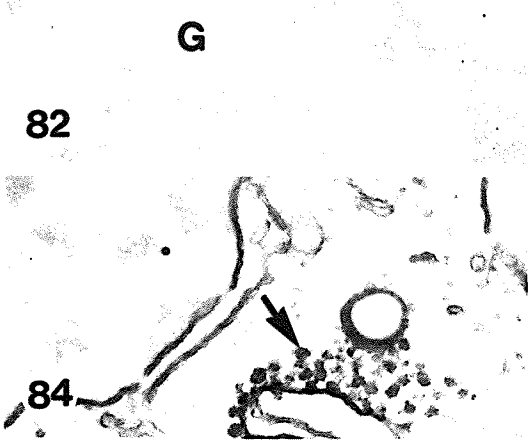
G
82
84

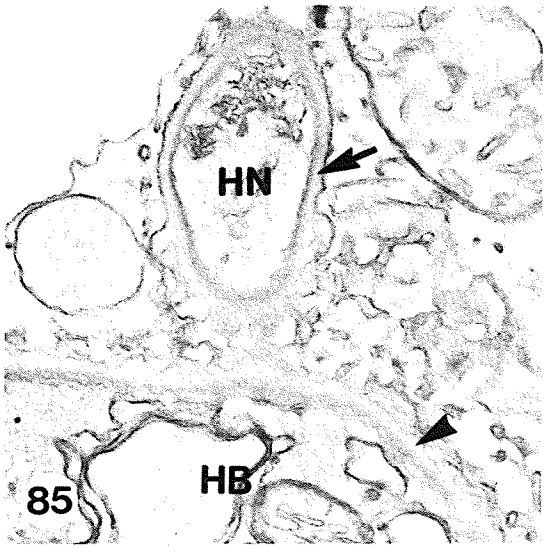
HN
HB
85

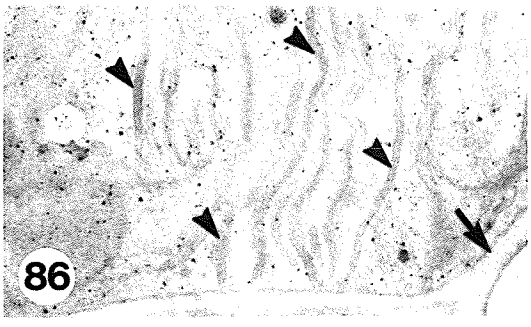
86

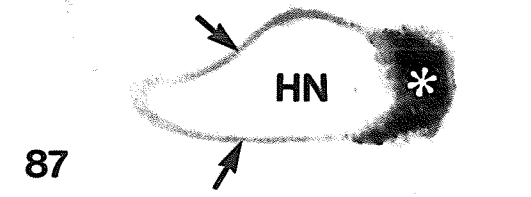
HN
*
87

LEGEND

Figures 88-90. Thiéry staining of fungal walls and/or the protrusion matrix in P. coronata avenae.

Figure 88. The protrusion matrix (arrowheads) and fungal walls (arrows) are intensely stained. Mitochondria (M) are weakly stained. Glt/OsO_4. PA-TCH-SP. x31,250.

Figure 89. The haustorial neck wall showing a thin, densely stained inner layer (IL) and a thick, lighter stained outer layer (OL). Glt/OsO_4. PA-TCH-SP. x62,500.

Figure 90. The two layers (IL and OL) are continuous around the haustorial body (HB). Glt/OsO_4. PA-TCH-SP. x60,700.

Figures 91-93. Controls for the PA-TCH-SP treatment; P. coronata avenae.

Figure 91. Mycelial wall (arrow) unstained in the control treatment. Glt/OsO_4. H_2O_2-TCH-SP. x29,100.

Figure 92. The HMC wall (arrows) and host wall (CW) unstained in the control treatment. Membranes, and a layer of extracellular substance (arrowheads) between HMC wall and CW are stained. Glt/OsO_4. TCH-SP. x52,900.

Figure 93. The HMC septum and protrusion matrix (arrowheads) unstained in the control treatment. Glt/OsO_4. PA-sodium borohydride-TCH-SP. x36,400.

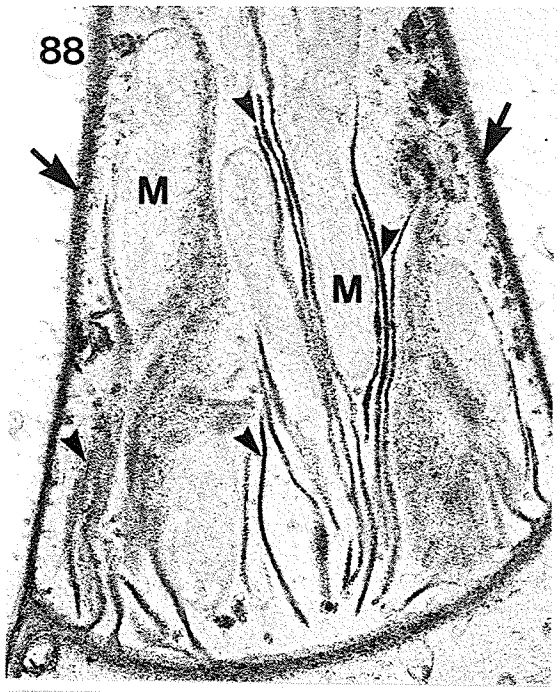
88
M
M

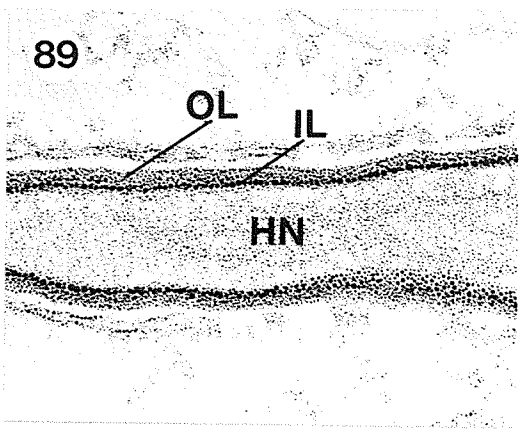
89
OL
IL
HN

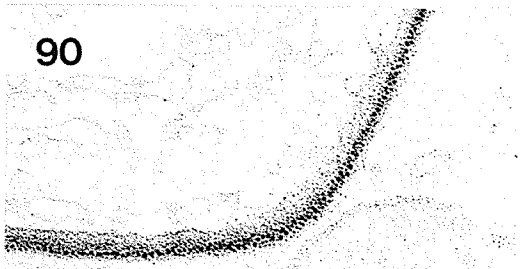
90


91

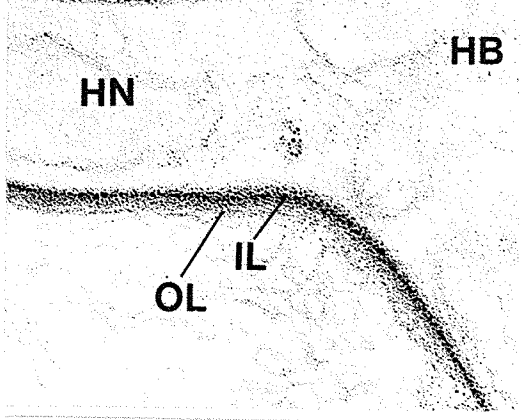
HB
HN
IL
OL

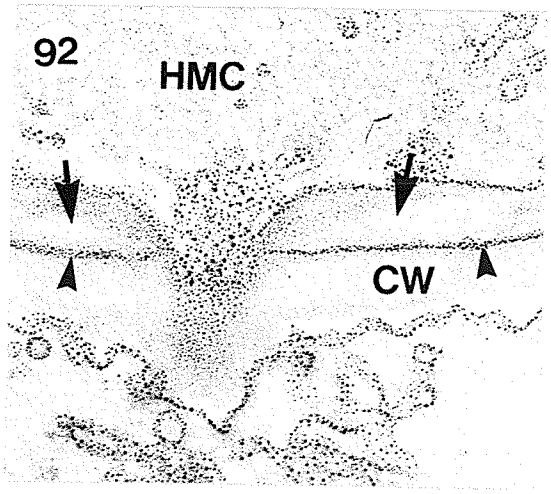
92
HMC
CW

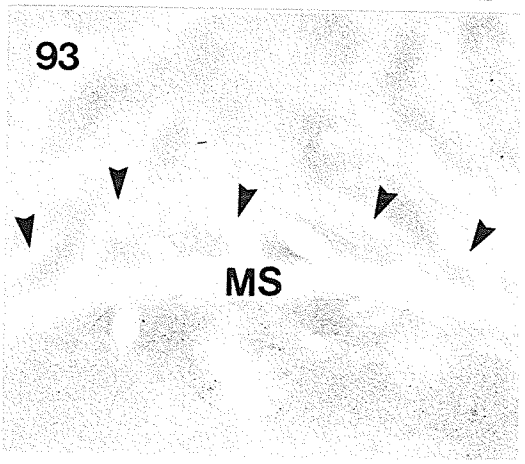
93
MS

LEGEND

Figures 94-99. Controls for the PA-TCH-SP treatments; P. coronata avenae.

Figures 94 and 95. Protrusion matrix (arrowheads) and membranes are intensely stained in the control treatment. The HMC septum is largely unstained. Glt/OsO_4. TCH-SP. Figure 94, x57,100. Figure 95, x50,000.

Figure 96. The haustorial neck wall (arrows) is intensely stained in the control treatment. Glt/OsO_4. TCH-SP. x34,000.

Figure 97. The haustorial body wall (arrowhead) is intensely stained in the control treatment, and is continuous with the neck wall (arrow). Glt/OsO_4. TCH-SP. x68,600.

Figure 98. No silver deposits in the haustorial wall (arrows). Glt/OsO_4. SP. x57,100.

Figure 99. Plastoglobuli and thylakoid membranes in a chloroplast of the Avena host are electron-dense due to their osmiophilia. Glt/OsO_4. Unstained section. x26,800.

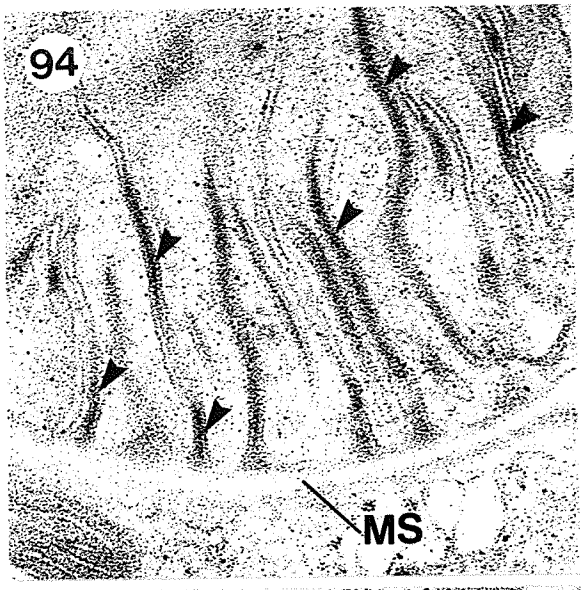
94
MS

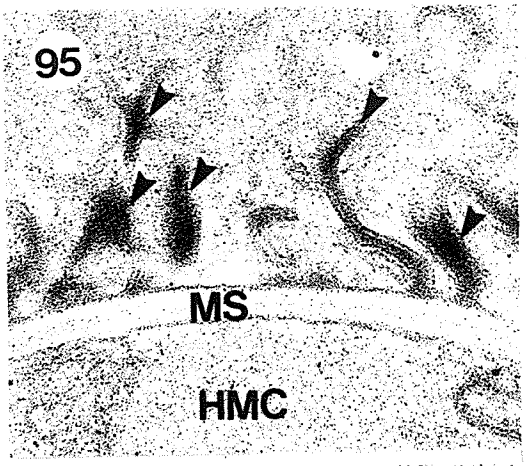
95
MS
HMC

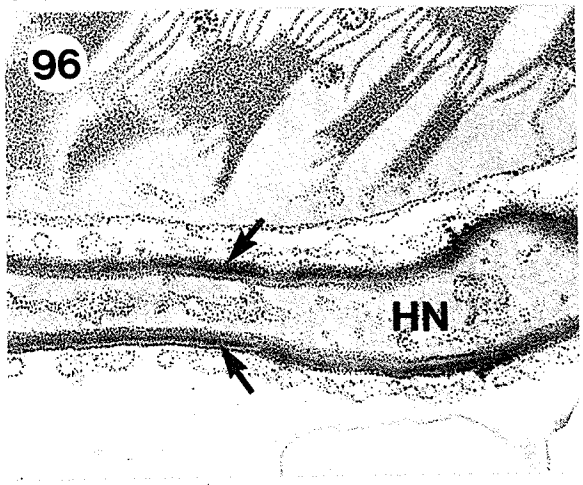
96
HN

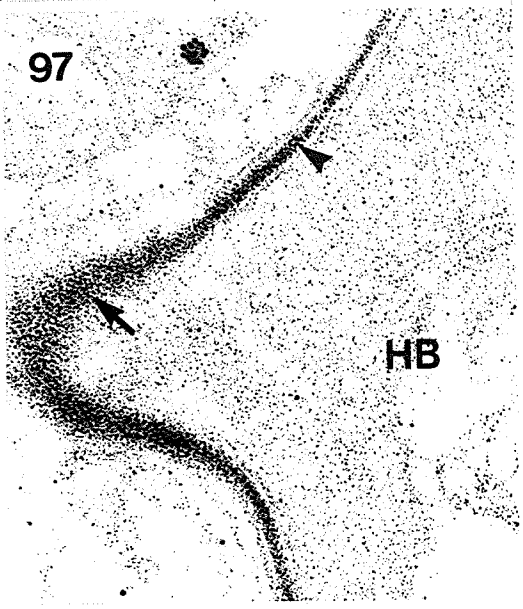
97
HB

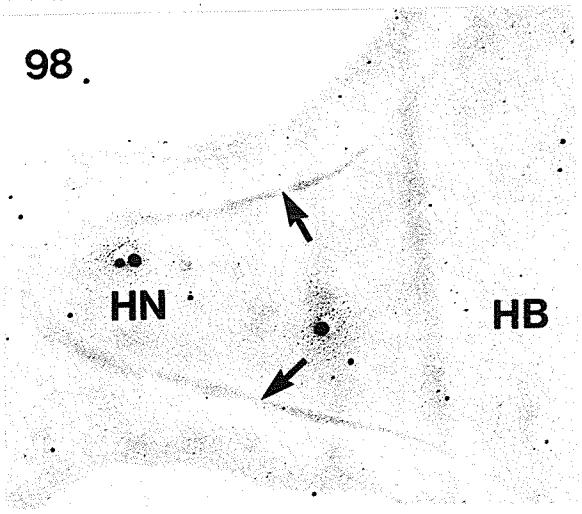
98
HN
HB

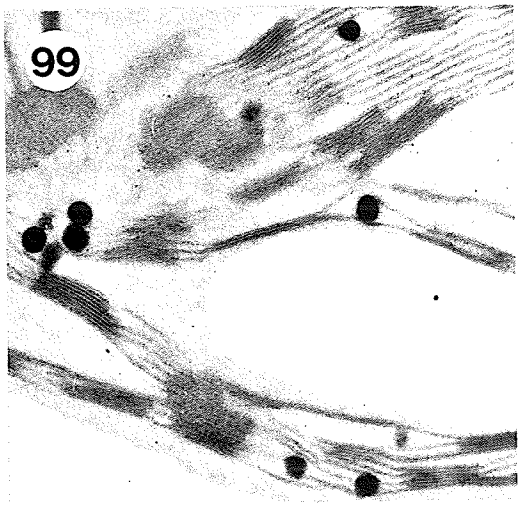
99

LEGEND

Figures 100-101. Thiéry staining of fungal walls and/or the protrusion matrix in P. coronata avenae.

Figure 100. The protrusion matrix (arrowheads), fungal wall (arrows) and HMC septum are stained. Glt. PA-TCH-SP. x44,900.

Figure 101. An oblique section of part of a haustorial neck (HN). The neck wall contains two layers (IL and OL); a thin, densely stained IL and a thick, lightly stained OL. Glt. PA-TCH-SP. x70,700.

Figures 102-103. The control treatment for the Thiéry stain of fungal walls and/or the protrusion matrix in P. coronata avenae.

Figure 102. The protrusion matrix (arrowheads) and HMC septum are unstained. Glt. TCH-SP. x42,900.

Figure 103. The haustorial neck wall (arrows) is largely unstained. The neck ring (open arrow) is electron-opaque. Glt. TCH-SP. x28,300.

Figures 104-105. Chloroplasts in the P. coronata-infected Avena host.

Figure 104. Plastoglobuli (arrowheads) unstained in the control treatment. Glt. TCH-SP. x50,000.

Figure 105. Plastoglobuli (arrowheads) unstained in the control treatment. Glt. Ua/Pb. x25,000.


100
MS

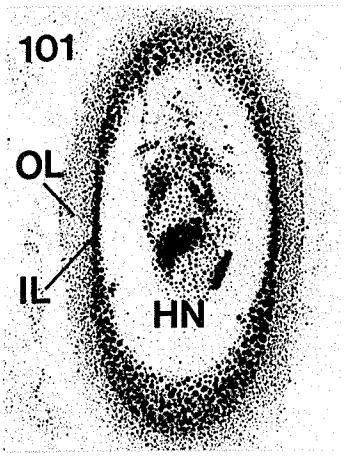
101
OL
IL
HN

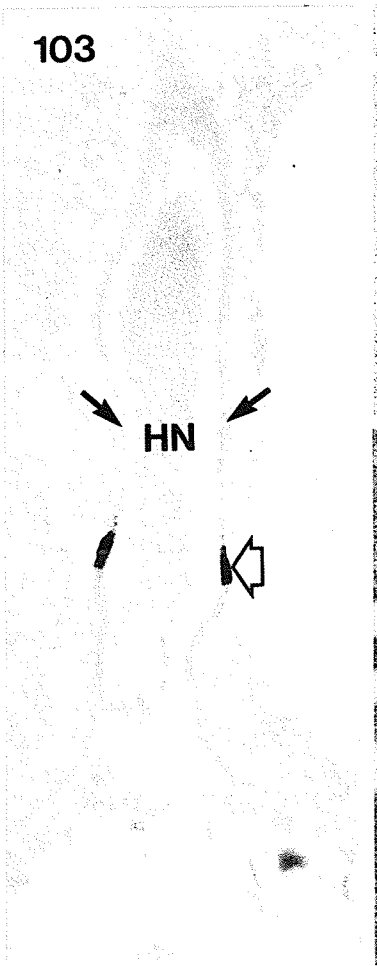
103
HN


104

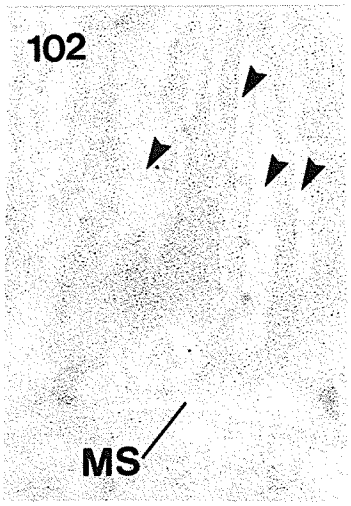
102
MS

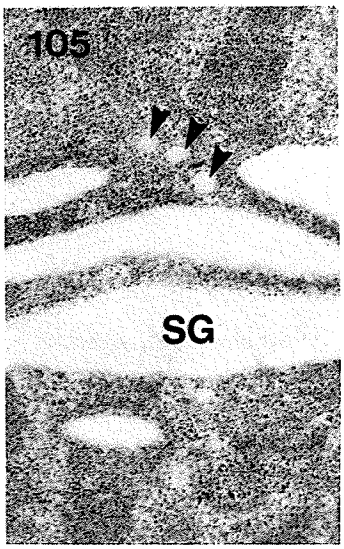
105
SG

LEGEND

Figures 106-113. P. coronata avenae and/or Avena host cells after lipid solvent extraction.

Figure 106. The haustorial neck wall (arrowheads) is largely unstained in the control treatment after extraction. Glt-acetone-OsO_4. TCH-SP. x50,000.

Figure 107. The protrusion matrix (arrowheads) is largely unstained in the control treatment after extraction. Glt-acetone-OsO_4. TCH-SP. x60,000.

Figure 108. The plastoglobuli (arrowheads) are unstained in the control treatment after extraction. Glt-acetone-OsO_4. TCH-SP. x50,000.

Figure 109. The plastoglobuli are electron-lucent after extraction. Glt-acetone-OsO_4. Ua/Pb. x25,000.

Figure 110. The haustorial neck walls (arrows) are lightly stained after extraction as compared to that in Figure 32. The neck ring (open arrow) is intensely stained. Glt-ether/ethanol-OsO_4. Ua/Pb. x38,900.

Figure 111. The protrusion matrix (arrowheads) and the HMC septum are lighter stained after extraction as compared to that in Figure 52. Glt-acetone-OsO_4. Ua/Pb. x47,500.

Figure 112. Thiéry staining of the protrusion matrix (arrowheads) after extraction. Staining intensity is reduced as compared to that in Figure 88. Glt-acetone-OsO_4. PA-TCH-SP. x40,000.

Figure 113. Thiéry staining of the haustorial neck wall (opposing arrows) after extraction. Staining intensity is reduced as compared to that in Figure 89. The host wall (CW) and HMC wall appear to be unaffected. Glt-chloroform/methanol-OsO_4. PA-TCH-SP. x45,700.

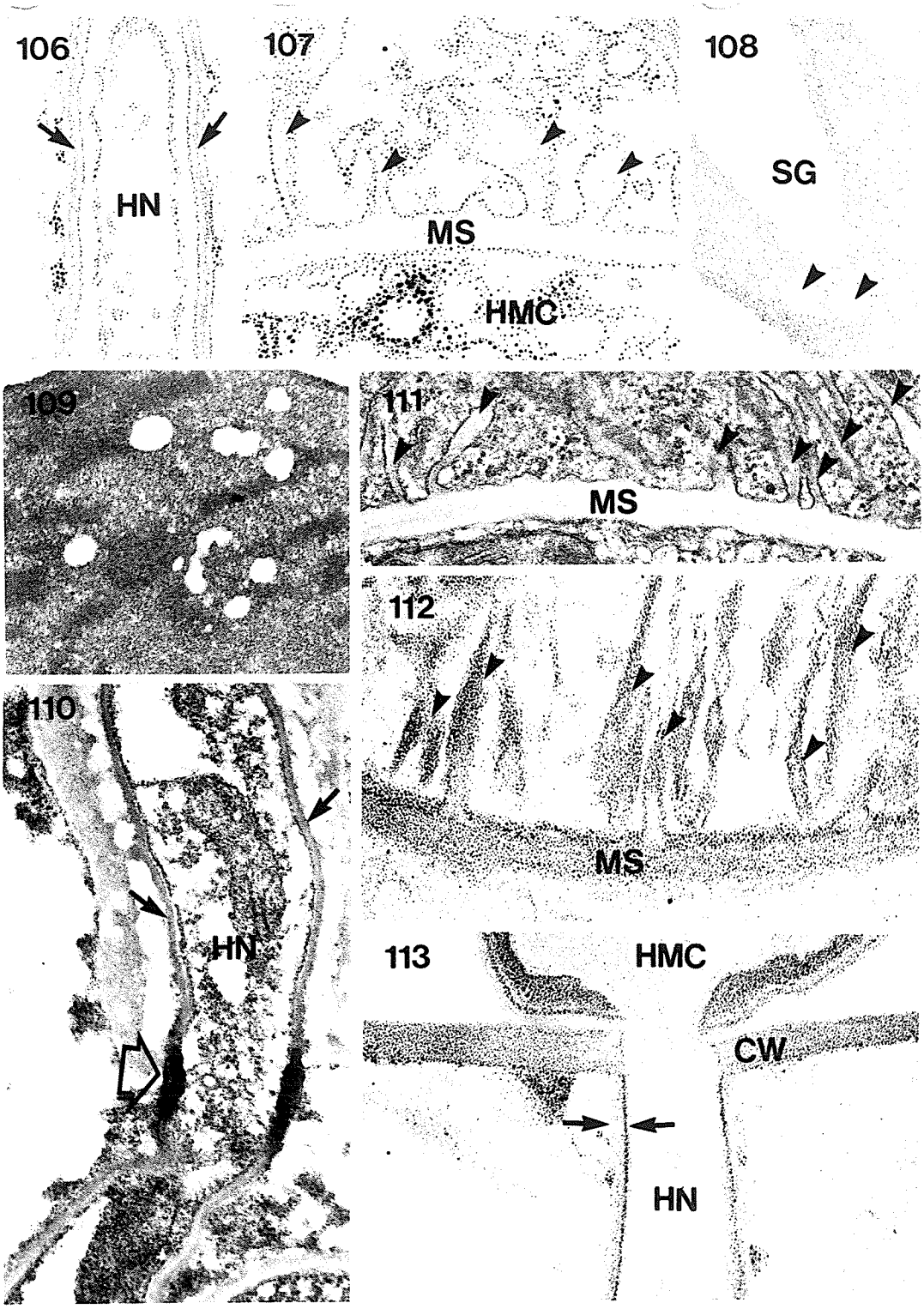
106
HN
107
MS
HMC
108
SG
109
111
MS
112
MS
110
HN
113
HMC
CW
HN

LEGEND

Figures 114-118. The Avena host cell (Fig. 114) and P. coronata avenae (Figs. 115-118) after protease treatment.

Figure 114. The host cytoplasm is eroded after treatment. Structural integrity of the chloroplast (CH) is markedly affected, but plastoglobuli remain electron-opaque. The host walls (CW) appear to be little affected. Glt-protease-OsO_4. Ua/Pb. x21,700.

Figure 115. The protrusion matrix (arrowheads) is largely electron-lucent after treatment with 1 mg/ml conc. of protease in buffer. Glt-protease-OsO_4. Ua/Pb. x34,000.

Figure 116. Extensive disruption of the septal protrusion occurred with 5 mg of protease/ml of buffer, but membrane structures delimiting the protrusions are still visible (arrows). Glt-protease-OsO_4. Ua/Pb. x55,400.

Figure 117. The HMC wall (arrow) is more fibrillar and less discrete after treatment than that in Figure 11. Glt-protease-OsO_4. Ua/Pb. x66,400.

Figure 118. Thiéry staining of fungal walls (arrows) and the HMC septum after treatment. Glt-protease-OsO_4. PA-TCH-SP. x28,300.

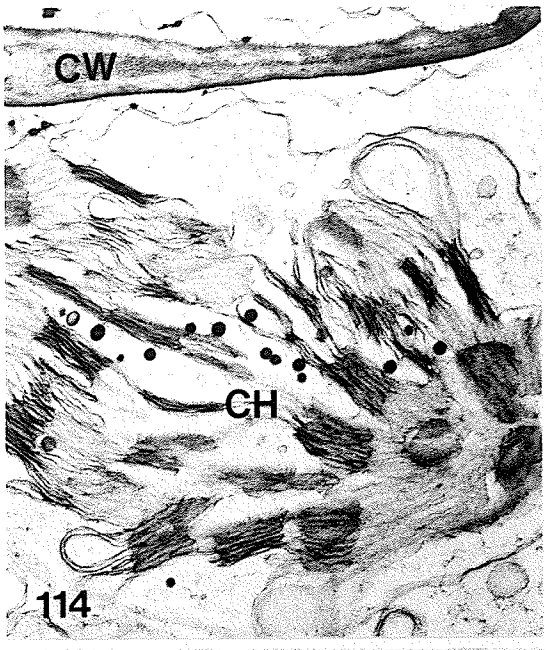
CW
CH
114


116


HMC
115

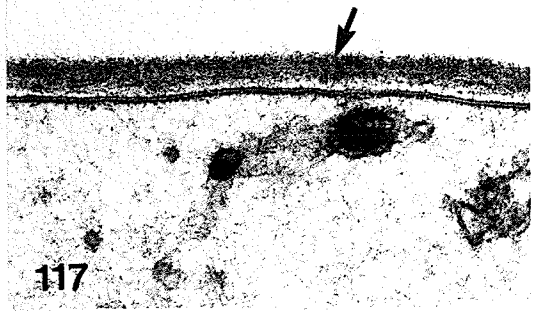
117

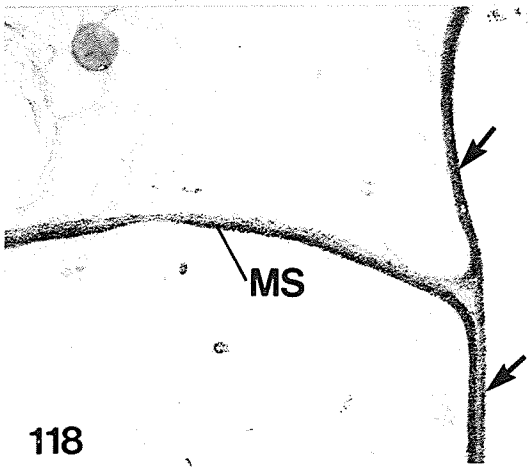
MS
118

LEGEND

Figures 119-123. Tissue of P. coronata avenae after protease treatment.

Figure 119. The haustorial neck wall (arrows) of a mature haustorium is electron-lucent after treatment, but the neck ring is unaffected, and is in its usual position along the haustorial neck. The neck wall (arrowhead) distal to the neck ring is more resistant to protease. Note separation of the HMC from its haustorium. Inset shows the presence of both bands (arrowheads) of the neck ring. A thin layer of fungal wall material still remains on the neck (arrow). Glt-protease-OsO_4. Ua/Pb. x31,100.

Figure 120. The haustorial body wall of a young haustorium is largely extracted, leaving a thin layer (arrow) which is continuous with that along the neck. Glt-protease-OsO_4. Ua/Pb. x58,900.

Figure 121. The haustorial body wall (arrow) of a mature haustorium is more resistant to protease than a young haustorium as shown in Figure 120. Glt-protease-OsO_4. Ua/Pb. x29,100.

Figure 122. Thiéry staining of the remaining wall material (arrow) of a young haustorium after protease treatment. Glt-protease-OsO_4. PA-TCH-SP. x42,900.

Figure 123. The TCH-SP type of staining is absent in the haustorial neck wall (arrows) after treatment. Note separation of the HMC from its haustorium, and leakage of cytoplasm from haustorial neck into the intercellular space (arrowhead). Glt-protease-OsO_4. TCH-SP. x27,100.

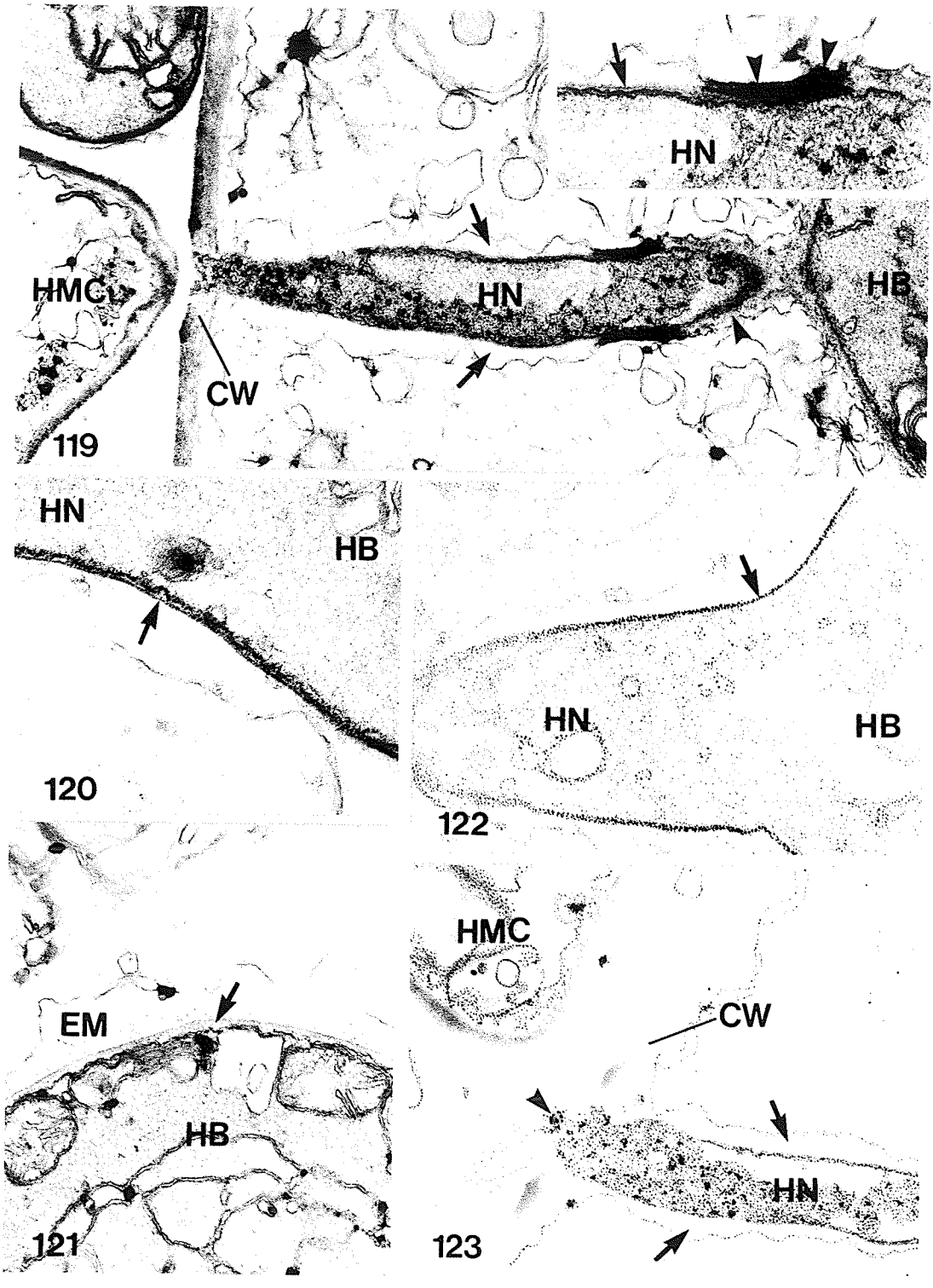
HN
HMC
HN
HB
CW
119
HN
HB
120
HN
HB
122
EM
HB
121
HMC
CW
HN
123

LEGEND

Figures 124-129. Concanavalin A binding to starch granules (Fig. 124) and fungal structures of P. coronata avenae (Figs. 125-129).

Figure 124. Con A binding to starch granules (SG). Glt. Con A-gold. Ua. x72,900.

Figure 125. Con A binding to glycogen granules (G). Glt. Con A-gold. Ua. x72,900.

Figure 126. Con A binding of the protrusion matrix (arrowheads). There is some binding to fungal wall (arrow), HMC septum, and cytoplasm. Glt. Con A-gold. Ua. x 50,000.

Figure 127. An oblique section of a haustorial neck through the neck ring region. There is Con A binding to the haustorial neck wall (arrow), but little to no binding to both bands of the neck ring. Glt. Con A-gold. Ua. x77,100.

Figure 128. Con A binding to the haustorial walls (arrows). Glt. Con A-gold. Ua. x72,000.

Figure 129. Con A binding to the protrusion matrix (arrow) and HMC septum was inhibited by the presence of methyl-α-D-mannopyranoside in the Con A-gold preparation. Glt. Con A-gold + methyl-α-D-mannopyranoside. Ua. x77,100.

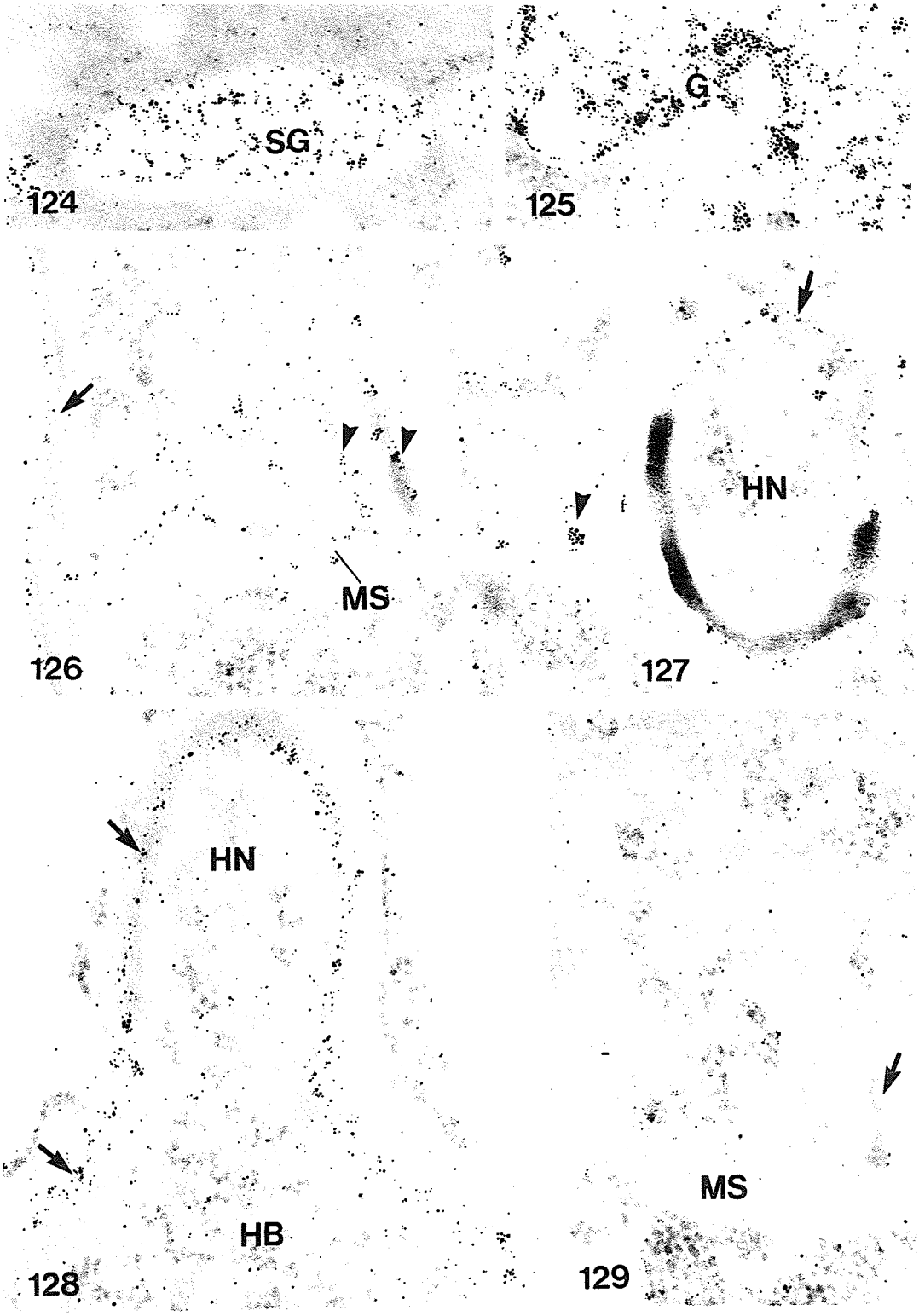
SG
124
G
125
MS
126
HN
127
HN
HB
128
MS
129

LEGEND

Figures 130-135. Avena host cells (Figs. 130 and 131) and P. coronata avenae (Figs. 132-135) after cellulase treatment.

Figure 130. The host wall (CW) is electron-lucent after treatment. Glt-cellulase-OsO_4. Ua/Pb. x23,100.

Figure 131. The thick outer layer (OL) of the host wall is largely electron-lucent after treatment. Inner layer (IL) of the host wall and starch granules (SG) are unaffected. Glt-cellulase-OsO_4. PA-TCH-SP. x28,900.

Figure 132. The protrusion matrix (arrowheads), fungal wall (arrow) and HMC septum are unaffected by the treatment. Glt-cellulase-OsO_4. Ua/Pb. x18,600.

Figure 133. The haustorial wall (arrow) is unaffected by the treatment. Glt-cellulase-OsO_4. Ua/Pb. x25,700.

Figure 134. Positive Thiéry staining of the protrusion matrix (arrowheads), fungal wall (arrow) and HMC septum after treatment. Glt-cellulase-OsO_4. PA-TCH-SP. x42,900.

Figure 135. Positive Thiéry staining of the haustorial wall (arrow) after treatment. Glt-cellulase-OsO_4. PA-TCH-SP. x53,600.

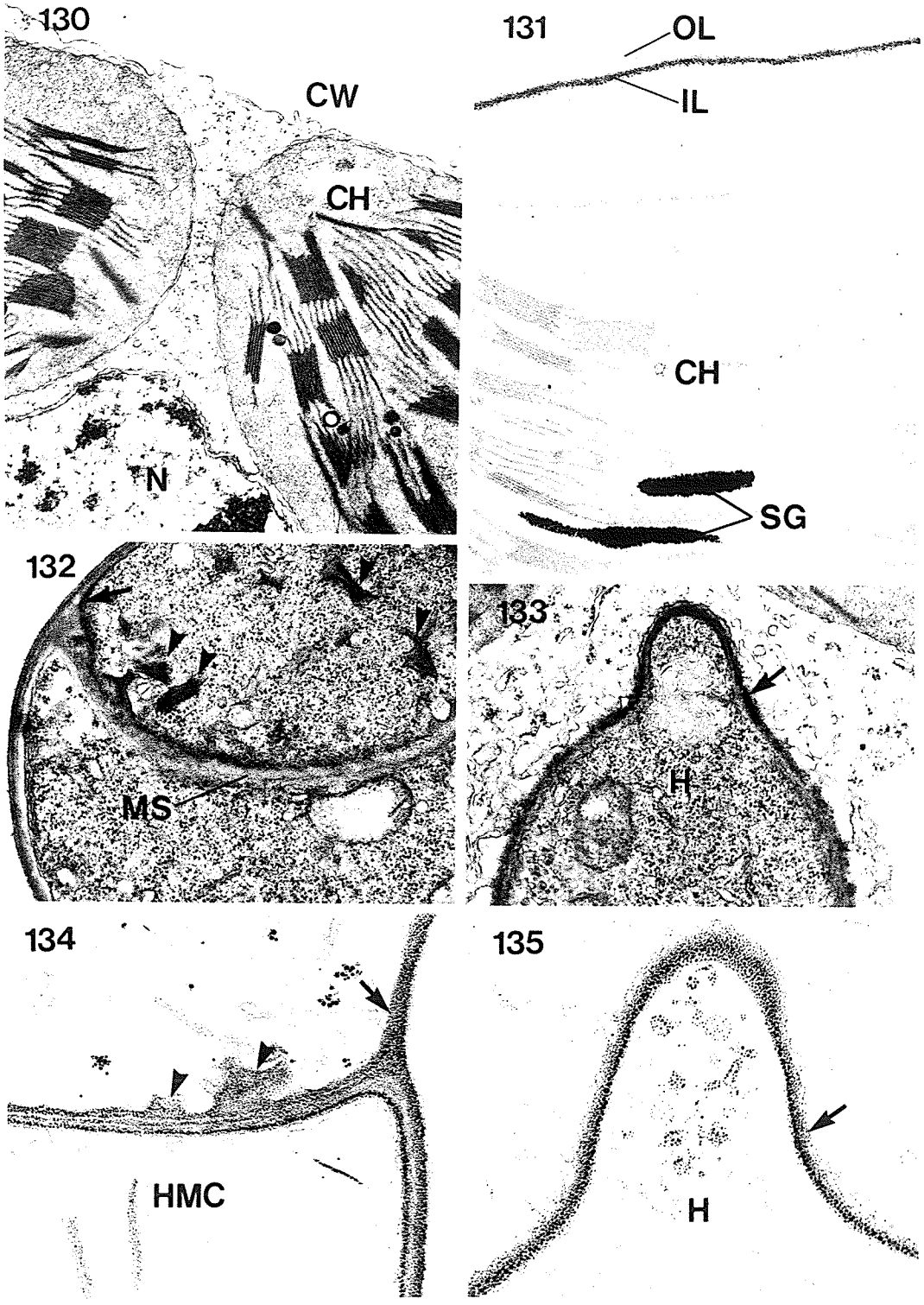
130
CW
CH
N
131
OL
IL
CH
SG
132
MS
133
H
134
HMC
135
H

LEGEND

Figures 136-141. Wheat germ lectin binding to fungal structures in P. coronata avenae (Figs. 136, 138-141) and P. graminis tritici (Fig. 137).

Figure 136. WGL binding to the fungal wall (arrow) and HMC septum, but not to the protrusion matrix (arrowheads). Glt. WGL-gold. Ua. x70,700.

Figure 137. WGL binding to the HMC wall (arrows) but not to the haustorial neck wall (arrowheads). Glt. WGL-gold. Ua. x47,100.

Figure 138. No WGL binding to the haustorial body wall (arrow) of a young haustorium. Glt. WGL-gold. Ua. x58,900.

Figure 139. WGL binding to the body wall (arrow) of a mature haustorium, but not to the EM. Glt. WGL-gold. Ua. x58,900.

Figure 140. No WGL binding to the neck wall (arrows) of a mature haustorium, or to both bands of the neck ring. Glt. WGL-gold. Ua. x79,300.

Figure 141. An adjacent section to that in Figure 139. WGL binding to the body wall (arrows) is inhibited by the presence of chitin oligomers in the WGL-gold preparation. Glt. WGL-gold. Ua. x52,900.

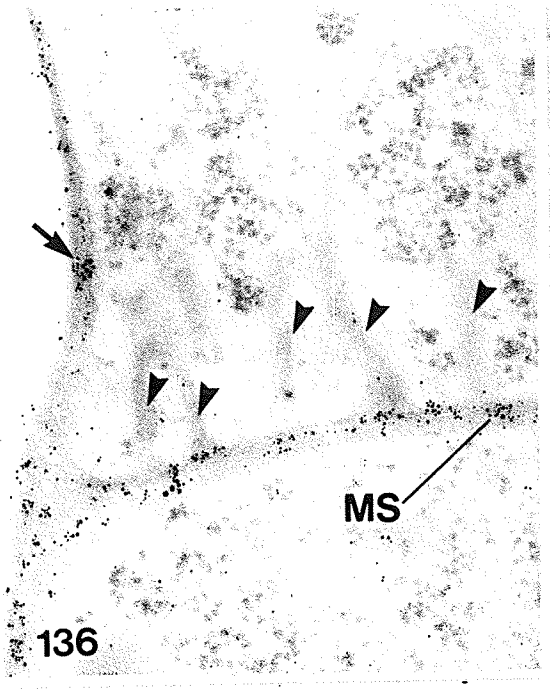
MS
136

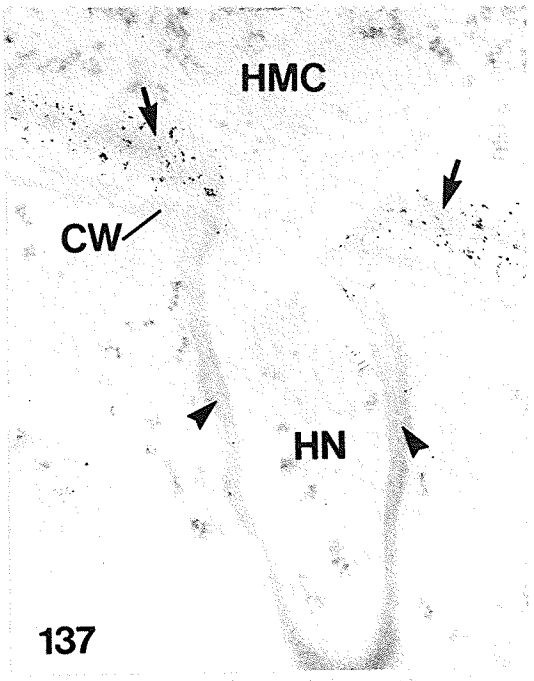
HMC
CW
HN
137

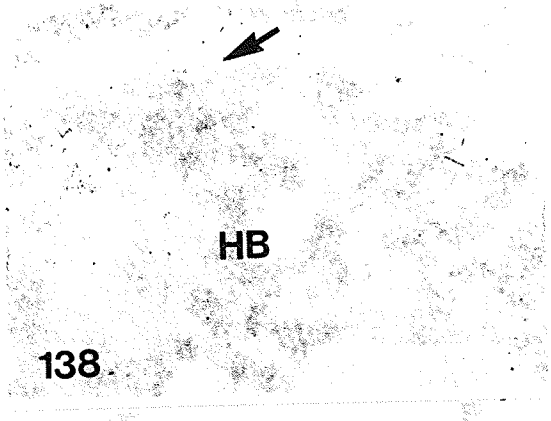
HB
138

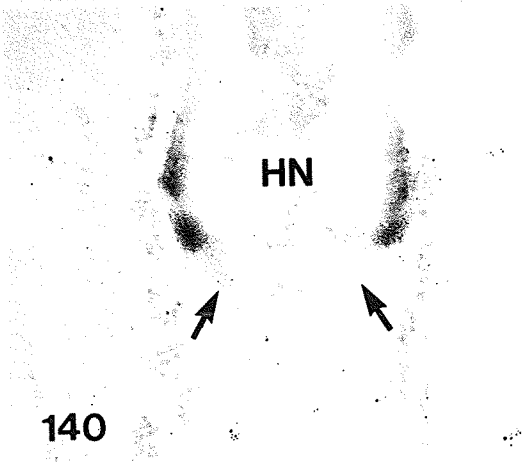
HN
140

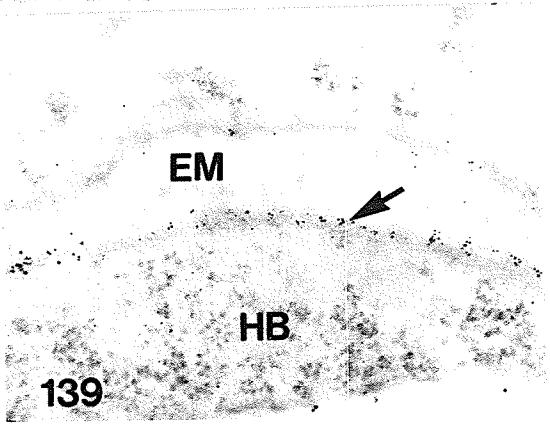
EM
HB
139

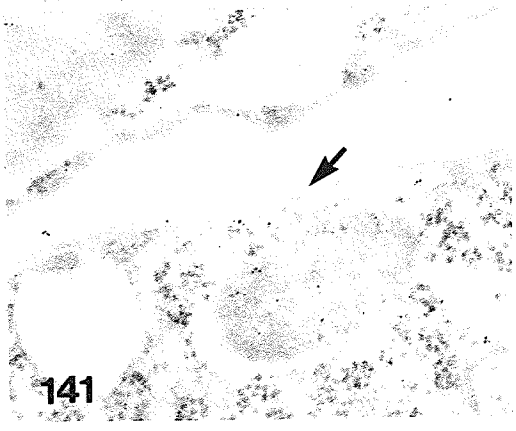
141

LEGEND

Figures 142-148. The extrahaustorial matrix of P. graminis tritici (Fig. 143) and P. coronata avenae (Figs. 142 and 144-148).

Figure 142. Thiéry staining of the extrahaustorial matrix (EM) of a haustorium during early expansion phase. The EM is not clearly differentiated from the body wall (arrow). Glt/OsO_4. PA-TCH-SP. x52,900.

Figure 143. Thiéry staining of the EM of a haustorium during the early expansion phase. Stained material is located in isolated patches, and the body wall (arrow) is intensely stained. Glt/OsO_4. PA-TCH-SP. x52,900.

Figure 144. Thiéry staining of the EM of a mature haustorium. The body wall is intensely stained, and the stained material of EM appears frayed. Contents of adjacent host cytoplasmic tubules (arrowheads) are stained, and membranes of these tubules are continuous (arrows) with the IPL. Glt/OsO_4. PA-TCH-SP. x64,300.

Figure 145. The EM is unstained in control treatment. Glt/OsO_4. PA-sodium borohydride-TCH-SP. x42,900.

Figure 146. The EM is unstained in control treatment. Glt/OsO_4. TCH-SP. x30,900.

Figure 147. Much of electron-opaque material is extracted from the EM and tubules (arrowheads) after cellulase treatment as compared to those untreated, eg. Figure 39. Glt-cellulase-OsO_4. Ua/Pb. x35,700.

Figure 148. Much of the stained material is extracted from the EM and tubules (arrowheads) after cellulase treatment as compared to those untreated, eg. Figure 149. Glt-cellulase-OsO_4. PA-TCH-SP. x40,100.

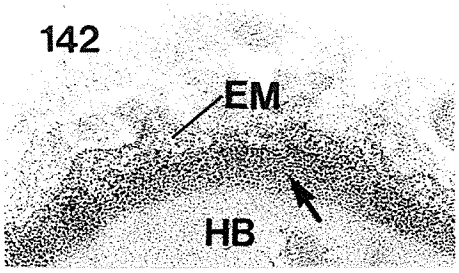
142
EM
HB

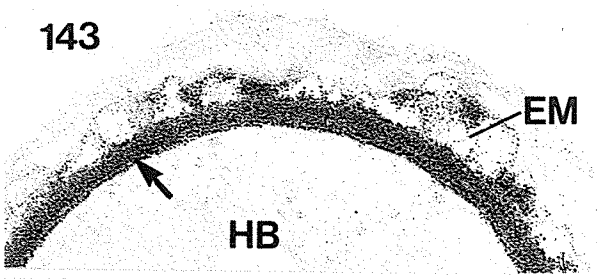
143
EM
HB

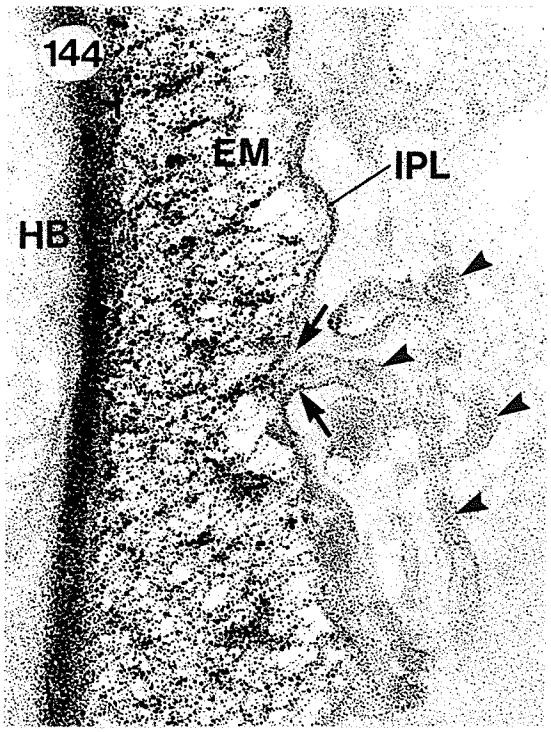
144
EM
IPL
HB

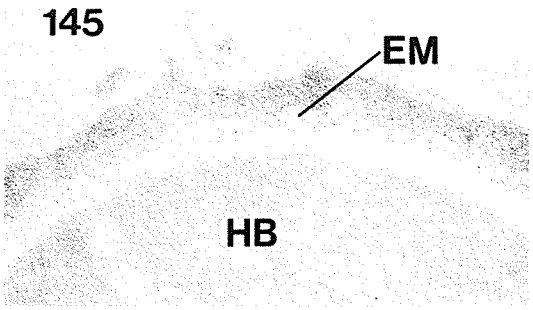
145
EM
HB

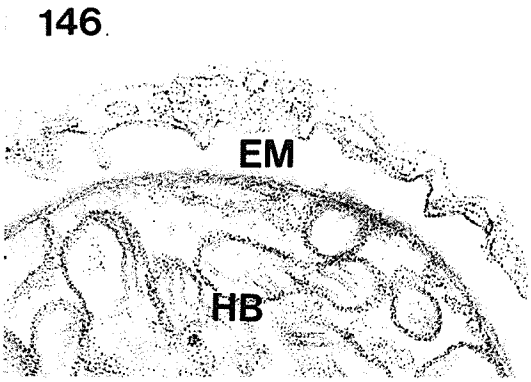
146
EM
HB

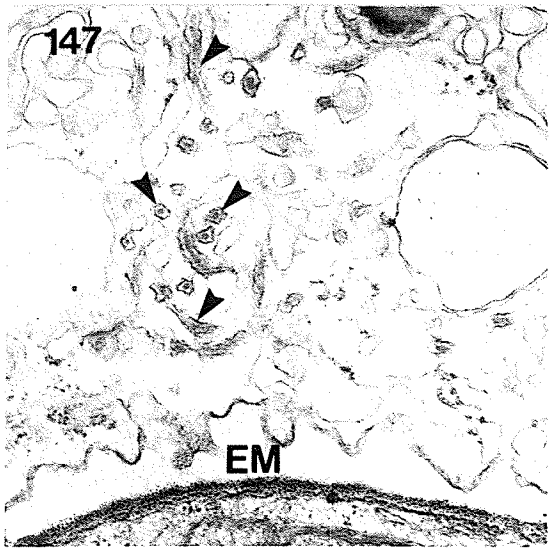
147
EM

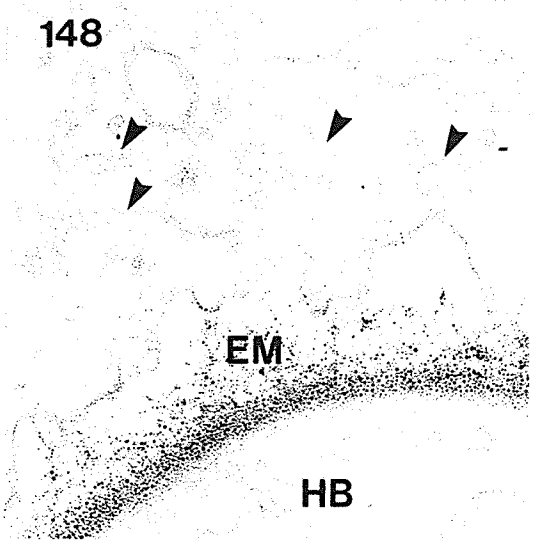
148
EM
HB

LEGEND

Figures 149-153. The extrahaustorial matrix of P. coronata avenae.

Figure 149. Both the extrahaustorial matrix (EM) and the haustorial body wall (arrow) are electron-lucent after lipid solvent treatment. Glt-chloroform/methanol-OsO_4. Ua/Pb. x47,100.

Figure 150. Positive Thiéry staining of the EM after lipid solvent treatment. The haustorial body wall (arrow) is more lightly stained but the staining of EM is unaffected, as compared to those in Figure 144. Glt-chloroform/methanol-OsO_4. PA-TCH-SP. x40,000.

Figure 151. The EM is electron-lucent and the body wall (arrow) of a young haustorium is largely extracted after protease treatment. Glt-protease-OsO_4. Ua/Pb. x36,100.

Figure 152. Much of stained material in EM is removed after protease treatment as compared to that in Figure 144. Haustorial body wall (arrow) is stained. Glt-protease-OsO_4. PA-TCH-SP. x51,400.

Figure 153. Heavy Con A binding to the EM (arrows) which is not clearly differentiated from the haustorial body wall. Glt. Con A-gold. Ua. x62,500.

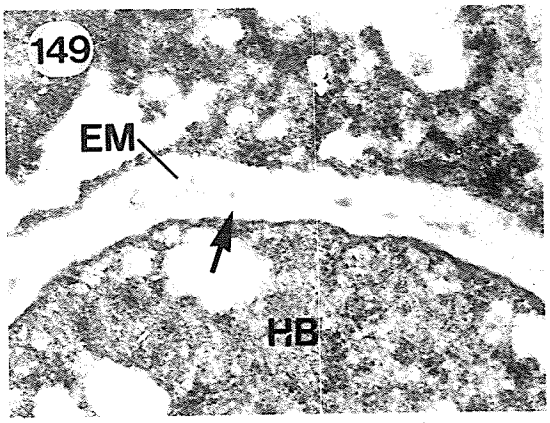
149
EM
HB

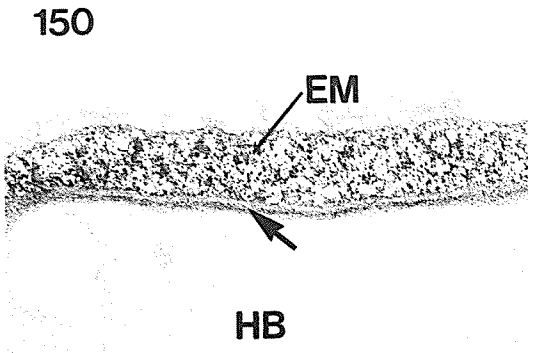
150
EM
HB

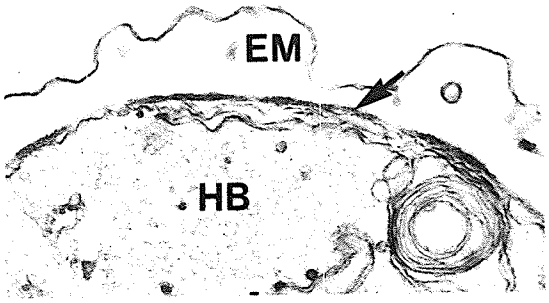
151
EM
HB

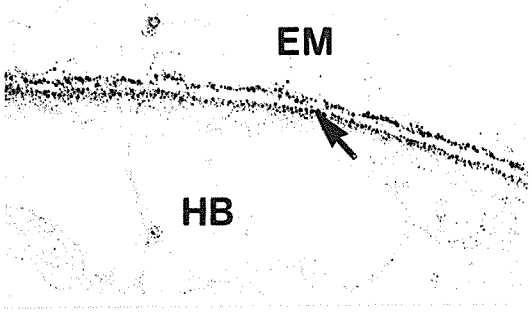
152
EM
HB

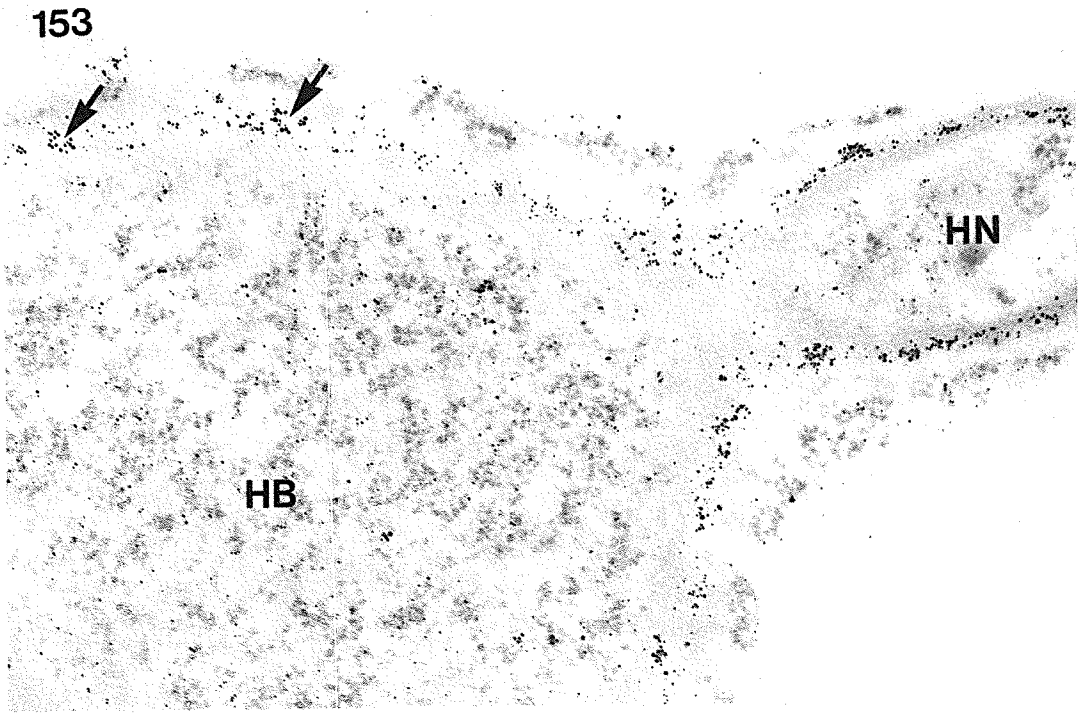
153
HN
HB

LEGEND

Figures 154-159. Cytochemistry of septal pore structures. Figure 155, *P. graminis tritici*. Figures 154, 156-159, *P. coronata avenae*.

Figure 154. The plug (arrow) of the pore of a young HMC septum is electron-lucent, and glycogen granules (arrowheads) are electron-opaque. Glt/OsO_4-$K_4Fe(CN)_6$. Unstained section. x62,100.

Figure 155. The plug (arrow) of the pore of a HMC septum is unstained by the Thiéry method. Glt/OsO_4. PA-TCH-SP. x20,700.

Figure 156. The plug (arrow) of a hyphal septum is unaffected by lipid solvent treatment. Glt-chloroform/methanol-OsO_4. Ua/Pb. x35,200.

Figure 157. Thiéry staining of a hyphal septum of the perforate type. The diaphragm (arrowheads) delimiting the septal pore structure is lightly stained. Glt/OsO_4. PA-TCH-SP. x57,900.

Figure 158. The diaphragm (arrowhead) delimiting the hyphal septal pore structure is unaffected by lipid solvent treatment, while other membranes have been extracted. Glt-chloroform/methanol-OsO_4. Ua/Pb. x43,900.

Figure 159. A hyphal septum with an open pore (arrowhead) seen after protease treatment. It is probable that the diaphragm delimiting the septal pore has been extracted. Membranes (arrow) still remained in place on the septum. Glt-protease-OsO_4. Ua/Pb. x47,100.

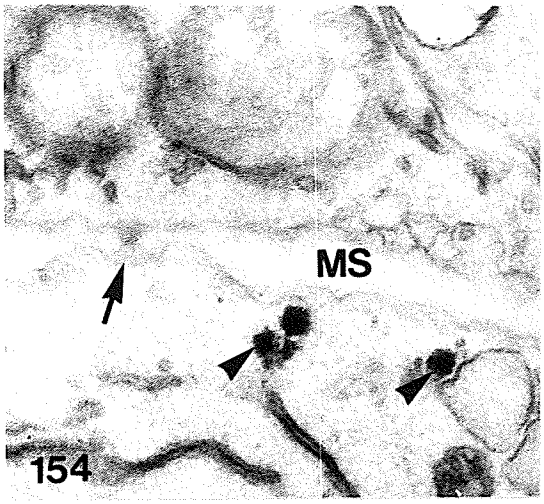

154

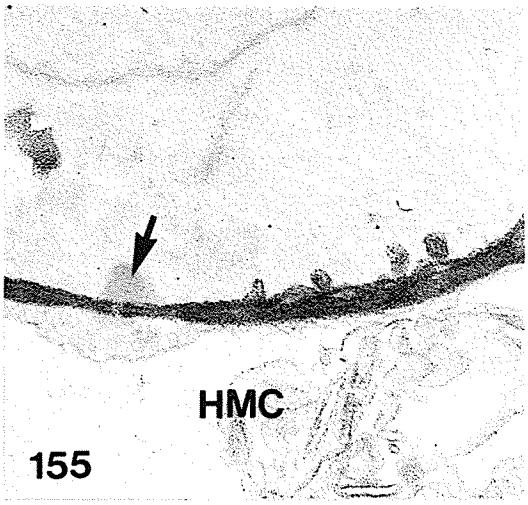

155

156

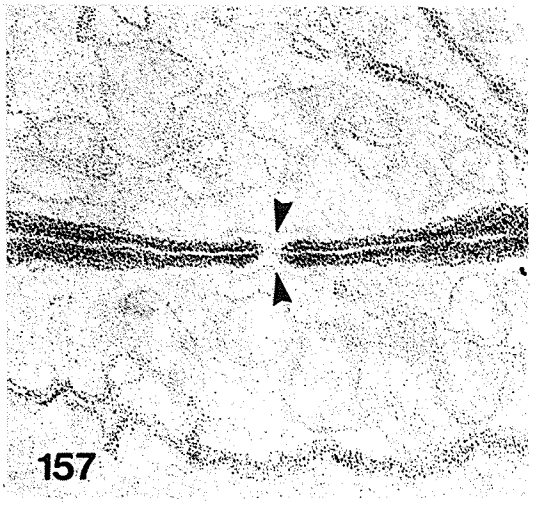

157

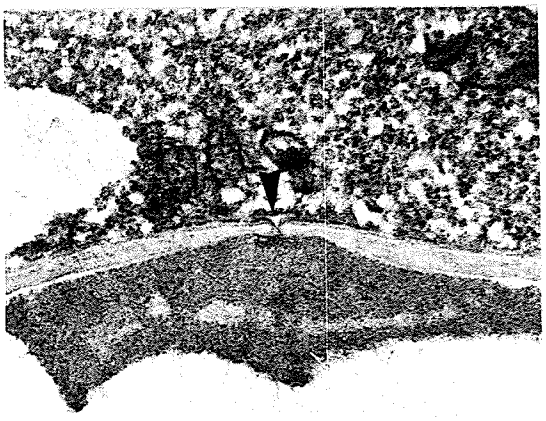

158

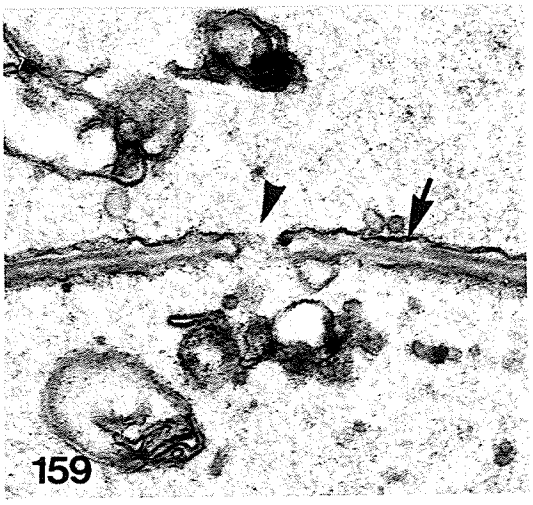

159

LEGEND

Figures 160-168. Cytochemistry of neck ring of P. coronata avenae.

Figure 160. An oblique, tangential section of a haustorial neck. A narrow strip of wall material (opposing arrows) separates the two bands of the neck ring. The larger band, closer to the haustorial mother cell, is designated as the α (alpha) band, and the smaller band, closer to the haustorial body, the β (beta) band. Glt/OsO_4. The section had been treated with H_2O_2 before staining with Ua/Pb. x73,300.

Figure 161. The haustorial neck with an electron-dense α band (large arrow) and an electron-lucent β band (arrowhead). Glt/OsO_4. PACP. x37,100.

Figure 162. An oblique cross-section of a haustorial neck with a densely stained region (α band, dark arrows) and an unstained region (open arrow). The neck wall (arrowhead) is moderately stained. Serial sections of the haustorial neck showed the unstained region to be the β band. Glt/OsO_4. PACP. x46,400.

Figure 163. An oblique cross-section from a serial set showing an electron-opaque α band and an unstained β band (open arrow). Glt/OsO_4. 3% periodic acid for 1 hour. x31,200.

Figure 164. An oblique section of a mature haustorium containing both bands (arrows) of the neck ring. Glt/OsO_4. PA-TCH-SP. x51,400.

Figure 165. The haustorial neck of a young haustorium with only the α band (arrow) present. Glt/OsO_4. PA-TCH-SP. x58,900.

Figure 166. The haustorial neck with electron-opaque neck ring in a control treatment. Glt/OsO_4. TCH-SP. x40,100.

Figure 167. An oblique section of a haustorial neck with electron-opaque neck ring in a control treatment. Glt/OsO_4. PA-sodium borohydride-TCH-SP. x47,100.

Figure 168. A semithin (blue interference colour) unstained section of a haustorial neck with two distinct electron bands in the neck ring. This section had been subjected to EDX analysis. The halos surrounding the two bands are due to carbonaceous contamination during analysis. The α and β bands on the top side of the neck appear to be separated from one another to a greater extent than on the bottom side. The proximity of these bands to one another affected the EDX analysis. Other areas analyzed were the haustorial neck wall (asterisk) and also the host cytoplasm adjacent to the neck ring. Glt. x41,300.

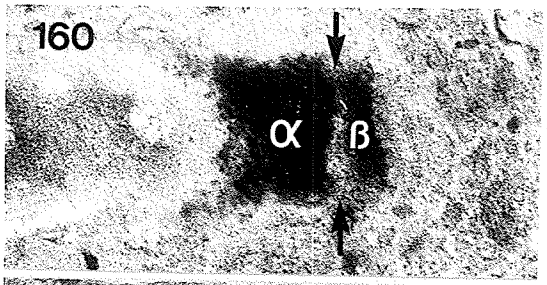
160
α
β

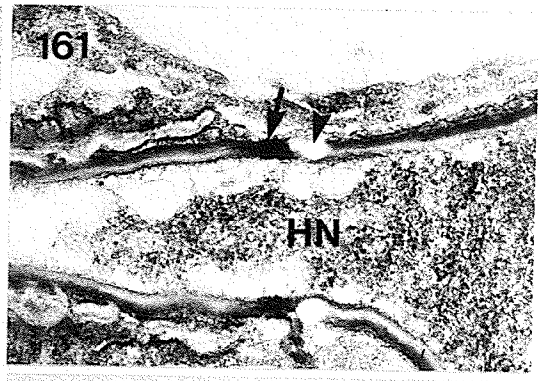
161
HN

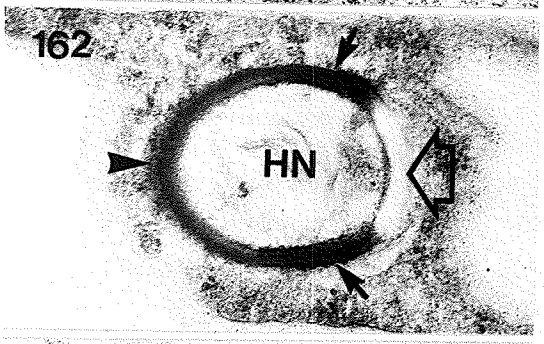
162
HN

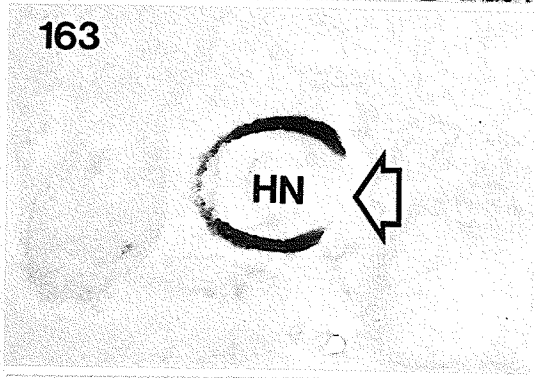
163
HN

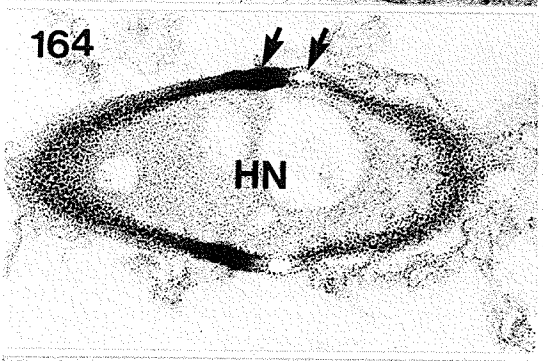
164
HN

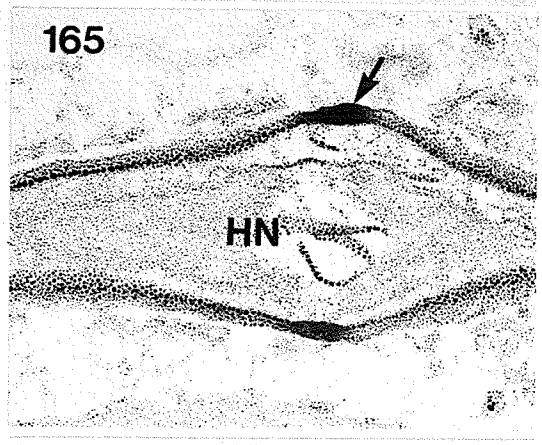
165
HN

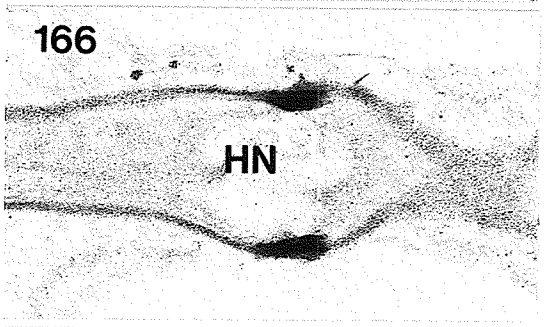
166
HN

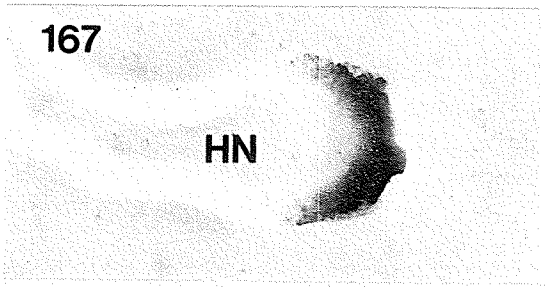
167
HN

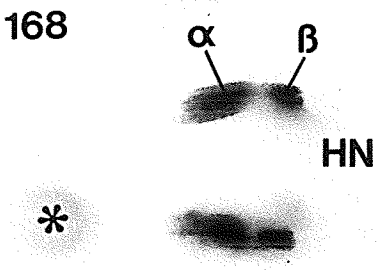
168
α
β
HN
*

LEGEND

Figures 169-174. EDX spectra obtained from the section in Figure 168 (except Fig. 173).

Figures 169 and 170 are spectra of the α band from the bottom and top sides, respectively. Silicon is the major element present.

Figures 171 and 172 are spectra of the β band from the bottom and top sides, respectively. Phosphorous, iron and possibly chlorine are the major elements present. The small amount of silicon, particularly in Figure 171, is probably due to interference by the α band.

Figure 173. EDX spectrum from a section with a different haustorium than that in Figure 168. Spectrum from the host cytoplasm near the neck ring showing traces of silicon, phosphorous, and chlorine.

Figure 174. EDX spectrum from the section in Figure 168 of the host cytoplasm near the neck ring. Traces of silicon and chlorine were detected.

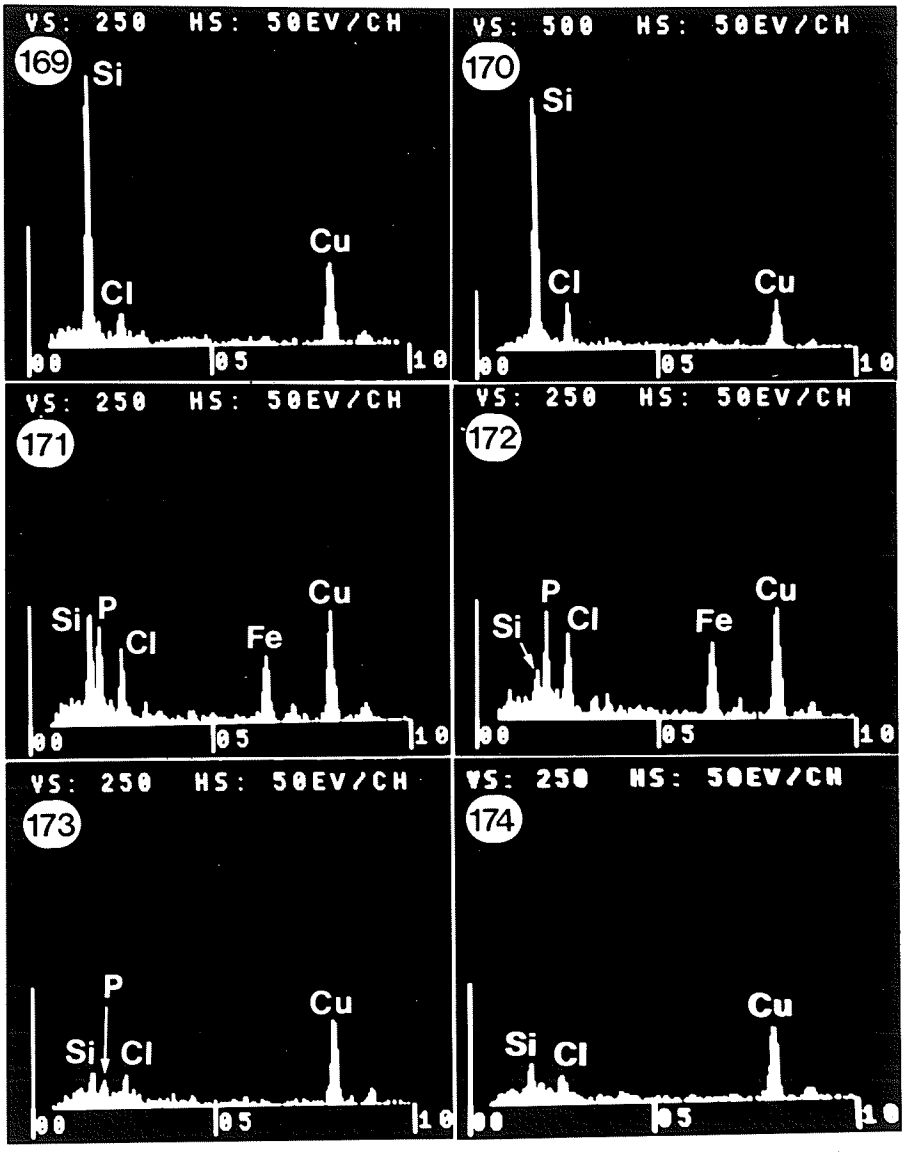
VS: 250 HS: 50EV/CH
169
Si
Cl
Cu
00
05
10
VS: 500 HS: 50EV/CH
170
Si
Cl
Cu
00
05
10
VS: 250 HS: 50EV/CH
171
Si
P
Cl
Fe
Cu
00
05
10
VS: 250 HS: 50EV/CH
172
Si
P
Cl
Fe
Cu
00
05
10
VS: 250 HS: 50EV/CH
173
Si
P
Cl
Cu
00
05
10
VS: 250 HS: 50EV/CH
174
Si
Cl
Cu
00
05
10

LEGEND

Figures 175-178. EDX spectra.

Figure 175. EDX spectrum obtained from the section in Figure 168 from the haustorial wall near the α band. Traces of silicon and chlorine were detected.

Figures 176 and 177. EDX spectra from a section with a different haustorium than that in Figure 168. Figure 176 is from the haustorial neck wall near the β band, showing traces of silicon and chlorine. Figure 177 is from the fungal cytoplasm inside the haustorial neck near the neck ring. A trace of silicon was detected.

Figure 178. EDX spectrum from an area of the Formvar-carbon support film on a copper grid free of any sections of tissue. There were silicon and copper present in amounts sufficient to account for silicon in the control analysis of non-neck band tissue, and for the copper in all analyses.

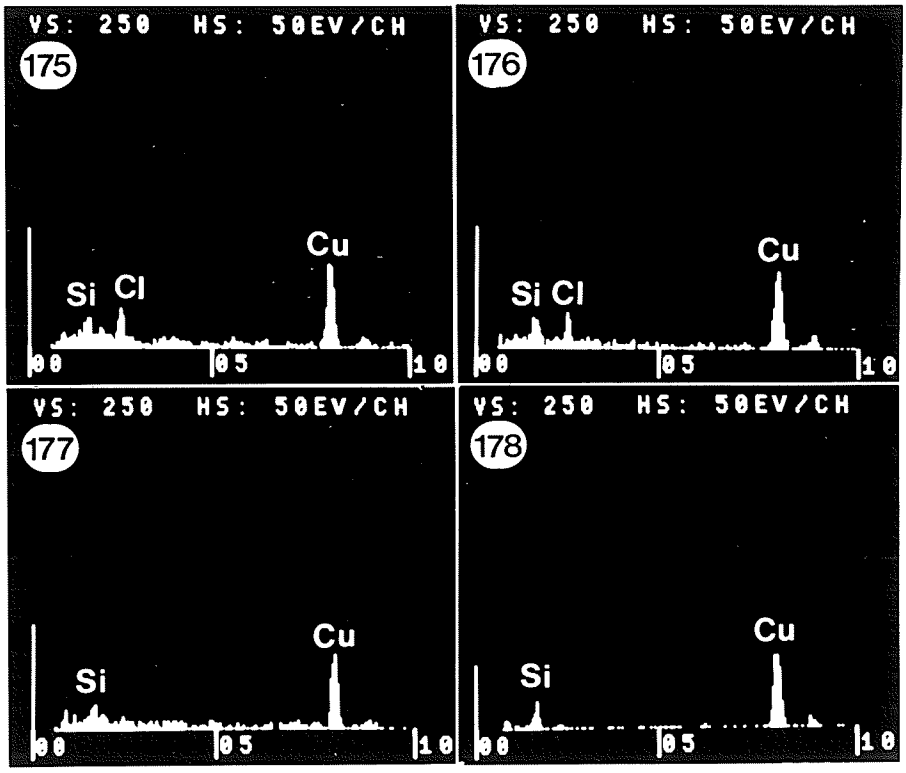
VS: 250 HS: 50EV/CH
175
Si
Cl
Cu
00
05
10
VS: 250 HS: 50EV/CH
176
Si
Cl
Cu
00
05
10
VS: 250 HS: 50EV/CH
177
Si
Cu
00
05
10
VS: 250 HS: 50EV/CH
178
Si
Cu
00
05
10

LEGEND

Figures 179-184. Electron-opaque deposits in the D-haustorial apparatus. Figures 180 and 181, P. graminis tritici. Figures 179 and 182-184, P. coronata avenae.

Figure 179. A near median section of the HMC septum. Electron-opaque deposits are found in the protrusion matrix (arrowheads), HMC septum, and HMC wall (arrows). A small portion of the HMC septum around the septal pore (open arrow) is free of these deposits. Glt/OsO_4. Ua/Pb. x47,100.

Figure 180. An oblique section through the penetration region. Granular electron-opaque deposits are found at the thickened region of the HMC wall (arrows). Glt/OsO_4. Ua/Pb. x35,700.

Figure 181. Heavy accumulation of electron-opaque deposits in the thickened region of the HMC wall (arrows) and in the rest of the HMC wall. Glt/OsO_4. Ua/Pb. x22,900.

Figure 182. Electron-opaque deposits found in protrusion matrix are indicated by arrows. The rest of the protrusion matrix is largely electron-lucent (arrowheads). The HMC septum and wall are free of electron-dense deposits at this stage. Glt. Ua/Pb. x40,700.

Figure 183. Electron-opaque deposits (arrows) in the protrusion matrix, but not in the HMC septum and wall. Glt. Unstained section. x46,100.

Figure 184. Electron-opaque deposits (arrows) accumulated mainly in the thickened region of the HMC wall at the site of host penetration. Glt/OsO_4. The section had been treated with 1% periodic acid for 30 minutes, and was not stained. x40,700.

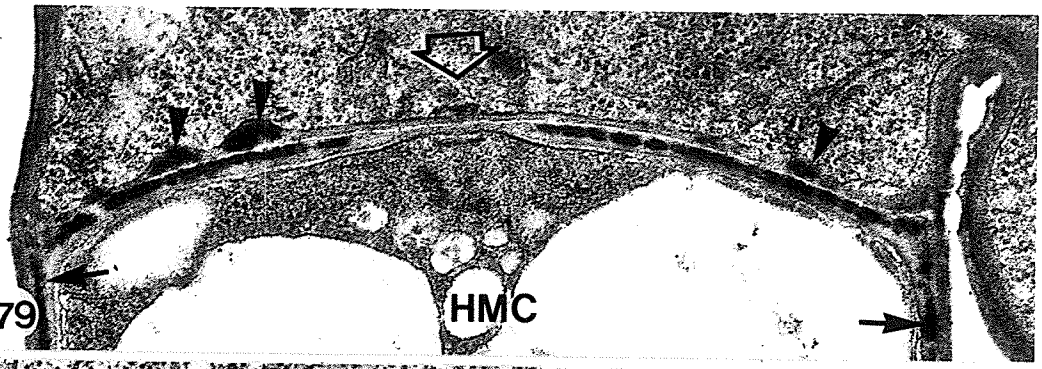
179
HMC


HMC
CW
180

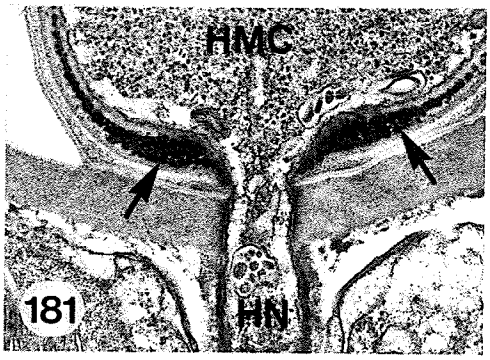
HMC
181
HN

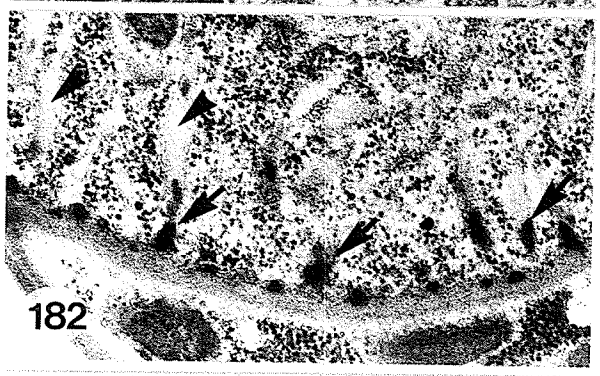
182

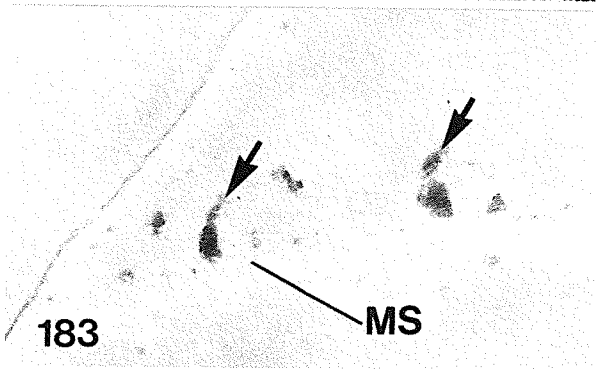
183
MS

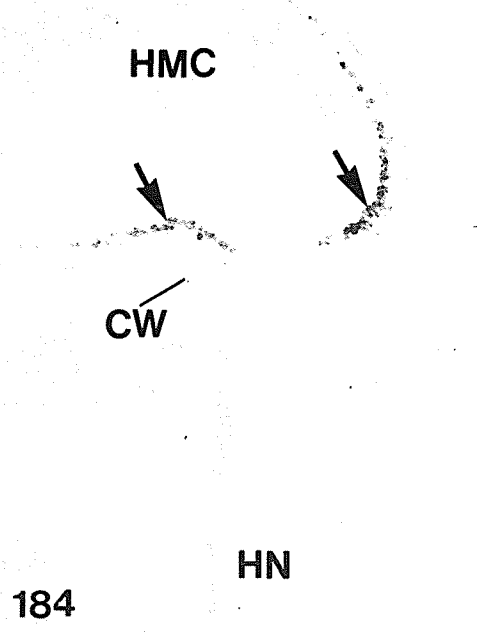
HMC
CW
HN
184

LEGEND

Figures 185-193. Electron-opaque deposits in the D-haustorial apparatus of P. coronata avenae, but not in the spore wall (Fig. 193).

Figure 185. Heavy accumulation of electron-opaque deposits in the protrusion matrix (arrowheads), and some amounts of the deposits appeared in the HMC septum (arrow) and HMC wall. Glt. Unstained section. x46,100.

Figure 186. Heavy accumulation of electron-opaque deposits in protrusion matrix (arrowheads), HMC septum (arrow) and HMC wall. Glt. Unstained section. x50,000.

Figure 187. Electron-opaque deposits (arrow) in the HMC wall after lipid solvent extraction. Glt-ether/ethanol-OsO_4. Unstained section. x20,000.

Figure 188. Electron-opaque deposits in the protrusion matrix (arrowheads) and HMC septum (arrow) and HMC wall after protease treatment. Glt-protease-OsO_4. Unstained section. x30,000.

Figure 189. Heavy accumulation of electron-opaque deposits in the HMC wall from a colony center. This HMC had collapsed. Glt/OsO_4. This section had been treated with 3% periodic acid for 1 hour, and was not stained. x24,300.

Figure 190. A semithin (blue interference colour) section showing heavy accumulation of electron-opaque deposits in the protrusion matrix (arrowheads), but not in the HMC septum and wall at this stage. Round electron-opaque deposits (arrow) are also found in the HMC protoplast. This section had been subjected to EDX analysis. Glt. Unstained section. x15,000.

Figure 191. A semithin (blue interference colour) section showing heavy accumulation of electron-opaque deposits (arrows) only in the thickened region of the HMC wall at the site of host penetration. This section had been subjected to EDX analysis. Glt. Unstained section. x45,000.

Figure 192. A semithin (blue interference colour) section showing heavy accumulation of electron-opaque deposits in the HMC wall and round electron-opaque deposits in the vacuole. This section had been subjected to EDX analysis. Glt. Unstained section. x26,700.

Figure 193. A section of a urediospore wall of P. coronata avenae. No electron-opaque deposits are observed. Glt. Unstained section. x18,000.

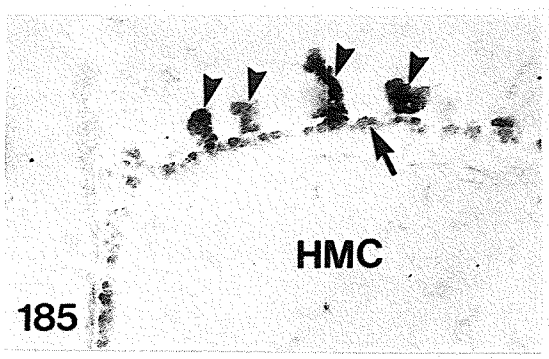
HMC
185

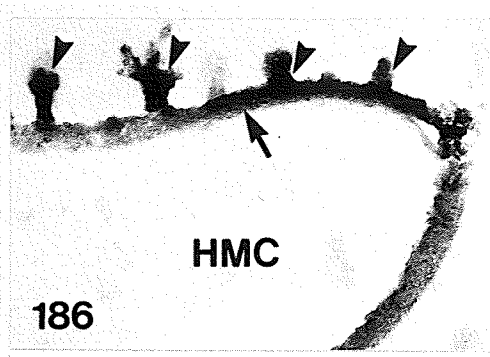
HMC
186

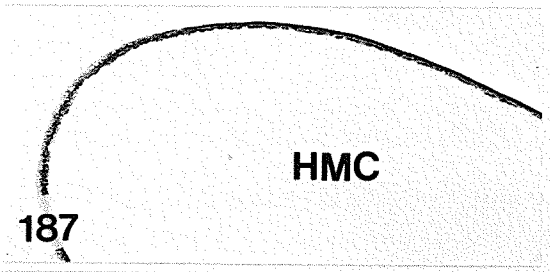
HMC
187

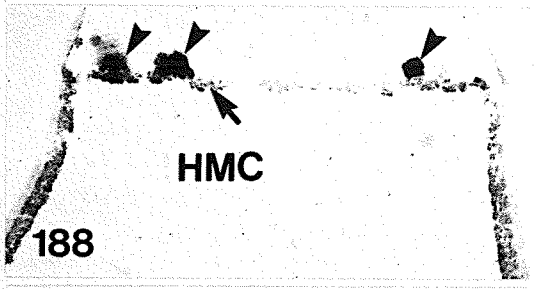
HMC
188

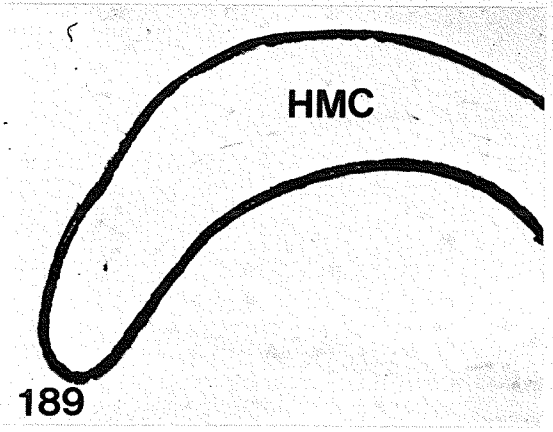
HMC
189

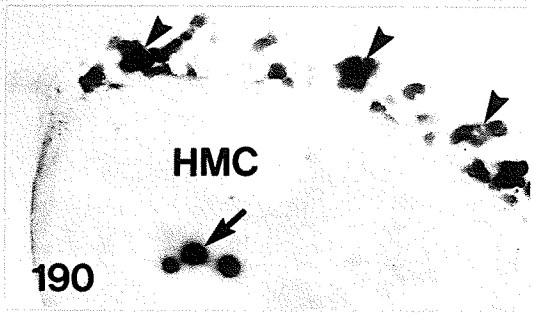
HMC
190

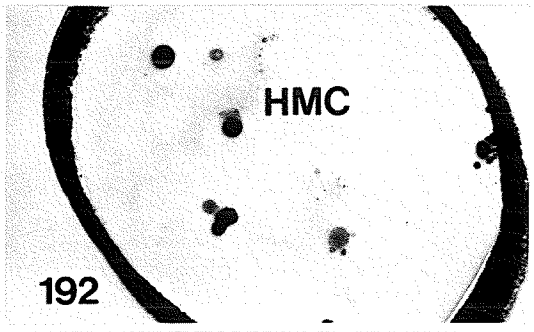
HMC
192

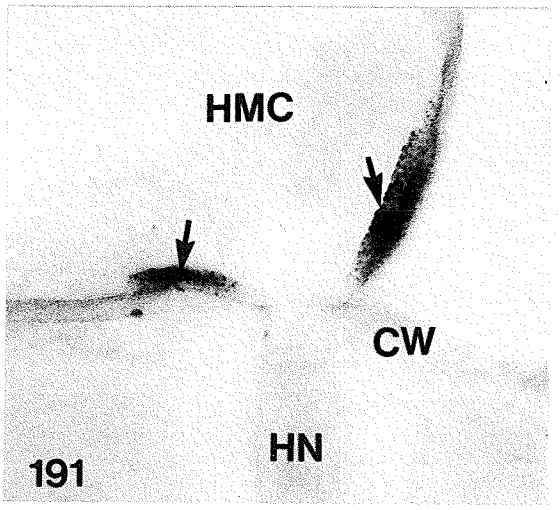
HMC
CW
HN
191

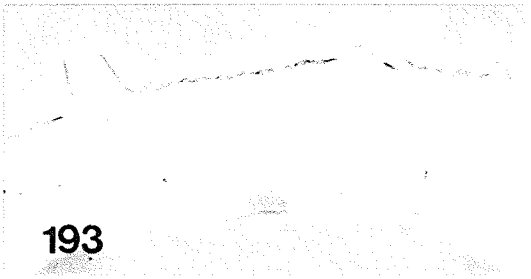
193

LEGEND

Figures 194-199. Electron-opaque deposits in P. graminis tritici (Fig. 199) and P. coronata avenae (Figs. 194-198).

Figure 194. A semithin (blue interference colour) section of part of a D-haustorium. Large electron-opaque deposits are found in the protoplast. This section had been subjected to EDX analysis. Glt. Unstained section. x12,600.

Figure 195. Large electron-opaque deposit (arrowhead) found in vacuole of a hyphal cell. Glt/$0s0_4$. Ua/Pb. x8,900.

Figure 196. Electron-opaque deposits (arrowheads) in a vacuole of a young HMC. Note the long membrane protrusions (open arrow) on the hyphal side of the HMC septum. Glt/$0s0_4$. Ua/Pb. x15,400.

Figure 197. Electron-opaque deposits (arrowheads) in vacuoles of a HMC after a young haustorium had formed. Note the angular membrane protrusions (open arrow) on the hyphal side of the HMC septum. Glt/$0s0_4$. Ua/Pb. x20,700.

Figure 198. Electron-opaque deposits (arrowheads) in vacuoles of a hyphal cell in the sporogenous tissue. Glt/$0s0_4$. Ua/Pb. x12,500.

Figure 199. Electron-opaque deposit (arrowhead) in a vacuole of a HMC. Glt/$0s0_4$. Ua/Pb. x25,000.

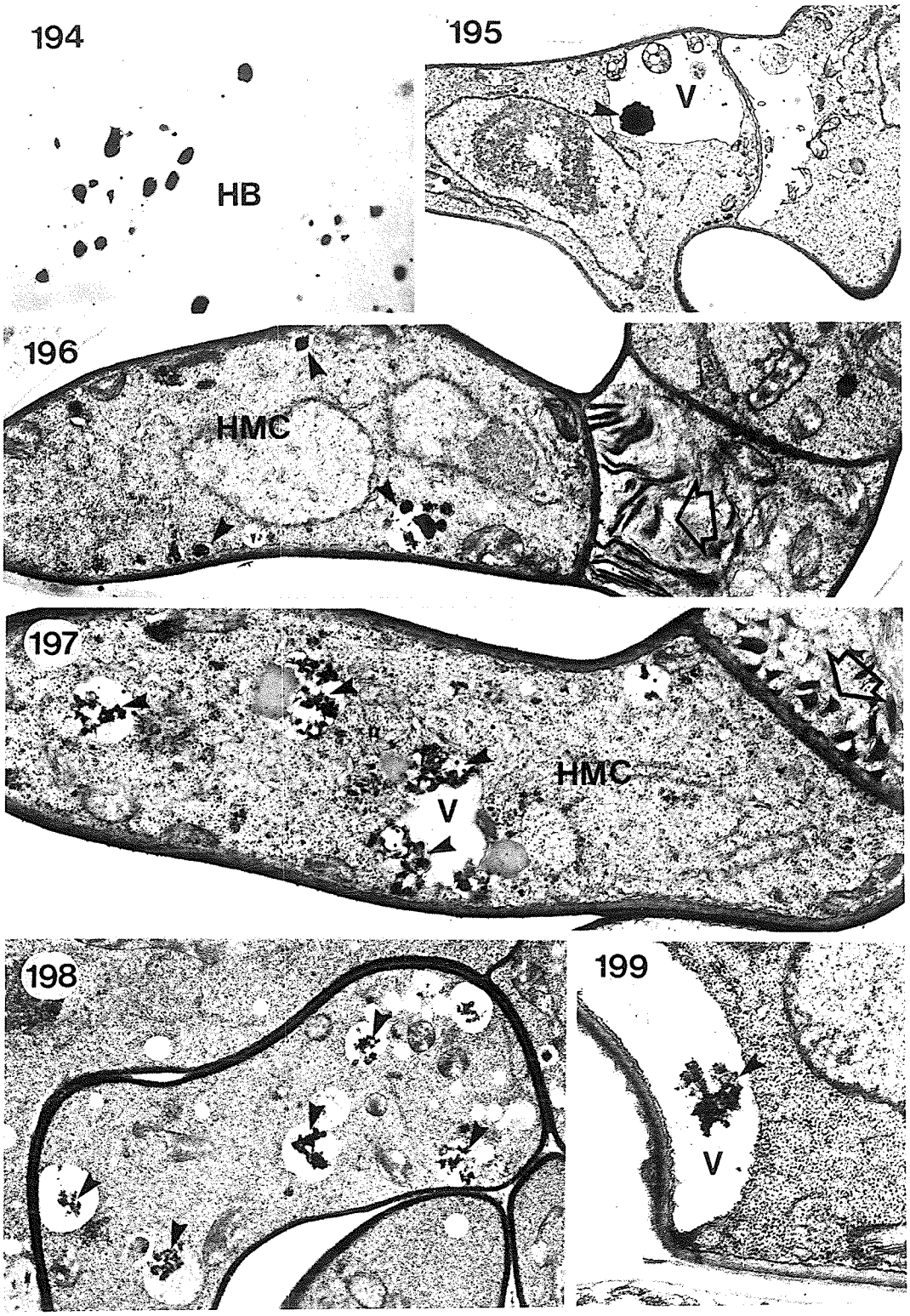
194
HB
195
V
196
HMC
197
V
HMC
198
199
V

LEGEND

Figures 200-205. EDX spectra.

Figure 200. EDX spectrum from the section in Figure 190 of the electron-opaque deposits in the membrane protrusion. Silicon is the major element present. The peak representing copper in this spectrum and in the following spectra, is assumed to have originated from the copper support grid.

Figure 201. EDX spectrum of the hyphal wall adjacent to the membrane protrusions shown in Figure 190. Only a small peak of silicon was detected, the amounts of which can be accounted for in the control analysis of the Formvar-carbon support film shown in Figure 178.

Figure 202. EDX spectrum from the section in Figure 191 of the electron-opaque deposits in the thickened region of the HMC wall at the site of host penetration. Silicon is the major element present in these opaque deposits.

Figure 203. EDX spectrum of the electron-opaque wall of an older HMC located near the center of an infection colony. Silicon is the major element present.

Figure 204. EDX spectrum of a HMC septum with electron-opaque deposits. Significant amounts of silicon were detected.

Figure 205. EDX spectrum of the wall of a HMC located at the edge of an infection colony. The wall of this HMC contains no electron-opaque deposits, and only a small peak of silicon was detected, the amounts of which can be accounted for in the control analysis of the Formvar-carbon support film shown in Figure 178.

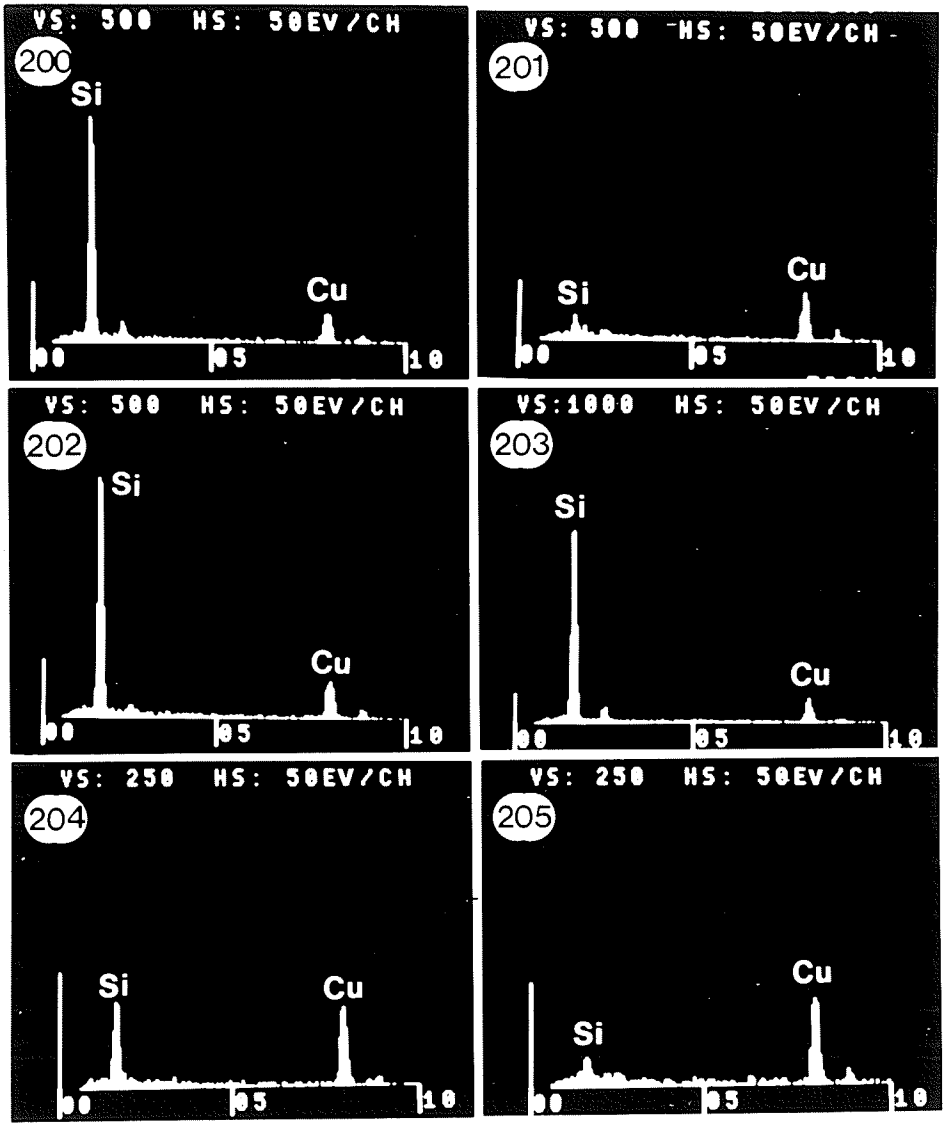
VS: 500 HS: 50EV/CH
200
Si
Cu
0
5
10
VS: 500 HS: 50EV/CH
201
Si
Cu
0
5
10
VS: 500 HS: 50EV/CH
202
Si
Cu
0
5
10
VS:1000 HS: 50EV/CH
203
Si
Cu
0
5
10
VS: 250 HS: 50EV/CH
204
Si
Cu
0
5
10
VS: 250 HS: 50EV/CH
205
Si
Cu
0
5
10

LEGEND

Figures 206-209. EDX spectra.

Figure 206. EDX spectrum of a HMC septum located at the edge of an infection colony. A trace of silicon was detected.

Figure 207. EDX spectrum of the wall of an air dried ungerminated urediospore of P. coronata avenae. The major peaks were of magnesium, phosphorous and potassium.

Figure 208. EDX spectrum from the section in Figure 194 of the large electron-opaque deposits in the protoplast of an older haustorium located near the center of an infection colony. Phosphorous was detected as the major element present, with some amounts of sulphur, iron and chlorine.

Figure 209. EDX spectrum from the section in Figure 192 of the round electron-opaque deposits in the protoplast of an older HMC located near the center of an infection colony. Phosphorous was detected as the major element present, with some amounts of sulphur and iron.

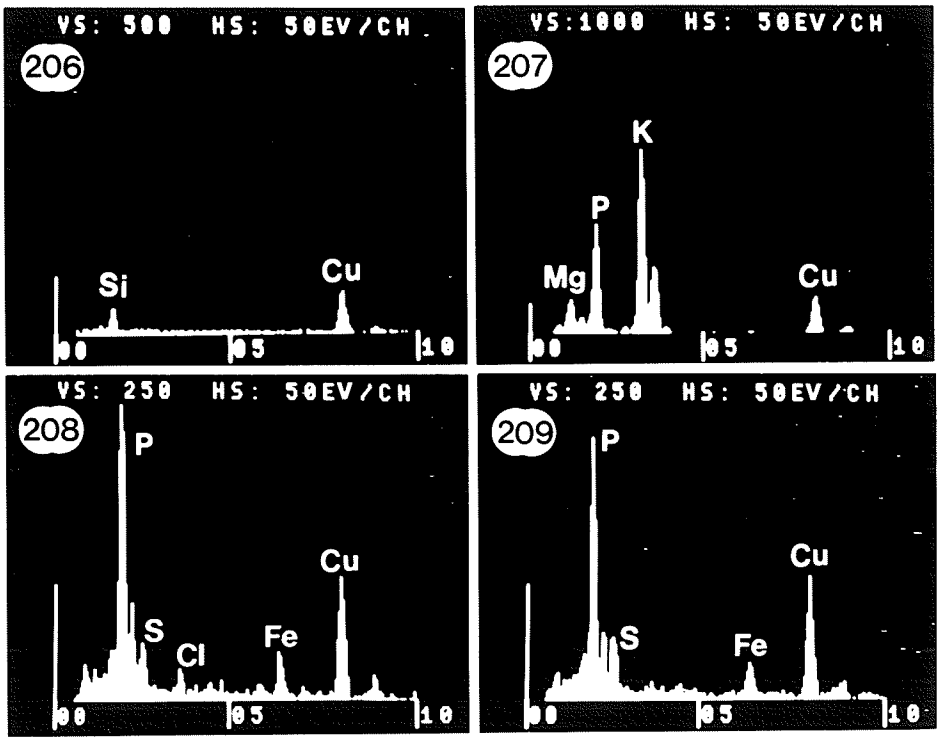
VS: 500 HS: 50EV/CH
206
Si
Cu
00
05
10
VS:1000 HS: 50EV/CH
207
K
P
Mg
Cu
00
05
10
VS: 250 HS: 50EV/CH
208
P
Cu
S
Cl
Fe
00
05
10
VS: 250 HS: 50EV/CH
209
P
Cu
S
Fe
00
05
10

LEGEND

Figures 210-215. Host cytoplasmic tubules adjacent to D-haustoria. Figure 215, P. graminis tritici; Figures 210-214, P. coronata avenae.

Figure 210. Proliferation of host cytoplasmic tubules and membranous whorls in the vicinity of a haustorium. The tubules contain an electron-dense matrix and a thread of denser staining material at their centers. The inset shows the continuity of a tubule (arrow) with the membranes of a whorl. Glt/OsO_4. Ua/Pb. x65,700. Inset, x46,100.

Figure 211. Tubules are distinct from host ER. Glt/OsO_4. Ua/Pb. x43,800.

Figure 212. Membranes of cytoplasmic tubules (arrow) are lighter stained than the invaginated host plasmalemma (IPL). Glt/OsO_4. PACP. x37,500.

Figure 213. A section through the distal end of a haustorium. The IPL is intensely stained, whereas membranes of the cytoplasmic tubules (arrowheads) are lightly stained. Glt/OsO_4. PACP. x38,600.

Figure 214. Host cytoplasmic tubules (arrowheads) in the vicinity of a haustorium, the contents of which are stained with the Thiéry method. Glt/OsO_4. PA-TCH-SP. x42,900.

Figure 215. Thiéry staining of the cytoplasmic tubules (arrowheads). The membranes of the tubule are continuous with IPL. Glt/OsO_4. PA-TCH-SP. x36,400.

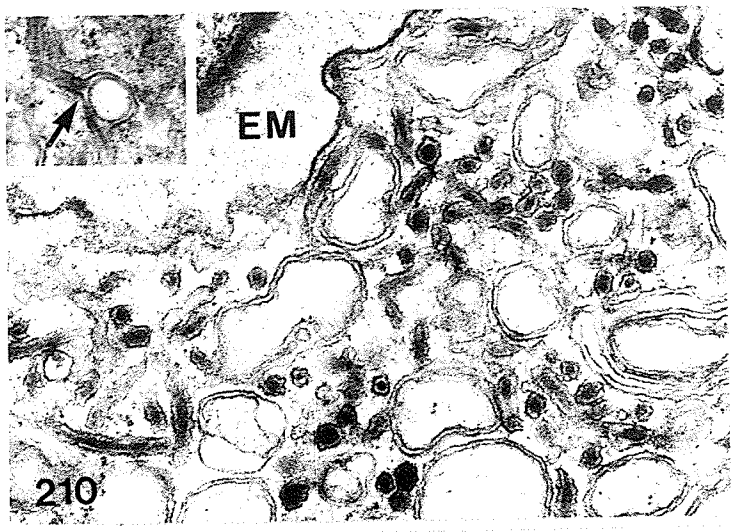
EM
210

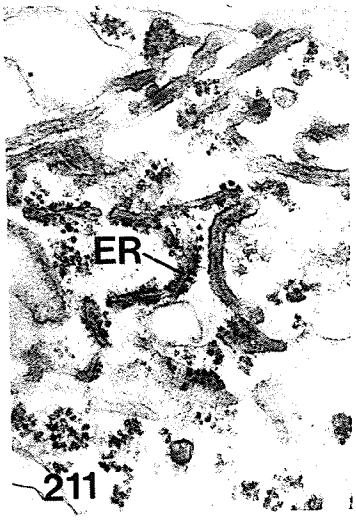
ER
211

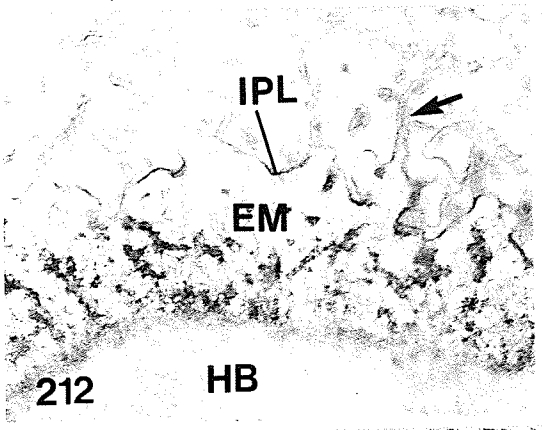
IPL
EM
212
HB

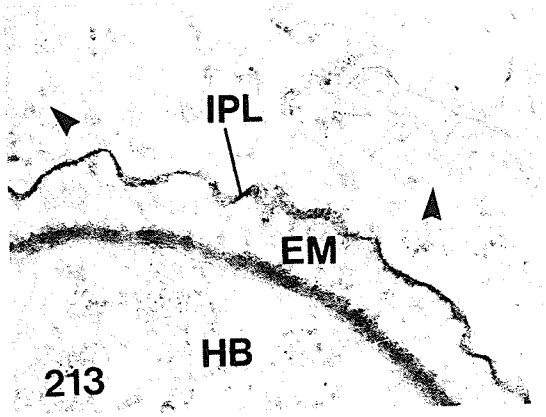
IPL
EM
213
HB

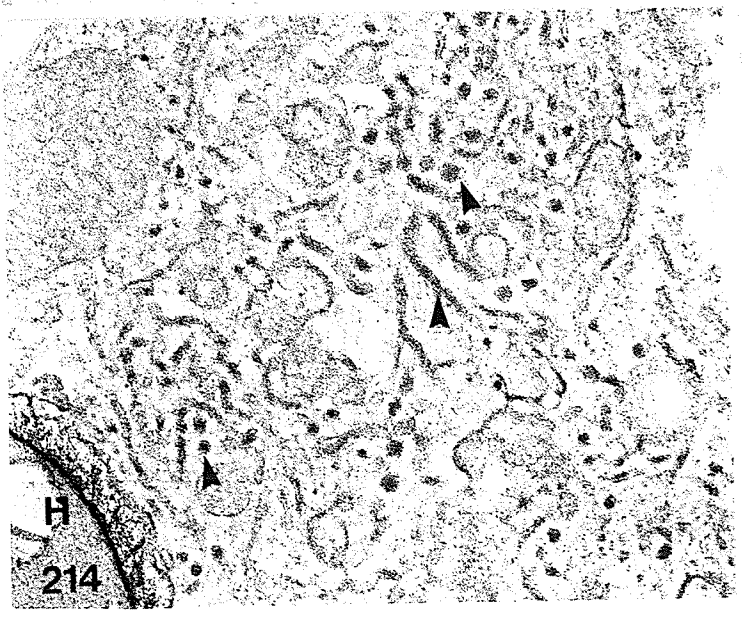
H
214

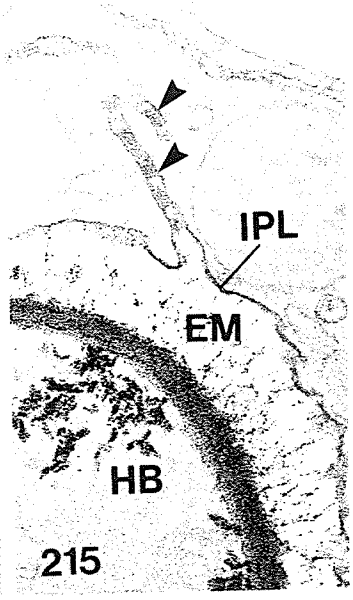
IPL
EM
HB
215

LEGEND

Figures 216-218. Haustorium-host nucleus association in P. coronata avenae.

Figure 216. A host nucleus (N) indented by a haustorial lobe (H). Glt/OsO_4. PA-TCH-SP. x16,000.

Figure 217. Cytoplasmic tubules found in the cytoplasmic region (asterisk) between the host nucleus (N) and a haustorium (H). Two lobes of the nucleus are seen. Glt/OsO_4-$K_3Fe(CN)_6$. Ua/Pb. x32,800.

Figure 218. Three lobes of a nucleus (N) indented by a haustorium are visible, and cytoplasmic tubules present in the cytoplasmic regions (asterisks) occur between the haustorium (H) and the nucleus. Glt/OsO_4-$K_3Fe(CN)_6$. Ua/Pb. x31,600.

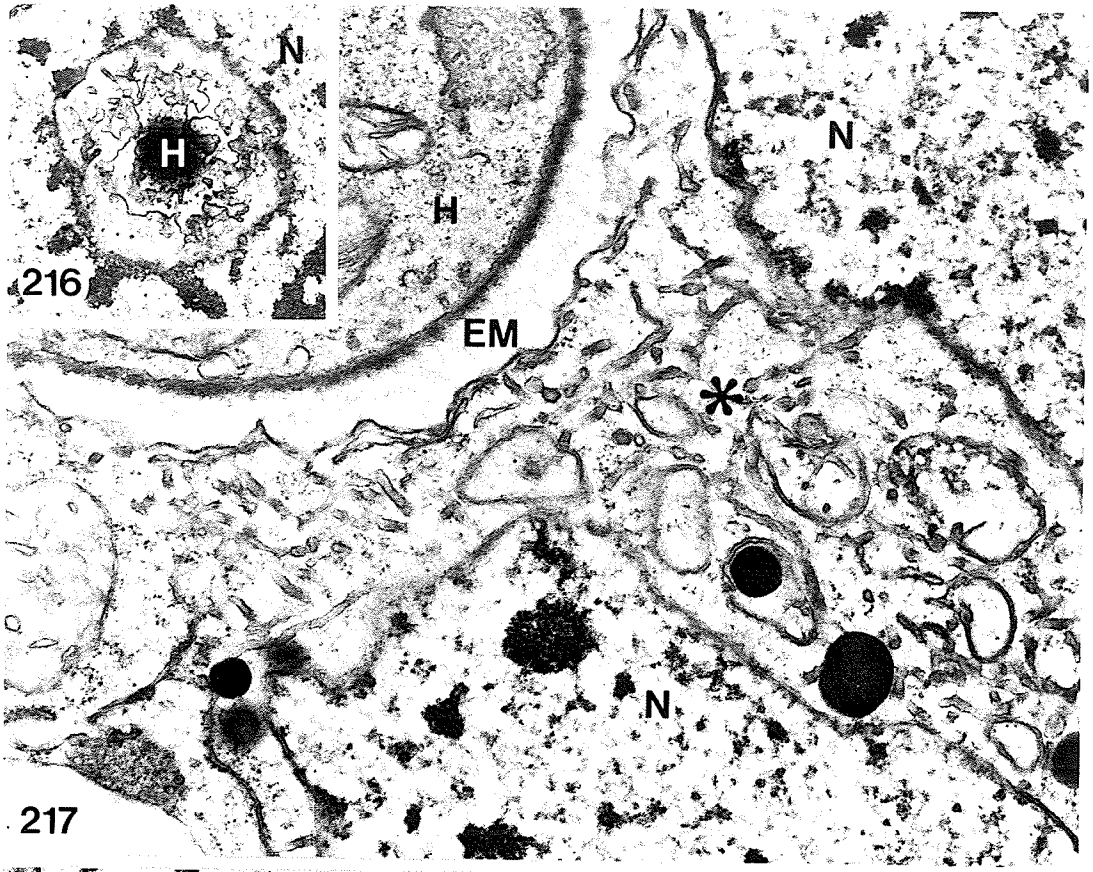
N
H
216
H
EM
N
*
N
217

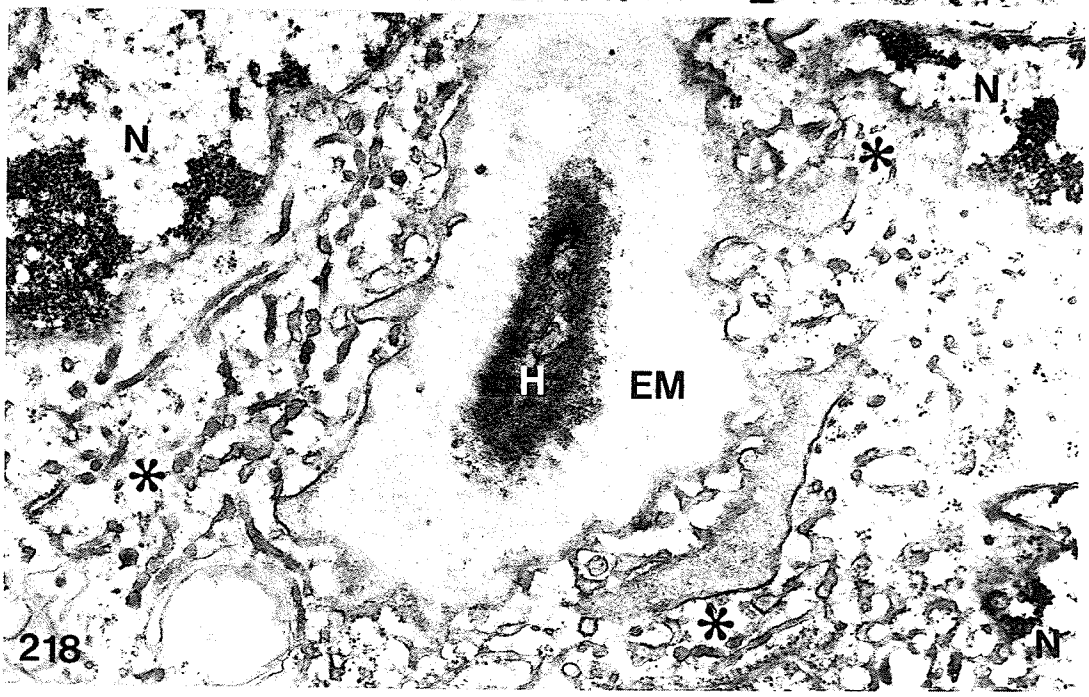
N
N
*
H
EM
*
*
218
N

LEGEND

Figures 219-221. Haustorium-host nucleus association in P. coronata avenae.

Figure 219. Close association between a haustorium (H) and the host nucleus (N). Cytoplasmic tubules are found in the region (asterisk) between haustorium and host nucleus. The nucleus is lobed. Glt/OsO_4-$K_3Fe(CN)_6$. Ua/Pb. x8,300.

Figure 220. A general view of the association of a mature haustorium (H) with the lobed portion of the host nucleus (N). Cytoplasmic tubules (arrows) are found in the region between the haustorium and nucleus, and not in other areas around chloroplasts (CH) and mitochondria. Glt/OsO_4-$K_3Fe(CN)_6$. Ua/Pb. x10,300.

Figure 221. Occasional association of cytoplasmic tubules with a chloroplast. It is likely that the host nucleus is located just out of the plane of sectioning. Glt/OsO_4-$K_3Fe(CN)_6$. Ua/Pb. x42,500.

219

220

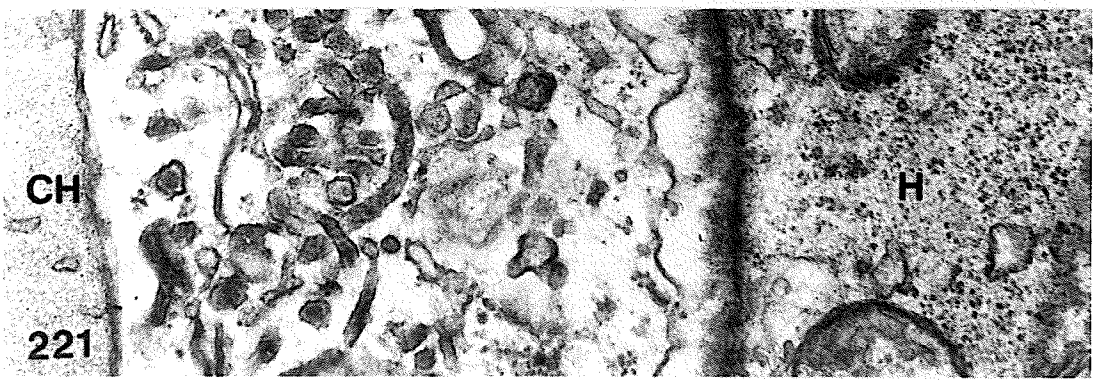

221

LEGEND

Figures 222-224. Host Golgi bodies and D-haustoria of P. coronata avenae.

Figures 222 and 223 are two adjacent sections of the same young haustorium. Only the α band is present in the neck ring. Golgi bodies (arrows) are found around the haustorial neck region. Vesicles with densely stained contents (open arrow) appeared to have budded off from the Golgi bodies. Glt/OsO_4. PA-TCH-SP. Figure 222, x27,100. Figure 223, x45,000.

Figure 224. Host Golgi bodies (arrows) found in the vicinity of a mature haustorial body. They appeared to be active in budding off vesicles. Glt/OsO_4-$K_3Fe(CN)_6$. Ua/Pb. x41,000.

Figures 225-227. Collars in dikaryotic infections of P. coronata avenae.

Figure 225. A small collar (C) around the haustorial neck of a haustorium. It is mainly electron-translucent, especially in the area around the neck. There are some electron-opaque patches in the collar. The collar is separated from the neck by both the host plasmalemma (arrow) and invaginated host plasmalemma (IPL). Glt/OsO_4. Ua/Pb. x60,700.

Figure 226. A large collar around the haustorial neck which is mainly electron-opaque. Glt/OsO_4. Ua/Pb. x29,100.

Figure 227. A section of part of a large collar with membranous material and electron-opaque patches. Glt/OsO_4. Ua/Pb. x26,800.

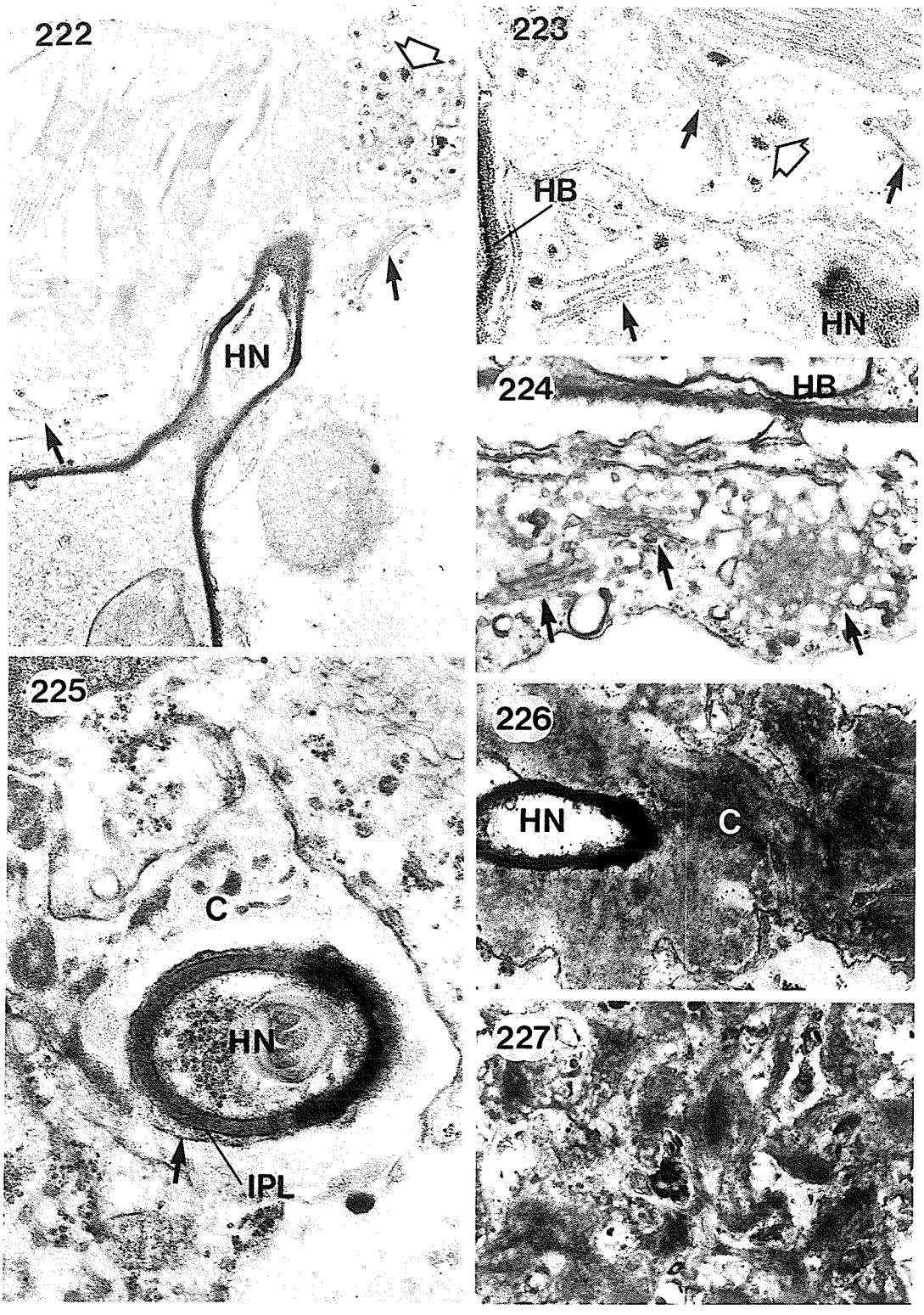
222
HN
223
HB
HN
224
HB
C
225
C
HN
IPL
226
HN
C
227

LEGEND

Figures 228-231. Collars in dikaryotic infections of P. coronata avenae.

Figure 228. A small collar (C) around a haustorial neck. Except for the immediate area around the neck, the material making up most of the collar is intensely stained, and it is continuous with the inner layer (IL) of the host wall. Glt/OsO_4. PA-TCH-SP. x31,000.

Figure 229. A large collar around a haustorial neck. Material making up most of the collar is intensely stained except for the small area immediately adjacent to the neck. The collar material is continuous with the inner layer (IL) of the host wall. Glt/OsO_4. PA-TCH-SP. x30,000.

Figure 230. An oblique cross-section of a haustorial neck surrounded by a well-developed collar (C), the material of which is intensely stained. Deposition of collar material is intense, and the inner layer of the host wall (IL) is very much thicker than the outer layer (OL). Wall appositions are observed at some distance away from the penetration site. Glt/OsO_4. PA-TCH-SP. x20,700.

Figure 231. An oblique section through the penetration region. Dense staining material (arrowheads) has been deposited against the haustorial neck and inner layer (IL) of the host wall. The IL is thinner than the OL. Glt/OsO_4. PA-TCH-SP. x50,000.

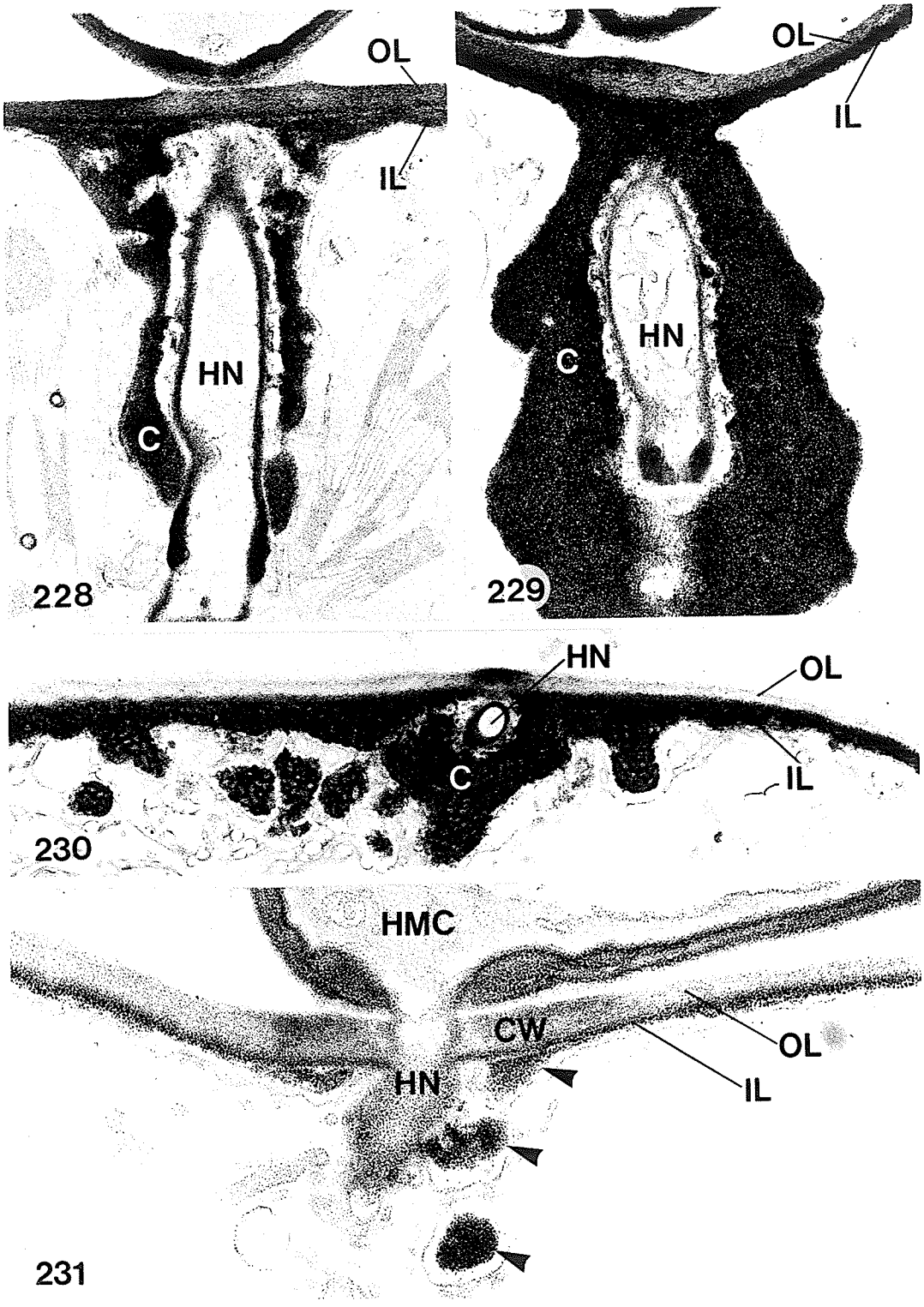
OL
IL
HN
C
228
OL
IL
HN
C
229
HN
OL
C
IL
230
HMC
CW
OL
IL
HN
231

LEGEND

Figures 232-235. Collars in dikaryotic infections. Figure 232, P. graminis tritici; Figures 233-235, P. coronata avenae.

Figure 232. A near tangential section through the penetration region. A well-developed collar has formed around the haustorial neck. Collar material is stained but is more diffuse and granular in appearance than that of P. coronata avenae. Glt/OsO_4. PA-TCH-SP. x26,800.

Figure 233. Small membrane-bound vesicles, some containing electron-opaque material (arrows) attached to the IPL along the haustorial neck. Glt/OsO_4-$K_3Fe(CN)_6$. Ua/Pb. x40,000.

Figure 234. An increased aggregation of vesicles (arrowheads) occurring around the haustorial neck. Glt/OsO_4-$K_4Fe(CN)_6$. Ua/Pb. x34,000.

Figure 235. A small collar with projections (arrowheads) radiating into the host cytoplasm. Glt/OsO_4. Ua/Pb. x44,900.

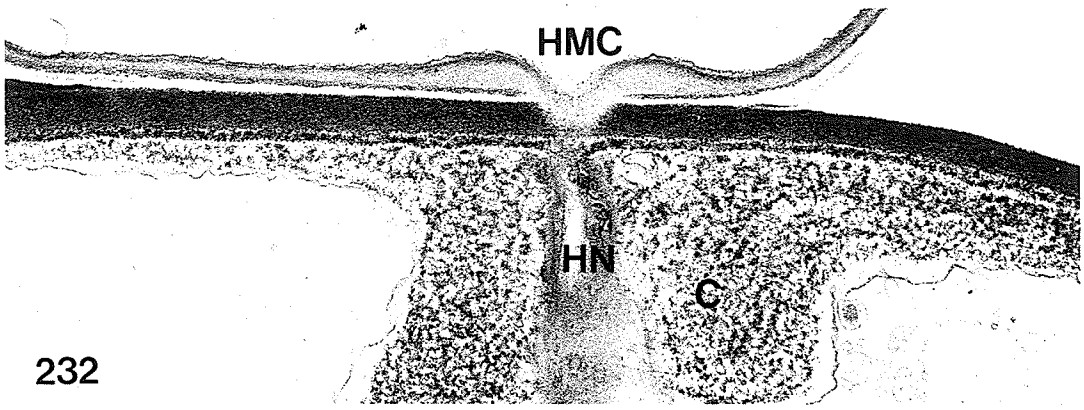

232

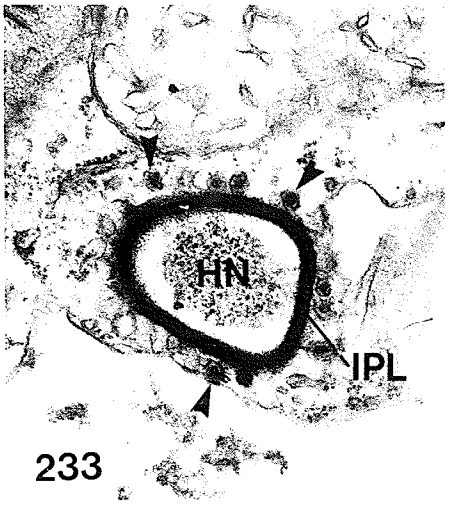

233

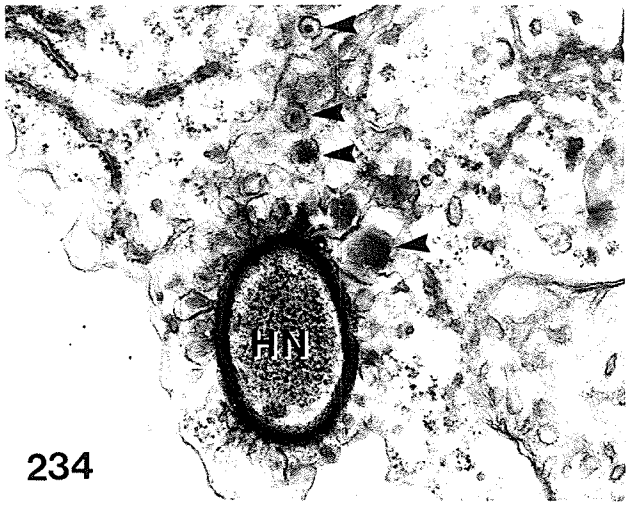

234

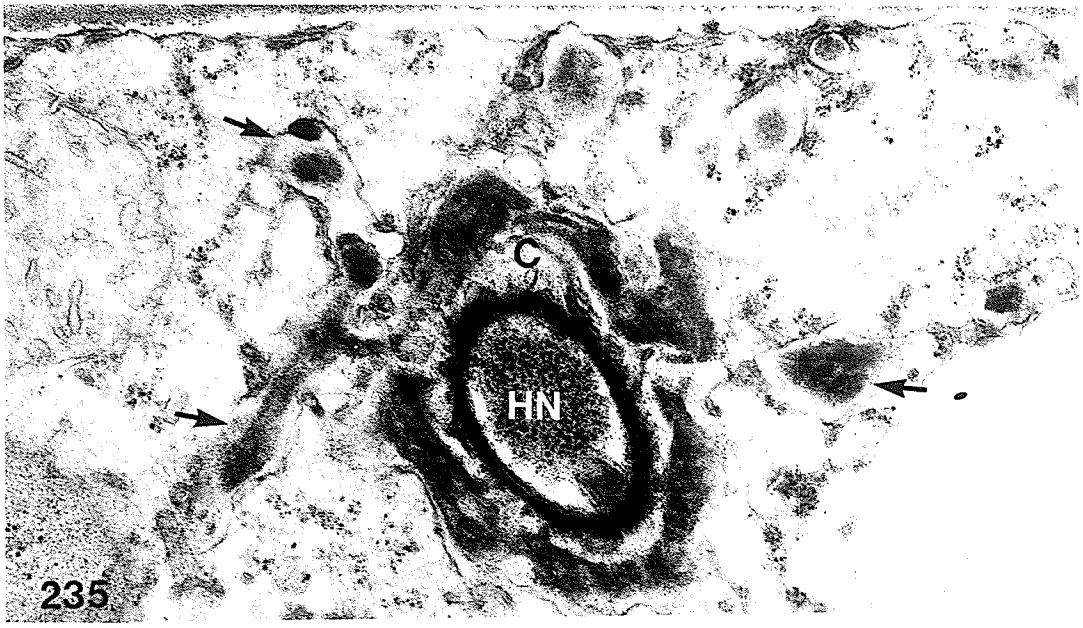

235

LEGEND

Figures 236-239. Collars in dikaryotic infections of P. coronata avenae.

Figure 236. A developing collar (C) with a projection (arrow). Serial sections showed that the nearby large vesicles (arrowheads) containing densely staining material were cross-sections of projections radiating out from the collar. Profiles of host endoplasmic reticulum (open arrows) and Golgi bodies (GB) are associated with these projections. Glt/OsO_4. PA-TCH-SP. x37,100.

Figure 237. An adjacent section to that in Figure 236. Projections of the collar are indicated by arrows. Note the close association of host endoplasmic reticulum (open arrows) with the collar. Glt/OsO_4. PA-TCH-SP. x31,400.

Figure 238. Intense Thiéry staining of collar material fixed with Glt alone. Glt. PA-TCH-SP. x18,600.

Figure 239. Collar (C) material unstained in a control treatment. Glt. PA-sodium borohydride-TCH-SP. x26,400.

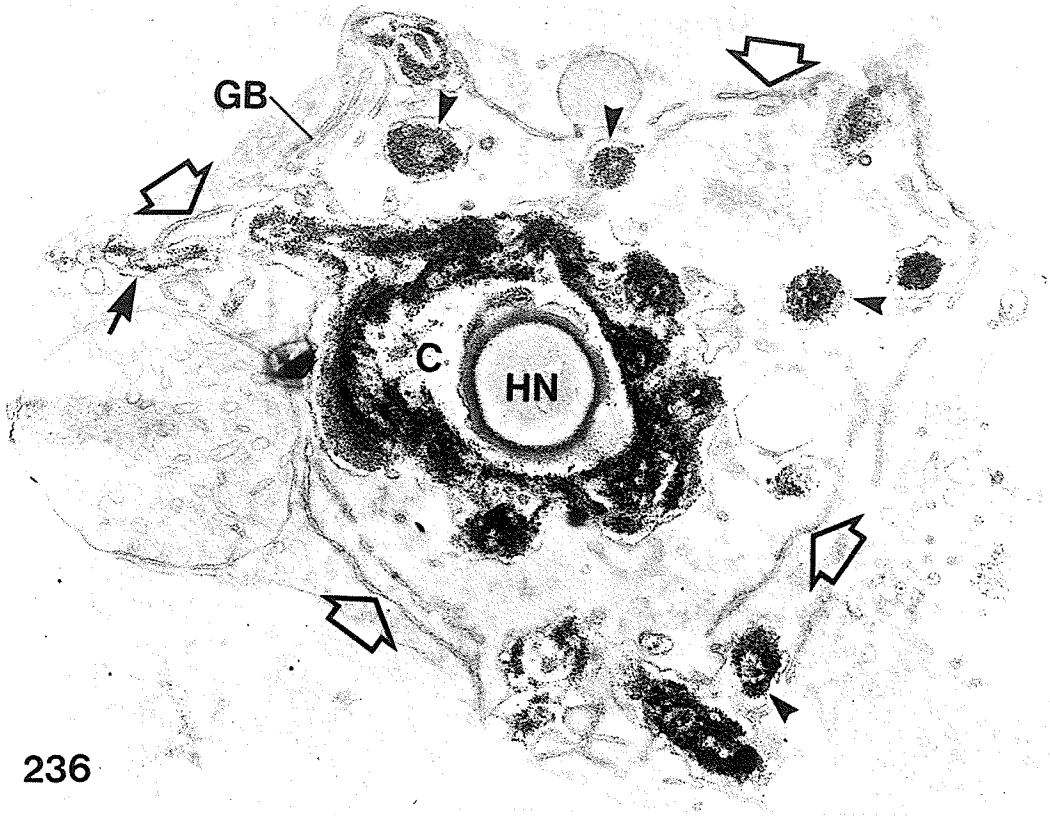

236

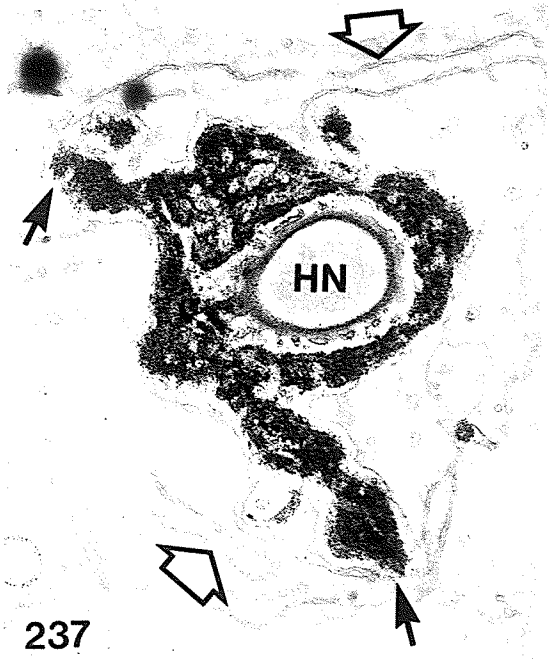

237

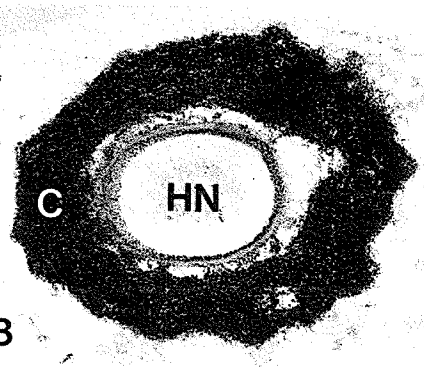

238

C HN

239

LEGEND

Figures 240-246. Collars in dikaryotic infections of P. coronata avenae.

Figure 240. Collar unstained in a control treatment. Glt. TCH-SP. x40,000.

Figure 241. Thiéry staining of the collar material after cellulase treatment. Glt-cellulase-OsO_4. PA-TCH-SP. x20,000.

Figure 242. The collar is electron-lucent after the de Bruijn staining method. Glt/OsO_4-$K_3Fe(CN)_6$. Unstained section. x40,000.

Figure 243. The collar (C) is unaffected by protease treatment, but the haustorial neck wall (arrow) is extracted. Glt-protease-OsO_4. Ua/Pb. x40,000.

Figure 244. Thiéry staining of a collar after protease treatment. Glt-protease-OsO_4. PA-TCH-SP. x30,000.

Figure 245. The collar appears to be unaffected by lipid solvent extraction. The haustorial neck is out of the plane of sectioning. Glt-ether/ethanol-OsO_4. Ua/Pb. x30,000.

Figure 246. Thiéry staining of a collar after lipid solvent extraction. Glt-ether/ethanol-OsO_4. PA-TCH-SP. x34,000.

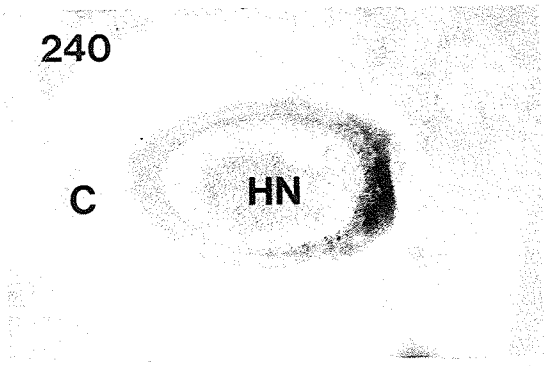
240
C
HN

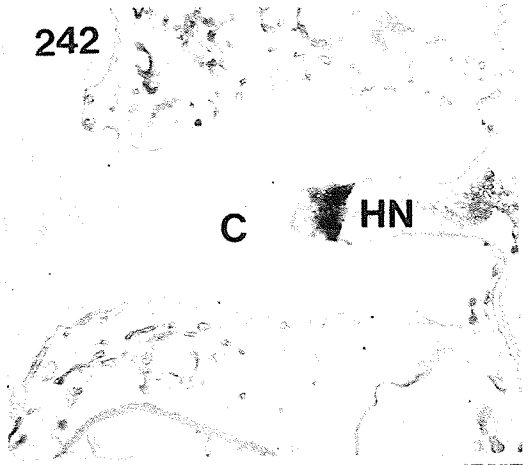
242
C
HN

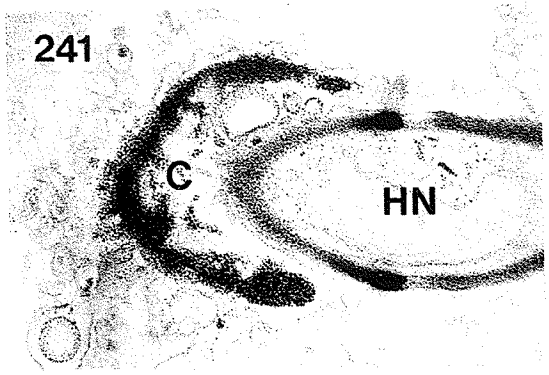
241
C
HN

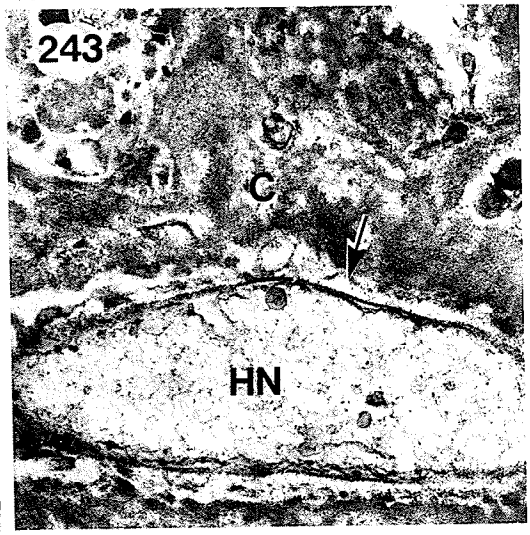
243
C
HN

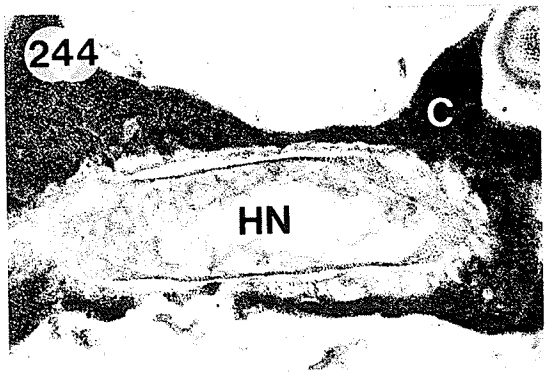
244
C
HN

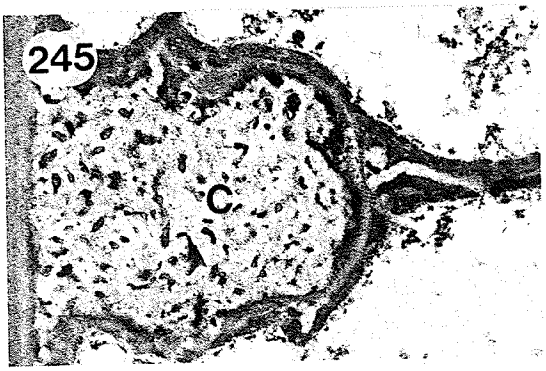
245
C

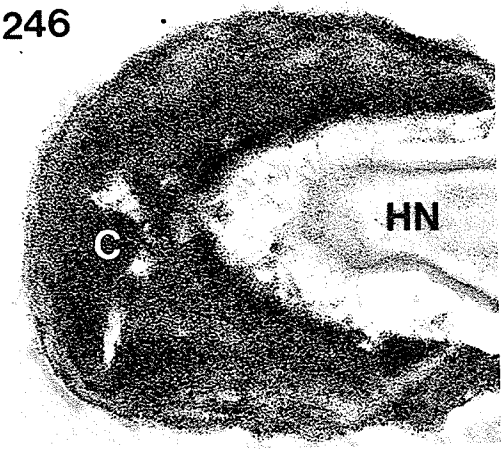
246
C
HN

LEGEND

Figures 247-251. Monokaryotic infections of P. coronata avenae.

Figure 247. Development of a protuberance (arrow) from a terminal cell (TC) during host-penetration. The fungal wall at the tip (arrow) of the protuberance is slightly thinner than that around the rest of the cell. Dense granules and membranous material are seen in the cytoplasm of the protuberance. There is no localized thickening of the fungal wall at the penetration site. A moderately-stained layer of extracellular substance is seen outside the terminal cell, which fills part of the angle of contact between host and fungus (arrowheads). Glt/OsO_4. PA-TCH-SP. x41,100.

Figure 248. The layer of extracellular substance (arrowhead) is moderately electron-lucent after staining with Ua/Pb, and the boundary between this layer and the fibrillar host wall is indistinct. Glt/OsO_4. Ua/Pb. x31,000.

Figure 249. The last fungal septum (arrow) delimiting the terminal cell (TC) found outside the host, which is located at some distance from the penetration region (asterisk), during early haustorium development. The septum contains two electron-opaque layers separated by an electron-lucent middle layer. Glt/OsO_4. Ua/Pb. x30,000.

Figure 250. The last fungal septum (arrow) occurring close to the site of penetration (asterisk), after the haustorium was more mature. Glt/OsO_4. Ua/Pb. x32,100.

Figure 251. A septum (arrow) in an older haustorium with normal appearing cytoplasm. Aberrant haustoria (arrowheads) are located in the same host cell. It is not known if these are different lobes of the same haustorium. Glt/OsO_4. Ua/Pb. x12,900.

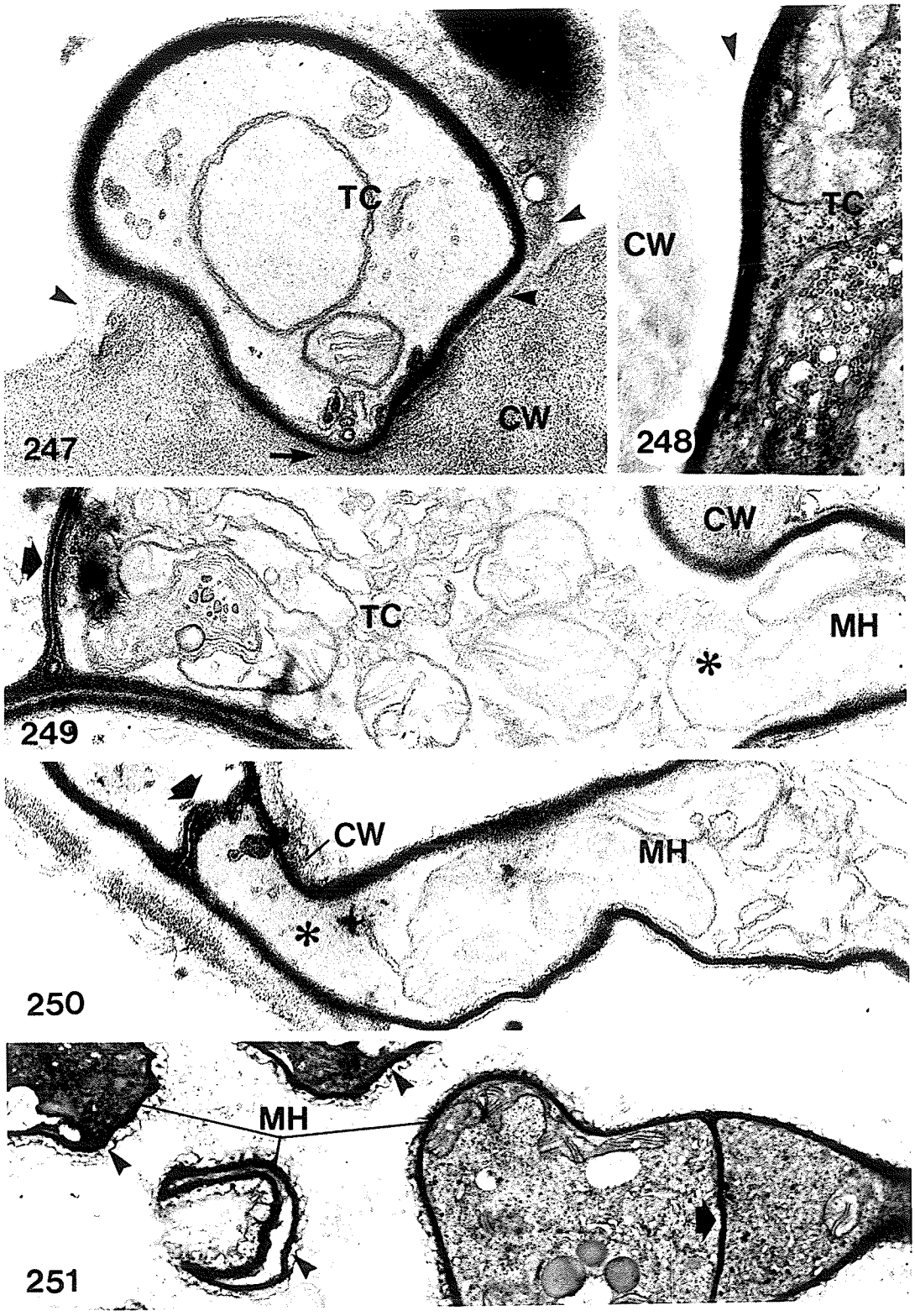
TC
CW
247
CW
TC
248
CW
TC
MH
249
CW
MH
250
MH
251

LEGEND

Figures 252-257. Monokaryotic infections of P. coronata avenae.

Figure 252. A hyphal septum (arrow) containing two electron-opaque layers separated by an electron-lucent middle layer. Glt/$0s0_4$. TCH-SP. x42,900.

Figure 253. Fungal walls are intensely stained, and they are similar in thickness throughout the penetration region. Apart from a slight constriction of the fungus at the penetration region, penetration occurred without causing any distortion in the host wall. Glt/$0s0_4$. PA-TCH-SP. x23,600.

Figure 254. An adjacent section to that in Figure 253 showing the same haustorium (MH). The fungal walls are intensely stained. The MH is filamentous in shape, there is no clearly differentiated neck region in this MH, and there is no neck ring. The constriction of the fungus seen in the host wall is due to the plane of sectioning. The nucleus of the terminal cell (TC) is seen as two lobes (N) at the penetration region, and migration of the nucleus into MH appears to be taking place. Note the separation of the invaginated host plasmalemma (arrows) especially at the distal region of the M-haustorium to form an EM. Glt/$0s0_4$. TCH-SP. x12,000.

Figure 255. A collar associated with an older haustorium (MH), which is largely vacuolated. Collar material is heterogenous with electron-opaque patches, and is fibrillar. Glt/$0s0_4$. Ua/Pb. x35,700.

Figure 256. A cross-section of a MH near the proximal region. The extrahaustorial matrix (EM) is electron-opaque, but can be differentiated from the fungal wall (arrowhead). Host endoplasmic reticulum (arrow) is seen associated with the MH. Glt/$0s0_4$. Ua/Pb. x44,600.

Figure 257. Cross-section of a haustorium (MH) in the mid-region. The extrahaustorial matrix (EM) is moderately electron-opaque, but not as dense as that in Figure 256. Small membrane-bound electron-translucent structures (arrowheads) are present in the cytoplasm of the haustorium. Glt/$0s0_4$. Ua/Pb. x34,000.

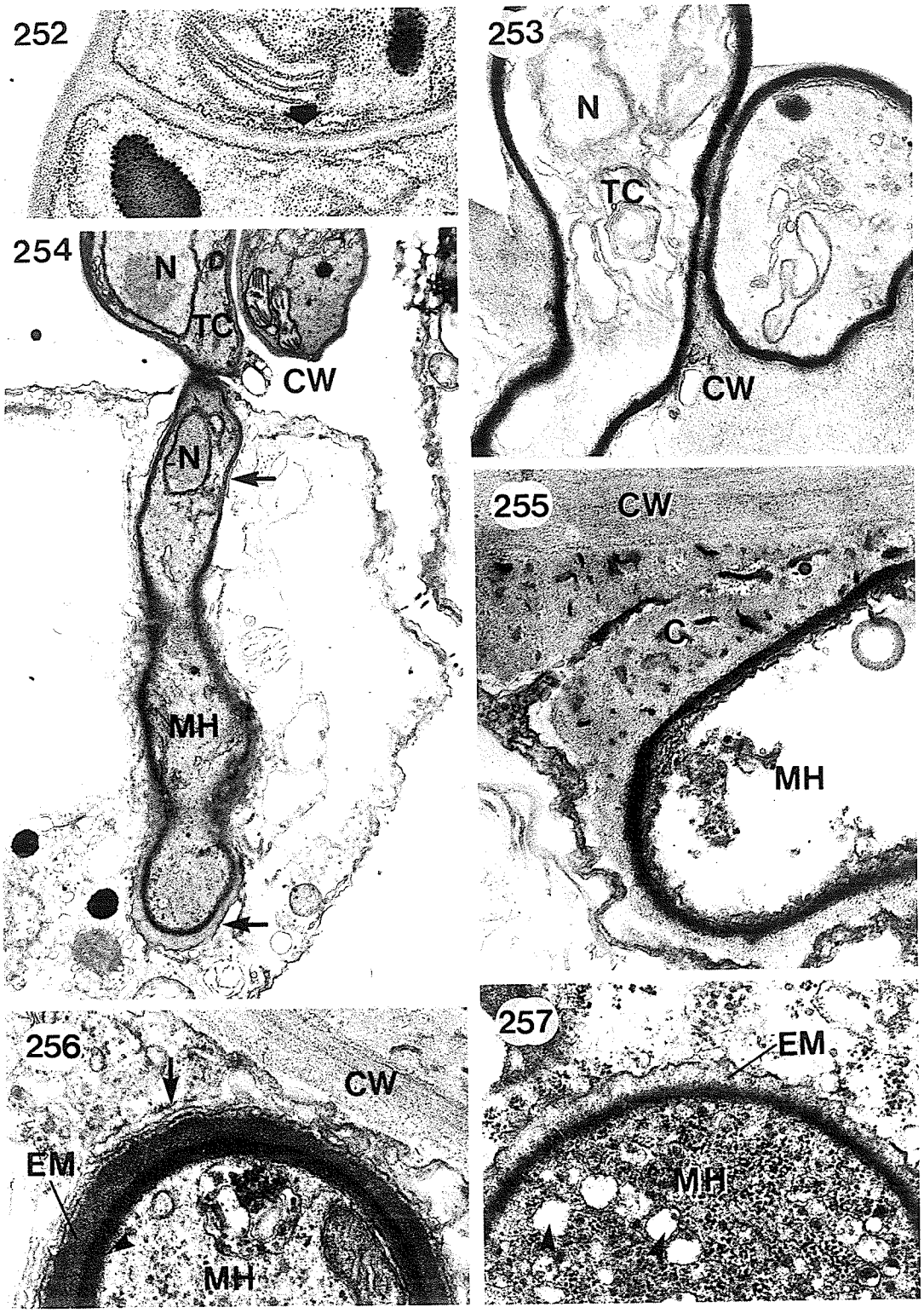
252
253
N
TC
CW
254
N
TC
CW
N
MH
255
CW
C
MH
256
CW
EM
MH
257
EM
MH

LEGEND

Figures 258-263. Cytochemistry of M-haustoria of P. coronata avenae.

Figure 258. A cross-section of a M-haustorium (MH) near the proximal end of the haustorium. The extrahaustorial matrix (EM) is electron-opaque but not as dense as the fungal wall (arrowhead). Note the presence of host endoplasmic reticulum (arrow) associated with the haustorium. Glt/OsO_4. PA-TCH-SP. x40,000.

Figure 259. A section of a haustorium (MH) through its distal end, showing a densely stained extrahaustorial matrix (EM). The fungal wall is indicated by an arrowhead. Glt/OsO_4. PA-TCH-SP. x41,000.

Figure 260. A closely adjacent section to that in Figure 258. Both fungal wall (arrowhead) and the extrahaustorial matrix (EM) are stained to the same extent in this control treatment. Glt/OsO_4. TCH-SP. x40,000.

Figure 261. A section of a haustorium (EM) through its distal end. The extrahaustorial matrix (MH) is more electron-lucent than the fungal wall (arrowhead) in this control treatment. Glt/OsO_4. TCH-SP. x43,000.

Figure 262. The extrahaustorial matrix (EM) of a haustorium (MH) and fungal wall (arrowhead) are largely unstained. Glt/OsO_4. PACP. x64,000.

Figure 263. The extrahaustorial matrix (EM) of a haustorium (MH) near its distal region is intensely stained. The fungal wall (arrowhead) is unstained, and the invaginated host plasmalemma (arrow) is lightly stained. Glt/OsO_4. PACP. x77,000.

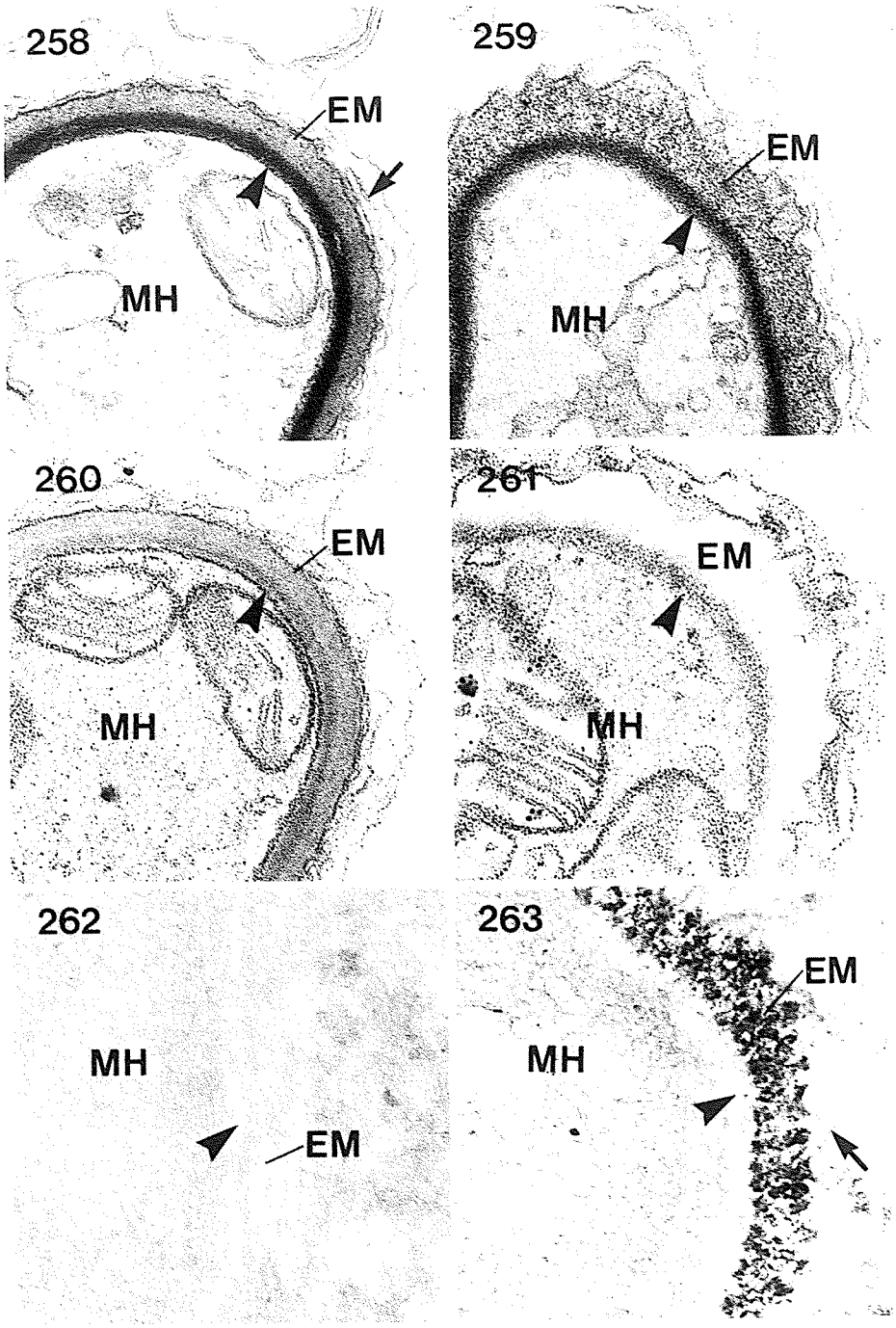
258
EM
MH
259
EM
MH
260
EM
MH
261
EM
MH
262
MH
EM
263
EM
MH

LEGEND

Figures 264-265. Aberrant M-haustoria.

Figure 264. Haustoria (arrows) with sharply contoured outlines and dense cytoplasm found in some mesophyll cells. Intercellular hyphal cells (arrowheads) are still healthy looking. Host cells show some sign of disorganization in the protoplasts. Glt/OsO_4. Ua/Pb. x6,600.

Figure 265. A M-haustorium in a sieve element (SE). This haustorium contains dense cytoplasm. The fungal structures (arrowheads) found in a mature xylem vessel (X) are more intercellular hypha-like and they lack an extrahaustorial matrix around them. Glt/OsO_4. Ua/Pb. x6,600.

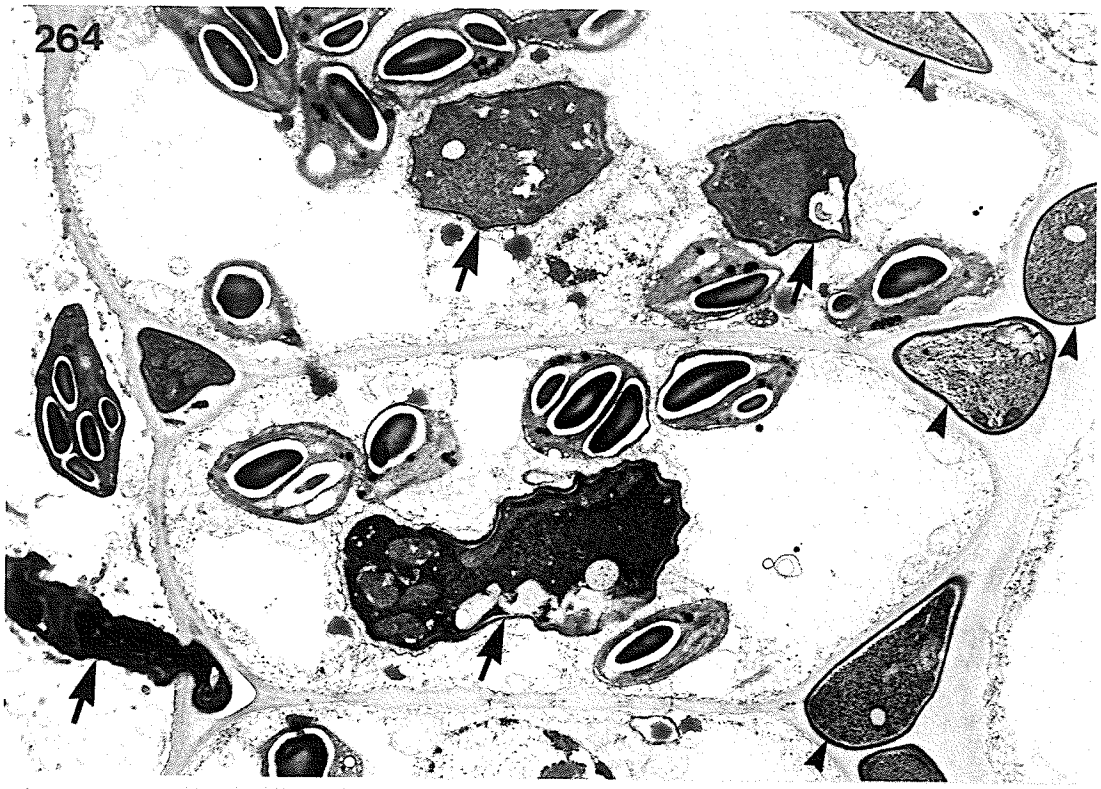
264

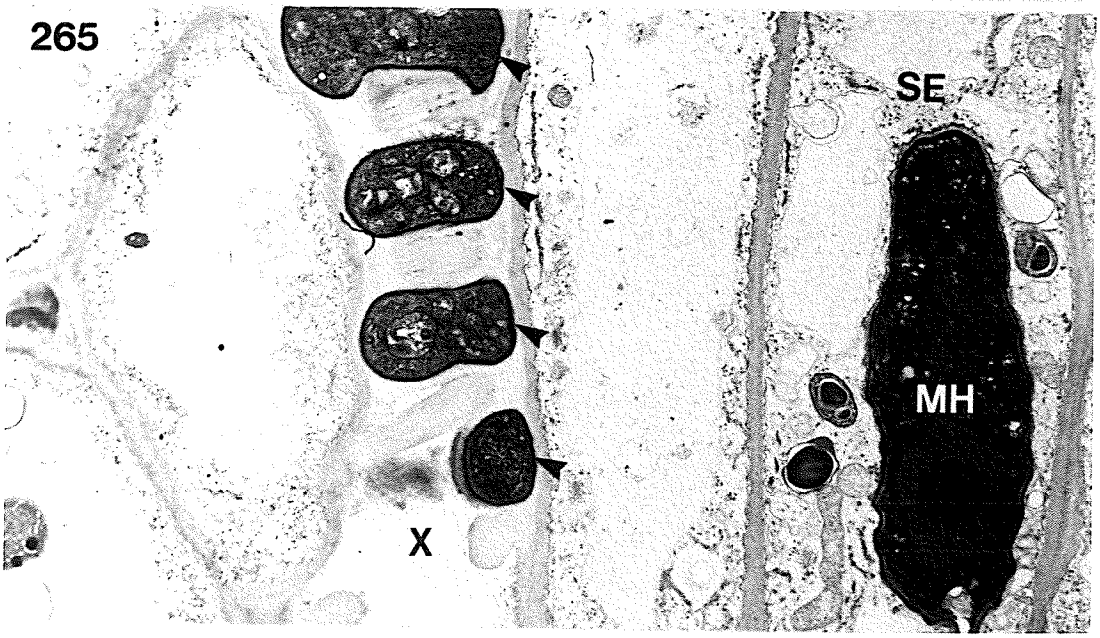
265
SE
MH
X

GENERAL DISCUSSION AND CONCLUSIONS

The structure of rust fungal haustoria has been extensively reviewed (see reviews by Bracker and Littlefield, 1973; Bushnell, 1972; Ehrlich and Ehrlich, 1971; Littlefield and Heath, 1979). However, a number of points of structure of the haustorial apparatus have remained unresolved, and very little is known of the chemical composition of component parts of the haustorial apparatus. With some exceptions, most studies to date have relied on conventional processing methods for electron microscopy, which may limit structural differentiation. By using more varied and more elaborate histochemical methods, it is possible to reveal structure in greater detail due to chemical differentiation of structural components.

In this thesis further details of structure, particularly during D-haustorium formation, have been presented. Although the D-haustorial apparatus in dikaryotic rust infections has often been referred to as a specialized structure, the structural and cytochemical details in the present study have indicated a much higher level of specialization and differentiation from the hyphal cells than has been previously indicated. This specialization is first apparent in the haustorial mother cell and its septum. The young haustorial mother cells of both P. coronata avenae and P. graminis tritici had a distinctive pattern of distribution of mitochondria around the periphery of their protoplasts, which was not found in the hyphal cell protoplasts. This pattern of mitochondrion distribution was later retained in the protoplasts of

mature D-haustoria. The haustorial mother cell walls also differed from the hyphal cell walls in terms of number of wall layers. This indicates that haustorial mother cell specialization begins with its formation, and it is not formed by mere extension of the hyphal tip. The septa that delimited the haustorial mother cells from the hyphal cells also differed structurally from those found in the rest of the mycelium. The haustorial mother cell septa contained more layers and the septal pore apparently was smaller than in the other septa. Light microscopists (Allen, 1923a; Ruttle and Fraser, 1927) remarked that certain hyphal tips that were about to form haustorial mother cells became swollen with their ends closely adpressed to the host cell wall. This suggests that induction of haustorial mother cell differentiation occurs prior to septum formation, and is probably brought about by host wall contact. Another significant difference between the haustorial mother cell septa and other hyphal septa was the characteristic development of long membrane protrusions on the hyphal side of the haustorial mother cell septum after its formation and during early stages of haustorium formation. No such structures were ever found in association with other hyphal septa.

The present ultrastructural study presented a detailed account of the development of D-haustoria of P. coronata avenae in their host cells. The results were generally similar to those reported for U. phaseoli vignae (Heath and Heath, 1975) and for M. lini (Littlefield, 1972). The haustoria of P. coronata avenae immediately after host wall penetration first appeared as finger-like projections. This projection subsequently became the haustorial neck after the haustorial body formed at the distal end. In U. phaseoli vignae (Heath and Heath,

1975), a thin fungal wall occurred through the penetration region, thus demonstrating continuity between the haustorial neck wall and haustorial mother cell wall. In the present study and as reported earlier (Harder, 1978), a thin fungal wall also occurred through the penetration region of the host wall, but it was so thin that it appeared to be absent in some cases. In P. graminis tritici, however, the fungal wall through the penetration region was thicker than that in P. coronata avenae and was revealed by the PACP or conventional Ua/Pb stains. Continuity was observed between the lens-shaped middle layer of the haustorial mother cell wall and the haustorial neck wall at the penetration site. Similar continuity was demonstrated in M. lini using the same PACP method (Littlefield and Bracker, 1972). In P. coronata avenae, although fungal wall material can be demonstrated to occur through the host wall in the penetration zone, the continuity of the fungal walls in this region is tenuous. The haustorial mother cells became detached from the haustoria by protease treatment.

The present histochemical studies showed that walls of young D-haustoria of P. coronata avenae had a unique composition not found in the haustorial mother cell or hyphal walls (Table 1). The walls of young haustoria characteristically contained protein as a major component, as indicated by their extraction with protease. They also contained an unsaturated lipid extractable with lipid solvents. This lipid component was also extractable with protease, suggesting that the lipid was a lipo-protein. Periodic acid-thiocarbohydrazide-silver proteinate (PA-TCH-SP) positive material was also abundant in walls of young haustoria. However, much of this PA-TCH-SP material in the haustorial walls was extractable with either protease or lipid solvents, suggesting

that it is also protein or lipid bound. As glucans are common wall components of fungi and as PA-TCH-SP is a general stain for polysaccharides, it is likely that some, if not all of the positive staining material seen in the haustorial walls was a polysaccharide(s), although it is known that some fatty acids and polypeptides are stained by this method (Hall, 1978). The presence of certain carbohydrate component(s) was confirmed by the presence of many Concanavalin A receptor sites on the haustorial walls. Thus, as with the lipids, the carbohydrate component likely occurs as a glycoprotein. The mycelial and haustorial mother cell walls also contained a lipid component, and histochemical reactions indicated that it was a saturated type. In contrast to the lipid found in walls of young haustoria, the lipid in mycelial walls was unaffected by protease treatment. Mycelial walls also contained PA-TCH-SP positive material but unlike that in walls of young haustoria, this material was resistant to both protease or lipid solvent treatments. Enzyme digestible protein thus was not a major component in the mycelial walls. Apart from the observation that these walls became more fibrillar in appearance after protease treatment, their staining characteristics remained essentially the same as the untreated ones. Wheat germ lectin receptor sites were found in all mycelial walls and septa, but not in walls of young haustoria. As haustoria matured, however, wheat germ lectin receptor sites were detected in the body walls but the neck walls were always free of wheat germ receptor sites. The detection of wheat germ lectin receptor sites in fungal walls indicates the presence of chitin (Horisberger and Vonlanthan, 1977; Molano et al, 1980). The above comparison studies therefore revealed a sharp contrast in chemical composition between

walls of haustorial mother cells and walls of young haustoria. Evidently, the thin fungal wall of the penetration peg marks the transition in chemical composition between the wall of the haustorial mother cell and that of the haustorial neck. Haustorium differentiation thus involves synthesis of new and unique materials, and it is not the result of a "simple" extension of the haustorial mother cell.

It is significant that the walls of young D-haustoria, particularly of the neck of P. coronata avenae had a unique composition not found in the mycelial walls, and available evidence suggests that the polysaccharide and protein components in the young haustorial walls are most likely present in more complex forms as glycoproteins. It is well established that race specificity in some plant - fungal systems is determined by specific plant recognition of fungus surface glycoproteins (Callow, 1977; Dow and Callow, 1978; Keen and Legrand, 1980; Wade and Albersheim, 1979). The finding of glycoproteins in the haustorial walls would suggest that the specificity factors may reside in these glycoproteins. This is in accordance with the results of previous studies (Samborski et al, 1977) which indicate that incompatibility between wheat and stem rust may be determined at the interface between host cells and newly formed haustoria. The invagination of the host plasmalemma and contact with the nascent neck wall may thus be one crucial step in the establishment of the host - parasite interaction. This view is consistent with the results of the M. lini - flax system (Littlefield and Bracker, 1972) which show that the invaginated host plasmalemma possesses distinctive features not present in the non-invaginated portion of invaded host cells. Change in staining properties of the invaginated host plasmalemma was also demonstrated in

the present study of the P. coronata avenae - oat system.

The characteristic membrane protrusions associated with the haustorial mother cell septa observed in the present study were also previously reported for U. phaseoli vignae (Heath and Heath, 1975), P. hordei (Reynolds, 1975) and possibly for M. lini (cited in Littlefield and Heath, 1979). Heath and Heath (1975) suggested that the occurrence of these membrane protrusions during early haustorium formation is to provide additional membrane area needed at this time to facilitate energy-requiring transport of materials across the septum. This would explain why there was a large accumulation of mitochondria in close association with the membrane protrusions during the maximum development as seen in the present study and in U. phaseoli vignae (Heath and Heath, 1975). However, there has been no information on their chemical composition to determine how they relate physiologically to the developing haustoria. The membrane protrusions in P. coronata avenae and P. graminis tritici were long flattened cisternae, closed at the end furthest from the haustorial mother cell septum. In plants and animals, membrane structures of similar shape have been regarded as functional sites where intensive secretion or absorption may take place (Berridge and Oschman, 1972; Gunning, 1977). However, as the maximum development of these protrusions coincided with the penetration of the host wall before the formation of the haustorium it is more likely that materials were being secreted into the haustorial mother cell, rather than out of it. The matrix of the septal protrusions was shown to contain unsaturated lipid, protein and PA-TCH-SP positive material as major constituents (Table 1) and it is of interest that the matrix of septal protrusions and the composite materials of the haus-

torial neck walls reacted similarly chemically, indicating a similar composition. Since the maximum development of the protrusions occurred during penetration of the host wall and a marked reduction in size of these protrusions occurred coincidentally with haustorial neck formation, it is possible that components of the membrane protrusions are used for the synthesis of the neck wall. Certain stages of early haustorium formation are ephemeral (Littlefield, 1972) suggesting that young haustoria are formed rapidly. To meet this requirement, large amounts of material would be needed quickly to synthesize the young haustorial necks.

The extrahaustorial matrix, ie. the interface between the invaginated host plasmalemma and the haustorial wall, has long been a subject of debate (Bracker and Littlefield, 1973; Littlefield and Heath, 1979). This is because the structural appearance of the extrahaustorial matrix may vary under different conditions of fixing and staining. This was demonstrated in the present study in that the extrahaustorial matrix in specimens fixed with glutaraldehyde alone was electron-lucent after conventional Ua/Pb staining, but stained intensely after PA-TCH-SP treatment for polysaccharides. For unknown reasons also, the extrahaustorial matrix in specimens fixed with glutaraldehyde alone stained more intensely after PA-TCH-SP treatment than those in specimens fixed with the conventional glutaraldehyde/OsO_4 process. The "electron-lucent" extrahaustorial matrix has been considered as an artifact of preparation (Allen et al, 1979). However, in the present study materials in this region could be demonstrated histochemically and these were removable with enzyme treatments. One possibility is that prepárative procedures solubilize materials and these

become re-distributed in the matrix region, resulting in positive staining. This possibility was not disproven in the present study, although it is considered unlikely because free or soluble materials are usually washed out of the tissue during preparation, as indicated by the enzyme digestion results. It is concluded that the extrahaustorial matrix is an integral structural component of the haustorial-host interface.

It is of significance that the composition of the extrahaustorial matrix of the D-haustorium of P. coronata avenae differed from that of the wall of the mature haustorial body. The present histochemical studies showed that it contained mainly PA-TCH-SP positive material, protein and some lipids but no wheat germ lectin receptor sites. It was probably free of chitin. Histochemical reactions suggested that the lipid in the extrahaustorial matrix was of the saturated type. The walls of mature haustoria on the other hand, were characterized by the presence of wheat germ lectin receptor sites and unsaturated lipid in addition to protein and PA-TCH-SP positive material. Thus the matrix does not appear to be a modification of the haustorial body wall.

The development of the extrahaustorial matrix of D-haustoria of P. coronata avenae was accompanied by a marked proliferation of tubules in the host cytoplasm between the D-haustoria and the host nuclei, and direct continuity between the tubules and the extrahaustorial matrix was frequently observed. Both the tubules and the extrahaustorial matrix lost electron-opaque material after cellulase treatment, indicating that cellulose was present in these structures. Although the cellulase preparation was free from measurable proteolytic activity, it may have contained other polymer-degrading enzymes besides cellulase.

Using similar enzyme preparations, Scannerini and Bonfante-Fasolo (1979) and Hickey and Coffey (1978) reported cellulose as a component of the extrahaustorial matrix in other plant/fungal interactions. The presence of cellulose in the extrahaustorial matrix of P. coronata avenae suggests that this component is of host origin since it has not been detected anywhere else in the fungus, and provides further evidence that the extrahaustorial matrix is an integral structural component of the haustorial-host interface. It is possible that deposition of cellulose in the extrahaustorial matrix is a response of the host to build a cellulosic wall at this interface.

In P. coronata avenae it is also significant that there was a close association of the host cytoplasmic tubule complexes with the host nuclei. Those portions of the host nuclei that were adjacent to these tubules were highly irregular in outline. Striking alterations in form and size of host nuclei of infected cells and the close contact of these nuclei with haustoria of P. poarum were reported in a recent study (Al-Khesraji and Lösel, 1980). Such nuclear alterations observed were interpreted as changes in nuclear content, or in the properties of the nuclear membrane, and a direct involvement of nucleic acid metabolism of the host during host-parasite interactions was thus implicated (Al-Khesraji and Lösel, 1980). The change in shape of the host nuclei and the occurrence of tubules mainly in the host cytoplasm between D-haustoria and host nuclei observed in P. coronata avenae may be of significance in this connection.

Although the tubule complexes differed from the haustorial mother cell septal protrusions cytochemically, they were structurally somewhat similar in being membrane-bound with a dense core. As indi-

cated above, this type of structure indicates intense secretory or absorptive activity. This presents the intriguing possibility of a high level of exchange between host and fungus, including products of nuclear metabolism. Direct connections were only seen between the tubules and the invaginated host plasmalemma, thus it is most likely that the flow of materials is in the direction of the haustorium.

Using energy dispersive X-ray (EDX) analysis, the neck ring of P. coronata avenae was shown conclusively to consist of two cylindrical bands, designated the α and β bands. The α band contained mainly silicon whereas the β band contained mainly iron and phosphorous. The EDX analysis also showed silicon to be present in large amounts in the walls of haustorial mother cells that were located mainly at or near the centers of the infection colonies. As mentioned earlier, the occurrence of silicon in fungal tissue is rare. It is, however, a rather common constituent of plant tissue particularly in gramineous plants, including oats (Jones and Handreck, 1965; Jones and Milne, 1963). The silicon in oat plants is taken up passively from the soil solution as monosilicic acid, and is distributed through the plant mainly via the transpiration stream (Jones and Handreck, 1965). However, the route of silicon uptake by the fungus needs to be ascertained as this may provide useful information on the physiologic role of haustoria. Assuming that a source of silicon is available to the fungus from the host, deposition or an active polymerization process must occur specifically in the membrane protrusions, haustorial mother cell and septal walls, and in the α band of the neck ring, and not anywhere else in the fungus. The mechanisms of silicon deposition in higher plants are still not clear, although many hypotheses, mainly attributing

deposition to the impedance of the evapotranspiration stream, have been put forward (Scurfield et al, 1974; Sargent and Gay, 1977; Sangster and Perry, 1976). However, recent evidence indicates that metabolic activity of some kind may also be involved in the formation of silicon deposits (Heath, 1979). Also, a metabolic role for silicon in the germination of E. graminis hordei was indicated (Kunoh et al, 1978). The specificity of the occurrence of silicon in the haustorial apparatus in the present study further indicates a controlled metabolic deposition of silicon.

Heath (1976) provided evidence that the neck ring of P. sorghi is capable of preventing apoplastic flow of substances along the haustorial neck and accordingly, the silicon deposits found in the neck ring of P. coronata avenae could very well function as a form of permeability barrier. The heavy silicification of haustorial mother cell walls and septa located at or near the infection colony centers is more difficult to explain. As mentioned earlier, structural changes in walls of haustorial mother cells located at the centers of older infection colonies have been reported in the same fungus by early light microscopists (Ruttle and Fraser, 1927). These haustorial mother cells were distorted and the appearance of their walls was described as glassy and swollen. In extreme cases, the lumen of the haustorial mother cells was almost obliterated. Significantly, the haustoria formed from these haustorial mother cells were also abnormal in appearance (Ruttle and Fraser, 1927). In the present study, the haustorial mother cells of P. coronata avenae showing heavy silicification in their walls eventually collapsed, and frequently they were found to be associated with aberrant, necrotic haustoria which were common in host cells at the

centers of older infection colonies. Necrosis of haustoria in these host cells would indicate incompatibility and would result in the production of deleterious interaction products. It is possible then that the heavy silicification seen in the above haustorial mother cell walls is a protective mechanism of the fungus and acts as a form of permeability barrier to prevent or minimize the passage of unwanted products from reaching the rest of the mycelium.

In the present study, phosphorous-rich iron-containing deposits were detected by EDX analysis in the protoplasts of haustorial mother cells and older D-haustoria of P. coronata avenae. These phosphorous-rich deposits were electron-opaque in unstained sections of glutaraldehyde fixed, unosmicated tissue. They were typically found within vacuoles, similar to the polyphosphates reported in other fungi (White and Brown, 1979; Bullock et al, 1980). Nishi (1961) has reported that large amounts of polyphosphate accumulated in spores of Aspergillus niger and was utilized during germination. A similar observation was made in the case of germinating urediospores of P. graminis tritici, as polyphosphates were found in almost every germ tube in the early stages of germination but were rarely detected at later stages (Bennett and Scott, 1971). Although at present there is insufficient information to ascribe a specific role for polyphosphate, a number of functions have been proposed (Harold, 1966; Bennett and Scott, 1971). Polyphosphates are thermodynamically high energy phosphate compounds and polyphosphate accumulation could be an energy storage mechanism. Accumulation of polyphosphate also allows large amounts of phosphorous to be stored in a non-leakable form (Farrar, 1976). Polyphosphate storage is also a mechanism for regulating orthophosphate levels in the cells under

fluctuating conditions. All of these possible roles are applicable in P. coronata avenae.

In the vesicular-arbuscular mycorrhizal system, it has been suggested that phosphates were taken up by the fungus from the soil, and after conversion, polyphosphates were translocated as vacuolar granules to active arbuscules (Callow et al, 1978). By analogy, it may be that phosphates were taken up by the haustoria of P. coronata avenae from the host cells and after conversion, polyphosphates were then translocated to other parts of the mycelium. This is consistent with the finding that much of the polyphosphate found in P. graminis tritici was located in the urediospores (Bennett and Scott, 1971), and the only source of phosphates was from the host.

In the present study electron-opaque deposits were common in small vacuoles in young haustorial mother cells of P. coronata avenae during early stages of D-haustorium formation. As these electron-opaque deposits were found in Ua/Pb stained sections of glutaraldehyde/OsO_4 fixed tissue, it is not known if these deposits were equivalent to the phosphorous-rich iron-containing deposits found in unstained sections of haustorial mother cells and haustoria that had been fixed with glutaraldehyde alone. However, if it could be determined through further studies that the commonly observed electron-opaque vacuolar deposits in these young haustorial mother cells are indeed phosphorous-rich, this would implicate the involvement of polyphosphates in haustorium formation. This is not unreasonable because large amounts of both energy and phosphorous would be required for the synthesis of at least phospholipids during haustorium formation.

The structural features of M-haustoria of P. coronata avenae

in Rhamnus were similar to those reported in other monokaryotic infections (see review in Littlefield and Heath, 1979; Al-Khesraji et al, 1980; Al-Khesraji and Lösel, 1980). They showed little of the structural specialization of the D-haustorial apparatus of P. coronata avenae found in the Avena host. This lack of structural specialization was first apparent in the mother cells. Unlike D-haustoria, the M-haustoria of P. coronata avenae were not associated with a distinct haustorial mother cell. As far as could be determined from the present study, no special structural differentiation occurred in the mother cells in producing the M-haustoria. Dikaryotic haustorium formation on the other hand involves formation of a specialized penetration peg in the thickened region of the haustorial mother cell wall at the site of host penetration, as shown in the present study and others (Heath and Heath, 1975; Littlefield and Bracker, 1972). The characteristic development of elaborate membrane protrusions and their association with a large mass of mitochondria in the haustorial mother cell septal region during early D-haustorium formation reported in the present study and in others cited earlier further add to the evidence that D-haustorium formation involves complex physiological processes (Heath and Heath, 1975). As mentioned earlier, membrane structures of similar shape have been regarded as functional sites where intensive secretion or absorption may take place. Similar structural changes were not observed during early M-haustorium formation in P. coronata avenae. The above findings suggest that in P. coronata avenae, monokaryotic haustoria differ from dikaryotic in their mode of formation in their respective hosts. Results from the present histochemical studies support this view. With D-haustoria, the thin fungal wall of the pene-

tration peg marks an abrupt change in composition of the haustorial mother cell walls, but the materials in the protrusion matrix were shown to be similar in composition to the walls of the young haustoria. This provides further evidence that new materials were being secreted into the haustorial mother cell for formation of a young D-haustorium with a unique wall composition. Walls of the M-haustoria on the other hand, were shown to be similar in composition and structure to those of the intercellular hyphae. Apart from a slight constriction at the site of host penetration, there was no clearly differentiated neck region, and there was no structural differentiation at the site of host cell penetration. The position of the last septum during growth of the M-haustoria also varied. As the haustorium continued to grow the septum was located nearer to the penetration site, and older haustoria themselves were septate. Also no structural differences could be found between the last septum and other septa anywhere in the intercellular mycelium. Evidently septation continued as though the M-haustorium is a normally growing hypha. The M-haustoria thus appear to be relatively undifferentiated hyphae, and they are formed by simple extension, or continued growth of the "mother cell", which in turn is also an undifferentiated hyphal cell.

Similar to that in D-haustoria, the host plasmalemma was invaginated by the M-haustoria, forming an extrahaustorial matrix between the invaginated plasmalemma and the fungal wall. Unlike that in D-haustoria, however, the extrahaustorial matrix was consistently electron-opaque, often staining with Ua/Pb and PA-TCH-SP, and it was clearly differentiated from the similar staining, but more discrete fungal walls. The question of whether the matrix is a fixation arti-

fact arises again. The present study showed that PACP positive material was located in the extrahaustorial matrix, but not in the host wall or in the haustorial wall. It is therefore unlikely that the matrix was an artifact resulting from preparation or from modification of the haustorial wall, even though it is possible that the thickness of the matrix has been accentuated by fixation as suggested by Littlefield and Heath (1979).

In general, the observations on P. coronata avenae support those on other rusts (see Gold et al, 1979; Littlefield and Heath, 1979), concerning the differences in structure between the M-haustoria (or intracellular structures) of the monokaryon and the D-haustoria of the dikaryon. In a more recent study, there is evidence that the typical dikaryotic haustoria and the monokaryotic intracellular structures of P. poarum on its alternate hosts also differed in other characteristics such as frequency of penetration of host cells, growth habit, close association with host nuclei and ability to infect vascular tissue (Al-Khesraji and Lösel, 1980). These findings suggested that the alternating phases of P. poarum differed in their nutrition and physiology, thus requiring two types of intracellular structures. While there is no quantitative data on frequency of penetration of host cells from the present study for comparison, the development of P. coronata avenae in both of its hosts is similar to that of P. poarum in some aspects. With both fungi, a close association occurred between host nuclei and haustoria but only in the dikaryotic phases. Also, the growth of the monokaryotic intracellular structures of both fungi was of limited extent and terminated within the host cells. They have not been observed to grow through and exit from the mesophyll cells. Only

the monokaryotic phases of either fungus invaded the vascular tissue of the hosts. This is significant because not all monokaryons invade the vascular tissue. Such is the case with the monokaryon of P. recondita (Gold et al, 1979). The ability of a rust fungus to invade vascular tissue may have a nutritional advantage. As pointed out by Al-Khesraji and Lösel (1980), the invasion of the host vascular tissue is likely to contribute substantially to the nutrition of the fungus, making it less dependent on intracellular structures elsewhere in the mesophyll.

The designation of M-haustoria as haustoria or as intracellular hyphae will doubtless remain controversial. However, as mentioned earlier, the exiting of the M-haustoria of P. coronata avenae from invaded cells has not been observed in the present study and in others (Harder, 1978; Allen, 1932b), as it has for some other rust fungi (see Littlefield and Heath, 1979), indicating at least some specialization of the intracellular structures of P. coronata avenae. Evidently, the M-haustoria of the rust fungi vary in their degree of specialization, and it will be difficult to establish precise criteria by which to designate them.

Table 1. Cytochemistry of the component parts of P. coronata avenae in its Avena host and of the host-parasite interface.

Chemical component	Hyphal wall	D-Haustorial Apparatus								Collar
		HMC wall	HMC[a] septal wall	Matrix of septal protrusions	Haustorium			Extra-haustorial matrix	Haustorium associated host cytoplasmic tubules	
					Neck wall	Body wall	Neck ring			
Protein	-	-	-	+	+	+	-	+		-
Lipid										
Unsaturated	-	-	-	+	+	+	-	-	-	-
Saturated	+	+	+				-	+	-	-
PA-TCH-SP[b] positive material	+	+	+	+	+	+	-[c]	+	+	+
Cellulose	-	-	-	-	-	-	-	+	+	-
Glycogen	-	-	-	-	-	-	-	-	-	-
Concanavalin A receptors (glucan and/or mannan)	+	+	+	+	+	+	-	+		
WGL[d] receptors (chitin)	+	+	+	-	-	+[e]	-	-		
Silicon	-	+[f]	+[f]	+[f]	-	-	+	-	-	
Iron and Phosphorous	-	-	-	-	-	-	+	-	-	

a haustorial mother cell
b periodic acid-thiocarbohydrazide-silver proteinate
c cannot be determined
d wheat germ lectin
e in mature haustoria
f in cells located at or near the center of the infection colony

BIBLIOGRAPHY

Abu-Zinada, A.A.H., A. Cobb, and D. Boulter. 1975. An electron-microscopic study of the effects of parasite interaction between Vicia faba L. and Uromyces fabae. Physiol. Plant Pathol. 5: 113-118.

Al-Khesraji, T.O., and D.M. Lösel. 1980. Intracellular structures of Puccinia poarum on its alternate hosts. Trans. Br. Mycol. Soc. 75: 397-411.

Al-Khesraji, T.O., D.M. Lösel, and Gay, J.L. 1980. The infection of vascular tissue in leaves of Tussilago farfara L. by pycnial-aecial stages of Puccinia poarum Niels. Physiol. Plant Pathol. 17: 193-197.

Allen, F.H.E., M.D. Coffey, and M.C. Heath. 1979. Plasmolysis of rusted flax: A fine structural study of the host-pathogen interface. Can. J. Bot. 57: 1528-1533.

Allen, R.F. 1923a. A ctyological study of infection of Baart and Kanred wheats by Puccinia graminis tritici. J. Agric. Res. 23: 131-152.

Allen, R.F. 1923b. Cytological studies of infection of Baart, Kanred and Mindum wheats by Puccinia graminis tritici forms III and XIX. J. Agric. Res. 26: 571-604.

Allen, R.F. 1930. A cytological study of heterothallism in Puccinia graminis. J. Agric. Res. 40: 585-614.

Allen, R.F. 1932a. A cytological study of heterothallism in Puccinia triticina. J. Agric. Res. 44: 733-754.

Allen, R.F. 1932b. A cytological study of heterothallism in Puccinia coronata. J. Agric. Res. 45: 513-541.

Allen, R.F. 1934. A cytological study of heterothallism in flax rust. J. Agric. Res. 49: 765-791.

Allen, R.F. 1935. A cytological study of Puccinia malvacearum from the sporidium to the teliospore. J. Agric. Res. 51: 801-818.

Armentrout, V.N., and C.L. Wilson. 1969. Haustorium-host interaction during mycoparasitism of Mycotypa microspora by Piptocephalis virginiana. Phytopathology 59: 897-905.

Bartnicki-Garcia, S. 1968. Cell wall chemistry, morphogenesis and taxonomy of fungi. Annual Review of Microbiology 22: 87-108.

Bary de, A. 1863. Recherches sur le développement de quelques champignons parasites. Ann. Sci. Nat. Bot. IV 20: 5-148.

Bennett, J., and K.J. Scott. 1971. Inorganic polyphosphates in the wheat stem rust fungus and in rust-infected wheat leaves. Physiol. Plant Pathol. 1: 185-198.

Berridge, M.J., and J.L. Oschman. 1972. Transporting epithelia. Academic Press, New York. 95 pp.

Boer, P. 1979. Glycosylation of yeast and fungal cell wall components. Biochem. Soc. Trans. 7: 331-333.

Bonnett Jr., H.T. 1968. The root endodermis: fine structure and function. J. Cell Biol. 37: 109-205.

Borland, J., and C.W. Mims. 1980. An ultrastructural comparison of the aecial and telial haustoria of the autoecious rust Puccinia podophylli. Mycologia 72: 767-774.

Bossányi, G., and G.M. Oháh. 1974. Activité phosphatique acide en relation avec la pénétration intracellulaire du parasite Puccinia graminis var. tritici dans la cellule du blé. Mycopath. Mycol. Appl. 54: 161-171.

Bowers, B., and E.D. Korn. 1974. Localization of lipophosphonoglycan on both sides of Acanthamoeba plasma membrane. J. Cell Biol. 62: 533-540.

Bracker, C.E., and L.J. Littlefield. 1973. Structural concepts of host-pathogen interfaces. In "Fungal Pathogenicity and the Plant's Response" (R.J.W. Byrde and C.V. Cutting, eds.), pp. 159-318. Academic Press, London.

Bruijn de, W.C. 1973. Glycogen, its chemistry and morphologic appearance in the electron microscope. 1. A modified OsO_4 fixative which selectively contrasts glycogen. J. Ultrastruct. Res. 42: 29-50.

Bullock, S., A.E. Ashford, and H.J. Willets. 1980. The structure and histochemistry of sclerotia of Sclerotinia minor Jagger. II. Histochemistry of extracellular substances and cytoplasmic reserves. Protoplasma 104: 333-351.

Bushnell, W.R. 1971. The haustorium of Erysiphe graminis. An experimental study by light microscopy. In "Morphological and Biochemical Events in Plant Parasite Interaction" (S. Akai and S. Ouchi, eds.), pp. 229-254. Phytopathological Society of Japan, Tokyo.

Bushnell, W.R. 1972. Physiology of fungal haustoria. Annu. Rev. Phytopathol. 10: 151-176.

Callow, J.A. 1977. Recognition, resistance and the role of plant lectins in host-parasite interactions. Advances in Botanical Research 4: 1-49. Acad. Press, New York.

Callow, J.A., L.C.M. Capaccio, G. Parish, and P.B. Tinker. 1978. Detection and estimation of polyphosphate in vesicular-arbuscular mycorrhizas. New Phytol. 80: 125-134.

Calonge, F.D. 1969. Ultrastructure of the haustoria or intracellular hyphae in four different fungi. Arch. Mikrobiol. 67: 209-225.

Chrispeels, M.J. 1976. Biosynthesis, intracellular transport, and secretion of extracellular macromolecules. Ann. Rev. Plant Physiol. 27: 19-38.

Clowes, F.A.L., and B.E. Juniper. 1969. Plant Cells. Blackwell Scientific Publications, Oxford & Edinburgh.

Coffey, M.D. 1975. Obligate parasites of higher plants, particularly rust fungi. Symp. Soc. Exp. Biol. 29: 297-323.

Coffey, M.D. 1976. Flax rust resistance involving the K gene: an ultrastructural survey. Can. J. Bot. 54: 1443-1457.

Coffey, M.D. 1977. Structural adaptations of obligate parasites. 2nd Int. Mycol. Congr. (Abstr.). pp. 109.

Coffey, M.D., B.A. Palevitz, and P.J. Allen. 1972. The fine structure of two rust fungi, Puccinia helianthi and Melampsora lini. Can. J. Bot. 50: 231-240.

Colley, R.H. 1918. Parasitism, morphology, and cytology of Cronartium ribicola. J. Agric. Res. 15: 619-660.

Courtoy, R., and L.J. Simar. 1974. Importance of controls for the demonstration of carbohydrates in electron microscopy with the silver methenamine or the thiocarbohydrazide-silver proteinate methods. J. Microscopy 100: 199-211.

Craig, A.S. 1974. Sodium borohydride as an aldehyde blocking reagent for electron microscope histochemistry. Histochemistry 42: 141-144.

Dow, J.A., and J.A. Callow. 1979. Partial characterization of glycopeptides from culture filtrates of Fulvia fulva (Cooke) Ciferri (syn. Cladosporium fulvum), the tomato leaf mould pathogen. J. Gen. Microbiol. 113: 57-66.

Ehrlich, H.G., and M.A. Ehrlich. 1963. Electron microscopy of the host-parasite relationships in stem rust of wheat. Am. J. Bot. 50: 123-130.

Ehrlich, M.A., and H.G. Ehrlich. 1970. Electron microscope radioautography of ^{14}C transfer from rust uredospores to wheat host cells. Phytopathology 60: 1850-1851.

Ehrlich, M.A., and H.G. Ehrlich. 1971. Fine structure of the host-parasite interfaces in mycoparasitism. Annu. Rev. Phytopathol. 9: 155-184.

Ehrlich, M.A., J.F. Schafer, and H.G. Ehrlich. 1968. Lomasomes in wheat leaves infected by Puccinia graminis and P. recondita. Can. J. Bot. 46: 17-20.

Eschrich, W. 1961. Untersuchungen über den Ab- und Aufbau der Callose. Z. Bot. 49: 153-218.

Farrar, J.F. 1976. The uptake and metabolism of phosphate by the lichen Hypogymnia physodes. New Phytol. 77: 127-134.

Faulk, W.P., and G.M. Taylor. 1971. An immunocolloid method for the electron microscope. Immunochemistry 8: 1081-1083.

Frey-Wyssling, A., and K. Mühlethaler. 1965. Ultrastructural plant cytology. Elsevier, Amsterdam.

Gold, R.E., and L.J. Littlefield. 1979. Light and scanning electron microscopy of the telial, pycnial and aecial stages of Melampsora lini. Can. J. Bot. 57: 629-638.

Gold, R.E., L.J. Littlefield, and G.D. Statler. 1979. Ultrastructure of the pycnial and aecial stages of Puccinia recondita. Can. J. Bot. 57: 74-86.

Goldstein, I.J., S. Hammerström, and G. Sunblad. 1975. Precipitation and carbohydrate-binding specificity studies on wheat germ agglutinin. Biochim Biophys Acta 405: 53-61.

Goldstein, I.J., L.L. So, Y. Yang, and Q.C. Callies. 1969. Protein-carbohydrate interaction. XIX. The interaction of Concanavalin A with IgM and the glycoprotein phytohemagglutinins of the waxbean and the soybean. J. Immunology 103: 695-698.

Gunning, B.E.S. 1977. Transfer cells and their roles in transport of solutes in plants. Sci. Prog. 64: 539-568.

Hall, J.L. 1978. Electron microscopy and cytochemistry of plant cells. Biomedical Press, New York. 444 pp.

Hanchey, P. 1980. Histochemical changes in oat cell walls after victorin treatment. Phytopathology 70: 377-381.

Harder, D.E. 1976. Mitosis and cell division in some cereal rust fungi. II. The processes of mitosis and cytokinesis. Can. J. Bot. 54: 995-1009.

Harder, D.E. 1978. Comparative ultrastructure of the haustoria in uredial and pycnial infections of Puccinia coronata avenae. Can. J. Bot. 56: 214-224.

Harder, D.E., R. Rohringer, D.J. Samborski, W.K. Kim, and J. Chong. 1978. Electron microscopy of susceptible and resistant near isogenic (sr6/Sr6) lines of wheat infected by Puccinia graminis tritici. I. The host pathogen interface in the compatible (sr6/P6) interaction. Can. J. Bot. 56: 2955-2966.

Harold, F.M. 1966. Inorganic polyphosphates in biology: structure, metabolism, and function. Bacteriol. Rev. 30: 772-794.

Hayat, M.A. 1970. Principles and techniques of electron microscopy: biological applications. Volume 1. Van Nostrand Reinhold Company. New York, Cincinnati, Toronto, London, Melbourne. 412 pp.

Hayes, T.L., F.T. Lindgren, and J.W. Gofman. 1963. A quantitative determination of the osmium tetroxide-lipoprotein reaction. J. Cell Biol. 19: 251-255.

Heath, M.C. 1971. Haustorial sheath formation in cowpea leaves immune to rust infection. Phytopathology 61: 383-388.

Heath, M.C. 1972. Ultrastructure of host and nonhost reactions to cowpea rust. Phytopathology 62: 27-38.

Heath, M.C. 1974. Light and electron microscope studies of the interactions of host and nonhost plants with cowpea rust - Uromyces phaseoli var. vignae. Physiol. Plant Pathol. 4: 403-414.

Heath, M.C. 1976. Ultrastructural and functional similarity of the haustorial neckband of rust fungi and the Casparian strip of vascular plants. Can. J. Bot. 54: 2484-2489.

Heath, M.C. 1979. Partial characterization of the electron-opaque deposits formed in the non-host plant, French bean, after cowpea rust infection. Physiol. Plant Pathol. 15: 141-148.

Heath, M.C., and I.B. Heath. 1971. Ultrastructure of an immune and a susceptible reaction of cowpea leaves to rust infection. Physiol. Plant Pathol. 1: 277-287.

Heath, M.C., and I.B. Heath. 1975. Ultrastructural changes associated with the haustorial mother cell during haustorium formation in Uromyces phaseoli var. vignae. Protoplasma 84: 297-314.

Heath, M.C., and I.B. Heath. 1978. Structural studies of the development of infection structures of cowpea rust, Uromyces phaseoli var. vignae. I. Nucleoli and nuclei. Can. J. Bot. 56: 648-661.

Heslop-Harrison, J. 1966. Cytoplasmic continuities during spore formation in flowering plants. Endeavour 25: 65-72.

Hickey, E.L., and M.D. Coffey. 1977. A fine structural study of the pea downy mildew fungus Peronospora pisi in its host Pisum sativum. Can. J. Bot. 55: 2845-2858.

Hickey, E.L., and M.D. Coffey. 1978. A cytochemical investigation of the host-parasite interface in Pisum sativum infected by the downy mildew fungus Peronospora pisi. Protoplasma 97: 201-220.

Horisberger, M., and J. Rosset. 1977. Colloidal gold, a useful marker for transmission and scanning electron microscopy. J. Histochem. Cytochem. 25: 295-305.

Horisberger, M., and M. Vonlanthen. 1977. Location of mannan and chitin on thin sections of budding yeasts with gold markers. Arch. Microbiol. 115: 1-7.

Hunsley, D., and J.H. Burnett. 1970. The ultrastructural architecture of the walls of some hyphal fungi. J. Gen. Microbiol. 62: 203-218.

Hunt, P. 1968. Cuticular penetration by germinating uredospores. Trans. Br. Mycol. Soc. 51: 103-112.

Jagels, R., and J.G. Garner. 1979. Variation in callose deposition in the ligules of seven species of Selaginella. Amer. J. Bot. 66: 963-969.

Jones, L.H.P., and K.A. Handreck. 1965. Studies of silica in the oat plant. III. Uptake of silica from soils by the plant. Plant and Soil 23: 79-96.

Jones, L.H.P., and A.A. Milne. 1963. Studies of silica in the oat plant. I. Chemical and physical properties of the silica. Plant and Soil 18: 207-220.

Karling, J.S. 1932. Studies in the Chytridiales. VII. The organization of the Chytrid thallus. Am. J. Bot. 19: 41-74.

Keen, N.T., and M. Legrand. 1980. Surface glycoproteins: evidence that they may function as the race specific phytoalexin elicitors of Phytophthora megasperma f. sp. glycinea. Physiol. Plant Pathol. 17: 175-192.

Kessler, G. 1958. Zur Charakterisierrung der Siebröhrenkallose Ber. Schweiz. Bot. Ges. 68: 5-43.

Kohno, M., H. Ishizaki, and H. Kunoh. 1976. Cytological studies on rust fungi. V. Intracellular hyphae of Gymnosporangium haraeanum Sydow in cells of Japanese pear leaves. Ann. Phytopathol. Soc. Jpn. 42: 417-423.

Kohno, M., H. Ishizaki, and H. Kunoh. 1977. Cytological studies on rust fungi. VI. Fine structures of infection process of Kuehneola japonica (Diet.) Dietel. Mycopathologia 61: 35-42.

Kozar, F., and H.J. Netolitzky. 1975. Ultrastructure and cytology of pycnia, aecia, and aeciospores of Gymnosporangium clavipes. Can. J. Bot. 53: 972-977.

Kunoh, H., and H. Ishizaki. 1980. X-ray microanalysis of air-dried conidia and conidiophores of Erysiphe graminis hordei. Can. J. Bot. 58: 133-135.

Kunoh, H., S. Takamatsu, and H. Ishizaki. 1978. Cytological studies of early stages of powdery mildew in barley and wheat. III. Distributions of residual calcium and silicon in germinated conidia of Erysiphe graminis hordei. Physiol. Plant Pathol. 13: 319-325.

Lalonde, J.-M.A., F.N. Ghadially, and K.L. Massey. 1978. Ultrastructure of intramuscular haematomas and electron-probe X-ray analysis of extracellular and intracellular iron deposits. J. Path. 125: 17-23.

Littlefield, L.J. 1972. Development of haustoria of Melampsora lini. Can. J. Bot. 50: 1701-1703.

Littlefield, L.J., and C.E. Bracker. 1970. Continuity of host plasma membrane around haustoria of Melampsora lini. Mycologia 62: 609-614.

Littlefield, L.J., and C.E. Bracker. 1972. Ultrastructural specialization of the host-pathogen interface in rust-infected flax. Protoplasma 74: 271-305.

Littlefield, L.J., and M.C. Heath. 1979. Ultrastructure of rust fungi. Academic Press, New York, San Francisco, London. 277 pp.

Lott, J.N., and M.S. Buttrose. 1978. Thin sectioning, freeze fracturing, energy dispersive X-ray analysis, and chemical analysis in the study of inclusions in seed protein bodies. Almond, Brazil Nut, and Quandong. Can. J. Bot. 56: 2050-2061.

Manocha, M.S. 1975. Autoradiography and fine structure of host-parasite interface in temperature-sensitive combinations of wheat stem rust. Phytopathol. Z. 82: 207-215.

Manocha, M.S., and K.Y. Lee. 1971. Host-parasite relations in myco-parasite. I. Fine structure of host, parasite, and their interface. Can. J. Bot. 49: 1677-1681.

Manocha, M.S., and K.Y. Lee. 1972. Host-parasite relations in myco-parasite. II. Incorporation of tritiated N-acetylglucosamine into Choanephora cucurbitarum infected with Piptocephalis virginiana. Can. J. Bot. 50: 35-37.

Manocha, M.S., and D.R. Letourneau. 1978. Structure and composition of host-parasite interface in a mycoparasite system. Physiol. Plant Pathol. 12: 141-150.

Manocha, M.S., and M. Shaw. 1966. The physiology of host-parasite relations. XVI. Fine structure of the nucleus in the rust-infected mesophyll cells of wheat. Can. J. Bot. 44: 669-673.

Manocha, M.S., and M. Shaw. 1967. Electron microscopy of uredospores of Melampsora lini and of rust-infected flax. Can. J. Bot. 45: 1575-1582.

Mares, D.J. 1979. A light and electron microscope study of the interaction of yellow rust (Puccinia striiformis) with a susceptible wheat cultivar. Ann. Bot. 43: 183-189.

Marinozzi, V. 1961. Silver impregnation of ultrathin sections for electron microscopy. J. Biophys. Biochem. Cytol. 9: 121-211.

Mendgen, K. 1975. Ultrastructural demonstration of different peroxidase activities during the bean rust infection process. Physiol. Plant Pathol. 6: 275-282.

Mendgen, K., and W.H. Fuchs. 1973. Elektronenmikroskopische darstellung peroxydatischer aktivitaten bei Phaseolus vulgaris nach infektion mit Uromyces phaseoli typica. Arch. Mikrobiol. 88: 181-192.

Mendgen, K., and R. Heitefuss. 1975. Micro-autoradiographic studies on host-parasite interactions. I. The infection of Phaseolus vulgaris with tritium labelled uredospores of Uromyces phaseoli. Arch. Microbiol. 105: 193-199.

Mills, J.T., and J. Chong. 1977. Ultrastructure and mineral distribution in heat-damaged rapeseed. Can. J. Plant Sci. 57: 21-30.

Molano, J., B. Bowers, and E. Cabib. 1980. Distribution of chitin in the yeast cell wall. An ultrastructural and chemical study. J. Cell Biol. 85: 199-212.

Morré, D.J. 1975. Membrane biogenesis. Plant Physiol. 26: 441-481.

Müller, L.Y., F.H.J. Rijkenberg, and S.J. Truter. 1974. Ultrastructure of the uredial stage of Uromyces appendiculatus. Phytophylactica 6: 73-104.

Nagahashi, G., R.T. Leonard, and W.W. Thomson. 1978. Purification of plasma membranes from roots of barley. Specificity of the phospho-tungstic acid-chromic acid stain. Plant Physiol. 61: 993-999.

Nelson, R.K., R.W. Scheetz, and C.J. Alexopoulos. 1977. Elemental composition of Metatrichia vesparium sporangia. Mycotaxon V: 365-375.

Nishi, A. 1961. Role of polyphosphate and phospholipid in germinating spores of Aspergillus niger. J. Bacteriol. 81: 10-19.

Northcote, D.H., and F.B.P. Wooding. 1965. Development of sieve tubes in Acer pseudoplatanus. Proc. Royal Soc. Lond. Ser. B 163: 524-537.

Orcival, J. 1969. Infrastructure des sucoirs et relations hôte-parasite dans des stades écidiens d'Uredinales. C.R. Hebd. Seances Acad. Sci., Ser. D, 269: 1973-1975.

Pady, S.M. 1935. The role of intracellular mycelium in systemic infections of Rubus with the orange rust. Mycologia 27: 618-637.

Pearlmutter, N.L., and C.A. Lembi. 1978. Localization of chitin in algal and fungal cell walls by light and electron microscopy. J. Histochem. Cytochem. 26: 782-791.

Pease, D.C. 1968. Phosphotungstic acid as an electron stain. In "Proc. 26th Ann. EMSA Meeting", p. 36. Claitor's Publishing Division, Baton Rouge, LA.

Rambourg, M.A. 1967. Détection des glycoproteines en microscopie électronique: coloration de la surface cellulaire et de l'appareil de Golgi par un mélange acide chromique phosphotungstique. C.R. Hebd. Seances Acad. Sci., Ser. D 265: 1426-1428.

Rambourg, M.A., W. Hernandez, and C.P. Leblond. 1969. Detection of complex carbohydrates in the Golgi apparatus of rat cells. J. Cell Biol. 40: 395-414.

Reynolds, B.A. 1975. Cytology and ultrastructure of brown rust in barley cultivars of varied resistance. Doctoral Thesis, University of London.

Rice, M.A. 1927. The haustoria of certain rusts and the relation between host and pathogene. Bull. Torrey Bot. Club 54: 63-153.

Rijkenberg, F.H.J., and S.J. Truter. 1973. Haustoria and intracellular hyphae in the rusts. Phytopathology 63: 281-286.

Rijo, L., and J.A. Sargent. 1974. The fine structure of the coffee leaf rust, Hemileia vastatrix. Can. J. Bot. 52: 1363-1367.

Robards, A.W., S.M. Jackson, D.T. Clarkson, and J. Sanderson. 1973. The structure of barley roots in relation to the transport of ions into the stele. Protoplasma 77: 291-311.

Robb, J., A.E. Harvey, and M. Shaw. 1975. Ultrastructure of tissue cultures of Pinus monticola infected by Cronartium ribicola. II. Penetration and post-penetration. Physiol. Plant Pathol. 5: 9-18.

Rohringer, R., J. Chong, W.K. Kim, and D.E. Harder. 1980. Cytochemistry of the host-parasite interface and the use of gold markers in cereal-rust interactions. In "Active Defense Mechanisms in Plants" (R.K.S. Wood, ed.), (In press).

Roland, J.C. 1973. The relationship between the plasmalemma and plant cell wall. Int. Rev. Cytol. 36: 45-92.

Roland, J.C., C.A. Lembi, and D.J. Morre. 1972. Phosphotungstic acid-chromic acid as a selective electron-dense stain for plasma membranes of plant cells. Stain Technol. 47: 195-200.

Russ, J.C. 1972. Energy dispersive analysis of X-rays and the scanning electron microscope. In "Thin-Section Micro-analysis", pp. 7-32. EDAX Laboratories, Raleigh, NC.

Ruttle, M.L., and W.P. Fraser. 1927. A cytological study of Puccinia coronata Cda. on Banner and Cowra 35 oats. Uni. Cal. Publ. Bot. 14: 21-72.

Samborski, D.J., W.K. Kim, R. Rohringer, N.K. Howes, and R.J. Baker. 1977. Histological studies on host-cell necrosis conditioned by the Sr6 gene for resistance in wheat to stem rust. Can. J. Bot. 55: 1445-1452.

Sangster, A.G., and D.W. Parry. 1976. Endodermal silification in mature nodal roots of Sorghum bicolor (L.) Moench. Ann. Bot. (London) 40: 373-379.

Sannes, P.L., S.S. Spicer, and T. Katsuyama. 1979. Ultrastructural localization of sulphated complex carbohydrates with a modified iron diamine procedure. J. Histochem. Cytochem. 27: 1108-1111.

Sargent, P., and J.L. Gay. 1977. Barley epidermal apoplast structure and modifications by powdery mildew contact. Physiol. Plant Pathol. 11: 195-205.

Savile, D.B.O. 1939. Nuclear structure and behavior in species of the Uredinales. Am. J. Bot. 26: 585-609.

Scannerini, S., and P. Bonfante-Fasolo. 1979. Ultrastructural cytochemical demonstration of polysaccharides and proteins within the host-arbuscule interfacial matrix in an endomycorrhiza. New Phytol. 83: 87-94.

Scott, J.E., and D. Glick. 1971. The invalidity of "phosphotungstic acid as a specific electron stain for complex carbohydrates". J. Histochem. Cytochem. 19: 63-64.

Scurfield, G., C.A. Anderson, and E.R. Segnit. 1974. Silica in woody stems. Aust. J. Bot. 22: 211-219.

Seligman, A.M., H.L. Wasserkrug, and J.S. Hanker. 1966. A new procedure (OTO) for enhancing lipid-containing structures by bridging osmium to osmium-fixed tissue with thiocarbohydrazide (TCH). J. Cell Biol. 30: 424-432.

Sharon, N., and H. Lis. 1972. Lectins: cell-agglutinating and sugar-specific proteins. Science 177: 949-959.

Shaw, M., and M.S. Manocha. 1965. The physiology of host-parasite relations. XV. Fine structure in rust-infected wheat leaves. Can. J. Bot. 43: 1285-1292.

Shiraishi, T., S. Ouchi, and H. Oku. 1976. Chitin component in haustorial wall of powdery mildew fungus of barley. Sc. Rep. Fac. Agr. Okayama Uni. No. 47: 21-24.

Silverman, L., and D. Glick. 1969. The reactivity and staining of tissue proteins with phosphotungstic acid. J. Cell Biol. 40: 761-767.

Snell, W.H., and E.A. Dick. 1971. "A Glossary of Mycology", Revised ed. Harvard University Press, Cambridge.

Spencer-Phillips, P.T.N., and J.L. Gay. 1980. Electron microscope autoradiography of ^{14}C photosynthate distribution at the haustorium-host interface in powdery mildew of Pisum sativum. Protoplasma 103: 131-154.

Spurr, A.R. 1969. A low-viscosity epoxy resin embedding medium for electron microscopy. J. Ultrastruct. Res. 26: 31-43.

Thatcher, F.S. 1943. Cellular changes in relation to rust resistance. Can. J. Res. Sec. C 21: 151-172.

Thiéry, J.P. 1967. Mise en évidence des polysaccharides sur coupes fines en microscopie électronique. J. Microscopie 6: 987-1018.

Thiéry, J.P. 1969. Role de l'appareil de Golgi dans la synthèse des mucopolysaccharides; étude cytochimique. I. Mise en évidence de mucopolysaccharides dans les vésicules de transition entre l'ergastoplasme et l'appareil de Golgi. J. Microscopie 8: 689-708.

Trocha, P., and J.M. Daly. 1974. Cell walls of germinating uredospores. II. Carbohydrate polymers. Plant Physiology 53: 527-534.

Tsuchiya, A., and K. Ogawa. 1973. Ultracytochemistry of the periodic acid (PA) phosphotungstic acid (PTA) reaction. J. Electron Micros. 22: 290.

Van der Valk, P., R. Marchant, and J.G.H. Wessels. 1977. Ultrastructural localization of polysaccharides in the wall and septum of the basidiomycete Schizophyllum commune. Experimental Mycology 1: 69-82.

Van der Woude, W.J. 1973. Significance of the specific staining of plant plasma membranes by treatment with chromic acid - phosphotungstic acid. Plant Physiol. 51: 15 (suppl.).

Van Dyke, C.G., and A.L. Hooker. 1969. Ultrastructure of host and parasite in interaction of Zea mays with Puccinia sorghi. Phytopathology 59: 1934-1946.

Wade, M., and P. Albersheim. 1979. Race-specific molecules that protect soybeans from Phytophthora megasperma var. sojae. Proc. Natl. Acad. Sci. 76: 4433-4437.

Walles, B. 1974. Ultrastructure of the rust fungus Peridermium pini (Pers.) Lev. Stud. For. Suec. 122: 1-30.

Wessels, J.G.H. 1969. A β-1,6-glucan glucanohydrolase involved in hydrolysis of cell-wall glucan in Schizophyllum commune. Biochem. Biophys. Acta 178: 191-193.

White, J.A., and M.F. Brown. 1979. Ultrastructure and X-ray analysis of phosphorous granules in a vesicular-arbuscular mycorrhizal fungus. Can. J. Bot. 57: 2812-2818.

Yudkin, L.Y., and B.G. Reiter. 1979. Electron microscopy study of the haustorial apparatus of the causal agent of brown rust in wheat. Mikol. Fitopatol. 12: 479-483.

Zimmer, D.E. 1970. Fine structure of Puccinia carthami and the ultrastructural nature of exclusionary seedling-rust resistance of safflower. Phytopathology 60: 1157-1163.